SYNTHESIS AND ENVIRONMENTAL CHEMISTRY OF SILVER AND IRON OXIDE NANOPARTICLES

By

SUSAN ALISON CUMBERLAND

A thesis submitted to
The University of Birmingham
For the degree of
DOCTOR OF PHILOSOPHY

School of Earth and Environmental Sciences
College of Life and Environmental Sciences
The University of Birmingham
March 2010

Abstract

Engineered nanoparticles are defined as having a dimension that is between one and one hundred nanometres. With toxicology studies reporting various degrees of toxicity the need to investigate nanoparticle fate and behaviour is vital. Monodispersed engineered nanoparticles were synthesised in-house to produce suitable materials to examine such processes. Iron oxide nanoparticles (5 nm) and citrate coated silver nanoparticles (20 nm) were subjected to different conditions of pH, ionic strength and different types of commercially available natural organic matter. Changes in particle size and aggregation were examined using a multi-method approach. Results showed that the natural organic matter was able to adsorb onto nanoparticle surfaces and improve their stability when subjected to changes in pH and ionic strength, where they would normally aggregate. The presence of higher concentrations of NOM in some cases promoted aggregation due to bridging. This work also concluded that silver nanoparticles could be produced in the presence of NOM without additional stabilisers and that they themselves were stable. This work has demonstrated that engineered nanoparticles could remain stable within a range of environmental conditions, and thus raise future pollution concerns.

Acknowledgements

Firstly, I would like to acknowledge my sponsors, NERC for funding this work.

I would also like to thank all the people that made this thesis possible. To my supervisor, Professor Jamie Lead, who took me on to do this project and gave much support, direction and opportunity.

The team at Exeter, Professor Charles Tyler, Dr Blair Johnson and Tessa Scown for the collaborative work that went into chapter 4 and supplying the tank water samples for analysis and Blair for supplying the fish mucus. There are many people that provided training and laboratory support, to which I would like to thank Ming Chu and Paul Stanley for help and support with the TEM and ESEM, Prof Colin Greaves for the XRD analysis. I would like to thank Mohammed Baalousha for his help and expertise with FFF and my first introduction to working with nanoparticles. Peter Bomford and Yon Ju-Nam for help and discussion about the nanoparticle synthesis, particularly Yon, whose early discussions led to developing the synthesis of the silver nanoparticles.

I would also like to thank Paula, Eva, Nadia, Breda and the rest of r325 for being such excellent team mates and providing moral support and Gillian Kingston for extra lab support and chats about horses! John Bridgeman for his patience and help

And lastly, to my partner, Steve, - for all the unlimited support he gave throughout for which I am eternally grateful- thank you!

Contents

List of figures

Chapter 2

Chapter 3

Chapter 4

Chapter 5

Chapter 6

Chapter 7

Chapter 8

List of Tables

Chapter 1

Chapter 2

Chapter 3

Chapter 4

Chapter 5

Chapter 6

Chapter 7

Chapter 8

Glossary

List of Abbreviations

AFM – Atomic Force Microscopy

BET – Brunauer, Emmett and Teller

CNT –- Carbon Nanotube

DLS – Dynamic light scattering

DOM – Dissolved organic matter

EDS/EDX – Energy dispersive x-rays-

EEM – Excitation Emission Matrix

EM – Electron microscopy

ENPs –- Engineered nanoparticles / manufactured nanoparticles

EPM – Electrophoretic mobility

ESEM –- Environmental Scanning Electron Microscope

Exo-PS- Exo cellular polysaccharide

FA- Fulvic Acid /

F*/*FFF –– Flow-Field Flow Fractionation - often shortened to field-flow fractionation (FFF)

HA-Humic Acid /

HDPE- High density polyurethane (plastic material)

HS – Humic Substances

ICP-MS – Inductively coupled plasma – mass spectrometer (elemental analyser)

IHSS – International Humics Substances Society

MALLS – Multi angle laser light scattering - particle sizer

MWCNT – Multi walled carbon nanotubes

NM – Nanomaterials

NOM – Natural organic matter

NP – Nanoparticle

NZVI – Nanosized zero valent iron

OS – Oxidative stress

PCS – Photon correlation spectroscopy

PEC – Predicted environmental effective concentration

PHA– Humic Acid / Fulvic Acid -/ Peat Humic acid

PM_{10} – Particulate matter – of 10 μm (aerosol and atmospheric science)

PNEC- Predicted no effect concentration

POM – Particulate organic matter

PS – Polysaccharide

ROS – Reactive oxygen species

SPR– Surface plasmon resonance

SRHA – Suwannee River humic acid

SS – Suspended sediments

SSA – Specific surface area - weight per area (g cm-3)

STM – Scanning Tunnelling Microscope

SWCNT – Single walled carbon nanotubes

TEM –- Transmission Electron Microscope

THF – Tetrahydrofluran

UF – Ultrafiltration

UHV – Ultra high vacuum

XRD – X-ray diffraction crystallography

1

Introduction

Chapter Summary

Nanoparticles (NPs, materials of 1-100nm in size) and their application in nanotechnology is an expanding area of science and industry. This is because NPs possess unique properties, that are absent in bulk materials, which are exploited in many areas of science and medicine. There are many potential benefits from nanoparticle applications in society, but there is concern arising from the number of toxicological studies reporting adverse and toxic effects. Equally important is to derive an understanding of NP environmental fate and behaviour once released to the environment. This information, once gained, will contribute to knowledge on NP exposure and, with the hazard data generated, will provide a better understanding of NP risk. The work in this thesis involves analysing and quantifying the interactions of three types of manufactured metal and metal oxide NPs with other naturally occurring substances. The research involved collaboration with eco-toxicologists; areas of joint research are briefly described. This chapter introduces NPs, their importance to science and society and their history and outlines the content in this thesis. It also lays out the aims and objectives of current research and outlines the chapters that follow.

1.1 Nanoparticles and their relevance

Nanoparticles (NPs) are defined as having at least one dimension between 1 and 100nm, where a nanometre is 10^{-9} metre. Within this category are numerous types of manufactured or engineered NPs (ENPs), including nanotubes or nanowires which are 100s nm long by only a few nm wide and nanodots, arguably, of only one dimension. Nanoparticles may also coalesce to form agglomerates and aggregates. Their behaviour has been described by DLVO theory based on the attractive and repulsive forces that surround each particle (Derjaguin and Landau, 1941; Verwey, 1947). Nanoparticles have properties that are very different to the larger or 'bulk' material and indeed this may be used as a definition of the NP phase. NPs have very large specific surface areas (SSAs) and surface energies, undercoordinated bonds, size-related quantum effects and other properties. There are many benefits arising from nanotechnology taking advantage of these novel properties including drug delivery in nanomedicine, solar panel technology and improved fuel efficiencies (Ball, 2001). As a result, manufactured NPs are finding their way into consumer products (see Table 1-1) and some of these maybe particularly harmful (Sandler, 2009), including Ag and carbon nanotubes (CNTs) (Navarro *et al.*, 2008a). For this reason there must be responsibility and regulation in the nanotechnology sector (Roco, 2005). This stated research is however, at an early stage and there remain many unanswered questions.

Table 1- 1 Examples of nanoparticle application, property and NP type

Application	**Property**	**NP type**	**Reference**
Food	Whitening agent e.g. icing sugar, milk powder	Titanium dioxide	(Lomer *et al.*, 2000)
Textiles e.g. socks	Anti bacterial properties, reduces washing	Silver	(Geranio *et al.*, 2009)
Sunscreen (high SPF)	Better UV protection, better transparency	Titanium dioxide Zinc oxide Silicon dioxide (coating)	(Serpone *et al.*, 2007)
Medicine	Drug delivery MRI imaging	Gold Iron oxide	(Lewinski *et al.*, 2008).
Plastics	Change properties Colour Strength	Iron oxide Titanium dioxide Carbon black	(Schmid and Riediker, 2008)
Self cleaning glass	Breaks down dirt of surface of glass	Titanium oxide	(DEFRA, 2005b)
Cell research	Fluorescence Imaging, Labelling	Quantum dots (e.g. Cd Se)	(DEFRA, 2005b)
LEDs Anti counterfeiting tags	Tuneable wavelength emitters	Quantum dots (e.g. Cd Se)	(DEFRA, 2005b)
Fuel additive	Improves combustion efficiency	Cerium oxide	(Oxonica, 2009)
Paints	Pigment Metallic lustre	Titanium dioxide Iron oxides Gold	(Schmid and Riediker, 2008)

Research into this field has been led from a number of disciplines (e.g. physicists, chemists and to some extent hydrologists). Colloidal scientists, consider NPs as a subset of colloids where a colloid is defined as being between 1 and 1000 nm and described as a "discrete, non-aqueous phase for contaminant binding, which does not sediment over reasonable timescales in the absence of further aggregation" (Lead and Wilkinson, 2006). Air pollution scientists have also been researching this size fraction as 'ultrafine' PM_{10} (10 μm) and are now focusing on $PM_{0.1}$ (100nm) as a size fraction with important health implications.

1.1.1 History

An early formalisation of working at the very small scale came from Feynman's 1960 lecture, "There's plenty of room at the bottom" (Feynman, 1960), is sometimes seen as the beginning of nanoscience, although the use of nanomaterials began several thousand years ago. He suggested that the entire Encyclopaedia Britannia could be written on a pin's head and proceeded to describe how nano-sized robots and computers could work and exist at this scale. In terms of understanding the presence of these materials, various techniques were then developed to allow us to 'see' the particles. In 1981 the scanning tunnelling microscope (STM) was developed. Following this, the atomic force microscope (AFM) was created in 1986, which could image NPs on a surface by tracking using a cantilever with the ability to interact with material and manipulate using attractive forces at this scale (Gibson *et al.*, 2007; Holister, 2002). A new allotrope of carbon (C_{60}) was discovered in the mid 1980s by Kroto, Smalley and colleagues (Kroto *et al.*, 1985) who shared the Nobel prize for this discovery in 1996. More recently, carbon nanotubes, which are now described as rolled graphene sheets, 1-2 nm in diameter by several 100 nm in length, where graphene is one carbon atom in height by up to a few microns length or breadth (sufficiently isolated from its environment to be free standing), were produced (Geim, 2009). The electronic structure of graphene, an individual layer of graphite, was first discussed by Wallace in 1947 (Avouris *et al.*, 2007; Wallace, 1947). Carbon nanotubes (CNTs) discovered in 1991 by Sumio Iijima (Iijima, 1991) are available as single walled (SWCNTs) and multi walled (MWCNTs). MWCNTs consist of layers of CNTs one inside each other and often engineered with surface-attached functional groups some of which have the ability to reduce the hydrophobicity of the CNT. CNTs and C_{60} show great potential in the motor industry when incorporated into rubber tyres (Colvin, 2003) and in resins and plastics for strengthening. They feature strongly in the electronic industry e.g. circuitry and flat panel screens. For the past few

years, rapid growth in nanoscience and nanotechnology has been observed. The major nanoparticles types produced in industrial quantities can be classified as inorganic metals (silver, gold, iron), metal oxides (TiO_2, ZnO_2, CeO_2, iron oxides etc), quantum dots (CdSe etc) and carbon based NMs (CNTs, fullerenes, graphene) (Ju-Nam and Lead, 2008). The list is not exhaustive (Table 1-1) and increasingly composite materials are produced, as are materials with a wide range of sizes, shapes and crystal structures etc.

1.2 Need behind the research

Although nanotechnology may provide huge and transformative benefits to society (Holister, 2002), there is the potential for risk to environmental and human health. NPs have proven toxicity (Lewinski *et al.*, 2008) and the potential for wide exposure (Sandler, 2009), but conclusions in the currently available literature are uncertain with many inconsistencies. A great deal is unknown about the eventual consequences of engineered nanoparticles (ENPs) released into the environment, but early studies have highlighted the importance of conducting research in this area (Oberdorster, 2004) and the exploration of NPs as novel hazards. Product life cycles containing NPs and the subsequent release of the nanoparticles from within these products to the environment has been discussed by a number of authors like Nowack and Bucheli (2007). Due to a lack of knowledge, much research is needed to understand the impact that nanoparticles will have, as a new contaminant, particularly due to their small size (Nel *et al.*, 2006) and potentially increased toxicity (Thill *et al.*, 2006). Currently, there is a great deal of attention given to cytotoxicity and its relation to oxidative stress caused by the formation of reactive oxygen species (ROS) (Sayes *et al.,* 2006), but the mechanisms behind bio-uptake, toxicity and bioaccumulation are poorly understood. NPs are known, because of their size and

unique surface chemistries, to pass though the cell membranes and cell walls causing call damage. In addition, there are few studies of NP environmental chemistry, fate and transport, which will in turn, inform bioavailability and exposure studies. In the environment, materials exist that fall within the nanoscale from natural processes (e.g. colloids) and thus NPs are already present in the environment. Natural nanoparticles, must therefore, exist as part of the natural chemical cyclic systems within the environment (Hochella, 2002) involved in solute and trace metal transportation. These natural NPs include chemical groups such as aquatic humic substances (HS) and metal oxides (Lead *et al.*, 1999). Moreover, natural colloids could interact with ENPs and change the ENP surface chemistry and affect bio-uptake. The ultimate result from introduction of manufactured nanoparticles and interaction with other NPs to the aquatic environment is uncertain. But several hypotheses could be made, for example, manufactured NPs could either remain in suspension or sediment due to aggregation and fall to the bottom (Lead and Wilkinson, 2007). NP removal from the system is unlikely, and sedimentation is not necessarily the final outcome, especially following emission disturbances or the impact of benthic feeders.

The synthesis of well defined NPs, their appropriate characterisation and an understanding of how NPs behave under environmentally relevant conditions, underpin all of these areas and represents the focus of this thesis.

1.3 Aims and objectives

The overall aim of this work is to investigate and quantify the interactions and behaviour of selected well defined and characterised nanoparticles under environmentally relevant conditions. The aims will be met by pursuing the following objectives:

1) To procure well defined nanoparticles by different synthesis methods (silver and iron oxides) and purchase from commercial suppliers (titanium dioxide).
2) To characterise physico-chemical characteristics of the nanoparticle
3) To investigate the effect of environmental conditions (NOM, pH and ionic strength) on objective 2.

Objective one and two will be exploratory investigations into suitable methodologies for NP production and characterisation. Whereas objective three will be taking the NPs characterised in objective two and subjecting them to some environmental conditions to investigate the changes in size, aggregation and surface coatings or other physico-chemical properties by changing solution conditions, for example, by adding humic and fulvic acids, counter ions and pH.

1.4 Guide to the thesis

This thesis is composed of nine chapters including five experimental chapters covering the background methodology and final discussion and recommendations for further work. The background, history and current use of NPs are discussed in more detail in chapter 2. This chapter also reviews cover nanoparticle toxicity, hazard and risks to the environment and to human health by synthesising the current literature and governmental reports. It concludes by recognising need for additional research in the fate and behaviour of NPs. Chapter 3 then outlines the generic techniques conducted in this research. It covers instrumentation, theory and some laboratory methods. Specific techniques and experimental details are provided in

subsequent chapters. Chapter 4 discusses the characterisation of commercial titanium dioxide nanopowders before and after exposure to freshwater fish (trout) over a nine day trial. This work was done in collaboration with Exeter University, where the exposures were performed. In chapter 5, results are presented from experiments investigating the interactions between in-house synthesised iron oxide nanoparticles and natural organic matter; in which the effect on particle size was measured, as a function of pH and humic concentration, by field flow fractionation. The work covered in chapters 6 to 8, focuses on silver nanoparticles. Chapter 6 describes the synthesis of monodisperse 15 nm citrate stabilised silver nanoparticles; chapter 7 reports the results of their interaction with NOM as a function of pH and ionic strength and chapter 8 explores alternative ways of producing silver nanoparticles capped with NOM in the absence of citrate and presents their full characterisation. The thesis discussion is presented in chapter 9, along with recommendations and areas for future research.

Finally, the content of chapter 5, on iron oxides was presented at a conference in Chicago 2008, with the abstract to be published in the conference proceedings and Chapter 7, was published in December 2009 in Chromatography A (Cumberland and Lead, 2009) (See Appendix 1). Other papers that the research conducted in this thesis has contributed to are Johnson et al. 2010 (see Appendix 2), Baalousha et al. (2008) (see Appendix 3) and Scown et al. 2009) (see Appendix 4).

2

Background

Chapter Summary

Manufactured nanoparticles (NPs) are being researched and produced in greater numbers with the industry predicted to be worth 1.5 trillion US dollars by 2015 (Aitken *et al.*, 2006). There are many types of inorganic metal and carbon-based manufactured nanoparticles which are increasingly being produced with numerous chemical attachments providing different surface chemistries. Yet, as some studies have revealed that NPs can have adverse effects on biota, the need for on-going research is clear. Research gaps include how NPs interact with environmental nano constituents and how NPs can be detected and analysed. The chapter begins by providing a definition for nanoparticles, and by differentiating NPs according to whether they are manufactured, incidental or naturally occurring. This leads to a section on NP synthesis and emerging applications. The second part of this chapter explores the concept of environmental risk by discussing environmental exposure, hazard, toxicity and risk. Environmental risk is then covered in more detail, with NP fate and behaviour explored under various chemical and environmental conditions, and important gaps in the literature are highlighted.

2.1 Definitions, classifications and history of NPs

Nanoparticles are defined as having at least one dimension that is between 1 and 100 nm, where a nanometre is 10^{-9} metres. To put this into context, a human hair is approximately 80,000 nm wide, and a red blood cell approximately 7000nm wide (RS/RAEng, 2004). This size definition, however, varies in its dimensions from country to country (OECD, 2009), and where it forms the basis of regulation may pose future problems as a result. Additionally, as NPs possess properties, that set them apart from their bulk counterparts, such characteristics may be taken into consideration when providing NP definitions in the future. The Royal Society and Royal Academy of Engineering (2004) have recently defined 'Nanoscience' as:

> *"The study of phenomena and manipulation of materials at atomic, molecular and macromolecular scales, where properties differ significantly from those at a larger scale"*

and 'Nanotechnologies' as;

> *"the design, characterisation, production and application of structures, devices and systems by controlling shape and size at nanometre scale"* (RS/RAEng, 2004).

To help further distinguish the origin of the nanoparticle, an additional definition was adopted by DEFRA (2005a) who defined 'engineered nanoparticles' as;

> *"nanoparticles manufactured to have specific properties or a specific composition".*

In Europe and UK regulatory policy terms, a definition based on size is perhaps the most robust of the definitions and should be adhered to when referring to nanoparticles. However, NPs property changes occur in particles that are much less than 50 nm and should be strongly considered in policy decisions (Auffan *et al.*, 2009).

Nanoparticle types fall within three genera: engineered NPs, those produced synthetically in industry, and are the focus of this work, but incidentally produced NPs, produced by man, but

without intent or purpose such as a by-product of burning fossil fuels, and naturally occurring NPs from chemical, geological or plant processes also exist. The work in this thesis examines engineered NPs as well as the interactions with other NPs in the environment.

2.1.1 Natural NPs

Naturally occurring (1-100 nm) nanoparticles are a subset of the group aquatic colloids, where colloids are aqueous macromolecules with a size range 1-1000 nm. Natural nanoparticles (1-100nm), are found in aquatic surface and ground waters (see Figure 2.1 (a) (Lead *et al.*, 2005; Lead and Wilkinson, 2006)) as suspended particles less than 25 nm (Baalousha and Lead, 2007b). Previous work with organic humic substances (HS), one specific form of NP, has revealed structures of around 1 nm (Lead *et al.*, 2000a). Natural nanoparticles (and colloids) are ubiquitous in the environment and may be biogenic or geogenic in origin (Buffle *et al.*, 1998). In biological systems, examples include DNA, and complex nanostructured proteins such as polysaccharides, viruses, and bacterial exudates that control a range of biological activities. Rock weathering, volcanoes, fires and sea spray are also responsible for producing nano-sized components (Hochella, 2002), other sources include, via microbial activity and through chemical hydrolysis (Wigginton *et al.*, 2007). Figure 2.1 shows the size range of many of these naturally occurring NPS and the techniques that can be used to detect them.

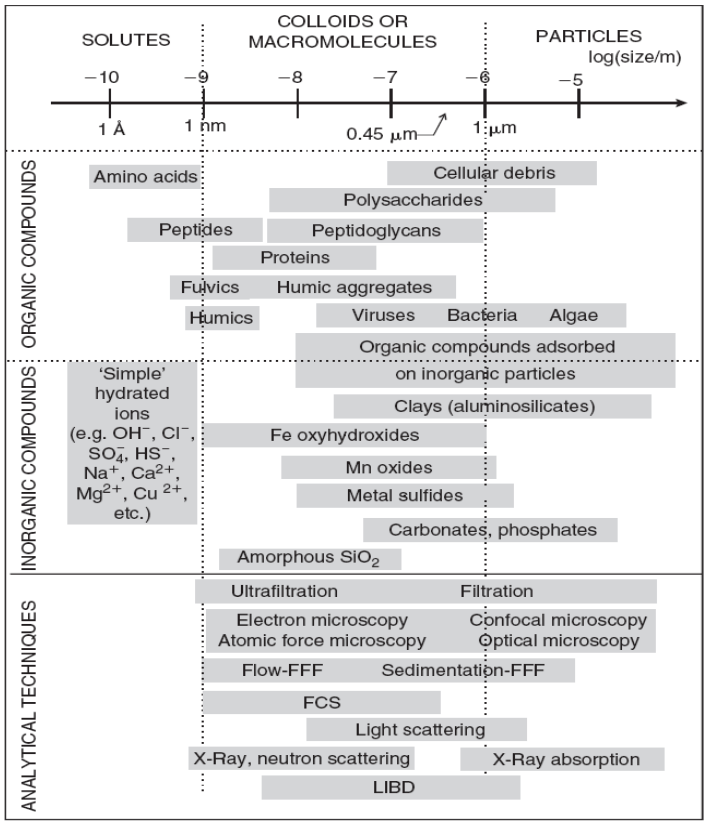

Figure 2. 1 Size distributions of various types of environmental colloids and particle and several of the analytical techniques used to characterise them. Techniques Abbreviated are: field-flow fractionation (F*/*FFF). fluorescence correlation spectroscopy (FCS): - laser induced breakdown detections (LIBD). Taken from Lead and Wilkinson (2006).

The duration over which small materials remain in the nanophase could be variable and will depend on environmental conditions and growth. For example, materials precipitating directly out of suspension will form minerals, However, a large fraction of nano-sized solid-phase materials exist at this size range for extended periods of time (Wigginton *et al.*, 2007). Well known examples of nanominerals, which remain in the nanoscale, include certain clays (aluminium-silicates) as well as iron and manganese oxyhydroxides (Hochella *et al.*, 2008; Hochella and Madden, 2005). The presence of nanomaterials in various soil types has also been reviewed by Wilson *et al.,* (2008).

Natural nanoparticles of organic origin, such as humic substances (HS), constitute the majority of the natural organic matter (NOM) fraction. A large proportion of this NOM, including HS, is present in the nanoscale. HS are macromolecules with various functional groups such as carboxylic, thiol, and phenols and are the product of the breakdown of lignin, plant and algae cellulose in surface waters. In marine systems, algae are the main contributors to NOM. Fulvic acid (FA) and humic acids (HA) are examples of aquatic HS, defined by their extraction method, but generally FA is soluble at all pH and humic acid (HA) is soluble at low pH and an example of a proposed structure for FA is given in Figure 2.2. Peat humic acid is hydrophobic and is able to bond readily with other surfaces (Aiken *et al.*, 1985), acting as a surfactant-like interface between water and other insoluble media (Hyung *et al.*, 2007). They have a hydrophilic group and a hydrophobic group and will change their conformation under certain pH and ionic conditions.

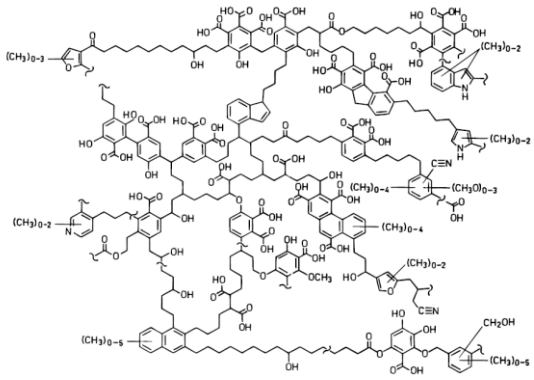

Figure 2. 2 Proposed chemical structure for fulvic acid. Taken from Buffle et al., (1998)

At 1-3 nm (or larger) in size fulvic acids are the smaller of the group with higher molecular weight soil and peat humics as large as 15 nm. These substances are available commercially from the International Humic Substances Society (IHSS), who have produced well defined characterized standard materials e.g. from the Suwannee River, US. Over thirty years of research have meant that the HS are well characterized (Alvarez-Puebla *et al.*, 2006), but cannot be

precisely defined structurally or functionally due to their heterogeneous nature, and are therefore defined by their extraction method. Humic substances have the ability to complex with trace metal ions and to reduce the oxidized forms of certain metals ions (Malcolm, 1985). The extent of this will depend on pH and ionic strength of the water (Leenheer *et al.*, 1998). Figure 2.3 (b) shows an AFM study of natural NPs from a UK river.

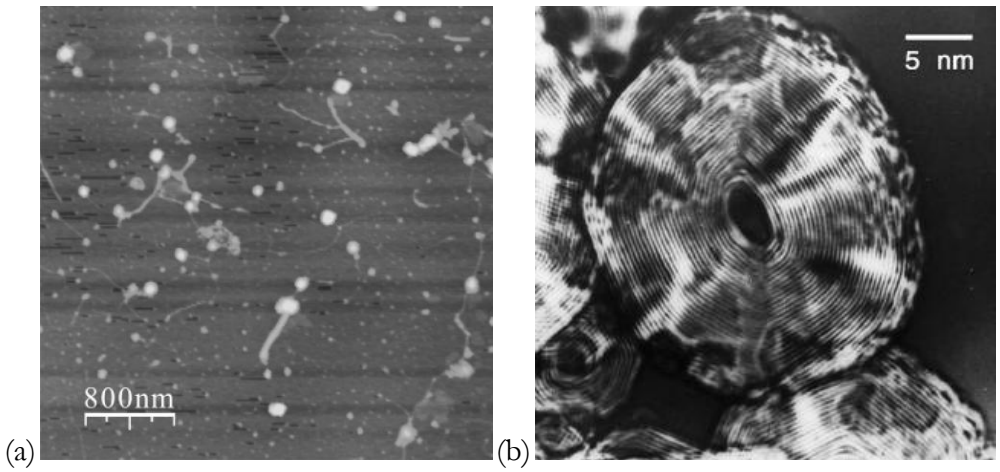

Figure 2. 3 Natural nanoparticles (a) AFM image of particles from the River Tame, UK taken from Lead *et al.,* 2005 (2005); (b)TEM image showing carbon 'onions' from the Allende meteorite. Taken from Buseck (2002).

Polysaccharides, a sub group of NOM (Balnois *et al.*, 2000), are complex carbohydrates formed by bacteria and fungi (Chenu, 1989) as exudates and the bacterial exudate, succinoglycan has been well studied. They are long fibular structures that can from rigid bi and tri dimers (Ridout *et al.*, 1997) able to interact and bind with other colloids and form an important role in forming protective biofilms due to their negative charge. Inorganic particles may bind along the length of the fibrils in a pattern resembling a pearl necklace (Buffle *et al.*, 1998). It is expected that these NOM types will play an important role as they may interact with ENPs (Chen and Elimelech, 2007; Cumberland and Lead, 2009; Diegoli *et al.*, 2008; Domingos *et al.*, 2009b; Giasuddin *et al.*,

2007; Hyung *et al.*, 2007), and because of their known ability to transport trace metals and persistent organic pollutants (POPs) (Lead and Wilkinson, 2006).

There are no known natural occurrences of carbon nanotubes (CNTs), however, rare findings of fullerenes (C_{60}) have been found in geological rocks over two billion years old, in meteorites from the Sudbury impact, Ontario and in Russian Shungite rocks (Buseck, 2002; Kovalevski *et al.*, 2005). The formation mechanisms of these fullerenes are unknown and could be extraterrestrial, although it is possible they were created on entry to the earth's atmosphere. Giant fullerenes or carbon onions are shown in Figure 2.3 (b) extracted from geological rocks (Buseck, 2002).

2.1.2 Incidentally produced NPs

Many nanoparticles are produced unintentionally as byproducts, mostly from combustion processes such as diesel engines exhausts and coal-fired power stations (Lin *et al.*, 2007). Moreover, the formation of very small particles by homogenous nucleation, may occur in hot combustion gasses and in metallurgical processes including welding (Biswas and Wu, 2005; Borm *et al.*, 2006). It is well known that atmospheric particles of size fractions less than 10 μm (PM_{10}) and less than 2.5 μm ($PM_{2.5}$) adversely affect the respiratory and pulmonary systems in humans via inhalation (Soto *et al.*, 2005). More recently, ultrafine, $PM_{0.1}$ has been found to be the most harmful (Borm *et al.*, 2006), particularly to the respiratory system, as ultrafine particles can 1) penetrate deeper into the alveoli, 2) pass through the cell membrane and 3) cause inflammation from the production of reactive oxygen species. Although the combustion of diesel is considered to produce the highest number of ultrafine particulates, LPG, considered as a cleaner fuel, results in larger nanoparticle emissions than those of unleaded gasoline (Biswas

and Wu, 2005). It is estimated that 50,000 kg year^{-1} of nano-sized materials are being produced through these un-intended anthropogenic sources in this way (Borm *et al.*, 2006). These type of NPs can also be transported in the atmosphere over large distances in cloud formations and can be deposited onto the soil and water bodies and result in secondary contamination or other environmental effects (Biswas and Wu, 2005). Moreover, NPs have been created for thousands of years as the products of combustion and food cooking (RS/RAEng, 2004).

An example of using incidentally produced NPs to create new, manufactured NPs, was demonstrated recently by Dunens *et al.* (2009) from fly-ash, Figure 2.4 (a), a residue of burning of coal in power stations. Fly-ash contains a large amount of metallic components such as SiO_2, Al_2O_3, Fe_2O_3, TiO_2, CaO, MgO and K_2O 1μm to 100μm in size and there are many problems associated with it as a waste product (Savage and Diallo, 2005). Moreover, this waste product can be used to produce multi-walled carbon nanotubes (MWCNTs), as seen in Figure 2. 4, as a cheap material for the building industry (Dunens *et al.*, 2009). However, this material may well be hazardous due to its presence of toxic components such as cadmium, arsenic and uranium.

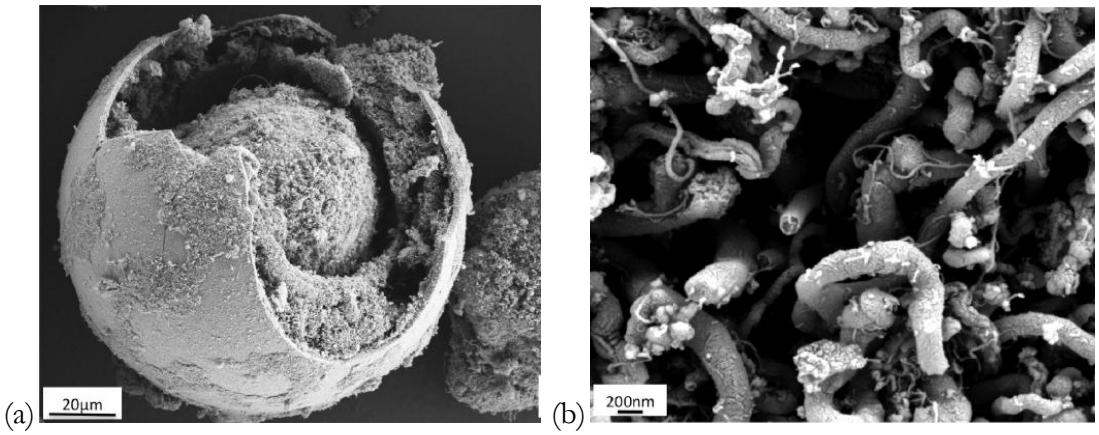

Figure 2. 4 SEM images of (a) 5 wt % Fe-Fly ash catalyst particle covered in MWNTs and carbon nanofibres; (b) is an enlarged image of the surface of the Fly-ash surface showing MWNTs intertwined within large CNFs on 2.5 wt % Fe loaded fly ash. Taken from Dunens *et al.,* (2009).

2.1.3 Intentionally produced NPs (manufactured NPs)

2.1.3.1 History of intentionally produced NPs

Nanoparticles have existed for centuries, where the word 'nano' comes from the Greek meaning dwarf (RS/RAEng, 2004). Decorations on ceramics found around the Mediterranean from as early as the IX century were produced from copper and silver salts which formed nanoparticle lustres beneath the glaze after heating to 600°C (Padovani *et al.*, 2003). Monks in the middle ages unwittingly made NPs in stained glass by heating various metals and metal salts with molten glass, which produced many different colours with high levels of transparency (Kerker, 1985; Link and El-Sayed, 2003). Gold and silver, in particular, were used and produced yellows, reds, violets and greens seen in the stained glass windows of churches and monasteries. Several centuries later scientists began this investigation in more detail. Michael Faraday first presented his lecture on '*Experimental relations of gold and other metals to light*' at the Royal Society in 1857 (Faraday, 1857). His experiments involved the thinning of gold leaf to less than 90 nm, to produce a translucent green colour on holding to the light and discovered that other colours could also be produced when the gold was subject to various conditions. The optical properties of silver nanoparticles were examined by Kerker, (1985) who used Mie theory to explain the absorption and scattering of light by finely divided particles. These observations can be attributed to size quantum effects of particles in the nanoscale due to a strong absorption in the spectrum providing the origin of the observed colour (Link and El-Sayed, 2003). More recently, scientists have reported many ways of producing aqueous suspensions of colloidal silver and gold in with varying sizes shapes and colours (An *et al.*, 2007; Ledwith *et al.*, 2007). A phenomena known as surface plasmon resonance (SPR), which is an interaction of the lightwaves on the surface of the particle (Link and El-Sayed, 2003; Miller and Lazarides, 2006), which is also responsible for NP colour and can be used to characterise the NP suspension

(Christian, 2009). Since the invention of the transmission electron microscope (TEM) in 1939 (Monthioux and Kuznetsov, 2006), observation has been possible at the nanoscale. Furthermore atomic force microscopy (AFM) (since 1986), has allowed height and manipulation of nano-sized particles (Gibson *et al.*, 2007).

Richard Feynman (1960), conceptualised the world of miniaturisation and the ability to scale down the entire Encyclopaedia Britannica onto the head of a pin (which has now been achieved (Corbett *et al.*, 2000)) and went on to discuss the practicalities of scaling down. In describing the potential to make nano robots and nano machines he further indicated that things simply do not scale down in proportion (Feynman, 1960). Further work on miniaturisation came in 1970s from the electronics industry, from a Japanese researcher, Norio Taniguchi, who in 1974, first coined the term 'nanotechnology' as the ability to engineer materials precisely at the nanometre level (RS/RAEng, 2004). The next revolution was the discovery of the fullerene (C_{60}), Figure 2.5(a), a spherical, football-shaped molecule consisting of 60 carbon atoms (Kroto *et al.*, 1985) which has subsequently received much attention. Identified in 1985, fullerenes were an additional allotrope of pure carbon to graphite and diamond (Ball, 2001; Buseck, 2002). Carbon nanotubes (CNTs), Figure 2.5(b) were synthesised and identified by Sumio Iijima in 1991 (Iijima, 1991). They are often described as rolled graphite or graphene (Buseck, 2002), which are likened to fullerenes joined end to end forming seamless tubes many 100s nm in length. CNTs can be single walled (SWCNT) or consist of more than one layer of carbon called multi-walled CNTs (MWCNT) (Aitken *et al.*, 2006). Inorganic NPs have increased in interest more recently as they have many uses and are discussed more fully in section 2.3. Illustrated in Figure 2.5(c) are of silica coated gold NPs and in Figure 2.5(d) are TEM image of silver nanoparticles.

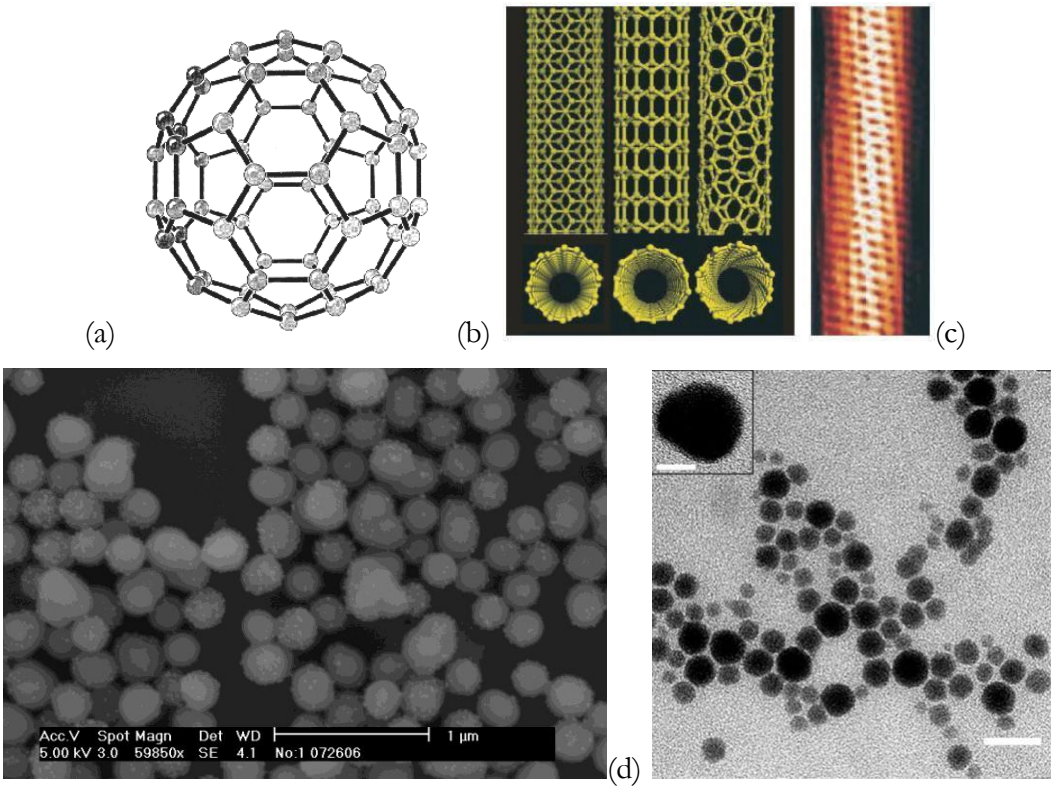

Figure 2.5(a) Schematic pictures of Fullerene C_{60} taken from http://www.godunov.com/Bucky/ and (b) Carbon nanotubes taken from www.ucd.ie/biophysics/cnt.html (c) SEM micrograph of Silica with gold NPs attached to surface taken from www.itg.uiuc.edu/exhibits/iotw/2006-09-05/ and (d) TEM micrograph of Silver NPs taken from www.sciencedaily.com/.../06/090601110403.htm.

2.1.3.2 Nanoparticle production and synthesis

Manufactured nanoparticles are produced by using either top down methods (lithography, grinding, ball milling etc) or by bottom up methods, via crystal growth of ions or atoms (see Figure 2.6). These processes can be controlled in such a way that many different types of structures are produced. The size range that holds so much interest is typically from 100 nm down to the atomic level (approximately 0.2 nm), because at just a few nm, nanoparticles show properties that are very different to those observed in the bulk. Decreasing the particle size, gives rise to an increased specific surface area, leading to better catalytic properties. At the small

scale, the dominance of quantum effects change the optical, magnetic or electrical properties of bulk material and are responsible to the main causes of change in NP behaviour (RS/RAEng, 2004).

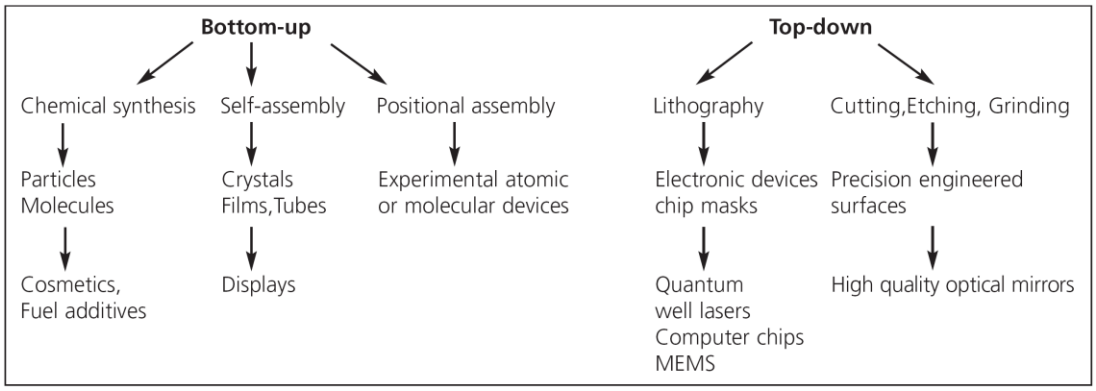

Figure 2.6 Routes of NP Manufacture illustrating top down or bottom up methods of NP synthesis. Taken from the Royal Society (2004).

Manufactured nanoparticles generally consist of a single-core, mixed-core or composite of inorganic metal, metal oxides or carbon. They can be embedded in materials such as glass or annealed onto surfaces (Kendall and Kosseva, 2005; Liz-Marzan and Lado-Tourino, 1996), depending on the required use. However, aqueous suspensions of metal nanoparticles often have an oxide (or oxy-hydroxide) layer formed on the outer surface (Loux and Savage, 2008) and may possess similar surface chemistries to other metal oxide NPs, but due to their small size may possess a larger number of metal atoms on the surface than in the bulk material (Christian *et al.*, 2008). Some of these types of metal oxide particles are charge stabilised, but uncharged or zero-valent particles may well be stabilised by other ways. Very often, NPs are coated with natural or synthetic organic polymers to improve stability sterically, for preventing aggregation or dissolving in aqueous, or to aid dispersion in creams and lotions in consumer products. NPs can also be engineered with additional components or surface modifications for specific purposes such as drug delivery. For example, in high sun protection factor (SPF) sunscreens

containing TiO_2 and ZnO NPs coatings provide functionability for anti-aggregation, even dispersal and are combined with anti-oxidants (e.g. carotene, Mn doping) to counteract the effects of reactive oxygen species (ROS) produced by the TiO_2 (Serpone *et al.*, 2007; Villalobos-Hernandez and Muller-Goymann, 2006).

Nanoparticle production can be achieved through wet chemistry synthesis such as forced hydrolysis and can yield fairly monodisperse suspensions. The methods for achieving monodisperse NPs are highly sensitive to the laboratory environments and more specifically, to temperature and acidity (Matijevic and Scheiner, 1978) and controlled NP growth through aging. Basic principles of NP wet synthesis begin with metal salts, such as ferric sulphate, ferric chloride or silver nitrate etc., being subjected to a chemical reduction or hydrolysis to produce a precipitation of metal solids or metal oxide clusters (Henglein and Giersig, 1999).

2.1.4 Special properties of nanoparticles

Manufactured nanoparticles hold a great deal of interest, because at a very small size, properties exist such as spatially contained electronic configuration related to quantum effects. These, which are not apparent in the bulk form, make NPs commercially interesting, but also a potential environmental risk. NPs are used in many different products including paints, washing machines, solar panels and cosmetics. This section looks at the importance of size, surface areas (SSA) and the light properties of surface plasmon resonance (SPR).

2.1.4.1 Size

The size (1-100nm) of nanoparticles has a significant impact on properties which fundamentally separates them from their bulk counterparts. The effect of size on a particle will alter the crystalline structure of the atoms and change the thermodynamic, electronic and magnetic properties (Auffan *et al.*, 2009). Any nanoparticle will have an exceptionally high specific surface area; however, the large surface area also means that NPs are likely to have a high surface energy and surface chemistry which is distinctly different from larger particles. Increased surface and small size also increases the catalytic activity due to the larger number of atoms available for surface reactivity and from the size-dependant alteration of the electronic structure (Auffan *et al.*, 2009). Moreover, as the particle gets smaller, e.g. below the 30-50 nm range, an increase in the band gap energy is seen, which is related to fluorescence wavelength (Auffan *et al.*, 2009). The properties of NPs appear to change distinctly, particularly around 30 nm qualitatively and quantitatively (Auffan *et al.*, 2009) and many properties are extremely enhanced below 10-15 nm. From an environmental health point of view, other things become important, such as increased toxicity. Biological interactions with NPs again differ from bulk materials, from those that are normally considered chemically benign, show toxicity as a NP e.g. TiO_2, possibly due to their ability to pass through the cell wall (Nel *et al.*, 2006), as one of a number of mechanisms.

2.1.4.2 Specific surface area

Nanoparticles, have a larger surface area per unit mass (i.e. specific surface area (SSA)) due to their small size (Nikolakis, 2006). SSA is the ratio of the external surface of the nanoparticles to the nanoparticle mass, expressed as metre squared per gram ($m^2 g^{-1}$) and can be measured by the Brunauer-Emmett-Teller (BET) method (Cai *et al.*, 1998; Madden and Hochella, 2005; Seo *et al.*,

2003) and calculated from displacement of N_2 gas over a powdered sample or microscopy. Reactivity is vastly increased as particles get smaller particularly as surface roughness (Pelley and Tufenkji, 2008) often further increases the SSA which enhances catalytic reactivity due to a larger number of reactive ions on the surface, than compared to a particle of greater mass (Auffan *et al.*, 2008). For example, when the size of iron 'ferragel' was decreased by Ponder *et al.* (2001), it became more efficient at promoting the oxidation of other metals (e.g. $Mn^{2+}_{(aq)}$). It was therefore postulated that the increased specific surface area resulted in an increase in the fraction of iron atoms on the particle surface, thereby creating a greater reductive capacity per gram. This surface effect was also reported by Auffan *et al.,* (2008) who measured by arsenic attachment to iron oxide which increased with decrease in particle size. This increased reactivity was found to be true even after surface area effect was normalised, this may be related to thermodynamics as a loss of surface energy (Auffan *et al.*, 2008), or changing electronic and geometric structure during the transition between the bulk and molecular structure of the iron oxide (Madden and Hochella, 2005). Not all substances behave in the same way probably due to differences in geometric shape and crystalinity and Ponder *et al.* (2001) found that silica supported ferragel had an SSA an order of magnitude higher than resin supported ferragel.

2.1.4.3 Surface plasmon resonance

The surface plasmon resonance (SPR) is the coherent oscillation of the conduction band electrons induced by interaction with an electromagnetic field (Hao and Schatz, 2004; Link and El-Sayed, 2003). The optical properties of NP suspensions of gold, silver and some other metals are due to their SPR and have been reviewed by Link and El-Sayed (2003). SPR absorbance spectras are sensitive to both NP size and surface chemistry, as SPR is absent for individual

atoms and bulk materials (Henglein and Giersig, 1999; Link and El-Sayed, 2003). Specific colours are generated which are size dependent and are produced as the electric field of an approaching light wave induces a polarization of the surface electrons. At the nanoparticle surface there is a net charge difference which creates a dipolar oscillation of all the electrons with the same phase and in turn creates a strong absorption in the spectrum associated with the observed colour. The metals, copper, silver and gold, show the strongest plasmon resonance and this is exhibited in the visible part of the electromagnetic spectrum (Link and El-Sayed, 2003). SPR occurs in particles from about 2 nm up to about 50 nm and is absent in much larger particles due to extinction of the resonated wavelength. The SPR can easily be measured from the spectral pattern using absorbance UV spectrophotometers, although interpretation in complex systems is difficult. Colours produced are associated with the size and shape of the primary particle, but may differ with particle type, aggregation state and with the coating ligand. This was demonstrated by Mock *et al.* (2002) who observed SPR in individual particles of different shapes and sizes, and noted that silver triangular NPs were absorbing at higher wavelengths. The presence of counter ions may also affect particle colour. While there is much discussion in the interpretation of SPRs they appear to be a good indication of the overall quality of nanoparticle when assessing nanoparticle synthesis (Henglein and Giersig, 1999).

2.1.5 Particle stability and aggregation

Particles in suspensions move and collide (collision factor) with each other because of 'Brownian motion' and are kept apart by strongly opposing surface charges (electro-static) which may be provided by the particle's own charge or by the surface coating ligand. If weak van der Waals attractive forces are dominant then particles coagulate (Stumm and Morgan, 1996). This may lead to coalescence of a few particles (agglomeration) or complete to a more

permanent aggregated state. The mechanism of aggregation is classically described in the literature as either homo- or hetero aggregation, i.e. that it will combine with itself or other with other chemicals (Buffle *et al.*, 1998). Aggregation is also described kinetically, so-called diffusion limited (DLA) and reaction-limited aggregation (RLA) (Leppard, 1992). In DLA, small colloids coagulate much faster than larger ones, producing loose aggregates with low fractal dimensions. With RLA, dense aggregates are produced from interactions between two colloids resulting in high fractal dimensions (Buffle and Leppard, 1995b) and occurs when there is negligible repulsive force between colloids (Amal *et al.*, 1990; Leppard, 1992).

The collision efficiency factor can be predicted using DLVO theory. DLVO theory is a mathematical model that was developed by two independent research groups circa, 1948, **D**erjaguin and **L**andau, and **V**erwey and **O**verbeek, with the name being taken from their initials (Derjaguin and Landau, 1941; Verwey, 1947). It attempts to calculate the interactions between particles in close proximity (Stumm and Morgan, 1996) by considering the effects of electrostatic interactions (attraction and repulsion due to the presence of two charged bodies) and van der Waals/ London forces (Balnois *et al.*, 2007). It is based on the assumption that the forces between surfaces or colloidal particles can be regarded as the sum of two forces. In the case of two similar particles, the particle charges will be of the same sign; therefore the forces due to these charges will be identical and hence repulsive, tending to stabilise the particle suspension.

If the particles get close enough together because the energy of the particles is sufficient to overcome the electrostatic repulsion, shorter range van der Waals/ London forces become

dominant and cause the particles to attach to each other. DLVO theory enables the electrostatic and van der Waals forces to be estimated quantitatively for certain geometries e.g.

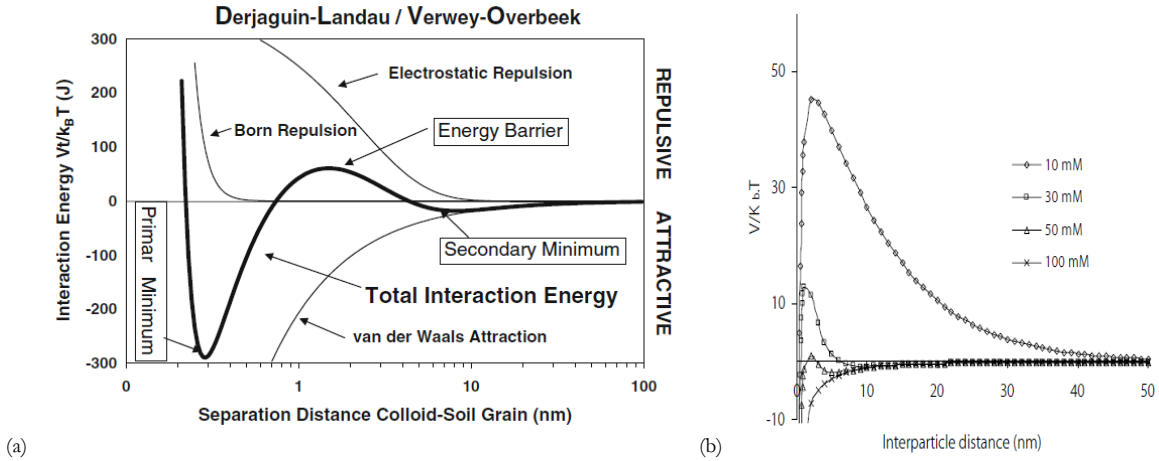

Figure 2. 7 (a) DLVO model for total interaction energies between a spherical NP and a flat collector (Christian *et al.*, 2008) (b) is the prediction of 65nm haematite particle interactions with increasing ionic strength ($NaCl^-$) at pH 5.7 (He *et al.*, 2008)

Figure 2.7 shows the energy associated with the repulsive electrostatic interactions, the energy associated with the attractive van der Waals interactions and the sum of these energies. It is predicted by DLVO theory that, for low ionic strength solutions (figure 2.7 (a)), the distance at which the effects of the charged surfaces is felt is large enough that there remains a sufficient energy barrier to maintain stability, at least in the short term, but as the ionic strength increases (figure 2.7b), this energy barrier becomes smaller eventually disappearing, and the suspension is then predicted to be very unstable, the attachment being within the 'primary energy minimum', and effectively irreversible. In some cases there develops a secondary energy minimum (figure 2.7(a)): when attachment occurs in this regime, it is reversible by mechanical action or by changing the ionic strength (or pH) of the solution.

In DLVO theory, the total interaction energy (V_T) between two surfaces can be calculated by

$$V_T = V_A + V_R,$$

Eq.2.1

where V_A and V_R are the energies (J) associated with the attractive van der Waals and the repulsive electrostatic forces. For identical spherical particles, V_A can be given by:

$$V_A(h) = -\frac{A}{6}\left[\frac{2R^2}{h^2+4Rh} + \frac{2R^2}{(h+2R)^2} + ln\left(1 - \frac{4R^2}{(h+2R)^2}\right)\right]$$

Eq.2.2

and V_R can be estimated using (Baalousha *et al.*, 2009):

$$V_R(h) = 32\pi\epsilon R\left(\frac{kT}{ze}\right)^2 \gamma^2 exp(-\kappa h)$$

Eq.2.3

where ε is the permittivity of the medium (F m^{-1}); R is the particle radius (m); γ is the surface potential (dimensionless); k is the Boltzmann Constant (J K^{-1}); T is the absolute temperature (Kelvin); h is the surface separation between particles (m); e is the electron charge; A is the 'Hamaker Constant', (J); κ is the inverse-Debye Huckel screening length (m^{-1}). κ can be calculated thus for electrolyte solutions containing a number of salts:

$$\kappa = \sqrt{\frac{e^2 \Sigma n_i z_i^2}{\epsilon kT}}$$

Eq.2.4

where, *n,* is the number concentration of ion, *i,* and z, is the valency of the ions.

In nanoparticles, unless the particles possess a strong static charge, aggregation is prevalent and clumping and sedimentation occurs. Aggregation is prevented by increased particle charge not allowing van der Waal's to act (standard DLVO). Where particle charge is weak, prevention of aggregation, which again is affected by suspension pH or ionic strength, requires further stabilisation, like adding a surface coating or ligand providing a surface charge through steric stabilisation and the formation of a double electrical layer. This leads to the deliberate modification of surface functionisation in ENPs, to change surface chemistry often in the form of organic ligands (Christian *et al.*, 2008).

The pH at which the net charge of a mineral's (or NP's) surface is neutral is called the point of zero charge (pzc), referred to as the pH_{pzc}. This is the pH value where the net surface charge is neutral. At this pH particle aggregation will result due to the lack of surface charge repulsion. Understanding NP stabilisation and aggregation as influenced by particle charge and the presence of ligands is an important aspect in predicting environmental ENP fate and behaviour.

2.2 Types and applications of manufactured NPs

The NP properties mentioned above have found many applications in various different product types. Manufactured nanoparticle have in recent years become available in products from paints to cosmetics and car tyres to self cleaning windows and printing inks to cosmetics (Aitken *et al.*, 2006; Schmid and Riediker, 2008). The most highly exploited nanoparticles are those of silver (Ag), titanium dioxide (TiO_2) and zinc oxide (ZnO), carbon fullerenes (C_{60}), gold (Au), the iron oxides Fe_2O_3 (and its many other forms), cerium oxide CeO, iron (Fe) and quantum dots (e.g. cadmium selenide, CdSe). They are, and many others, will become increasingly more important

economically as the electronic industry becomes dependent on nanotechnology for miniaturisation.

A scoping study was undertaken by DEFRA in 2005 which identified the major players in the nanotech industry. These primary areas represent the intersection of several important variables including high market value, high social priority, and availability of relevant materials. Several key current nanotechnology R&D areas are summarised below (DEFRA, 2005b):

- **Human Health:** drug delivery, imaging, cancer therapeutics
- **Defence:** energetic materials, lightweight armour composites
- **Energy:** hydrogen storage, improved efficiency, catalysis
- **Agriculture:** increased crop yields, secure packaging, chemical/biological detection
- **Environment:** water filtration, reduced air emissions, remediation

2.2.1 Applications

2.2.1.1 Metal NPs

One of the most prevalent NP types in production today is silver (AgNPs) To date, silver is used in more consumer products than any other nanomaterial (Luoma, 2008). Ag NPs, because of their antimicrobial properties, have wide spread applications in hospitals, such as medical bandages and dressings for use in surgery and in dressings for treating burns, as they can be embedded in various materials and textiles (Duran *et al.*, 2007). Colloidal silver has also been marketed as a putative health tonic (Ohbo *et al.*, 1996; White *et al.*, 2003), however, there are reports that ingesting this material (and silver nitrate) has led to conditions such as argyria

(greying of skin pigment), and adverse;y impact the intestinal flora, although this is largely untested. Gold is also used in nano medicine for drug delivery as gold NPs can target cancer cells (Connor *et al.*, 2005; Malam *et al.*, 2009).

Uses of Ag NPs in domestic products are becoming more common in washing machines, fridges (Maneerung *et al.*, 2008) and food containers to reduce surface mould growths. Ag NPs embedded into socks, to reduce odours, has been shown to leach silver into the environment from washing (Benn and Westerhoff, 2008; Geranio *et al.*, 2009). Likewise, silver may leach from anti-fouling membranes, when used as an application in water purification (Zodrow *et al.*, 2009).

As environmental sensors, gold and silver have shown potential due to their optical responses when in contact with environmental contaminants (Rickerby and Morrison, 2007) such as silver NPs which can be used to detect herbicide (Dubasa and Pimpan, 2008). For applications in treatment of contaminated groundwater, zero-valent iron can be used to form underground reactive barriers (Bigg and Judd, 2000; Cantrell *et al.*, 1995; Gu *et al.*, 2002; Ponder *et al.*, 2001; Scherer *et al.*, 2000; Zhang, 2003). For catalytic breakdown of persistent organic pollutants (POPs) to methane, hydrogen gas and carbon dioxide (Li *et al.*, 2006), although an oxygen depletion has been reported (Zhang, 2003).

2.2.1.2 Metal oxides

Iron oxide and TiO_2 NPs as examples of metal oxide NPs, have many applications, for example, as pigments in paints (Aitken *et al.*, 2006), food (Lomer *et al.*, 2000) and cosmetics (EWG, 2009).

Different crystal structures of metal oxide NPs often show different reactivity properties, such as, rutile and anatase forms of TiO_2 (Melnyk *et al.*, 2005) and haematite and magnetite in iron oxide, among others. In medicine, metal oxide NPs (and gold) have been highly researched as potential drug delivery agents in treating cancer (El-Ansary and Al-Daihan, 2009; Thevenot *et al.*, 2008), as have magnetic iron oxides in MRI imaging (Lewinski *et al.*, 2008). Wide band-gap photocatalysts, such as TiO_2 (Melnyk *et al.*, 2005) and ZnO NPs, are effective ingredients in transparent sun protection creams (Borm *et al.*, 2006; Serpone *et al.*, 2007; Tan *et al.*, 1996; Villalobos-Hernandez and Muller-Goymann, 2006), solar panel technology (Koparde and Cummings, 2007; Mor *et al.*, 2006), and self-cleaning glass able to catalyse organic matter (Hyett *et al.*, 2006). Cerium oxide (CeO) NPs, are currently used as additives to improve diesel fuel efficiency by 11.4% (Oxonica, 2009; Thill *et al.*, 2006). The emissions of which have not been environmentally tested, but CeO NPs have proven to be toxic (Thill *et al.*, 2006).

2.2.1.3 Carbon

Carbon nanoparticles (C_{60}, CNTs and carbon black) are commercially of interest, as mentioned previously, however, fullerenes and CNTs are very toxic, hydrophobic and aggregate easily. The electronics industry has largely benefited from carbon-based NPs in flat panel displays and computing. CNTs and fullerenes can be an ingredient for polymers and resins adding strength and flexibility (Mueller and Nowack, 2008). Carbon NPs are also used in the printing industry as a very precise mechanism for getting ink onto paper. Historically, carbon black (CB), not previously considered a nanomaterials (NM) (Gottschalk *et al.*, 2009), has been in use longer than fullerenes, as an industrial form of soot used in various applications such as filler in rubber compounds, primarily in automobile tyres and vulcanising. Carbon black, typically has a particle

size range between 20 and 300 nm indicating that a proportion exists in the nanoscale (Nowack and Bucheli, 2007). Pollution from these materials is likely to be from degradation of the product or from combustion.

2.2.2 International economics of manufactured NPs

Nanotechnology is anticipated to become a trillion dollar industry by the 2015 (Aitken *et al.*, 2006). Indeed, despite the current economic climate, millions of pounds, euros, dollars etc are being pumped into research R&D in contrast, a vastly smaller amount is directed to studying the risks that nanoparticles present to the environment. It was found that in 2005, 52 companies were involved in manufacturing, processing and/or using NMs in the UK. At that time, the UK NM manufacturing industry was still very much at the development stage. In 2005, only 19 companies could be identified as NM manufacturers. Another 11 were processing NMs and 22 were using or developing applications for NMs (Aitken *et al.*, 2006). Internationally, the nanotechnology industry is dominated by US companies (49%), followed by Europe (30%), and the rest of the world (21%). UK NM industry contributes to around 9% of the global nanotechnology sector. In view of the large number of emerging new materials and applications, this situation is likely to change in the near future (DEFRA, 2005b). Within the European Union, the UK accounts for nearly one-third of the market (Aitken *et al.*, 2006).

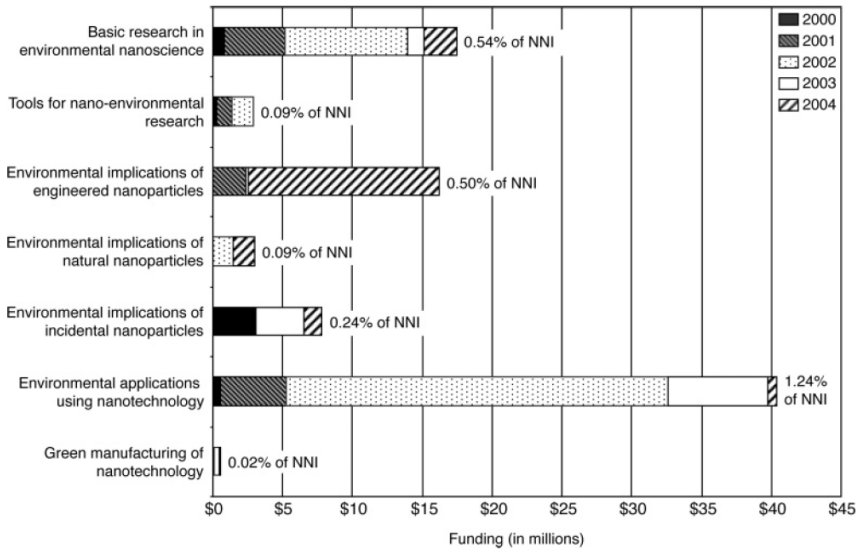

Figure 2.8 Estimated NNI environmental research, 2000-2004. Taken from Dunphy-Guzman et al (2006)

Figure 2.8 shows the National Nanotechnology Initiative (NNI) US government spending on nanotechnology and the environment, estimated by Dunphy-Guzman *et al.,* (2006), for the years between 2000-2004. The bulk of the funding identified was directed towards "environmental applications using nanotechnology". With the next most prominent category of funding recognised as, "basic research in environmental nanoscience". They also estimated that 2.7 % of US federal grant money, $88.2 million, from a total of $3.26 billion, was allocated to environmental nanotechnology by the NNI over the observational time period (Dunphy Guzman *et al.*, 2006b). This indicates the scale of the investment into nanotechnology and the proportion of funding allocated into research of the consequences of this industry (Arnall and Parr, 2005).

With this large growth and investment into nanoparticles, there is ground for concern that the industrial use of nanoparticles is running ahead of research into the environmental impact of nanoparticles. In order to be able to assess the potential impact of nanoparticles a clearer understanding of environmental risk is required. However, only if risk can be shown to be

sufficiently high can industry and government officials be encouraged to take note. To reach such level of awareness requires a more detailed understanding of environmental risk and its constituents.

2.3 Nanoparticles and the environment

The rising use of manufactured nanoparticles increases the likelihood that nanoparticles will enter the environment. Research has indicated that materials considered benign in the bulk form may show toxic or adverse effects when nano-sized (Adams *et al.*, 2006; Grassian *et al.*, 2007). For instance, TiO_2 NPs are toxic to bacteria (Adams *et al.*, 2006) whereas bulk titanium is routinely used in human implants, and macro titania powders are used in food and paint due to their biocompatibility. A similar point could be made in relation to the toxicity of silver NPs, and the use of the bulk metal in dental amalgams. With the consensus that some NPs are cytotoxic they are also likely be hazardous to environmental and ecological health, depending on bioavailability. Therefore environmental risk assessment analysis is vital in order to be able to understand the environmental impact of NPs. Independent assessments of the NP exposure and the NP hazard need to be made and how this may change under different conditions. The combination of these two would then provide an overall indication of environmental NP risk. Where:

$$\text{Risk} = \text{Exposure} \times \text{Hazard}$$

In order to define the overall risk posed by ENPs to the environment both exposures as well as biological hazards must be evaluated (CBEN, 2010). The following section applies the environmental risk model to nanoparticles in the aquatic environment, and in doing so describes

current research knowledge as well as areas where more research is required. The three sub-sections that follow explore exposure, hazard and risk in turn.

2.3.1 Exposure

The most widely produced NPs are likely to be TiO_2 and silver NPs, because of their antibacterial and photocatalytic properties. As the volume of production increases, so too does the likelihood of exposure (Luoma, 2008). The chance of exposure will be greater close to the manufacturer at beginning of the NP lifecycle, or alternatively at the end of the NP product lifecycle from landfill leaching or where sewage treatment waste is disposed. In other situations, exposure may occur directly from the injection of NPs into contaminated ground waters (Owen and Depledge, 2005; Zhang, 2003). Yet whilst the presence of high concentrations of ENPs in the environment is a major concern, it may not necessarily lead to higher exposure. For instance, aggregation may occur. This scenario is, however, currently under-researched. The effects of potential NP surface morphological transformations prior to reaching a receptor such as an algae cell are also unknown (Alvarez *et al.*, 2009). Finally, not all organisms or humans may necessarily be exposed to released ENPs, as this will depend on dispersal and the existence of potential pathway routes.

2.3.1.1 Pathways of nanoparticles to the environment

In considering the potential for NP exposure it is necessary to consider the different routes or pathways through which NPs can enter the aquatic environment. These pathways could be through soil, water, sediment or air (Blaser *et al.*, 2008; Gottschalk *et al.*, 2009). For example, silver NPs products may release Ag^+ ions which could be transported though waste waters and sewage from textiles and washing machines (Blaser *et al.*, 2008; Gottschalk *et al.*, 2009; Mueller

and Nowack, 2008) whereas CNTs can become airborne after incineration (Mueller and Nowack 2008).

Figure 2.9 considers the potential pathways of silver NPs to the aquatic environment that may occur during the manufacturing and life-time of a product containing silver NPs. In industrial processes this may include, the release of NPs via equipment rinsings that had previously contained NPs, and discharges, leakages or spills resulting in wastewater effluents containing NPs even if the initial rinses are collected for proper disposal (Biswas and Wu, 2005; Mueller and Nowack, 2008).

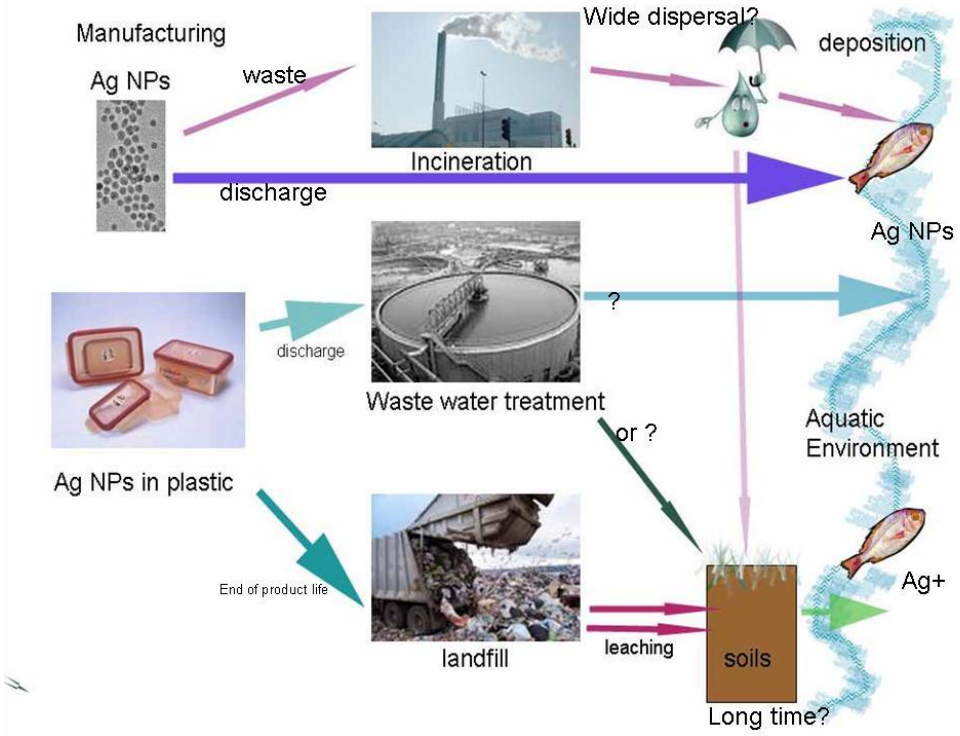

Figure 2. 9 Hypothetical pathways of a product containing silver nanoparticles from manufacture to end of life, and how they might reach the aquatic environment.

Recent studies have shown the processes through which NPs can enter aquatic systems. Kaegi *et al.* (2008), for example, demonstrated how NPs can be naturally weathered from painted exterior walls into storm drains. Focusing on waste water treatment works, both Kiser *et al.* (2009) and Jarvie *et al.* (2009) have shown that NPs are capable of passing through primary treatment stages relatively unaltered. An additional consideration is international variation in waste management practices. For example, in Europe the majority of sewage sludge is spread onto agricultural land, whereas in the UK this is only around 60% (Jarvie *et al.*, 2009). Another disposal method is the incineration of sewage sludge, which enables the release of airborne NPs (Mueller and Nowack, 2008). In atmospheric systems deposition of released airborne NPs is likely but the concentration of particles will be low due to high dispersal rates.

2.3.1.2 Fate and behaviour of manufactured NPs in the aquatic system.

Understanding the eventual fate and behaviour of NPs upon reaching the environment is critical as this will determine the extent to which organisms are exposed. The precise fate of NPs is uncertain because of different matrixes found in surface waters (Nel *et al.*, 2006). Previous work has established that HS can bind and carry trace metals, solutes and organic pollutants (POPs) suggesting that the fate of ENPs will depend on their behaviour when in contact with natural HS and other colloids (Ross and Sherrell, 1999; Tipping and Higgins, 1982; Tipping *et al.*, 2002). Synergistic toxic effects may also occur when NPs are present in chemical aqueous mixtures (Alvarez *et al.*, 2009; Handy *et al.*, 2008c) leading to uncertainties, thus requiring more research in this field.

The diagram presented in Figure 2. 10, considers the movement of exposure and modifications of released manufacture NPs. In type 1, they pass through the environment unchanged, in type 2 there are modifications in association with NOM. In type three, aggregation occurs and in type 4, there are dissolution of ions, and reformation into other chemicals (Alvarez *et al.*, 2009). The presence of organic ligands may provide stabilisation by attaching to the particle's surface (electro-steric) (Navarro *et al.*, 2008a) or destabilisation by bridging with HS and fullerenes (Chen and Elimelech, 2006; Chen and Elimelech, 2007).

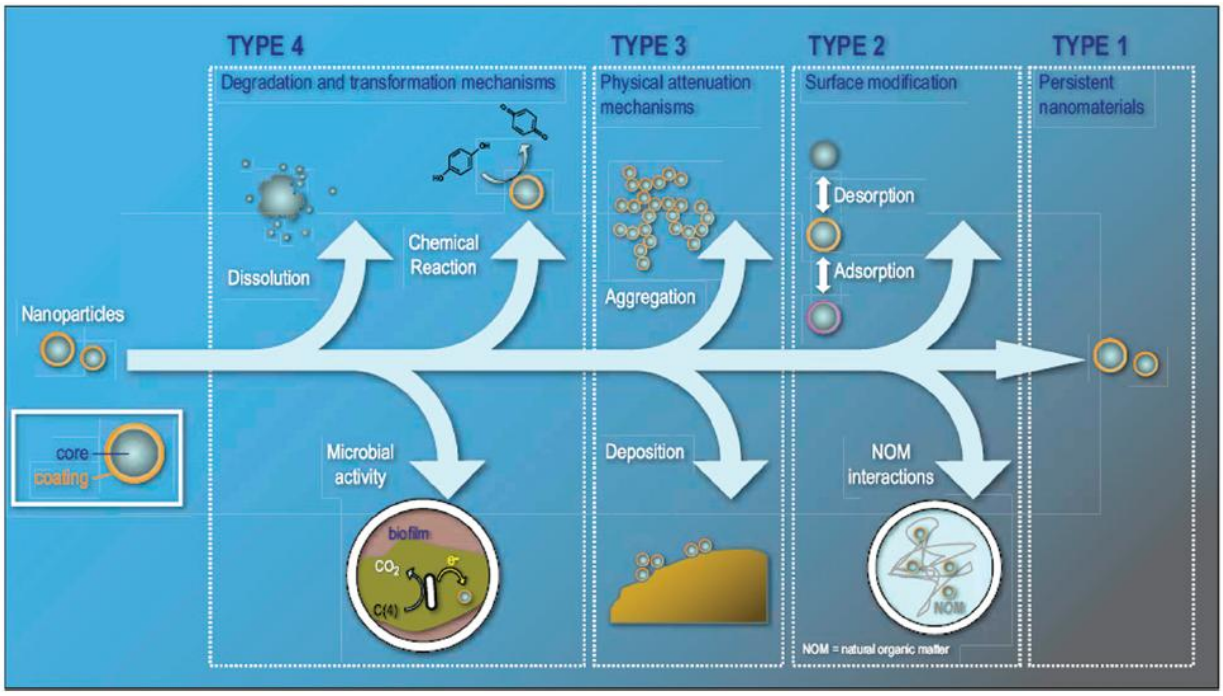

Figure 2. 10 Possible nanoparticle modifications in the environment for four scenarios types; From NPs unchanged and persistent in type one to complete change in type four. Taken from Alvarez *et al.,* (2009)

Experimentally, mixing NP with natural HS has already been conducted by a few researchers. For example, Hyung *et al.* (2007) found that carbon nanotubes showed improved dispersion and stability in the presence of HS, probably by forming a surface layer which may be tightly bound as in a film, or through various functional groups resulting in loops. Domingos *et al.* (2009b)

showed that TiO_2 NPs were generally sterically stabilised in the presence of fulvic acids, resulting in some disaggregation of small nanoparticle aggregates. It was possible for zerovalent iron (NZVI) to bind to humic acid and thus be removed from suspension containing 20 mg L^{-1} HA. Further testing from bond measurements revealed that a complex chemical reaction occurred between NZVI and HA (Giasuddin *et al.*, 2007). Humic acid has also been shown to have a significant effect on the structure of gold aggregates and evidence has been found that SRHA are able to substitute and/or over-coat the citrate and acrylate anions on the gold nanoparticles surface (Diegoli *et al.*, 2008).

In the natural environment, the fate, mobility, and bioavailability of nano-TiO_2 will be greatly influenced by particle size and charge. Domingos *et al.,* (2009b), found that at all pH values, sorption of fulvic acids on to TiO_2 NPs resulted in steric stabilisation and some disaggregation of small NP aggregates. These findings suggest that in the natural aquatic environment, the dispersion and mobility of TiO_2 nanoparticles might occur to a much greater extent than predicted in the absence of natural organics (Domingos *et al.*, 2009b).

2.3.1.3 Detection and analysis

Presently, environmental detection and identification of nanoparticles is impossible in un-amended samples (Tiede *et al.*, 2009). This is because of the large background of natural NPs and the difficulty in distinguishing between manufactured NP and other sources of the same material. In principle, it may be possible to quantify NPs in the environment however, identification using isotopic, fluorescent or other potential signatures has not yet been found. The current research emphasis is towards a multi-method analytical approach; however, this

requires further method development. In all environments, the ability to detect concentrations of NPs at natural levels is an immediate research priority to provide baseline data on which to benchmark further studies (Ju-Nam and Lead, 2008). These methods will be essential for characterisation when conducting hazard and toxicity studies. Furthermore, for universal comparisons between research groups, there is need for the development and use of NP reference materials to assist in knowledge building about NP fate and behaviour.

2.3.2 Hazard and toxicity of ENPs

Nanoparticles have shown adverse effects on cells and aquatic organisms. These effects have been extensively reviewed (Baun *et al.*, 2008; Handy *et al.*, 2008b). The precise mechanism or particular characteristic of NPs that causes the toxicity is not clear. Nanoparticle shape, crystal structure, size, surface area and catalytic properties as well as concentration could all be responsible as all have shown positive results in terms of toxicity. It is likely though, that NP size is a key factor in uptake as very small particles are able to pass through cell membranes via phagocytosis causing the production of reactive oxygen species (ROS), which causes oxidative stress (OS) (Jeng and Swanson, 2006; Long *et al.*, 2006; Oberdorster *et al.*, 2005; Stone *et al.*, 1994).

In Figure 2.11, the possible mechanisms for cytotoxicity are shown, including the production of ROS, showing interactions with the surface chemistry of the nanoparticles. Under conditions of excess ROS production, oxidative stress occurs in cells. This is essentially referred to as a state in which glutathione (a produced antioxidant) is depleted while oxidized glutathione accumulates (Nel *et al.*, 2006) e.g. by creating free oxygen radicals (O_2•). The outcome of this

can result in damage to DNA. For example, modelled carbon nanotubes have been shown to bind to DNA (Zhao *et al.*, 2005). This could either induce cancerous cells from cellular nucleotide mutations or ultimately cell death either from cell membrane rupture or mitochondrial damage (Li *et al.*, 2003).

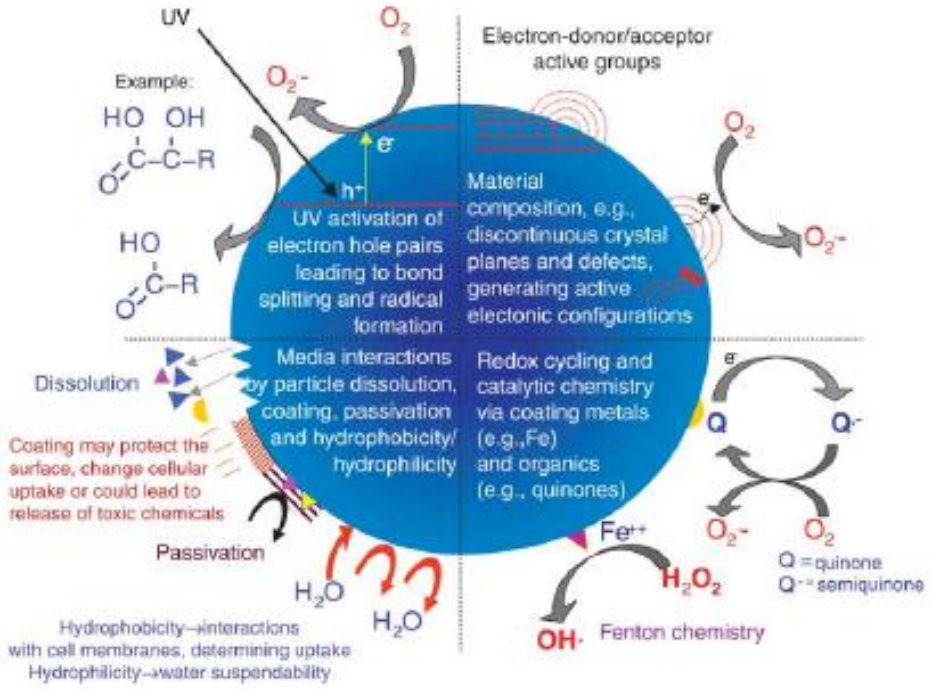

Figure 2.11. Possible mechanisms by which nanomaterials interact with biological tissue. Examples illustrate the importance of material composition, electronic structure, bonded surface species (e.g., metal-containing), surface coatings (active or passive), and solubility, including the contribution of surface species and coatings and interactions with other environmental factors (e.g. UV activation). Taken from Nel et al. (2006).

Obersdorster (2004), conducted a study looking at the effect of fullerenes (suspended in Tetrahydrofuran (THF)) on largemouth bass and found oxidative stress in the brain and gills with increased aggressive behaviour compared to the control tanks. However, questions were raised in the literature on the actual toxicity of the C60, since THF (and perhaps its degradation products) used to stabilise the particles, could have attributed to the oxidative stress. Henry et al

(2007) demonstrated that toxicity in zebra fish, measured by gene expression, exposed to C60 did not occur with the pure substance, but could have resulted from products generated by the THF vehicle. Additionally, work in cytotoxicity has demonstrated that cell wall damage can occur through other mechanisms such as cell pitting (Choi et al., 2008; Thevenot et al., 2008).

Literature investigating the toxicity of silver NPs has been summarised in Table 2-1 . The table reveals that at the cellular level the concentration of silver required to kill *E.coli* bacteria ranged between 50-75 μg mL^{-1} (ppm) (Morones *et al.*, 2005; Sondi and Salopek-Sondi, 2004; Yoon *et al.*, 2007) regardless of NP size and capping agent used. Other bacteria tested appeared to be more or less sensitive and some species were still viable in the presence of 65 nm silver NPs, however, biofilms were affected (Fabrega *et al.*, 2009b). The test with *E. coli* by Choi and Hu (2008), found that these levels were much reduced when working with nanoparticles less than 21 nm capped in PVP. However, lung cells proved to be very sensitive with an EC_{50} of 1 μg mL^{-1} for 30 nm particles (Soto *et al.*, 2005). When compared to silver nitrate (Ag^{+}) Navarro *et al.,* (2008b) found that lower silver concentrations were needed for NPs than for ions to have the same inhibitory effect on algae photosynthesis. Ag NPs did not induce ROS in trout (Farkas *et al.*, 2010), but the associated mitochondria, revealed an EC_{50} of 1.1 mg L^{-1}. In summary Table 2-1 demonstrates high levels of different toxicity responses to Ag NPs within recent research and that test parameters such as the EC_{50}, results can be up to a magnitude in difference in concentration. A determination of ROS for indication of oxidative stress is often made, however as Choi and Hu (2008) pointed out stress can be caused by other environmental factors. Therefore, results from multiple tests are also important when assessing Ag NPs toxicity.

Table 2-1 literature survey of Silver NPs toxicity data

Test Organism	Particle characteristics	Effects	Reference
Escherichia coli	12.3 ± 4.2 nm SSA 158 m^2 g^{-1}. Ag NPs capped with Daxad 19, washed, freeze dried and used in agar.	Damaged cell by pitting of cell wall. More effective biocide on agar than in suspension. A concentration of 50–60 μg cm^{-3} caused 100% inhibition of bacterial growth on agar compared to EC_{50} 100 μg cm^{-3} when grown in media.	(Sondi and Salopek-Sondi, 2004)
Escherichia coli, *Bacillus subtilis*	40 nm (range 25-65 nm) Commercial no further characterisation	B. subtilis (32 μg mL^{-1}) was more sensitive than E. coli (58 μg mL^{-1}) for 90% antimicrobial efficiency. 100 nm Cu NPs were more toxic to *B. subtilis* (28 μg mL^{-1}) and *E. coli* (33 μg mL^{-1})	(Yoon *et al.*, 2007)
E coli *V cholera* *P aeruginosa* *S. typhus*	16 ± 8 nm conc ranging from 1-100 ug ml^{-1} Ag NPs inside carbon matrix suspended in water	Bactericidal effect is size dependant. all NPs smaller than 10 nm by membrane attachment and dysfunctional permeability and respiration 75 ug ml^{-1} killed all microorganisms Can penetrate the bacteria and damage DNA NPs release Ag^+ ions to further enhance toxicity.	(Morones *et al.*, 2005)
Escherichia coli	9 ± 5 nm , 15 ± 9 nm 14± 6 nm, 12 ± 4 nm 21±14 nm (made in house capped in PVP)	EC_{50} were Ag NPs 0.14 mg/L, Ag colloids 0.25 mg/L, Ag ions 0.27 mg/L Ag NPs were more toxic to nitrifying bacteria than Ag^+ ions at the same Ag $conc^n$. Particles less than 5 nm found to penetrate cell membrane.	(Choi and Hu, 2008)
Pseudomonas putida	65 ± 30 nm SSA 2.4 m^2g^{-1} in citrate and SRFA	Looked at cell uptake and effect on biofilms. Cell viability was unchanged in the presence of AgNPs. Biofilms were notably damaged by sloughing off. Ag NPs were observed to be in or on the bacteria's surface.	(Fabrega *et al.*, 2009b)
Chlamydomonas reinhardtii	40nm (10-200nm) Aggregates 1200 nm Carbonate coated Ag NPs Ag^+, Ag NPs, $AgNO_3$ and cysteine	1-5 hour exposures measured effect on photosynthetic yield. EC_{50}- $AgNO_3$ 184-188 nM(1-2 hr), Ag NO_3 Cystine 200 nM (1hr), Ag NPs 829-3300 nM (1-5 hr) (as total Ag). EC50-Ag NO_3 Cyst 57-61 nM (1hr), Ag NPs 8-33 nM (1-5 hr) (as free Ag)	(Navarro *et al.*, 2008b)
Lung cells	30 nm 100-1000nm aggregates	EC_{50} = 1 ug/mL silver was the most toxic compared to other NPS test and was more toxic than asbestos.	(Soto *et al.*, 2005)
Rainbow trout	>10nm AgNPs 80nm AgNPs + DOC, 5-10nm AuNP 100nm AuNPs + DOC Ag , Au with citrate, media and/or DOC	Ag did not induce ROS, Gold (Au^+ and Au NPs) increased ROS production with AuNPs more potent. Ag NPs more toxic (mitochondria) than Ag^+, (EC_{50} = Ag^+, 2.5, Ag NPs 1.1, AgNPs DOC, 2.6 mg L^{-1}) Gold (Au+, Au NPs) did not show toxicity to mitochondria or cell membranes. DOC did not influence results	(Farkas *et al.*, 2010)

Toxicity data for metal oxides is tabulated in Table 2-2 (TiO_2 studies are further covered in chapter 4). For these NPs a wider range of test organisms and greater variation in test results compared to Ag NPs can be observed. Results tend to be confusing and trends difficult to establish from the dataset. For example, in research that exposed *Daphnia magna* to a range of TiO_2 NP sizes and crystal structures, toxicity levels ranged from 100% mortality with TiO_2 NPs less than 200 nm at 10 mg L^{-1} with the lowest effective concentration (LC_{50}) of 5.5 mg L^{-1} (Lovern and Klaper, 2006). By way of contrast, in a similar exposure to *Daphnia*, there was no effective calculable concentration for 25 nm NPs (Hund-Rinke and Simon, 2006). The differences in results could be due to presence of THF, formation of aggregates or the effect of washing the NPs.

For human cells, data exists within the same magnitude, for example, iron oxide NPs affected mesothelioma cells with 3.75 ppm of 50 nm NPs causing 100% death (Brunner *et al.*, 2006) to lung cells with an EC_{50} of 10 ppm with 20 and 60 nm NPs (Soto *et al.*, 2005). This data can be compared to that of Sayes *et al.* (2006) where 10 nm titania anatase particles gave an LC_{50} 3.6 ppm with human cells.

Generally when comparing the literature in this way, discrepancies and gaps are seen with some reports incomparable to others due to a lack of NP characterisation, reference material and similarity of comparable tests. Most studies did report concentration effects but certainly, other factors are at play. It is therefore impossible to establish the effects of NP size, capping agent, SSA or whether free ions were responsible for toxicity. Mechanisms for NP uptake and toxicity are suggested such as NPs incorporation into vesicles (Brunner *et al.*, 2006; Limbach *et al.*, 2007) or through cell wall pitting (Choi *et al.*, 2008).

Table 2-2 literature summary of toxicity of metal oxides NPs

Organism	Particle characteristics	Effects	Reference
E. coli *B. subtilis*	66nm, 950 nm 44 μm TiO_2 (mixture rutile and anatase and pure anatase), 14 nm, 930 nm, 60 μm SiO_2, 67nm, 820 nm 44 μm ZnO	Size of particles different from that advertised. Light intensity modulates the toxicity of TiO_2, but not ZnO or SiO_2 SiO_2 least toxic. ZnO most toxic (10 ppm 90% Growth reduction fore *B. Subtilis*) *B subtilis* more sensitive to toxicity than E.coli to all NPs 90% growth reduction averaged from 1000 ppm to 5000 ppm for all particles	(Adams *et al.*, 2006)
Lung cells	40 nm (5-100nm) TiO_2 anatase 20-60 nm (5-15 nm dia.) TiO_2 rutile 20 nm (5-40 nm) TiO_2 anatase 50 (5-140 nm) Fe_2O_3	EC_{50} 10 ug/mL about the same for both types of particles EC_{50} 5.5 ug/mL Fe_2O_3	(Soto *et al.*, 2005)
Dermal and lung epithelial cells (human)	10 nm TiO_2 anatase NPs 3 nm TiO_2 anatase and rutile NPs 5 nm TiO_2 rutile NPs	Anatase x 100 more toxic than rutile. TiO_2 less toxic than fullerenes Nano-TiO_2 anatase induced an LC_{50} of 3.6 ug/mL Nano-TiO_2 rutile induced an LC_{50} of 550 ug/mL Nano-TiO_2 particles produced greater levels of ROS than nano-TiO_2 rutile particles	(Sayes *et al.*, 2006)
Human MSTO and rodent 3T3 cells	50 nm Fe_2O_3 SSA 93 $m^2\ g^{-1}$ 36 nm ZnO SSA 57 $m^2\ g^{-1}$ 20 nm TiO_2 SSA 188 $m^2\ g^{-1}$ uncoated in cell culture	3 -6 day exposure Compared to asbestos Viability tests (100%) Quite toxic to MSTO cells ZnO 15 ppm, FeO 3.75 ,TiO_2 reduced by 50% less toxic to 3T3cells ZnO 15 ppm, FeO 30 TiO_2 reduced by 50%	(Brunner *et al.*, 2006)
Lung epithelial cells	20-75 nm all particles Fe_2O_3 and TiO_2	30 ppm conc all promote increase in ROS after 4hr Limited characterisation	(Limbach *et al.*, 2007)
Daphina magna	200 nm, TiO_2 and $TiO_2$with THF Filtered/ unfiltered (sonicated)	Filtered, smaller particles had highest mortality 100 % mortality at 10 ppm; LC_{50} 5.5 ppm. Sonicated did not kill daphnia	(Lovern and Klaper, 2006)
Daphina magna	< 20 nm TiO_2 anatase 10,000 nm bulk TiO_2 in reconstructed water	NP More toxic than bulk counterparts Nano-TiO_2 EC_{50} = 35 mg L^{-1} Bulk TiO_2 was 275 mg /L Daphnia easily ingested the nanomaterials	(Zhu *et al.*, 2009)
Desmodesmus subspicatus *Daphnia magna*	25 nm TiO_2 mostly anatase 100 nm TiO_2 anatase Particles were tested washed and unwashed without characterisation	For algae concentration curve effects were seen 25 nm unwashed EC_{50} 44 mg /L, washed EC_{50} 32 mg/L. For 100 nm TiO_2 lower toxicity no EC_{50} values calculated. For daphnia no clear concentration curve effects could be calculated for either product. But some immobilisation was seen above 1.5 mg/L and increased once illuminated.	(Hund-Rinke and Simon, 2006)
Rainbow trout	21 nm TiO_2 & 5% rutile 25% anatase	Aqueous (tank) exposure to TiO_2 NPs did not cause mortality. Signs of mucus secretion. Higher incidence of aneurisms on secondary lamellae Did not accumulate titanium over 14 days Fish suffered from oxidative stress	(Federici *et al.*, 2007) (Johnston *et al.*, 2010) (Scown *et al.*, 2009)
Curcorbita maxima pumpkin plant	20 nm Aggregates up to 2um -ve charged Fe_3O_4	There were no apparent visual differences in the plants after 20 days of growth indicating no toxicological effects. Translocation of iron oxide NPs occurred to all parts of the plant with the highest concentration found at base of the stem probably due to aggregates.	(Zhu *et al.*, 2008)

(LOEC) lowest observable effect concentration
(NOEC) – no observable effect concentration.

LC_{50} – lowest concentration at which half test organisms are unviable
EC_{50}- effective concentration at which half test organisms are unviable

Exposure study length is imperative and short, high concentration and longer exposures at lower concentrations are valid and need to be tested to fully understand the environmental indications. However when considering the environmental exposure, NPs may have changed considerably, especially in the presence of natural organic matter.

2.3.3 Environmental risk of manufactured nanoparticles

The risks emanating from NPs are determined by their potential hazards (such as toxicity), as well as by the extent to which the material will come into contact with an organism (Mueller and Nowack, 2008). Risk is usually defined as a product of hazard and exposure. For nanomaterials to present a risk, there must therefore be both a potential for exposure and a hazard, such as toxicity, that results after exposure (Wiesner *et al.*, 2006). To determine the risk from NPs to human and aquatic environments requires knowledge of the exposure, toxicity, transportation, and fate and behaviour in fresh and marine aquatic medium (Moore, 2006). It is also important to know likely NP concentrations (Nowack and Bucheli, 2007) and whether NPs are in suspension or are air-borne (Lovern and Klaper, 2006). Additional evidence suggests that the greatest risk from ENPs emanates from the smallest ones, nominally less than 30 nm (Auffan *et al.*, 2009), and the level of toxicity will vary between NP and organism type (Auffan *et al.*, 2009; Borm *et al.*, 2006).

Whilst assessing risk is difficult, we may be able to make reasonable predictions (Moore, 2006). This has been attempted by Bernard Nowack's team at EMPA, Switzerland (Gottschalk *et al.*, 2009; Mueller and Nowack, 2008). In their model they compare the predicated environmental effective concentration (PEC) to the predictive non effective concentration (PNEC) to give an RQ value (Mueller and Nowack, 2008; Nowack, 2009). PNEC values are typically gained from

toxicological studies where the expected concentrations have been extrapolated to the point at which there is no adverse effect on organisms. Therefore if the PEC/PNEC ratio is smaller than one, risk can be considered low (Mueller and Nowack, 2008).

Through this model silver nanoparticles in soil and water were found to pose little or no risk to the environment, RQ (PNEC/PEC) registering less than 0.001, whereas PEC values for TiO_2 concentrations posed slightly more risk at 0.7 to 16 μg /L (Nowack, 2009)(page 76). This outcome is notable, as Ag NPs are considered to pose one of the greatest risks to the environment due to high use, solubility and toxicity. Moreover their route through waste water into the aquatic environment will become available to sensitive organisms such as algae, daphnia, bacteria, fish and plants (Geranio *et al.*, 2009). A similar pathway is expected for TiO_2 NPs but may have a different fate due to differences in surface chemistry. As already indicated many nanoparticles show anti-microbial or toxic properties. Mutations are also a possibility resulting in NP resistant bacteria, although from a recent study the likelihood of this was low (Mühling *et al.*, 2009).

The literature evidence is therefore contradictory as not all studies have found adverse effects from the exposure of NPs. For example, Nyberg *et al.,* (2008) found minimal impact on bacterial colonies in sewage sludge exposed to fullerenes. This uncertainty thus allows for complacency and delayed action. In 2007, for example, the US National Nanotechnology Initiative (NNI) stated that: "It is not possible yet to make a rigorous assessment of the level of risk posed by [engineered nanomaterials]. Further assessment protocols have to be developed, and more research is required to enable assessment of potential EHS risks from nanomaterials"

(NNI, 2007). The majority of the report was orientated towards the promoting the use of nanotechnology.

The risk of NP to either the environment or to public health is strongly influenced by the ability of NPs to aggregate. Nanoparticles that form aggregates in the water column are likely to sediment and fall to the bottom. Here they will be less available to pelagic organisms but may be available to benthic feeders and biofilms (Mühling *et al.*, 2009). To date, very little work has been done using environmental materials such as soils, sediments and river or lake waters due to their complexity (Mühling *et al.*, 2009). However, it is difficult to transfer the results of some such *in vitro* studies directly to [more complex] environmental situations (Nowack and Bucheli, 2007). Depending on the degree of severity of toxicity of engineered NP there is a risk posed to human health and to the environment if NPs are left untracked (Roco, 2005).

Overall, the calculation of risk that nanoparticles pose to the environment is one of extreme complexity and requires much more data produced from original research which can then be applied to theoretical models. Currently the risk-reward benefit favours the use of NPs, i.e. we carry on using NP technology even though there are risks associated with it because of actual and perceived benefits e.g. medicine, electronics, energy and environment.

2.4 Conclusion

Internationally there is rapid growth in the use of materials containing NPs because of their unique and special properties. It has been found that some of these NMs have biocidal properties and are being exploited for this reason. The risk of nanoparticles to human health is

unknown, but many studies have already indicated that there are adverse effects at the cellular level. Unfortunately, this may also mean that exposure in the environment may cause adverse effects the scale of which is currently under-researched. Moreover, the exact mechanisms that affect toxicity also hold some uncertainly. Additionally the external environmental factors such as pH, ionic strength, and other chemical complexities in the aquatic environment may change the original properties of the EMPs. The fate of NPs will depend on the environmental conditions and the NP type, size and charge. The formation of larger aggregates by high molecular weight NOM compounds will favour the removal of ENPs into sediments and is likely to decrease their bioavailability (Navarro *et al.*, 2008a) or simply transfer the problem to benthic feeders. Difficulties which arise include the detection of engineered NPs in the environment as is impossible to tell how much is going to reach the environment and what effects they will have. One such approach to meet these challenges is to provide adequate test materials through in-house nanoparticle synthesis. This will ensure the choice of stabiliser, nanoparticle test size (a range of monodisperse suspensions of known size), concentration and thorough characterisation methods. A data set that may help identify the mechanisms that are at play in terms of environment fate, behaviour and would provide towards toxicity assessments. Furthermore, these nanomaterials need to be tested at ranges of pH, ionic strength and in the presence of naturally occurring nanomaterials such as the humic substances. The following work in Chapter 3 outlines the instrumentation, materials and methods that were used for characterisation and to explore the topic nanoparticle fate in the aquatic environment in a laboratory study.

3

Methodology

Chapter Summary

Nanoparticle (NP) characterisation is critical when conducting studies concerning synthesis, fate, behaviour and biological interactions of NPs. Techniques applied can be both quantitative and qualitative and characteristics of size, particle coating, charge and aggregation and others are considered. Techniques covered in this chapter include particle sizing by separation using field-flow fractionation (F/FFF), transmission electron microscopy (TEM), scanning electron microscopy (SEM), and dynamic light scattering techniques and others such as x-ray diffraction (XRD), which measures crystal structure, and BET analyser for specific surface area (SSA) analysis. Other particle properties are also explored such as charge, surface plasmon resonance (SPR), and fluorescence. Some experimental details of NP synthesis and sample preparation are also provided in this chapter for clarity, while the synthesis method development is covered in chapters 6, 7 and 8. Many problems arise during the preparation and observation processes leading to sample perturbation and aggregation and thus an accurate 'picture' can be difficult to develop. No single technique can be considered definitive i.e. one that completely characterises NPs, so a multi-method approach is adopted where complex systems are difficult to characterise.

3.1 Introduction

A number of different analytical techniques can be employed to characterise nanoparticles (NPs) both qualitatively and quantitatively. NP characterisation is important in the field of fate, transport, and behaviour in the environment and in biological media for toxicity studies because NPs can behave differently in different media. The driving mechanisms behind NP behaviour are less well understood in complex systems and information about NP size, shape, charge and aggregation will aid this challenge. NP behaviour is dominated by surface chemistries of charge, size, ligand attachment and crystallinity. Results from toxicology studies suggest a number of NP characteristics, such as size and shape, may be important in toxicity and therefore mechanisms such as oxidative stress and cell pitting. Such characteristics include:

- Size (measured by F/FFF, Microscopy, XRD, DLS/PCS)
- Surface area (measured by BET)
- Solubility/dissolution/ion concentration (AAS, ICP-MS coupled with ultra-filtration)
- Coating/ stabilisers (electrophoresis/zeta potential/GC-MS/IC)
- Particle number concentration (EM, FM, NTA, FCS)

The fate and transport of engineered nanoparticles (ENP) in the environment may determine bioavailability through solubility, aggregation or other chemical binding and are dependent on other chemical and physical environmental conditions such as ionic strength, pH and NOM. In order to understand why such parameters are important it is useful to work with monodisperse ENP samples and study their characteristics with and without the presence of other constituents. In the absence of a single comprehensive technique, the application of several methods is required for a more complete assessment. Reviews by Buffle and Leopard (1995a)

and more recently by Tiede *et al.* (2009) suggest a multi-method approach is required (Domingos *et al.*, 2009a). In all environments, the ability to detect concentrations of NPs at natural levels is still lacking and requires further development (Ju-Nam and Lead, 2008).

Analytical techniques currently available for NP observation, which have been developed by physicists for examining and manipulating atomic and nanoscale materials, can also be applied to environmental science applications at this scale. Many of these techniques are prone to sample perturbation, therefore the multi-method approach can reduce bias. The techniques listed in Table 3-1 are used for the uniform ENPs and can be applied for characterisation of ENPs with natural NPs and NPs with complex surface chemistries.

For example, one technique used in this thesis is field-flow fractionation (FFF). FFF is a chromatography–like technique able to separate a mixture of particle sizes of relevant size range. If multiple detection methods are available online, valuable information can be gained and this method is therefore well suited for nanoparticle analysis (Baalousha *et al.*, 2008; Gimbert *et al.*, 2007). Dynamic light scattering (DLS), on the other hand, is quicker to obtain results, but has the tendency to overestimate size, due to light scattering from larger particles. The weighting towards the larger fraction, in DLS is due to dust, aggregates and the presence of a smaller number of larger particles it is therefore more suited to samples containing mono-modal and monodisperse particles. In this chapter, the scope and limitations of each instrument are examined, and the information each instrument provides, its theory and the experimental approach adopted in this work for each analysis are discussed. Sample preparation is discussed together with requirements to obtain accurate, repeatable results.

Table 3-1 Suitable methods used for analysing nanoparticles

Technique	Approximate size range	Dimension	Advantages	Disadvantages
Filtration	100 -1000s nm	No specific dimension	Straight forward technique, fast separation, several size fractions can be obtained by sequential filtration	Size ranges are approximate, non-size separation, perturbation may occur via clogging ior gel layer formation, poor size resolution. Possible change in sample.
Ultrafiltration (UF)	1-3 nm	No specific dimension	Can produce fractions from analysis of the dissolved concentration, less prone to artefacts than filtration	Slow , expensive membranes produces one fraction only
Field flow fractionation (FLFFF)	1-1000 nm	Hydrodynamic diameter H_d Diffusion coefficients D is primary measurement, converted to H_d	Size distribution, produced and excellent resolution, non-destructive (as UF and F)	Samples must be pre-fractionated and preconcentrated, possible sample changes in column.
Transmission electron Microscopy (TEM)	<1- 1000 nm	Particle diameter, size distribution, fractal dimensions can be produced, particle number concentration measurable, chemical information with X-EDS or EELS	Samples are stable for long periods after preparation. Direct observation. Electron beam penetrates samples why advantage?	Sample change through desiccation and ultra high vacuum conditions, organic and other material can alter significantly under electron beam. Staining for organics may be necessary.
Environmental Scanning electron microscope (ESEM)	> 500 nm	Surface morphology	Can use sample in high humidity, thus avoiding damage by drying. EDS available	3D hard to measure size Cannot penetrate surface Resolution at micrometer size
Dynamic light scattering (DLS)*	1- 5,000 nm	Light scattering by counting photons gives a hydrodynamic diameter from diffusion coefficients	Rapid, simple to operate	Tends to overestimate size if large particles present or polydisperse sample, requires high sample concentration
Zeta potentiometry and Electrophoretic mobility (EPM)	N/A	EPM modelled as zeta potential	Rapid measurement of point of zero charge and charge information	.
Surface plasmon resonance (SPR)	about 5 -50 nm	UV-vis light absorbance 200-800 nm Actual size not easily determined	Very quick, good indication if a monodisperse sample and if extensive aggregation has occurred. Very good for silver and gold NPs	Difficult to interpret if in complex matrix Not yet quantitative
X-ray diffraction (XRD)	nm to um	Crystal structure Measures primary particle size	Gives further information on particles structure, better with larger particles	Can only analyse as powder
Surface area analysis (BET)	5 nm to several um	Surface area $m^2 g^{-1}$		Resolution only as large as the size of the gas used, can only analyse as powder
Fluorescence spectrometry	N/A	N/A	Used to determine fluorescent florophores. Can detect florescent NPs such as CdSe and TiO_2 and cerium oxide May be able to determine particle bonding to fluorescent moieties	Metal quenching or enhancement occurs then is hard to quantify

(* alternative name = correlation spectroscopy (PCS))

3.2 Nanoparticle characterisation techniques

3.2.1 Filtration and ultrafiltration

Filtration can be a suitable way to separate particles of different sizes within fluids. It is often a necessary part of sample preparation prior to further analysis, for example measurement with inductively coupled plasma-mass spectrometry (ICP-MS). However, particle interactions with the membrane can lead to non-size separation and sample perturbation. Traditionally, in natural systems, 0.45 μm pore size has been used as the particulate/dissolved cut off point in environmental studies. Other pore sizes can be used to obtain fractions of less than 200 nm and 100 nm with cellulose type materials. Membranes are available in a wide range of materials which have to be considered according the sample and analysis required, for example glass the fibre filter shown in Figure 3.1, pore size of 0.7μm.

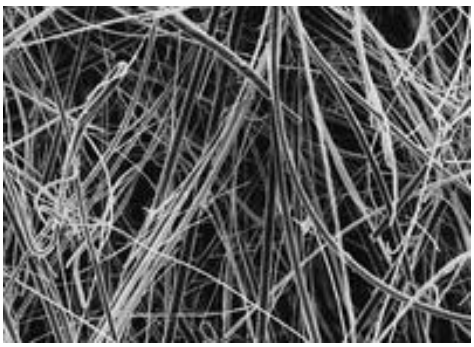

Figure 3.1 SEM image of glass fibre 'F' 0.7 μm filter paper. Taken from: http://www.millipore.com/catalogue/module/c255)

Calibration of pore size is normally with standard particles obtaining retention value of 90%. Ultrafiltration (UF) (Assemi *et al.*, 2004; Bae and Tak, 2005; Benedetti *et al.*, 2003; Diallo *et al.*, 2005; Ross and Sherrell, 1999; Stolpe *et al.*, 2005) uses much smaller pore sizes of 1-10 k Da (Figure 3.2) and retains the nanoparticle fraction, while the permeate approximates to the

truly dissolved fraction. The particular role of UF in the area of manufactured NPs is to separate the dissolved phase metal from the NP metal suspension (for inorganic NPs), either due to the synthesis or from dissolution of the NP over time (Ju-Nam and Lead, 2008). Filtration is performed in the presence of an inert gas such as N_2 to force the sample through under high pressure (Guo and Santschi, 2007).

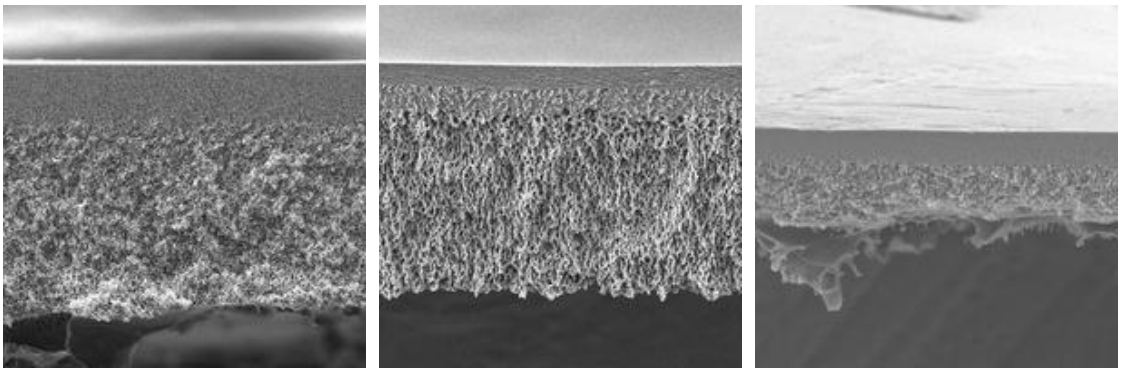

Figure 3.2 TEM images of filtration membranes: Left to right 1) UF membrane; 2) ultrafiltration Discs, PLAC, Ultracel regenerated cellulose, 1 kDa NMWL, 76 mm 3) Ultrafiltration Discs, PBCC, Biomax polyethersulfone, 5 kDa NMWL, 76 mm. Taken from www.millipore.com

3.2.1.1 Experimental conditions

Experimental procedures are outlined in Table 3-2 for standard vacuum filtration or UF under N_2 gas. Membranes were pre-washed with 10% HNO_3 acid solution followed by adequate rinsing with water to remove acid traces and leachable metal ions. This was followed by rinsing with a few millilitres of sample. The storage of UF membranes in acid was found unusable due to performance loss, probably from a reduced pore size (from experimentation). Therefore, UF membranes were stored in pure water (for repeated use with the same sample only).

Table 3-2 Methods applied for filtration and ultrafiltration processes. Volumes are approximate

Step Process	Method 1 Standard filtration	Method 2 To determine dry weight of sample	Method 3 Ultrafiltration e.g. for cleaning NPs
1	Filter 100mL acid (discard)	Filter 100mL acid (discard)	Filter 100mL acid (discard) Gas pressure high
2	Rinse with 200mL pure water (discard)	Rinse with 200mL pure water (discard)	Rinse with 200mL pure water (discard)
3	Rinse with few mL of sample if available (discard)	Oven dry	Add known volume of sample
4	Filter sample	Weigh	Filter 70 -75% of sample (into measuring cylinder). Keep filtrate gas pressure low
5		Filter sample (accurately known volume)	Top up filter housing with ultra pure water of same volume lost
6		Weigh to constant weight and substrate 2nd wt from 1st wt.	Repeat steps 4 & 5 several times or until leached ions are not detectable can also replace with salts or citrate on last top up

The UF apparatus shown in Figure 3.3, was used for nanoparticle washing by a diafiltration method i.e. by releasing of 70% of the suspension and replacing it with the same volume of pure water, to keep the sample hydrated. This was repeated several times and finally replaced with pure water or $NaNO_3$ to maintain ionic strength. Care was taken to avoid excess stripping of surface ions or ligands from the NP (i.e. repeated washings) which would have resulted in an unstable nanoparticle suspension.

Figure 3.3 Ultrafiltration equipment assembly. Sample is placed in chamber, N_2 gas is passed over the sample from the top with the filtrate collected from the bottom. The sample can be stirred to reduce aggregation as the sample concentrates.

3.2.2 Flow field-flow fractionation (F*l*FFF)

Flow Field-flow fractionation (F*l*FFF) is a suitable tool for nanoparticle characterisation as the whole size range can be accurately obtained through separation. This procedure operates with minimal sample perturbation and by using various on-line detection methods, material can be associated with the size fraction such as trace metals or NOM. This section explores the theory behind F*l*FFF. It describes how the separation occurs and how particle size is achieved by calculation of the channel volume and flow conditions using F*l*FFF theory.

*3.2.2.1 F*l*FFF theory*

Samples containing particles within the nano and colloidal scale can be analysed for their particle size distribution via separation using flow field-flow fractionation (F*l*FFF). F*l*FFF is a chromatography-like technique, well described in the literature (Giddings, 1993; Giddings *et al.*, 1992; Schimpf *et al.*, 2000) and is one of a family of F*l*FFF methods where separation occurs along a thin ribbon-like channel with an applied field. This channel consists of Perspex blocks surrounding ceramic frits, as illustrated in Figure 3.4.

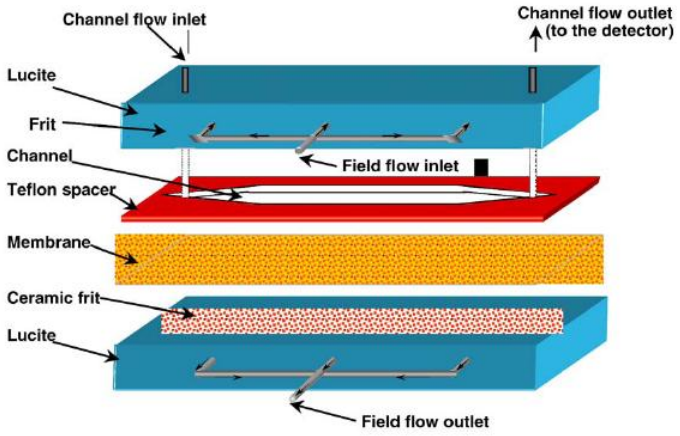

Figure 3.4 Schematic diagram of F*l*FFF channel. Taken from Assemi et al. (2004).

In flow field-flow fractionation, the separation channel is normally asymmetrical (tapered), or as used in this study, symmetrical. Between the frits, an ultrafiltration membrane is placed

to prevent small particles passing through. Separation takes place within the channel by an eluent or carrier solution, usually a low ionic strength salt solution or surfactant in pure water. The particles are carried along it via a parabolic velocity profile where the smallest particles are carried foremost as shown in Figure 3.5.

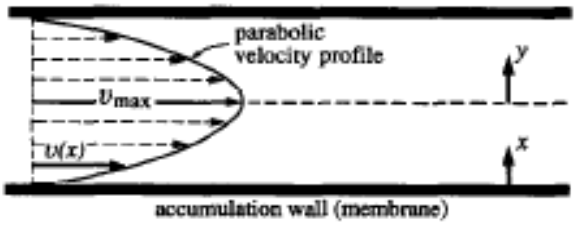

Figure 3.5 Edge view of F*/*FFF channel showing parabolic flow velocity profile. Taken from Assemi *et al.* (2004).

Separation of the particles occurs after injection, via a (20 μL) sample loop, into the top of the F*/*FFF channel (Figure 3.6(a)). A stop-flow procedure operates where the cross-flow remains on but the channel flow off, forcing the sample towards the accumulation wall Figure 3.6(b). Separation occurs after a period of relaxation. The mixed sample is allowed to diffuse away from the accumulation wall; individual species spread into zones of a specific thickness which is determined by their diffusion coefficients and hydrodynamic diameter and the applied flow field. On re-start of the channel-flow the smallest particles are carried first along the parabolic flow Figure 3.6(c) and the fractionation begins (Thang *et al.*, 2001).

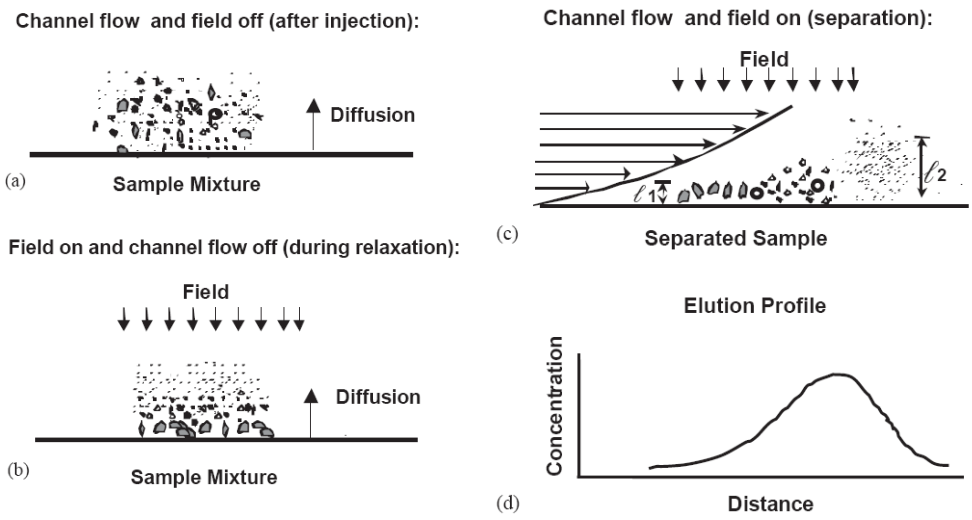

Figure 3.6 Schematic diagrams of separation process within the FFF channel. (a) The formation of sample clouds under the applied field (b) in the FFF channel (c) with channel flow applied smaller size particles diffuse back faster and elute earlier due to interaction with the faster flow streams of the laminar flow taken from (d) the resulting fractogram. Taken from Assemi *et al.* (2004).

3.2.2.2 Components

The membrane acts as the accumulation wall and prevents loss of samples through the ceramic frits. Beckett *et al.* (1992) reported that the sorption to membranes could be dependent on the membrane material and is identified as a primary factor for the sample losses during fractionation (Thang *et al.*, 2001). Several membrane materials are available for use in the F*l*FFF channel. For example, polyethersulfone has been reported to have affinities for humics; whereas cellulose membranes, are reported to have a humic recovery of only 35-37% (Assemi *et al.*, 2004; Thang *et al.*, 2001) and sample sorption is reported with acrylic membranes (Assemi *et al.*, 2004). Beckett *et al.,* (1992) found regenerated cellulose to be the most suitable membrane. For some samples, this may be related to the charge of the membrane, where sorption is due to attraction of oppositely charge particles. The membrane is also subject to compression and the volume inside the F*l*FFF changes and needs to be recalculated regularly to establish the particle size (Giddings *et al.*, 1992). If too much sample is injected onto the membrane, then sample overloading (i.e. too much material in the channel or on the membrane) may occur leading to odd elution peaks (Caldwell *et al.*, 1988).

Choice of carrier solution is important to minimise sample interactions and maximise separation. Several types of carrier matrix have been reported, including sodium azide, (Dycus *et al.*, 1995), sodium nitrate, sodium dodecyl sulphate (SDS) and other surfactants, of ionic strength 10^{-4} M to 10^{-2} M. The conformation of the macromolecules can be significantly affected above pH 10 and therefore this is not recommended (Thang *et al.*, 2001). Moreover, the use of sodium azide, NaN_3, as a solution of known viscosity has been used to calculate the F*l*FFF channel volume (Thang *et al.*, 2001) can be used to reduce microbial activity in the sample. Increasing the ionic strength of the carrier will inevitably increase elution times (Schimpf *et al.*, 2000). The eluent is circulated by means of hydrolytic (HPLC) pumps and control the flow and pressure of the cross flow and channel flow. The channel flow enters at the top and comes out at the bottom and the cross flow is pulled though the frits perpendicular to the channel flow to create the field (Figure 3.4). Most F*l*FFF systems operate with a re-circulating cross flow and this factor should be considered when working with ICP-MS as ions cannot easily be removed, thus affecting sample contamination.

Once separated, the sample can be detected by various methods, usually in-line from the channel end, but equally samples can be collected via fractionators for analysis off line. UV is the most common detection method, but F*l*FFF has also been coupled with different detection methods such as fluorescence (Hassellov, 2005), and multi angled laser light scattering (MALLS) (Baalousha *et al.*, 2005) and ICP-MS (Lesher *et al.*, 2009). Ion detection via ICP-MS couple to F*l*FFF is the most promising method for NP detection in natural samples as elements are directly associated with particle size (Lyven *et al.*, 2003; Stolpe *et al.*, 2005). F*l*FFF has also been combined with electron microscopy for single particle structural and chemical analysis (Baalousha *et al.*, 2006; Gimbert *et al.*, 2007; Gimbert *et al.*, 2006) and with atomic force microscopy (AFM) for the quantification of the structure e.g. permeability

and sphericity of nanoscale natural colloids, where some soft colloids and NPs are permeable to solvents and solutions, however, these are not necessarily intrinsic properties of NPs (Baalousha and Lead, 2007a; b).

The void peak is the first elution peak to appear and should be well separated from the main peak and the sample peak, which can be performed by altering the cross-flow rate. The void peak contains components of the samples which are too small to be removed by the crossflow, as well as particles which elute 'sterically' due to their interaction with the FFF membrane. In FFF theory, the void volume, or channel volume, and its elution time is required in the calculation of particle measurement eluting from the FFF channel (Giddings *et al.*, 1992) (see Eqs 3.1- 3.6). The diffusion coefficient of the particles is calculated from sample retention time and channel void volume (analogous to retention volumes used in chromatography) using equations described in the FFF theory (Giddings *et al.*, 1992). The hydrodynamic diameter of the particles can thereafter be calculated from diffusion coefficient using the Stoke-Einstein equation (Eq. 3.7)

3.2.2.2 Experimental (i) particle size calculation calculations

Particle size and hydrodynamic diameter was derived, according to Schimpf *et al.* (2000), through the application of FFF theory to the fractograms of the eluted samples. In FFF theory, the retention parameter, *l,* is a measure of the average distance a particle diffuses away from the wall when under the force from the crossflow (illustrated in figure 3.3). Small particles with large diffusion coefficients have higher *l* values than larger particles with small diffusion coefficients. The retention parameter, *l* can be written as $l=D/U$, where, *D,* is the diffusion coefficient ($m^2\ s^{-1}$) and *U* is the cross flow in $m\ s^{-1}$. To express this in terms of the volumetric cross flow, V_c ($m^3\ s^{-1}$), *U* is multiplied by the channel area (*LB*), so that, *l* =

DLB/V_c, where V_c, is the volumetric cross flow (m^3 s^{-1}). In FFF theory, lambda (λ), the dimensionless retention parameter, is l divided by the channel thickness, w, $\lambda = l/w$, so that when combined with previous equation, λ can be expressed as:

$$\lambda = \frac{DLB}{V_C w} = \frac{DV_o}{V_C w^2}$$

Eq. 3.1

Where Vo is the void volume (m^3). The retention ratio, R, describes the retention volume (V_r) in relation to the void volume (V_0): $R = V_o / V_r$, where the retention volume is the measured volume eluted between injection and recovery of a particle (V_r'). With the dead volume (V_d) subtracted, which is defined as the volume between the end of the channel and the detector (0.09 mL) estimated from the tube size (NB: as the channel flow stops at the injection point this is the only calculated dead volume), R is expressed as:

$$R = \frac{V_o}{V_r' - V_d}$$

Eq. 3.2

In practice, V_0 can be obtained from the retention volume of the 'void peak', i.e. a peak of very small ions and other species that are not retained by the FFF, and therefore elute at the start of the separation. The retention parameter R is related to lambda and is important as lambda describes the separation conditions inside the channel (Hassellov and Kaegi, 2009).

$$R = 6\lambda \coth\left[\frac{1}{2\lambda}\right] - 12\lambda^2$$

Eq.3.3

A lambda approximation of equation 3.3 (Schimpf *et al.*, 2000) can be applied.

$$\lambda = \frac{R}{6(1-R)^{1/3}}$$

Eq.3.4

However lambda from Eq 3.4 is a reasonable approximation, and is used only to establish w together with the Stokes-Einstein equation (eq 3.5). As the hydrodynamic size of the particle (H_d) is directly related to its diffusion coefficients, D, the Stokes-Einstein equation, 3.5, is applied in FFF theory in this instance.

$$H_d = \frac{kT}{3\pi\eta D}$$

Eq.3.5

By combining Eq 3.5 with the re-arranged Eq3.1, $D = \lambda Vc\ w^2/Vo$, (LBw =Vo) we get

$$H_d = \frac{kTLB}{3\pi\eta V_c w\lambda}$$

Eq.3.6

where *k* is the Boltzmann constant 1.33 x 10^{-23} m^2 kg s^{-2} K^{-1}, *T* is the temperature in Kelvin, *L* and *B* are the channel dimensions in metres, V_c is the cross flow rate in $m^3\ s^{-1}$, η is the viscosity of water (0.00089 Pa s at 298 K), H_d is the hydrodynamic diameter (metres) and w (metres). In order to obtain hydrodynamic size data from FFF fractograms, the dimensions of the channel length, breadth and width *(LBw),* are required. The dimensions for this work were; L=27.7cm, B=2.5 cm, the thickness of the spacer defining the FFF channel was 0.254 cm. However, the channel thickness is reduced due to the presence of the membrane, so *w* must be calibrated (Giddings *et al.*, 1992). This was performed by standard latex beads of known size and by rearranging Eq 3.7 to obtain w.

$$w = \frac{kTLB}{3\pi V_c \eta H_d \lambda}$$

Eq.3.7

From the retention volume of the standard latex beads, *R* was calculated using Eq 3.2, and λ was calculated by Eq. 3.4. Thereafter, from the known values of H_d of the latex beads, the

true value of *w* was obtained using Eq.3.7. As the thickness of the channel is not fixed, but varies with crossflow, salinity and pH of the FFF carrier etc., recalculation of the channel thickness, using Eq. 3.7, is required every time the F*l*FFF conditions change e.g. channel flow, eluent (concentration, pH) cleaning etc. Once w is known, particle sizes for the unknown samples can be then obtained by the application of equation 3.7 to each time data point with λ calculated from equations 3.4 and 3.2. Finally, because Flow-FFF separates materials according to their diffusion coefficients data can be converted from H_d using the equation below (which is eq 3.5 rearranged.)

$$D = \frac{kT}{3\pi\eta H_d}$$

Eq.3.10

To test the calibration, the theory was applied to the fractogram data from the elutions standard suspensions and additionally a correlation was made between particle retention time and known particle size

3.2.2.3 Experimental (ii) separation and conditions

Experimental conditions for FlFFF are presented in Table 3-3. Samples were injected through a 20 μL sample loop via a Rheodyne valve, controlled by a standard PC running the Flow 2.1 software (Postnova). A regenerated 1 kDa (UF) cellulose membrane was used throughout the experiments. The eluent carrier solution in this work was a low ionic strength, 10^{-4} or 10^{-3} M (Table 3-3), and the pH was adjusted to match the sample conditions. Eluent was run through the channel overnight to equilibrate the membrane and put through a degasser before delivery. Calibration of the void volume and sample size was by injection of polyacrylamide beads (*Duke Scientific Corp.)* of known particle size 20 ± 1.5 nm, 33 ± 1.4 nm and 50 nm or 80 nm, both ± 2 nm.

Sample detection in the system here was by UV (*Varian*) set at 254 nm (detector 1)as HS absorbs at this wavelength, however, an additional 400 nm detector (detector 2) (*Perkin Elmer*) was added later for silver NP detection. Peaks were baseline corrected with peak software and exported to an Excel spreadsheet and FFF theory applied (equations 3.1 to 3.8). Diffusion coefficients and hydrodynamic diameters were calculated (equations 3.7 – 3.8).

Table 3-3 F/FFF parameters used in this study

	Chapter 5 Iron oxides NPs	Chapter 7 Silver NPs
Channel flow rate	1 ml min^{-1}	1 ml min^{-1}
Cross flow rate	0.5 to 1 ml min^{-1}	0.4 to 1 ml min^{-1}
Sample loop size	20 uL	20 uL
Eluent [NaNO3]	10^{-4} M	10^{-4} M or 10^{-3} M
Eluent [Ca NO3]	-	10^{-4} M
Membrane	Regenerated cellulose 1kDa	Regenerated cellulose 1kDa
Detector 1-Varian	λ254 nm	λ400 nm
Detector 2- Perkin Elmer	-	λ254 nm

The membrane was regularly cleaned by dismantling the channel assembly, (see Figure 3.4,) and running under pure water. This was necessary to reduce the signal to noise ratio and to clear the channel of microscopic debris to prevent sample overloading. For example, when using HS in the channel, the channel was cleaned every 10-15 samples. Post cleaning the channel was equilibrated overnight and calibrated the following day with standards due to the change in membrane thickness. Occasionally a mild solvent such as ethanol was injected into the channel as a sample. For the positively charged Fe oxide (iron oxyhydroxide) NPs, repeated injections with concentrated sample were necessary to change the charge on the membrane so that separation could take place. This was not required for the negatively charged Ag NPs.

Data acquisition for detector 2 was via a Campbell CR23X datalogger (normally designed for environmental weather stations) as FFF Postnova computer and software did not support this operation. Being both useful and flexible, the supporting Loggernet software also enabled a 'live' view of the incoming data. Data was downloaded after each run and exported into Excel where it was baseline corrected prior to calibration. Data capture was every 15 seconds, as an average of 3 seconds. The program for the Campbell logger was compiled by the author with assistance from Ian Oakes-Green at Campbell Scientific.

3.2.3 Dynamic light scattering (DLS)

Dynamic light scattering (DLS), alternatively known as photon correlation spectroscopy (PCS), is a sizing technique that uses lasers to measure particle size from intensity fluctuations from particle Brownian motion recorded at 90° and sometimes at back scatter. Such fluctuations arise due to constructive and destructive interactions of the scattered light due to the Brownian motion of particles. An autocorrelation function, is used to extract the diffusion coefficient of the particles from the intensity fluctuations of the light scattered by particles, which can then be converted to hydrodynamic diameters (H_d), using the Stokes-Einstein equation (Eq. 3.6). The DLS delivers an intensity–weighted correlation function, and therefore an intensity weight (z-average) diffusion coefficient (table 6.3) and hydrodynamic diameter (Hassellov and Kaegi, 2009).

Mie theory can be applied to convert the z average hydrodynamic diameter distribution to volume or number distributions. This can be done by calculating the volume or number of particles that yield the observed intensity in each size class. Such calculation requires exact knowledge of the refractive index of the particles being studied. The application of Mie theory for the calculation of number and volume weighted distributions from intensity

distributions can lead to some errors of DLS whereby artificial peaks may result from the deep minima in the scattering predicted by Mie theory (Filella *et al.*, 1997). Additionally, Mie theory assumes spherical shape of particles, which is not always the case. The presence of irregular shaped particles and fractal aggregates can skew the DLS result for number and volume-weighted averages. Therefore, the most reliable method of reporting particle size from DLS is through the z-average.

3.2.3.1 Advantages and limitations of dynamic light scattering

DLS has many advantages over other sizing techniques, especially its simplicity and *in-situ* measurements minimise sample perturbation. Time and temperature measurements can also be controlled easily. However, limitations mean that it is best suited to spherical, mono-disperse and mono-modal samples. The presence of larger or non-spherical particles can skew sizes and reduce accuracy, as larger particles diffract more light than smaller particles. If interpreted correctly its sensitivity towards the larger particles can be used to detect the onset of early aggregation where it is not visible in the sample. Comparison with other techniques such as FFF and TEM can help with interpretation of size distribution, e.g. when peaks are compared to tailing in FFF Fractograms. Additionally, the software can convert the intensity to a volume or number based distribution. The z-average (nm), calculated as the root mean square radius of gyration, is normally reported as this is the most universal number when compared with data from other instruments, but used with caution due to its representation of the data. Limits of detection are around 3-5 nm for most light scattering systems (Filella *et al.*, 1997), the manufacturers (Malvern) claim a limit of detection of less than one nm (Kaszuba *et al.*, 2008) with an upper limit of several micrometers. However, this technique requires high sample concentrations that are likely to result in some NP aggregation Since the aggregation rate is proportional to the square of the particle

concentration, the collision frequency is thus higher (Kallay and Zalac, 2002). Indeed, Domingos *et al.* (2009a) found that diameters obtained from DLS were consistently higher than the other techniques with, aggregates providing a disproportionate influence on the analytical signal.

3.2.3.2 Experimental conditions

Measurements in this work were obtained using a HPPS (Malvern instruments) and from May 2008 a zetasizer (Malvern instruments) that combined particle sizing and electrophoresis (section, 3.3.7). Standard operating procedure (SOP) files were created for consistency in the method. Low volume disposable cuvettes were used throughout; the sample was injected using syringe needles or glass Pasteur pipettes to avoid air bubbles. Refractive indexes (RI) for the samples were taken from the Malvern manual of refractive indexes as in Table 3-4 and values were used as parameters in the instrument software.

Table 3-4 DLS refractive index and absorbance measurement parameters (Malvern).

Particle	Refractive index	Absorbance	Cell type
Iron oxide (hematite)	3		Low volume
TiO_2	2.4-2.9		Low volume
Ag	0.54	3	Low volume

3.2.4 Electron microscopy (EM)

3.2.4.1 Transmission electron microscopy (TEM)

Transmission electron microscopy (TEM) is suited to NP characterisation; with images providing information on shape, size and, with suitable data analysis, other properties e.g. fractal dimensions, shape factors and particle size distributions. Furthermore, additional

spectroscopic detectors such as energy dispersive x-rays (EDX), parallel electron energy loss spectroscopy (PEELS), can gain chemical and elemental information. After suitable sample preparation by placing the wet sample on grids, e.g. copper, covered with a surface film to aid sample adhesion and affixing by air drying or centrifugation, particles are analysed under an electron beam in a ultra high vacuum (UHV). The disadvantages of TEM are due to this UHV which causes desiccation and the powerful electron beam may cause damage to the viewed sample particularly if organics are present. Particle focusing is greatly aided by the use of a holey film, as the edge of the film can be used as a focusing guide. Particle size analysis is performed on the recorded digital image, and calibrated using the scale bar provided on good quality micrographs, either manually or automatically. Several hundred are required to produce a particle size distribution to achieve a proportionate number of representative particles and reduce subjective error in particle selection.

3.2.4.2 Experimental conditions

Samples were viewed with a Phillips Technai F20, Figure 3.7(a) fitted with Oxford Instruments ISIS EDS, and Gatan digi PEELS, with a point resolution of 0.24 nm and a focal length of 1.77 mm. Sample preparation involved dropping 10 μL of a diluted sample onto carbon coated copper grids (purchased from *Agar*) loosely covered and air dried between locking tweezers. The initial practice of mopping off the excess droplet after 15 minutes was halted as it was suspected that migration of very small particles could go on the tissue and introduce contamination from paper fibres. Corrected dilution was important to prevent aggregation of samples upon drying so that individual particles could be observed.

(a)  (b) 

Figure 3.7 Images of electron microscopes, (a) transmission electron microscope (TEM) Phillips Technai F 20 and (b) the ESEM Philips XL30 ESEM-FEG

3.2.4.3 Environmental scanning electron microscopy (ESEM)

Environmental scanning electron microscopy (ESEM), Figure 3.7(b), enables surface scanning of the sample resulting in apparent three dimensional images. The advantages of ESEM are realized by elimination of the UHV of traditional SEMs in the microscope chamber, samples wet or dry can be then be viewed under high pressures up to 10 torr. This is achieved inside the microscope by separating the vacuum environment in the chamber from the high vacuum environment in the column.

3.2.4.4 Experimental conditions

The samples were viewed with a Philips XL30 ESEM-FEG fitted with a Oxford Inca 300 EDS system. Sample preparation involved dropping the raw aqueous sample onto a gold coated mica surface, a contact was achieved to the gold by using a mounting of silver paint. Excess moisture was driven off the sample once it was placed inside the chamber until about 80% humidity. At 100% humidity the sample cannot be viewed due to the surface water. SEM scans the surface of the sample and can provide detailed 3D type images, but the resolution is low maybe to about 0.5 μm, ESEM has the added advantage of examined the

subject under high humidity, whilst it is impossible to view the image at 100% humidity, at 80% images are very clear. EDX is an EM utility that focuses the electron beam onto a very localised area of the samples and enables gain of elemental composition. The disadvantage over TEM is that resolution is at best to 500 nm, and direct particle measurement is limited due to viewing over the surface, whereas TEM directs the electron beam through the sample.

3.2.5 Brunauer, Emmett and Teller (BET) surface area analyser

Surface area was determined by the Brunauer, Emmett and Teller (BET), N_2 gas porosimiter 2010 BET surface area analyser (Micromeritics ASAP 2010 CE). Particles specific surface area (SSA) is calculated by use of the Brunauer, Emmett and Teller (BET) equation or the multilayer adsorption theory (Brunauer *et al.*, 1938). The technique uses gas absorption, usually nitrogen at liquid nitrogen temperature, and is based on the theory of assuming that each first layer absorbed molecule serves as a site for the adsorption of a molecule into the second layer and so on (Allen, 1997). The eventual change in volume of gas absorbed to the surface is used to calculate the surface area and assumes that there is no gas interaction on the particle's surface. The sample has to be in powder form and is given in grams per metre squared ($m^2 g^{-1}$).

3.2.6 X-ray diffraction (XRD)

X-ray diffraction crystallography (XRD) is a technique that uses x-rays to establish the crystal structure, geometery and particle size of the material examined based on the elastic scattering of X-rays. The pattern gained from the angle of diffraction, can be compared against standards of known samples of pure substance. Particle size can also be calculated

from the dominant peaks using Scherrer's formula (Eq.11) based on the half-value breadth *B* of the diffracted beam and can be expressed as:

$$B = \frac{K\lambda}{\left(L\cos\frac{x}{2}\right)}$$

Eq.3.11

where, λ is the wavelength of the incident x-rays, *L* the linear dimension of particle, x/2 the Bragg angle and *K* a numerical constant for which Scherrer, in 1918 obtained the value, $2(\ln 2/\pi)^{1/2} = 0.93$, where ln is the natural log (Langford and Wilson, 1978; Patterson, 1939). This formula is valid for a particle sizes of a few nm to several hundred, however a homogenous sample with a small particle size range is considered more important when obtaining accurate particle sizes (Borchert *et al.*, 2005). Analysis was conducted with a Siemens 5000 crystal fractionator, a powdered sample was placed on analytical tape and placed inside the machine, where x-rays were fired at it.

3.2.7 Electrophoretic mobility (EPM) and zeta potential

Electrophoretic mobility (EPM) (10^{-8} m^2 V^{-1} s^{-1}), is the velocity per unit voltage gradient of a particle in a liquid across which has been applied a voltage gradient: its value is dependent on the charge at the boundary between the atoms moving with the particles and those remaining with the bulk solution. (Duval, 2007; Jiang *et al.*, 2009). Sometimes converted to zeta potential (V), ζ, using the Smoluchowski equation: $\zeta = \mu U/\varepsilon$, where ε is the electric permittivity of the medium (C^2 N^{-1} m^{-2}) (Jiang *et al.*, 2009), and zeta, ζ, is the potential at this slipping plane (Jiang *et al.*, 2009). Zeta can be used to determine the point of zero charge (pzc), or the iso-electric point of a solution, which is the point at which particles do not move in an applied field (Sposito, 1989). It is dependent on the pH of the solution, where the pH_{pzc} is the pH at which the particle has a net neutral charge and is relevant only for hard particles. Kosmulski (2002) has reported pzc values of metals and metal oxides

providing details of collated results from the literature. The measurement is useful as it provides information about the stability of charge stabilised NPs in suspension and can be related to particle size in terms of shrinkage or expansion of the outer layer of the particle. In the case of particle outer layer shrinkage, particle-particle distance potentially decreases, allowing van der Waals forces to act thus increasing the potential for aggregation. The DLVO theory predicts an increase in total interaction energy with an increase in particle size (Stumm and Morgan, 1996).

3.2.7.1 Experimental conditions

In this study, analysis of EPMs was performed on a Malvern Zetamaster in a quartz capillary cells for chapters 4 and 5 and then on Malvern Nanosizer, in disposable plastic cuvettes (Malvern). Both types of cell were flushed with pure water between each sample. A one point calibration was performed either with pure water which would give a value close to zero, or with standard solution (Malvern) of known zeta potential with at least 5-12 measurements taken for each sample. Samples were then plotted as a function of pH.

3.2.8 Surface plasmon resonance (SPR)

The surface plasmon resonance is defined by Link and El-Sayed (2003) as being the coherent motion of the conduction-band electrons caused by interaction with an electromagnetic field. In short, it is the interaction of photons with the surface of the NP which provides the observed colour. The SPR of NPs are particularly strong with silver (max absorption, 400 nm) and gold (max absorption, 520 nm) of a particle size from about 2-50 nm. For spherical particles less than 20 nm, this is explained by Mie's theory, for other shapes and larger particles other theories have been applied (e.g. see Link and El-Sayed (2003)). The maximum absorbance band can increase in height as particle size changes (6-10 nm) as well as shift from left to right with larger sizes, the latter will depend on the number density of particles in the size range (Van Hyning and Zukoski, 1998) with particle shape

having the strongest influence on the peak maxima SPR (Mock *et al.*, 2002). This method, although currently not quantifiable, gives a good indication of sample polydispersity, where aggregated particles will display a further shoulder or peak at a higher wavelength (Miller and Lazarides, 2006; Mock *et al.*, 2002).

3.2.8.1 Experimental conditions

In the SPRs presented in this thesis the work was carried on UV–vis (WPA *lightwave*) in 1 cm pathway quartz cuvette with a wavelength range between 200-800nm. The instrument was baseline corrected each day using a sealed cell containing pure water. Measurements were taken in triplicate and generally showed extremely good repeatability. Absorbance was plotted against wavelengths 200 -800 nm or the selected region of interest.

3.2.9 Fluorescence

Excitation-emission matrix (EEM) fluorescence spectrometry examines the fluorescence properties of materials including organic materials containing aromatic compounds, such as carboxylic acid and phenols. Some NPs also have fluorescent properties depending on size and band gap. Fluorescence occurs when light is absorbed at one wavelength and emitted at a different (longer) wavelength.

3.2.9.1 Experimental conditions

Sample fluorescence analysis was carried out with a Varian Cary Eclipse spectrophotometer in a 1 cm pathway low fluorescence quartz cuvette. EEMs were obtained using a slit width of 5nm with voltage of 750 v at 5 nm, wavelength range was from 200-500 nm and was extended to 600 nm when measuring peat humic acid. Samples and blanks were run in triplicate and peaks were handpicked using Cary Eclipse software and the maximum fluorescence values taken for an area of EX/EM. Data was corrected to 20 Raman units and

was done by taking the Raman value of a sealed water-cell at 370 nm (Baker, 2002; Cumberland and Baker, 2007) as the bulb intensity varies on a daily basis and the equation below applied:

Corrected intensity = (Raman units/20) x the uncorrected units

Quinine sulphate standard was not used for sample calibration. High fluorescing samples were diluted to avoid inner filtering effects (IFE) (Mobed *et al.*, 1996; Spencer *et al.*, 2007) and machine filters were applied for nanoparticle analysis to avoid refractive light scattering. For NP analysis, filters were added to eliminate refraction including the Raleigh Tyndall second order scatter line.

3.2.10 Total organic carbon (TOC)

Total or dissolved organic carbon (TOC, DOC) measurements were undertaken with a shimadzu 5050 carbon analyser. Where samples typically filtered to gain DOC. Standards were obtained from Reagacon and diluted by the machine. Measurements were either taken in duplicate to a CV of 2, whereby, two samples were measured and if a CV greater than two was obtained, a third measurement was taken and the outlier discarded, because of variability the procedure was changed to analysis in triplicate, with a SD obtained. Glass vials were acid washed and oven dried to remove excess carbon. Blanks were with Milli Q water inserted every 10 samples as well as before and after the run. Blanks were subtracted from the measurements.

3.2.11 Graphite furnace atomic absorption spectrometry (GFAAS)

Detection of metal ions in solution was analysed by graphite furnace atomic absorption spectrometer GF-AAS (THGA Perkin-Elmer AAnalyst 600). The lamp was a hollow cathode ray tube (5UA Ag –A B51 539) set to maximum current of 10 mA. Silver ions were

detected at 328.1 nm with a slit width of 0.7 L and concentration raw values from peak areas. Samples and blanks were all at 0.1 % HNO_3 and the matrix modifiers used were $MgNO_3$ and Pd. Standards were diluted by the AAS from 0-100 μg L^{-1}. Table 3-5 describes the GFAAS program for sample analysis.

Table 3- 5 AAS method for sample analysis for ramping times. Taken from Perkin-Elmer instrument manual.

Step	Temp oC	Ramp Time (s)	Hold Time (s)	Internal flow
1	110	1	30	250
2	130	15	30	250
3	800	10	20	250
4	1500	0	3	0
5	2400	1	3	250

3.3 Laboratory techniques

3.3.1 Sample preparation

Sample preparation was conducted with utmost care, as preparation is as important as the analysis itself. In most preparation steps, a range of factors must be considered, including types of material used for preparation and storage. For example, glass, is the traditional material for sample preparation as it inert, low in organics and if treated correctly, and can be cleaned and reused easily. Material adhesion to glass, which can result in material loss and cross-contamination, can often be rectified by soaking in acid solutions. However, more persistent chemicals, such as TiO_2 and CeO_2 NPs, which leave white deposits on glass surfaces (from experimental), led to using plastic as the preferred material for storage. Plastic is available in different types of material densities and with different properties. Polypropylene (PP) is highly fluorescent, but high density polyurethane (HDPE) is useful for

this type of analysis due to low fluorescence. Metal is only suitable where chemical assays are not required but maybe suitable for CNTs and C_{60}. Analysing blanks are the only reassurance that chemical contamination is not a factor in analytical processes.

3.3.2 Glassware preparation

All new and used plastic vials and glassware were soaked overnight in 10% HNO_3 as a matter of course and were triply rinsed in distilled water before use. Laboratory detergent (e.g. Decon/ LIPSOL) was used for particularly dirty items, and rinsed before acid washing. Vials intended for carbon analysis were oven dried at 140 degrees to remove carbon traces. Volumetric flasks were not heat dried as their volume may change with heating. Rubber bungs, 'o' rings and metal objects were never placed in the acid bath. Disposable plastic cuvettes for light scattering were used out of the box and discarded once used, because scratches may increase contamination and interfere with measurements.

3.3.3 Preparation of commercial NOM

Suspensions of fulvic acid were prepared from IHSS Suwannee River dried fulvic acid (SRFA) by weighing the appropriate amount and dissolving in ultra pure water (Barnard nanopure) and left for at least 24 hours to equilibrate at a concentration of 400 mg L^{-1} which was then diluted to the desired HS suspension to be used. The peat humic acid (PHA), also obtained from the IHSS, was prepared in a similar way, however due to its hydrophobicity a few drops of 1M NaOH were added and mixed quickly. The increased pH increased PHA solubility. The suspension was readjusted to pH 7 using HNO_3. Polysaccharides are less soluble than the HS and the suspension was prepared as for SRFA but a known weight of the exo-polysaccharide, succinoglycan, was suspended in water in a 100 mL volumetric flask and stirred for 24 hours. The resulting suspension was then filtered

through a pre-weighed 0.1 μm cellulose nitrate filter paper according to procedure 2 in Table 3-2. The filter paper was re-weighed and the difference subtracted from the original weight and the concentration recalculated and diluted to 5-25 mg L^{-1}.

3.3.4 Measurement of dissolved iron

Dissolved iron from UF fractionated iron oxide samples were determined by UV absorbance. Standards were prepared from iron chloride in HCl and measured at pH 2. This was found to be a more suitable method than by atomic absorption methods. The results are presented in chapter 5. The maximum absorbance value was at 304 nm (Steiner and Lazaroff, 1974) and Figure 3.8 (a) show a 5 mg L^{-1} sample with a peak at 304 nm. This produced a good calibration curve (r^2> 0.998) Figure 3.8 (b) from standard solution made from $FeCl_3$ in HCl adjusted to pH 2. Ferric ions (Fe^{3+}) absorb strongly in the 295- to 304-nm region (Steiner and Lazaroff, 1974).

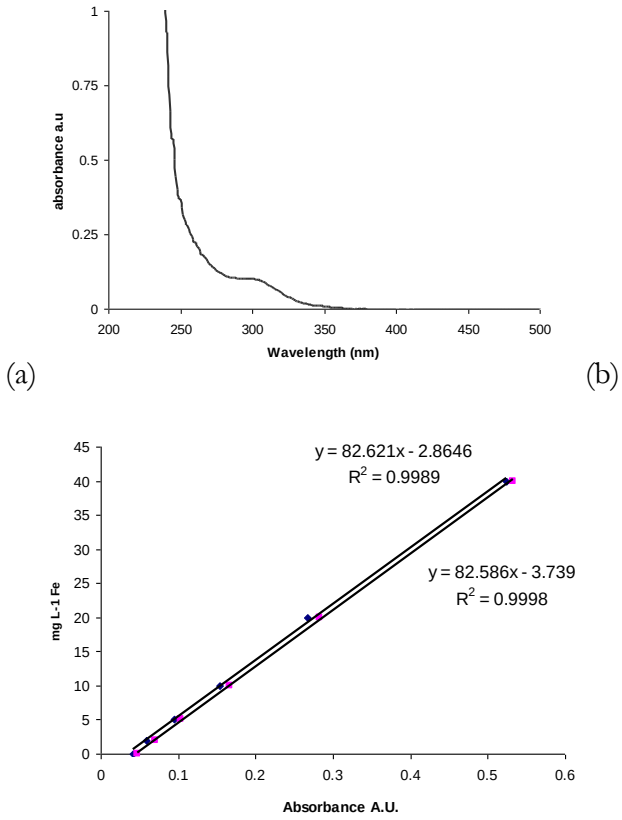

Figure 3.8 (a) Typical spectrogram trace for 5 ppm standard solution with peak showing at 304 nm. (b) Calibration curves for standards using $FeCl_3$ in HCl solution at pH2.

3.4 Statistical methods

3.4.1 Descriptive statistics

Data were analysed in Excel to give descriptive statistics of particle size for mean, mode, median and standard deviation. Standard deviation is an estimation of the average spread of the data given in the same units of the original data. It is calculated as the square root of the variance, where the variance is the sum of the squares of the differences between each individual measurement and the mean divided by the number of measurements minus one, and is used to indicate in the current case the variation in repeat measurement values, where there are at least three replicates.

In order to determine particle size from TEM measurements, particle number and size were derived manually by using the TEM software and drawing calibrated lines across the particle's image. These data were then analysed in Excel to determine the maximum, minimum, range and spread. Frequency distributions were obtained via the application of the Excel data analysis add-in functions and displayed as histograms (where the data are grouped into bins (or small data ranges) and the bar charts plotted in either excel or sigma plot (Systat)).

3.4.2 Parametric and non-parametric statistics

Parametric (normally distributed) and non-parameteric (non-normally distributed) tests were applied to the data to see whether significances differences lay between the sample means, for example, particle size, as a function of solution condition. The t-test (parametric) is used to test whether the differences between two data sets are significantly different from zero, whereas the Mann-Whitney (non-parametric) looks for differences between two independent samples. Where there are several sets of paired data, the analysis of variance (ANOVA) can be applied and is the overall test to determine whether groups means differ. All of these types of analysis were performed using the statistical function packages available in sigma plot (Systat).

To assess the relationship or correlation between two sets of data, the data is plotted as an x-y scatter plot. The closer these datum points are to forming a straight line that is not horizontal or vertical, the better the relationship, R^2, is. R^2 values were calculated in Excel, either from the equation produced by the plotted graph, or by using the 'slope', 'intercept'

and 'correl' functions to produce the relationship, y = mx+c. The nearer the R^2 value is to one the better the relationship. One of the most common uses for the correlation function is for instrument calibration, but equally it can be used to determine how strongly independent variables are related to each other.

3.5 Conclusion

Many analytical methods can be suitably applied to NP characterisation and this chapter has summarised the main techniques applied to the work in this thesis. However, each method has its advantages and limitations and is the main reason for using such a wealth of techniques. Moreover, analysis is often performed with a different particle phase, for example, powder is required for BET and XRD, while FFF and DLS measure the hydrodynamic diameter in the aqueous phase. TEM on the other hand examines dry samples under ultra high vacuum (UHV). Whereas ESEM can overcome this by operating in high humidity, the spatial resolution is poor compared to EM techniques which examine under UHV. Furthermore, values achieved from sizing using DLS can be affected by the presence of larger particle or aggregates but analysis is rapidly performed in situ and doesn't involve interactions with a column or membrane. Sample perturbation has to be minimised; for instance, measurement of concentrated samples may lead to aggregation. Nevertheless, a great deal of information can be gained on particle size, charge, surface area, crystallography, shape, aggregation and bonding state from this multi-method approach. Therefore, in this project a multi-method approach is the favoured option for analysis of NPs (Domingos *et al.*, 2009a). The proceeding chapters in this thesis take these techniques to characterise manufactured NPs, either as prepared or after change in suspension conditions (pH, HS concentration, and ionic strength) to further knowledge in environmental behaviour.

4

Characterisation and behaviour of TiO_2 NPs exposed to trout, their tank waters and exudates

Chapter Summary

Trout *(Oncorhynchus mykiss)* were exposed to commercially available titanium dioxide nano and macro-sized powders at two different concentrations over a nine day exposure at Exeter University by Dr Blair Johnston, Tessa Scown and Professor Charles Tyler in collaboration with, Dr M Baalousha and Professor Jamie Lead. Following exposure, the fish were killed at nine days and results from tissue examinations are published in Johnston *et al.,* (2010) (Appendix 2). The tank waters were characterised at University of Birmingham, by electron microscopy, light scattering and fluorescence. The trout responded immediately to the TiO_2 NPs by producing mucus, showing no other symptoms. This chapter looks at the behaviour of the TiO_2 NPs after exposure to fish and examines the fluorescence of TiO_2 NP with mucus comparing with CeO_2 NPs. Analyses were conducted by the author except where indicated.

4.1 Introduction

Titanium dioxide nanoparticles (TiO_2 NPs) are one of the major types of nanoparticles currently used in industry. Of about 15 different types of engineered NPs identified in Switzerland, silicon dioxide (SiO_2) and titanium dioxide (TiO_2) were the two predominant nanoparticle types with over 400,000 kg produced annually (Schmid and Riediker, 2008). Commercially, titania is of interest due to its ability to scatter light effectively (Li *et al.*, 2007) and traditional applications for bulk TiO_2 have included paints (Braun *et al.*, 1992), and personal care products such as sunscreen and toothpastes. The production of nanoparticulate titania has seen the development of transparent, high sun protection factor (SPF) sunscreens (Serpone *et al.*, 2007). In the advancement of medical research, TiO_2 NPs have been found to act as an anti-tumour agent by inhibiting the growth of cancer cells (Huang *et al.*, 2000; Li *et al.*, 2007; Thevenot *et al.*, 2008). At the nanoscale TiO_2 is a very effective semi-conductor and photocatalyst, due to its wide band gap of 3.2 eV (see Figure 4.1) and is used in solar panel technology.

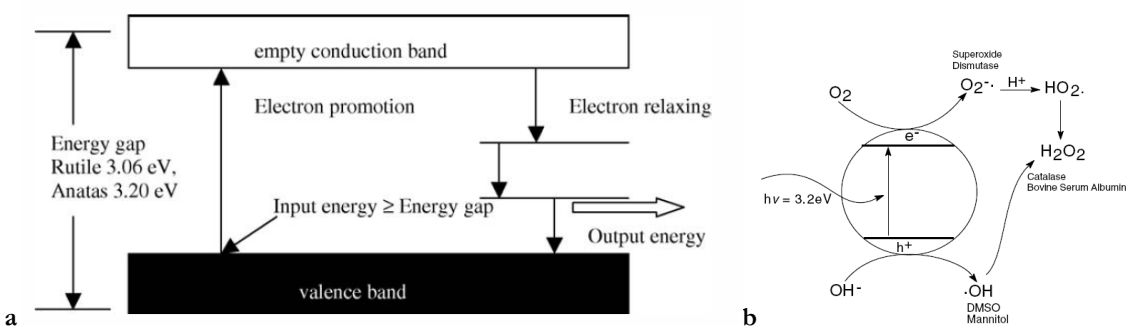

Figure 4.1(a) Diagram showing the absorption of UV light by electronic transition in titanium dioxide showing rutile or anatase modifications where the dark area is occupied by electrons (From Villalobos-Hernandez and Muller-Goymann (2006)). (b) Scheme illustrating, in simple terms, the photophysical and photochemical events that occur when metal-oxide semiconductors, such as TiO_2 and ZnO, are photoactivated by the absorption of UV radiation. Taken from Serpone et al. (2007).

Under light, the titainia is able to photocatalytically degrade organic molecules (Mahmoodi *et al.*, 2007). This make it useful, together with ZnO NPs in applications such as solar panels,

self cleaning glass (Paz *et al.*, 1995) and drinking water purification (Kim *et al.*, 2009; Theron *et al.*, 2008). The degradation of NOM by TiO_2, is also aided in the presence of ozone and other oxidants (Kim *et al.*, 2008). Figure 4.1b shows the production of the OH free radical in the photocatalytic reaction. Because of these properties TiO_2 also exhibits anti-bacterial and other toxic effects due to its ability to produce reactive oxygen species (ROS) under light (see Figure 4.1). Under some conditions TiO_2 NPs has also observed to be toxic in the dark (Adams *et al.*, 2006).

4.1.1 Factors affecting the toxicity of TiO_2

Bulk TiO_2 has a history of being relatively non-toxic and safe to use in contact with skin and ingestion via food additives. However, a number of published studies have reported adverse and toxic effects from nano-sized TiO_2 in test organisms (Adams *et al.*, 2006; Long *et al.*, 2006; Sayes *et al.*, 2006). This toxicity could be due to the titania's size, surface area, crystalline structure, concentration, catalytic or photocatalytic properties (Jiang *et al.*, 2009). The literature also indicates that more than one factor may be responsible for TiO_2 NP toxicity. Titania's ability to readily form aggregates (Domingos *et al.*, 2009b) also needs to be considered, because like other NPs, aggregation may reduce toxicity (Grassian *et al.*, 2007; Warheit *et al.*, 2006). Nevertheless, several conflicting reports exist in the literature about the toxic mechanism and effectiveness of TiO_2. For example, with trout fish *(Oncorhynchus mykiss)* exposed to TiO_2 NPs no acute toxicity was observed in short term exposures for either water or diet (Federici *et al.*, 2007; Handy *et al.*, 2008a). Even when administered intravenously at 1.3 mg kg^{-1} of body weight into rainbow trout (Scown *et al.*, 2009), Ti was found in tissues samples (kidneys), There did not appear to be any overall ill-effects (Handy *et al.*, 2008a; Scown *et al.*, 2009). However, NP exposure has shown to provoke irritation and aggressive behaviour in trout (Oberdorster, 2004; Smith *et al.*, 2007). Where other fish have

responded to TiO_2 NP exposure by excessive mucus production from epithelia cells (Johnston *et al.*, 2010) resulting in NP interactions leading to flocculation and sedimentation. While NPs are removed by sedimentation in the short term, the long-term bioavailability of NPs is unclear (Handy *et al.*, 2008b).

4.1.2 TiO_2 toxicity response to size and specific surface area

As a factor of toxicity, size shows much importance, as very small particles are able to pass though membranes and though not proven, may pass through dermal layers (Crosera *et al.*, 2009). This highlights concern towards the use of NP ingredients in sun cream and other lotions (Serpone *et al.*, 2007). In toxicity studies, a difference in size has been seen with TiO_2 NPs although not significant in a dark/ light study (Hund-Rinke and Simon, 2006) where 25 nm particles were more toxic than 100 nm. Another factor responsible for NP toxicity is the specific surface area (SSA). Nanoparticle SSA increases as the particle gets smaller, with catalytic activity and other reactivity enhanced possibly contributing to toxicity. The surface area effects of TiO_2 toxicity were investigated by Warheit *et al* (2006) and Grassian *et al.* (2007), exposing airborne particles to rats and mice in sub-acute inhalation studies of TiO_2 NPs. They found no difference in toxicity between small particles with a large surface area (>100 m^2 g^{-1}), compared to larger particle sizes, with comparatively smaller surface areas (Grassian *et al.*, 2007; Warheit *et al.*, 2006).

4.1.3 Aggregation and TiO_2 toxicity

TiO_2 aggregation could affect toxicity arising from sample preparation techniques (Jiang *et al.*, 2009; Lovern and Klaper, 2006) such as filtering verses sonication. For example, *Daphnia magna* mortality to TiO_2 NP_S gave a dose response curve EC_{50} at 10 mg L^{-1}, with filtered particles. However, with sonicated particles, the concentration required to have the same

effect was higher, at 300 mg L^{-1}. On examination of the particle size, sonicated particles were found to be 100-200 nm in size with observed aggregation and clumping (Lovern and Klaper, 2006). This indicated that filtering exposed more of the smaller particles to the daphnia whereas sonication was unable to fully break apart the aggregated particles resulting in reduced exposure due to less surface area contact from the larger particles. In the study by Grassian *et al.* (2007), exposing mice to TiO_2, aggregated particles, which had a lower specific surface area (SSA), were cleared from lungs more readily than individual particles of less than 10 nm. Another study by Warheit *et al.* (2006) exposed TiO_2NPs to rats. They found that lung inflammation from inhaled NPs was reversible and remarked that large aggregates had formed in the airways thus reducing the effect of injury to the lungs. Toxicity therefore, appeared to be dependent, not on the primary particle size, but on its ability to readily form aggregates (Grassian *et al.*, 2007) and that toxicity could perhaps be reduced by aggregation. Using unstable NPs and particles that are prone to aggregation, may result in an inaccurate assessment of NP toxicity and even misleading conclusions, as the NPs will be lost from suspension through sedimentation (Jiang *et al.*, 2009).

4.1.4 TiO_2 NPs and crystal structure

Differences in toxicity have been observed from different crystal structures (Sayes *et al.*, 2006) and common polymorphs for TiO_2 are anatase, rutile and brookite (Koparde and Cummings, 2007). The smaller TiO_2 NPs generally contain more anatase than rutile, which forms a larger crystal lattice. Rutile NPs are reported to be more hydrophilic than anatase of the same size, due to the orientation of titanium or oxygen surface ions (Koparde and Cummings, 2007). Anatase is a better photocatalyst than rutile, due to inherent differences in crystal structure, but even in the absence of light, in the study of Sayes *et al,* (2006) anatase

was reported to be 100 times more toxic to human cells, than rutile and produces the most ROS generation (Warheit *et al.*, 2006).

4.1.5 Toxicity and catalytic and photocatalytic properties of TiO_2 NPs

Of most interest are the catalytic and photocatalytic properties of TiO_2 NPs. They are considered reactive under light or dark condition and are able to produce free radical, oxygen species. However, ROS produced in living tissue (from TiO_2 catalyst) can potentially lead to oxidative stress and to cancer (Long *et al.*, 2006). As a bactericide, titanium dioxide NPs have been found to be effective (due to this ability to photocatalytically produce ROS) for gram positive, *E coli* and gram negative *Bacillus subtilis* (Adams *et al.*, 2006). Toxic effects on other organisms are less certain, and other factors may be responsible. Moreover, light emission from UV pre-exposed TiO_2 may be time delayed or phosphorescent (Hund-Rinke and Simon, 2006; Melnyk *et al.*, 2005). Toxicity studies using pre-illuminated TiO_2 NPs revealed that there was an effect (to bacteria) compared to similar particles of ZnO and SiO_2 (Adams *et al.*, 2006) and with daphnia and green algae (Hund-Rinke and Simon, 2006; Zhu *et al.*, 2009), indicating that the NPs were effective for some time post illumination.

4.1.6 Fate and behaviour

There are relatively few studies concerning the fate and transport of TiO_2 NPs. NOM interactions with other nanoparticles have had more attention than TiO_2 NPs, whereby NOM has generally been found to stabilise nanoparticles where they would normally aggregate (Domingos *et al.*, 2009b). The factors affecting behaviour determine whether the nanoparticles are going to remain in the water column or aggregate and become available to aquatic benthic feeders. Like the other nanoparticles examined in this thesis, TiO_2 NPs have also been reported to interact with NOM (Domingos *et al.*, 2009b) and proteins (Zattoni *et*

al., 2007) by forming coatings (Kim *et al.*, 2009). Furthermore, TiO_2 can facilitate the transport of trace metals for example; mercury onto SiO_2-TiO_2 nanocomposites (Gao *et al.*, 2008) and TiO_2 facilitated cadmium uptake into carp (*Cyprinus carpio*) tissues (Zhang *et al.*, 2007). While their actual environmental fate is unknown it is likely that TiO_2 metal oxide NPs will behave similarly in the environment to other metal oxides NPs.

4.1.7 Aims and objectives

The aims of this chapter are to characterize the behaviour of uncoated TiO_2 nanoparticles when exposed to fish in a nine-day exposure. Sub-objectives were to:

1) Characterise prepared titania NPs as powder or in pure water using DLS, XRD, ESEM, EPM and other methods.

2) Characterise TiO_2 NPs interactions with fish mucus and examine their associated fluorescence.

4.2 Methodology

4.2.1 Fish experiment

An exposure experiment was set up and conducted at Exeter University. Purchased rainbow trout were kept in a large tank before exposure. The concentration ranges (0, 0.5 and 5 mg L^{-1}) of the TiO_2 NPs were chosen by the Exeter group, to reflect likely dose-response curves of the exposed trout. Table 4-1 shows the experimental tank set up. Sixty litre (60 L) tanks were set up under semi static conditions between 9 and 11°C containing TiO_2 nano and macro particles ((*Sigma Aldrich*) where the mean estimated size of the macro particles were; 177 nm; stdev ± 39 nm; number = 131) based on ESEM tank waters at t = -1 (pre-sonicated – by placing in a ultra sonication bath for 30 minutes) suspensions of 500 or 5000 μg L^{-1} with and without fish or 5000 μg L^{-1} TiO_2 bulk particles with fish (eight per tank). An

additional tank containing suspended titanium was also set up for the benefit of the toxicology study, but this tank was not analysed further at Birmingham. Prior to exposure, fish were maintained in 500 L tanks supplied *via* a flow-through system with reconstituted RO water, where the various ion concentrations were; Na^+ = 8.27 mg L^{-1}, K^+ 2.07 mg L^{-1} , Mg^{2+} = 4.38 mg L^{-1}, Ca^{2+} = 24.50 mg L^{-1} and pH = 7.56. The tanks were left for 24 hours with air stones providing continual movement of the water column then half drained and re-dosed with a fresh suspension of NPs to allow for any loss of NPs from suspension due to NPs adhering to the glass wall of the tank, which may affect the actual tank concentration. A 66% water change of 40L was undertaken every 2 days (for ethical reasons), on days 2, 4, 6 and 8 and TiO_2 replenished accordingly, as potential loss of TiO_2 could occur, from using an automatic water change system. The light source over the tanks was by normal fluorescent lighting set on a 12hr on, 12hr off light-dark cycle.

Table 4-1 Experimental set up of the fish tanks at Exeter University

Tank ID	Condition	Fish present
Tank 1	500 μgL $^{-1}$ TiO_2 Nanoparticles	No Fish
Tank 2	5000 μgL $^{-1}$ TiO_2 Nanoparticles	No Fish
Tank 3	Control no NPs	8 Fish
Tank 4	5000 μgL $^{-1}$ TiO_2 Macroparticles	8 Fish
Tank 5	5000 μgL $^{-1}$ TiO_2 Nanoparticles	8 Fish
Tank 6	500 μgL $^{-1}$ TiO_2 Nanoparticles	8 Fish

4.2.2 Mucus collection

In the absence of any standard published method, fish mucus was collected (by Blair Johnston at University of Exeter) by placing a live trout in a plastic bucket for a short duration and stroking it. The fish was subsequently returned to its tank. The secreted mucus was then transferred directly to a dark glass bottle stored on ice. The collected fresh sample,

on ice was sent up to the University of Birmingham on ice for immediate analysis by fluorescence.

The remaining mucus/water sample was centrifuged at 2500 rpm for 10 minutes in 15 mL plastic tubes to reduce water content and the supernatant carefully discarded. The remaining precipitate was frozen and then freeze dried. The resultant powder was weighed (18.2 mg) and retained. When used it was re-hydrated in water by stirring for 24 hours. It was then filtered through a large pore size pre-weighed glass fibre filter paper (GF/F 0.7 μm) and the solution concentration was thus obtained by subtracting the difference in weight from the original dried mucus. 18.8 mg dry mucus, minus loss of polysaccharide (PS) on filter paper (5.5 mg) dissolved in 94 mL of pure water. The resulting stock solution was 143.6 mg L^{-1} and diluted as required.

4.2.3 Materials

Powdered TiO_2 NPs (advertised particle size 25-75 nm) were obtained from Sigma Aldrich (UK). For initial characterisation, the TiO_2 powders were suspended in pure water at 5, 10 and 200 mg L^{-1} and sonicated for 10 minutes prior to analysis by DLS, ERM. Surface area was determined using a Brunauer, Emmett, Teller N_2 gas porosimiter 2010 BET surface area analyser (Micromeritics ASAP 2010 CE). Size and crystallography were measured by XRD (Siemens D5000) at room temperature by Colin Greaves in the Department of Chemistry, University of Birmingham. Tryptophan standard was from VWR and made up in pure water.

4.2.4 Instrumentation

Particle size analysis of tank waters were obtained by dynamic light scattering (DLS) (Malvern HPPS) in disposable plastic cuvettes and run in triplicate. Electrophoretic mobilities (EPM) were measured with a Zetasizer (Malvern instruments). The sample was injected into a pre-flushed quartz capillary cell and at least 10 replicates obtained. Particle size and EPM zeta potential for the TiO_2 suspension were obtained with a nanosizer 5000 (Malvern instruments). Environmental scanning electron microscopy (ESEM) was carried out using a Philips XL30 ESEM-FEG equipped with x-ray energy dispersive spectometer (EDS), using Oxford Inca 300 software. The wet sample was dropped onto a gold plated glass slide and silver paint applied around the edges to ensure good contact. Relative humidity was reduced to 80% at 10 torr at 4^{o} C. Total organic carbon analysis (TOC) was measured by a undertaken using a Shimadzu 5050 carbon analyser, using the TC/IC method certified standards were obtained from Reagacon® and dilutions from 0-50 mg L^{-1} were performed by the machine. Analyses were performed in triplicate unless a CV < 2 was found in the first 2 replicates. Fluorescence excitation, emission matrices (EEM) were produced using a Cary Eclipse spectrophotometer. Emission (Em) wavelengths were 280-500nm and excitation (Ex) was 200- 480 nm at 750 v with a slit width of 5 nm, in a 1 cm pathway quartz cuvette. In some instances, wavelength filters were also applied to eliminate the second order 'Raleigh-Tyndall' scatter line due to NP scattering interference to fluorophore peaks. Comparisons of the two methods (with and without filter) are presented in appendix 5, results agreed by less than 10% error showing comparability between methods.

4.3 Results

4.3.1 Characterisation of the titanium dioxide

Characterisation (Figure 4.2, Figure 4.3, and Table 4-3) of the titanium dioxide powder from dynamic light scattering (DLS) revealed an intensity –weighted average particle size of 222 nm for concentrations of 5 and 10 mg L^{-1}, which was larger than the advertised size of 25-75nm. Interestingly, the measurement, Figure 4.2 (b), at the higher concentration of 200 mg L^{-1} shows a bi-modal distribution with a particle size greater than 1600 ± 200 nm with the presence of larger aggregates up to 6 μm. The bigger particle size is probably due to aggregates forming because of the higher TiO_2 concentration. Since the aggregation rate is proportional to the square of the particle concentration, the collision frequency is thus higher (Kallay and Zalac, 2002).

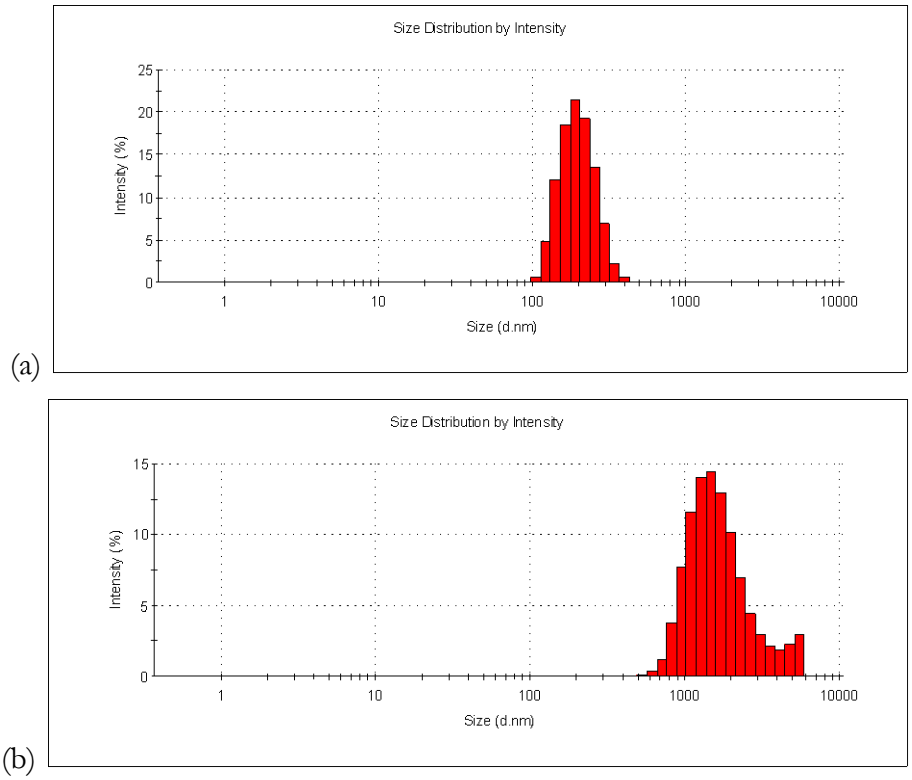

Figure 4.2 DLS histograms of TiO_2 nanopowders size by intensity, (a) 10 mg L^{-1}; histogram peak =190 nm, z-average, 222 nm and (b) 200 mg L^{-1}; modal histogram peak =1484 nm.

The electrophoretic mobilities (EPM) are presented in, Table 4-2. The largest EPM value -2) was achieved for the lowest concentration, 5 mg L^{-1}, and could again be due to higher aggregation at higher concentration (electro static charges) as EPM and particle size are related, due to shrinkage or expansion of the outer layer and is explained more fully in section 3.2.7. The pzc was not established in this work, but at concentrations of 10 mg L^{-1} in pure water the NPs had an EPM value of -0.4 10^{-8} m^2 V^{-1} s^{-1} at pH 5.8. Reported values for pzc are between pH4 and pH 6 depending on crystal structure (Kim *et al.*, 2009; Kosmulski, 2002). Table 4-3 is a summary of particle size for various techniques.

Table 4-2 DLS size and EPM charge results for the TiO_2 at concentration 5, 10, 200 mg L^{-1} in pure water and not tank waters. DLS measured at 5 mg L^{-1} TiO_2.

TiO_2	suspension	EPM	std dev	n	z-average	Stdev	range	n
mg L^{-1}	pH	10^{-8} m^2 V^{-1} s^{-1}			nm		nm	
200	5.32	-0.6	*0*	5	1562	*199.9*	500-6000	3
10	5.88	-0.4	*0.1*	10	227.4	*10.8*	100-450	6
5	5.79	-2.1	*0.3*	10	218.2	*5.3*	100-450	3
0	6.02	0	*0.2*	4				

Table 4-3 Summary of the size data for the TiO_2 nanopowder; (s) donates solid and (aq) aqueous measurement

	manufacturer (s)	XRD (s)		DLS (aq)	BET (s)
	nm	Anatase (nm)	Rutile (nm)	nm	m^2 g^{-1}
Size	25-75	75	110	220	20.8
st dev		*5*	*10*	*8*	

The XRD pattern at 25ºC, revealed a mixture of anatase and rutile (Figure 4.3). Particle size was using Scherrer's formula (Patterson, 1939) based on peak FWHM (full-width at half maximum) analysis, see chapter 3. The anatase was 75 ± 5 nm and rutile component was a

larger crystallite size of 110 ± 10 nm. Surface area was found to be 20.8 m^2 g^{-1} by BET analysis which gave a particle diameter of 68 nm from equation 4.1 and agrees with data from the manufacturer's value and for anatase (XRD). As diameter (*d*) is related to area and assuming particles are spherical geometric equations can be applied for a volume, V (m^3), where, $V = \pi d^3 / 6$ and area, A (m^2), where $A = \pi d^2$ and density, ρ, is in g m^{-3}. The equation for SSA (a_s) is $A/V / \rho$, therefore to convert *SSA* to *d*, simplifies to (Janz *et al.*, 2010);

$$d = \frac{6}{a_s \rho}$$

Eq.4.1

where; *d* = diameter in m and *SSA* (a_s) is m^2 g^{-1}, ρ (TiO_2) = 4.23 10^6 g m^3,. Fluorescence of pure TiO_2 showed low absorbance and high refractivity due to its ability to scatter light. There was a peak at emission 420 nm for most wavelengths, particularly at excitation 255/260 nm which is comparable with the reported values (Melnyk *et al.*, 2005).

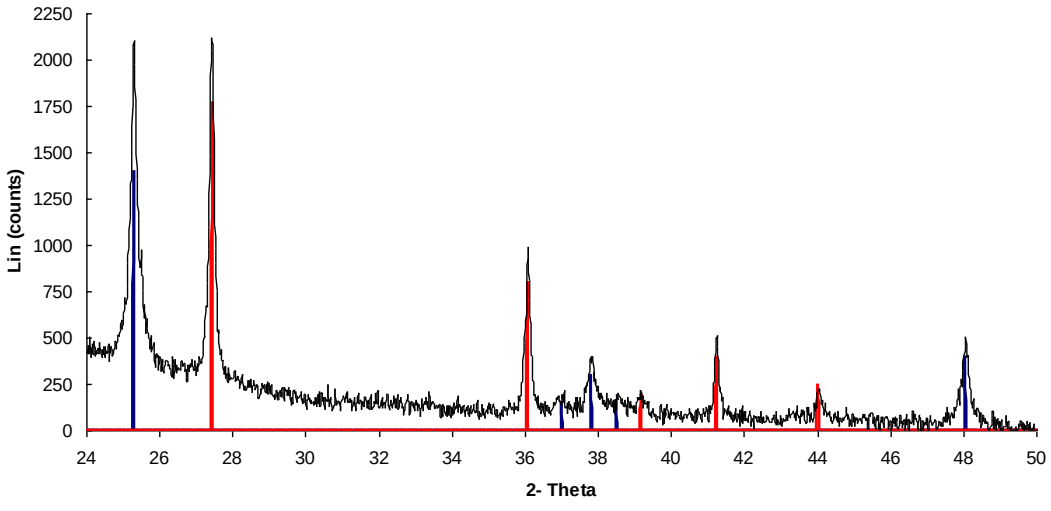

Figure 4.3 XRD pattern of TiO_2, anatase is in blue and rutile is represented in red, analysis was at 25°C.

4.3.2 Characterisation of fish tanks days 1-9

Tanks were analysed four times during the nine day experiment, just prior to adding fish (Time, T = -1 day); at 24 hours after adding fish (T = 24 hours); at 5 days (T= 5 day) and on the final day (T=9 day) before the fish were killed for analysis. *In-situ* measurements of pH and conductivity were taken daily at Exeter and are presented in Figure 4.4. Tank pH range is between pH 6.3 and 8, well within ranges normally expected for aquatic lowland river pH. Interestingly, the dip in pH co-insides with the introduction of fish on day one. Tanks 1 and 2 also follow this pattern, albeit to a lesser extent with no fish. Otherwise, tanks follow the same pattern of daily pH change. Conductivity ranges from 200-250 μS cm^{-1}, with the exception of elemental titanium which ranges from 350 – 400 μS cm^{-1}. This may be due to the ammonium nitrate present in the Ti standard, but exact solution composition is unknown .In the presence of fish, the conductivity is higher than in absence of fish (tanks 1 and 2).

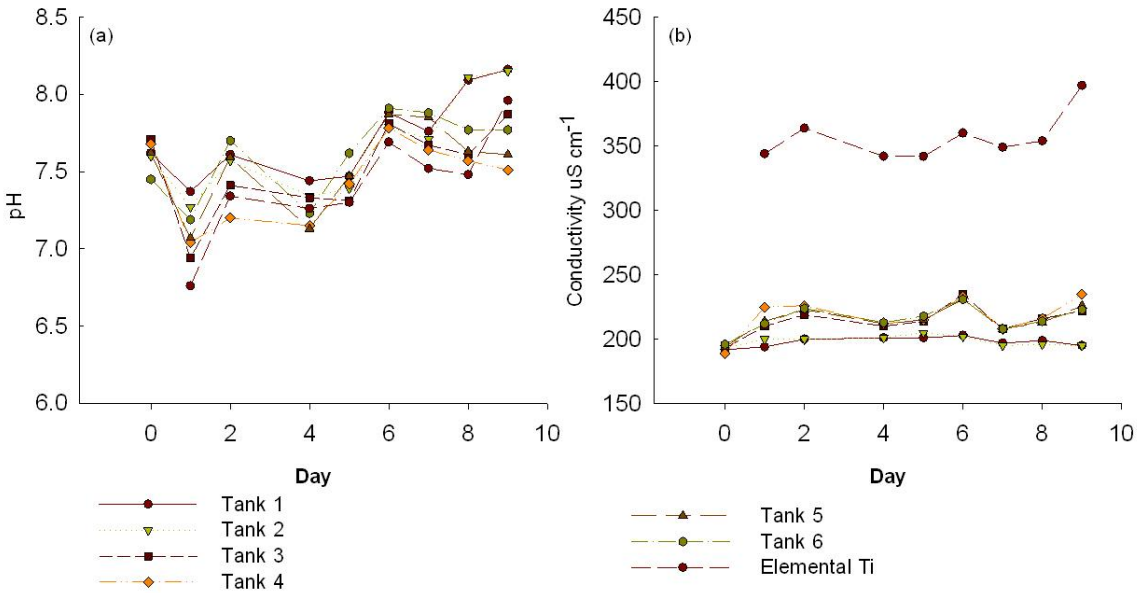

Figure 4.4 Daily *in situ* measurements of the fish tanks for a) pH and b) conductivity measurements were taken by Tessa Scown at Exeter University

Figure 4.5 shows particles taken on day 2 from tank 5 containing macro particles. The insert shows the outlined particles which were measured using digital micrograph software. Average particle size (187 nm) shown here is in agreement with size from DLS shown in Table 4-2. Almost immediately after adding the fish, large agglomerates were observed and the milky appearance of the waters containing the TiO_2 nanoparticles cleared. It was hypothesised that exudates produced by the fish accelerated the aggregation of the TiO_2 NPs causing the NPs to settle to the bottom of the tanks.

(a)

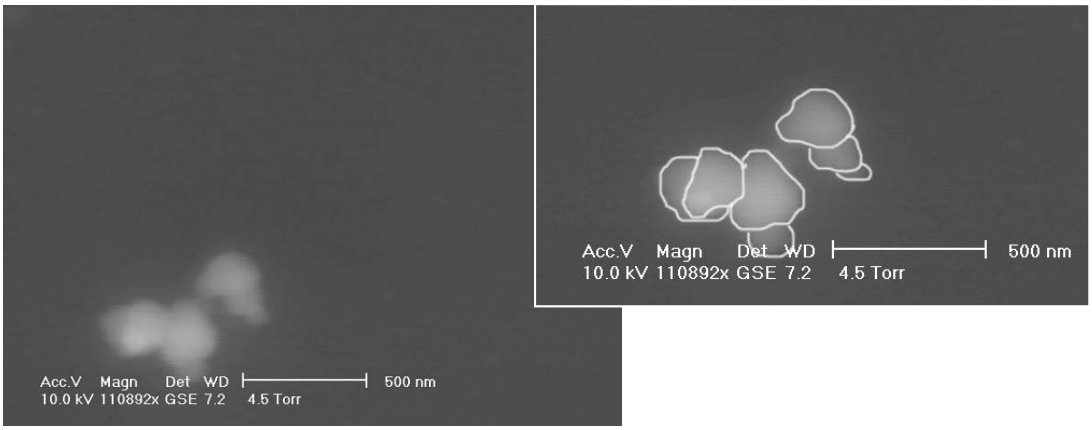

Figure 4.5 Figure 1 ESEM image TiO_2 NPs of day 2 tank 5 inset shows enlargement and the particles outlined in white are between 100 and 250 nm (mean 187 nm)

Analysis of the sediments from the fish tanks by ESEM, (see Figure 4.6, (b) to (d)), at 9 days revealed dense amorphous aggregates in the tanks containing electron dense, particles of high contrast and corresponding EDS analysis of these aggregates confirmed the presence of titanium embedded within the matrix. The image shown in Figure 4.6 (a), of the control experiment with fish is probably tank debris of biological origin and EDS analysis did not reveal the presence of any titanium. Figure 4.6 (b) contained bulk titania at 5000 μg L^{-1} and shows the TiO_2 and mucus together (scale is 10 μm) a similar structure is also seen in Figure 4.6 (c), of the TiO_2 NPs at 5000 μg L^{-1} (scale is 5 μm) and Figure 4.6 (d), TiO_2 NPs 500 μg L^{-1} (scale is 2 μm). EDS also revealed the presence of other salts, used to formulate the synthetic tank waters.

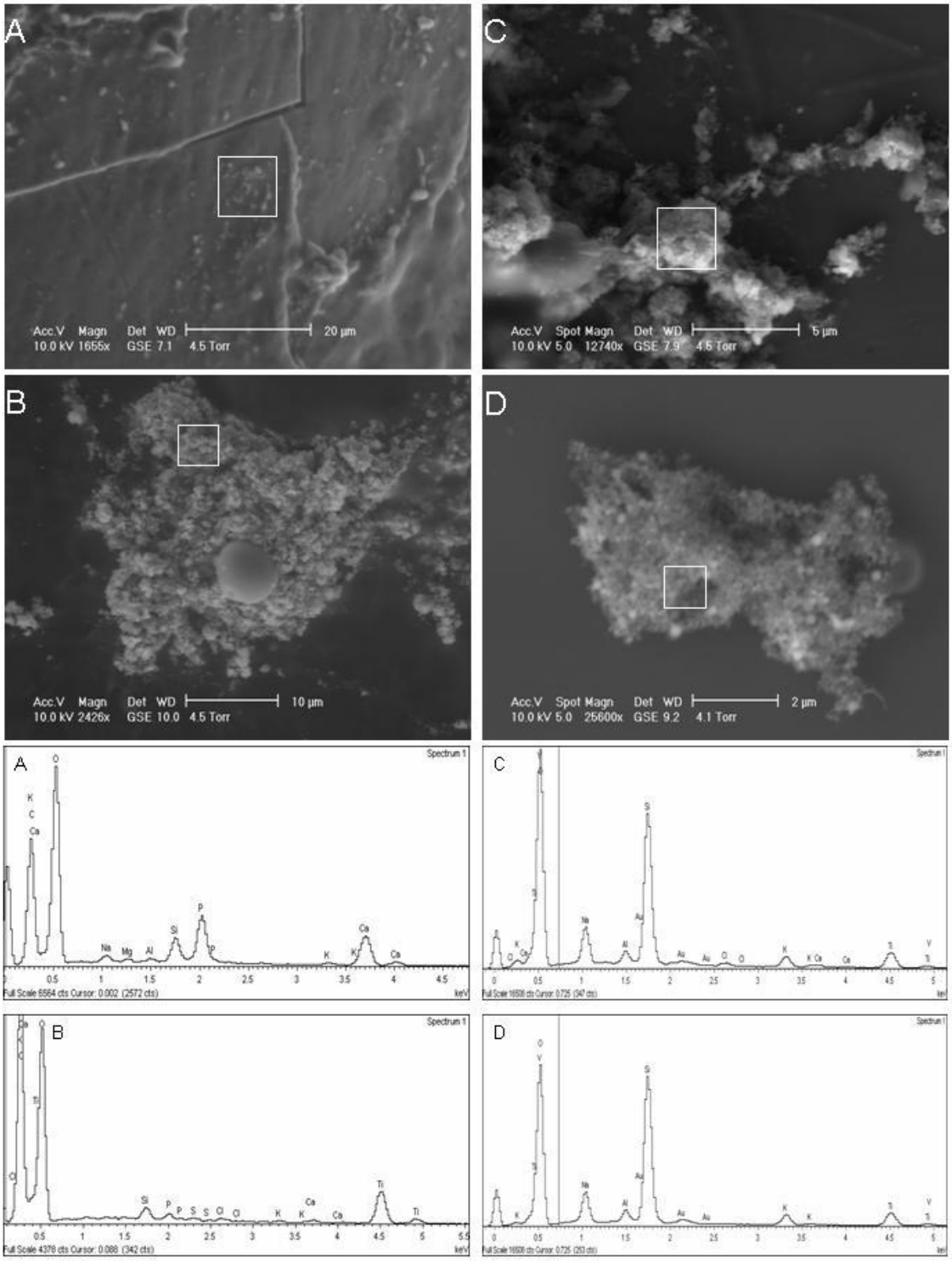

Figure 4.6 Environmental scanning electron micrographs of fish tank waters showing EDX spectrum analysis (white square) at day 9 for, a) Fish no particles, b) Fish with 5000 µg L^{-1} bulk TiO_2, c) Fish with 5000 µg L^{-1} TiO_2 NPs, d) Fish with 500 µg L^{-1} TiO_2 NPs. Images were analysed at 4.5 Torr, 10kV 80% humidity at 4 ^oC and are representative of the 25 plus images taken of each sample (Taken by the author, and published in Johnston et al., (2010)).

Particle size analysis of the tank waters was analysed by DLS, shown on four occasions over the 9 day period (**Figure 4.7**). Z-average, rather than number average, as discussed in chapter 3 section 3.2.3, was considered the most suitable because the presence of aggregates would make the number-average inaccurate. Z-averages show a general particle size increase over time although tanks 2, 3, 5 and 6 show a decrease in suspension particle size on day 9 which may be due to larger particles sedimenting (removal from water column). Stokes' law (Eq 4.2 below), the settlement velocity, W_s (m s^{-1}), can be applied to establish the time taken for the NPs to settle to the bottom of the tank, working on the assumption that particles are spherical (van der Perk, 2006).

$$W_S = \frac{(\rho_S - \rho_w) g d^2}{18\mu}$$

Eq.4. 2

Where ρ_s is the density of TiO_2 (4 kg m^{-3}), ρ_ω is the density of water (0.999 kg m^{-3}); μ is the dynamic viscosity of water (1.3 10^{-3} kg m^{-1} s^{-1} at 10 ^{O}C), g is gravity (9.8 m s^{-2}), d = diameter of the particles in metres. So for pure TiO_2 NPs of 220 nm it would take 13.6 weeks to settle over a distance of 50 cm at 10 ^{O}C, however for particles of 1000 nm this would be reduced to 4 days and for 3000 nm, 11 hours.

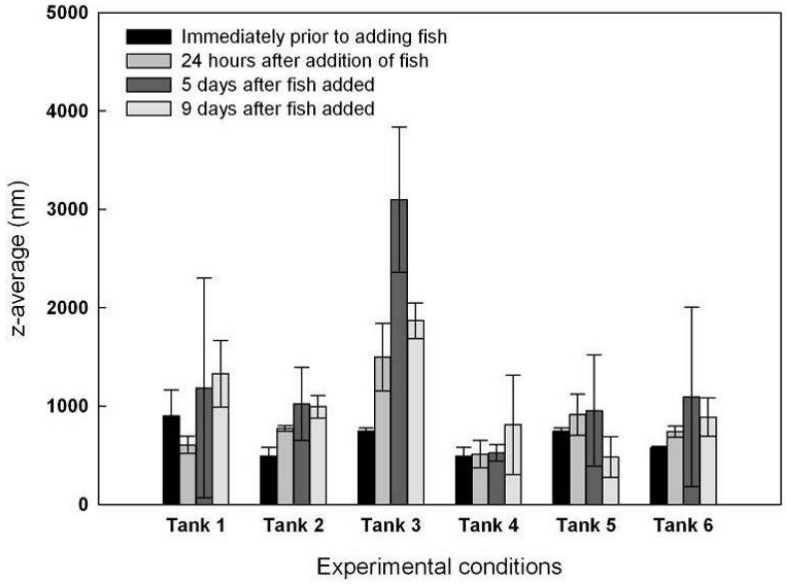

Figure 4.7 Particle size results from DLS show the z-averages (nm) for all tanks taken at 0, 1, 5 and 9 days error bars are standard deviations of at least three measurements.

The tank containing the fish only showed a massive increase in particle size on day 5 to 3000 nm. This is certainly due to biological particulate matter. Interestingly, Tank 4, containing the macro (bulk) particles, showed the smallest particle size overall. In Figure 4.7 trends are difficult to assess due to the large error bars (standard deviations). In DLS this may indicate instability in terms of NP size. However there was an exception with tank 3 that contained the fish only, which showed an increase in particle size on day five which could be solely attributed to organic material, since there were no NPs present. Figure 4.8 shows the corresponding EPMs for the period. Generally, EPM values are between -1 and -1.6 10^{-8} m^2 V^{-1} s^{-1} and this value is not sufficient under these conditions to maintain particle repulsion and so for particles to remain in suspension.

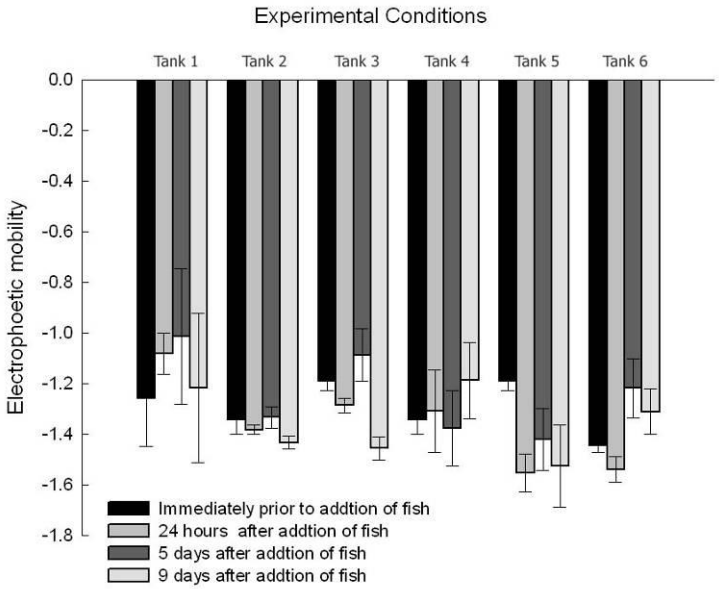

Figure 4.8 Electrophoretic mobility (10^{-8} m^2 V^{-1} s^{-1}) for the fish tanks sampled prior to adding fish, at 24 hours, 5 and 9 days.

There was a clear difference in TOC concentration between tanks that contained fish and those that were absent of fish (see Figure 4.9), showing that the fish contributed to TOC in the tanks. Data ranges from 1 mg L^{-1} to 3.5 mg L^{-1} over the period whereby, concentration increased in only tank 3 containing fish after 24 hours with concentration reaching

maximum levels around 3-3.5 mg L^{-1}after day 5 (See Table 4-2). Actual trends from figure 4.7, however, cannot be drawn due to large error bars.

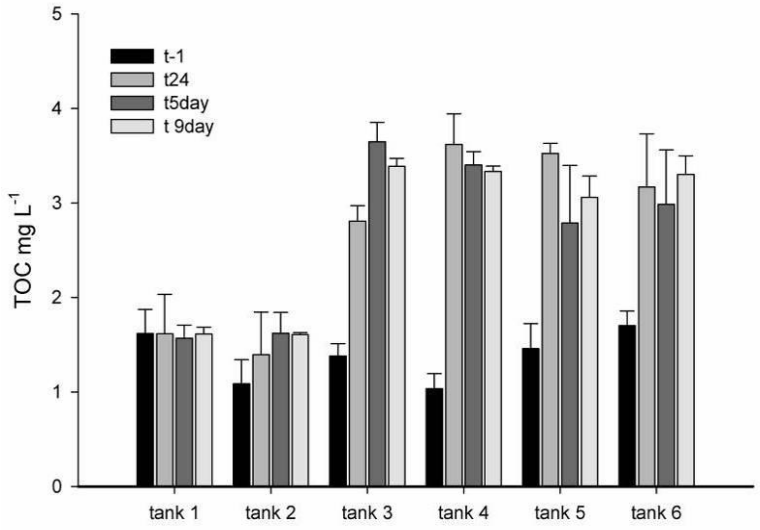

Figure 4.9 Total organic carbon measurement of fish tank waters taken at 0, 1, 5 and 9 days error bars represent standard deviations of two measurements.

4.3.2.1 EEM fluorescence fish tank analysis

As with TOC measurement there was a difference in fluorescence intensity between the tanks containing fish compared to tanks without fish. Fluorescence, excitation-emission matrix (EEM), shown in Figure 4.9, analysis can give an optical breakdown on carbon type, the two peaks, shown more clearly in Figure 4.10(d) (Ex λ230 nm and Ex λ280 nm) are associated with the amino acid, tryptophan nominally known as tryptophan-like (Baker and Inverarity, 2004).

Fluorescent EEMs in Figure 4.10 are for tanks, with and without fish, and with and without TiO_2 NPs, sampled on day 1 at 24 hours and on day 5. There is a general increase in fluorescence from day 1 to 5 with tank waters that had contained fish, compared to tank waters without fish and agrees with the TOC data in Figure 4.8. The tank containing NPs

only, does not show either significant change in fluorescence intensity or indication of peak shifting.

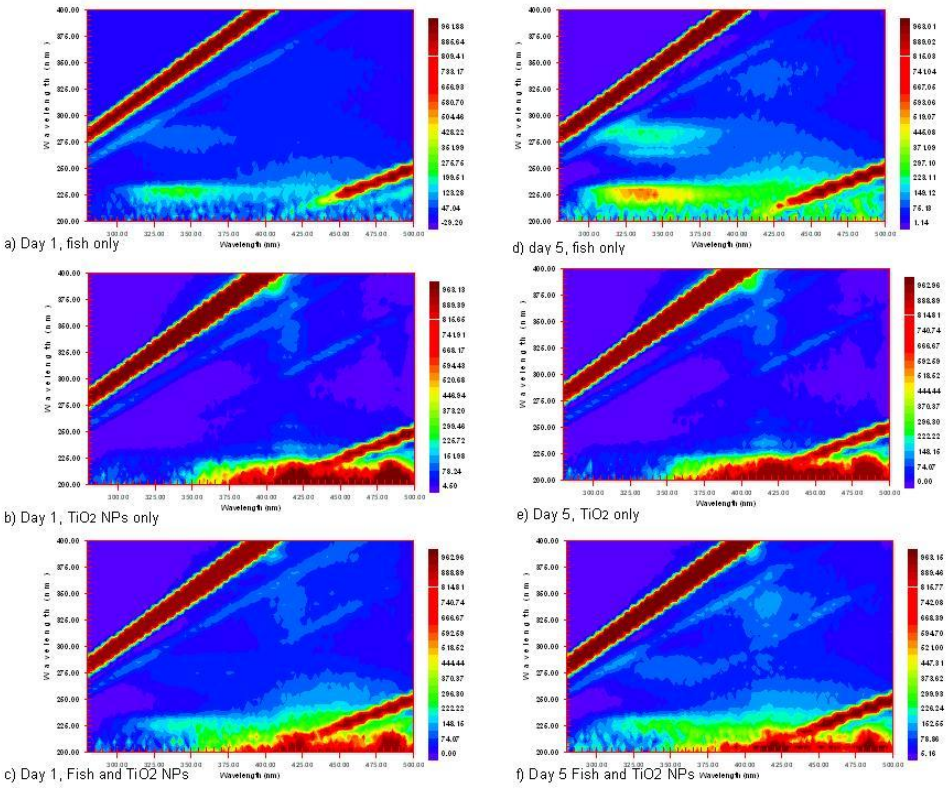

Figure 4.10 EEMs for (a-c) days 1 and (d-f) for day five for the tanks with fish only (top), TiO_2 NPs only (middle) and fish and NPs (bottom). X = emission (nm) and y= excitation (nm). NB colour scale bar varies between plots.

In both tanks containing NPs, a vertical scatter line at Em λ420 nm is observed which can be attributed to the TiO_2 NPs, fluorescence was also observed to emit at λ420 nm from several excitation wavelengths and could be attributed to scattering from the TiO_2. However, Em at λ260 nm for TiO_2 is reported in the literature (Melnyk *et al.*, 2005). Figure 4.11 shows the Raman corrected fluorescence intensity of peaks at Ex 230 nm and Ex 280 nm. Qualitative similarities of the data in Figure 4.9 and Figure 4.11 indicate a relationship between TOC and tryptophan fluorescence, where the EX/Em 230/350 nm and TOC give $R^2 = 0.67$ Peak 2 at Ex 280nm, indicating that a good proportion of the OC is fluorescent in the tryptophan region. Fish were observed to shed mucus quite visibly and was the probable

material of the fluorophore. Mucus and its relationship with the TiO_2 NPs is the subject of the following investigation.

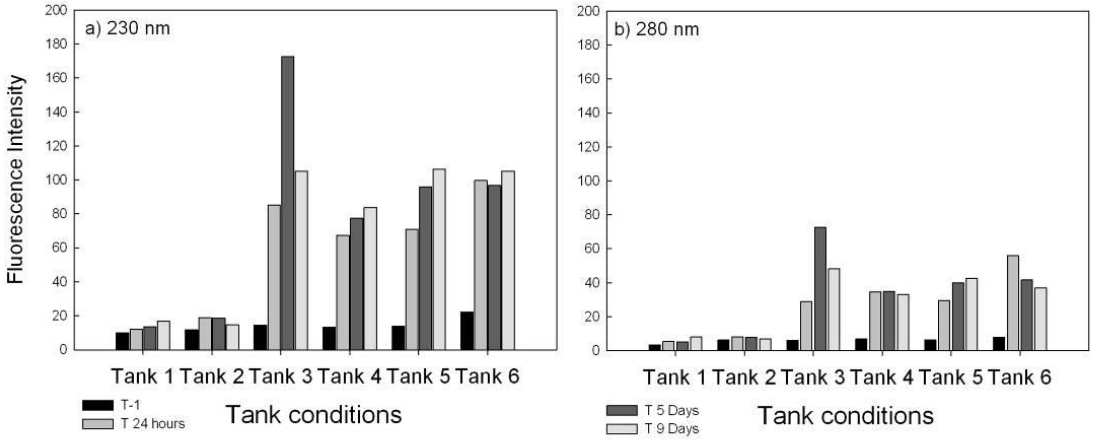

Figure 4.11 Shows the max intensity tryptophan–like fluorescence peak a) ex 230 Em 325- 330nm and b) EX 280 nm for the fish tanks at just before fish added, day 1, day 5 and day 9.

From the fluorescence traces in Figure 4.12, the tanks with fish show a reduction in fluorescence intensity in the presence of TiO_2 NPs. Figure 4.12, shows the fluorescence in tanks with and without fish and with and without TiO_2 NPs (5 mg L^{-1}) for tanks samples taken over the nine day exposure. For excitation λ 230, λ 280 nm (tryptophan-like) and λ 260 nm (TiO_2 NPs) (Melnyk *et al.*, 2005). The peak at λ 450 nm is a second order Raman scatter line and should be ignored.

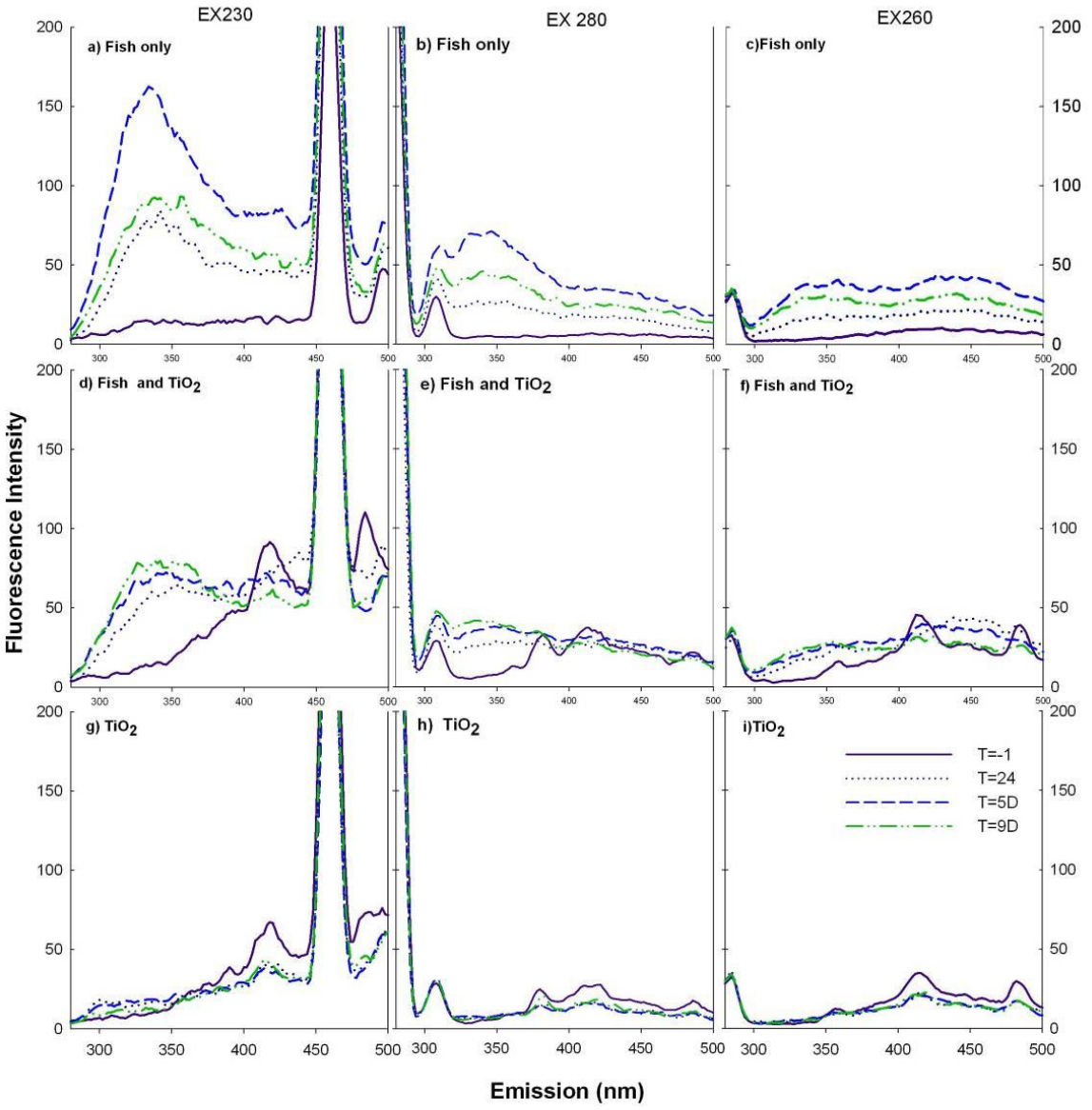

Figure 4.12 Fluorescence emission spectra at Ex 230nm for days 0-9 for fish only (top) fish and TiO_2 NPs (middle) and TiO_2 only (bottom), where TiO_2 concentration is 5 mg L^{-1}. Spectra shown λ_{ex}= 230, 280 and 260 nm. Peaks have been corrected to 20 Raman units and data smoothed by averaging 3 data points for each data point plotted.

With the fish only tank, a steady increase in the tryptophan-like fluorescence is observed over the first 5 days to over 150 fluorescence intensity units (FIU), but a reduction is seen at day 9 to less than 100 FIU probably because of aggregation and sedimentation. In the tank containing fish and TiO_2 NPs, the peak at Em 330 nm is 75 FIU, very much reduced compared to the tank water containing only fish. No fluorescence is observed at the lower wavelengths for TiO_2 NPs only. However, a peak at Em 420 nm is observed in Figure 4.12

(d) and (g). This peak is reduced after day 1, probably due to loss of NPs by sedimentation and coincides with the increase in particle size seen in **Figure 4.7** and in EEMs, Figure 4.10(e).

The fluorescence examined at Ex 260 nm, also shows a peak at Em 420 nm, this peak is not observed in the fish–only sample so is probably associated to the TiO_2. The peak below Em 300nm is a scatter line and should be ignored. At Ex 260 shows a distinct, pattern for the TiO_2 Figure 4.12 (f) and (i) with twin peaks at Em 420 and 480, a similar pattern appears at Ex 230 nm. Neither peak is present in the tank containing fish only. At 24 hours the tanks with fish and the tanks containing both fish and titania show the same level of fluorescence, but at day five and day nine the differences are that the tank containing both fish and titania show reduced fluorescence intensity.

4.3.3 Characterisation of the fish mucus

Collected fresh fish mucus showed two clear fluorophore peaks in Figure 4.13 at Ex 230 nm and at Ex 280 nm which was consistent with tryptophan fluorophores. To date there is relatively little information in the literature describing fish mucus fluorescence and this experiment was conducted to try to establish the quantity of mucus in the tank waters and to establish its relationship and behaviour with the TiO_2 NPs.

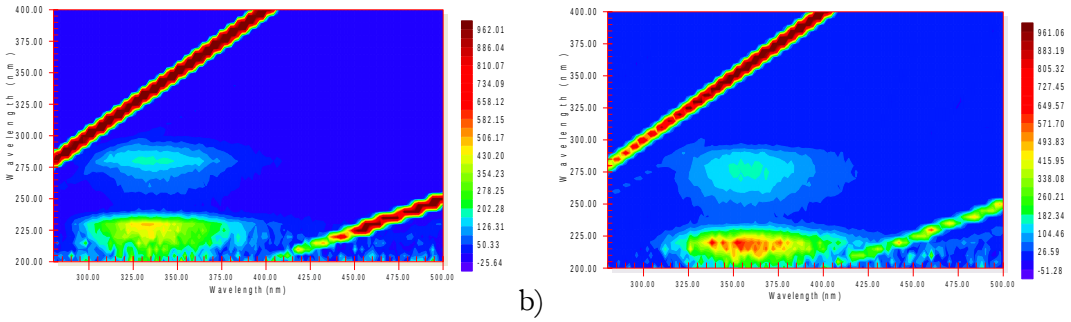

Figure 4.13 Fluorescence EEMs a) of fresh fish mucus diluted x 5. b) tryptophan standard 80 µg L^{-1}.

The fresh, raw mucus, in Figure 4.13 (a), demonstrated a strong fluorescent signal in the tryptophan-like regions (peak T1 and T2) and required dilutions of 5 times and 10 times to ensure that inner filtering effects were eliminated. Similar peaks were observed same region from the fish tank waters. The tryptophan standard also showed florophores in this region (Figure 4.13 (b)). The aquarium water on its own did not show fluorescence. Further experiments were conducted on the re-hydrated filtered (0.7 μm) sample and then mixed with TiO_2 NPs at concentrations of 0, 0.5 and 5 mg L^{-2}. A stock solution of tryptophan standard (*VWR*), was used to make a series of standard solutions and fluoresced using the same method.

4.3.4 Quantification of mucus from fluorescence

The fresh mucus was quantified from the amount of dry residue obtained in mg after freeze-drying 500 ml of the fresh mucus and water. A stock solution was then made from this freeze dried material which was 18.8mg/ 500 ml equating to 37.6 mg L^{-1} and solutions were then made from this diluted stock. From the amount of dilution of the fresh mucus, this was calculated linearly e.g. a five times dilution which was equal to 7.52 mg L^{-1} which gave a corrected fluorescence intensity of about 398 units. The resultant freeze-dried powder was re-hydrated by the method outlined in section 4.2.2. In comparison to the tryptophan standard, the mucus fluorescence was compared and quantified and compared with the TiO_2 NP doped fish tanks. The intensity per gram of mucus was less for the freeze dried substance than for fresh material, about 10%. Figure 4.14 compares the slopes between fresh and dried mucus.

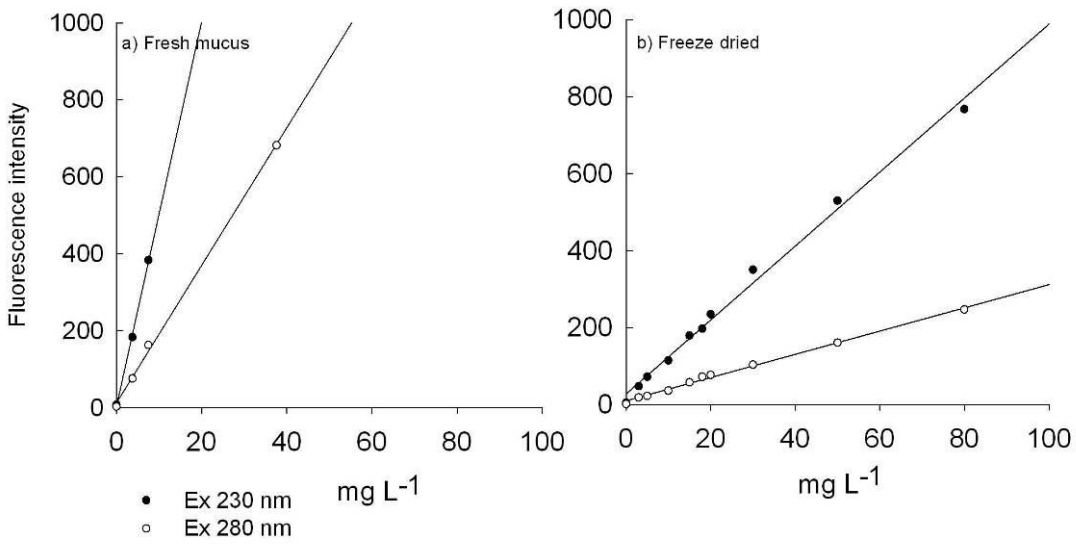

Figure 4.14 Fluorescence correlations of (a) Fresh mucus (b) freeze–dried mucus dilution at 230 (filled circle) and 280 nm (open circle).

Figure 4.14(a) shows the fluorescence response to dilutions of fresh mucus at 230 nm and 280 nm and Figure 4.14 (b) is the maximum fluorescence intensity of the freeze dried mucus at different concentrations 0 - 80 mg L^{-1} for Ex 230 and 280 nm. A linear relationship was observed for both sets of data and the regression equations are presented below (Eq 4.3 to 4.6). The gradient for the fresh mucus is much steeper than for the dried mucus indicating its higher fluorescence per gram of dry matter. Intercept values donate fluorescence background values.

$y = 49.962x + 3.5637$ $R^2 = 0.9986$, λ 230 nm

Eq.4.3

Eq.4.$y = 17.884x + 12.309$ $R^2 = 0.9987$, λ 280 nm

Eq.4.4

$y = 9.6067x + 27.938$ $R^2 = 0.9933$, λ 230 nm

Eq.4.5

$y = 3.0168x + 9.966$ $R^2 = 0.9952$, λ 280 nm

Eq.4.6

Equations Eq.4.3 and Eq.4.4 are the regression equations for the fresh mucus in Figure 4.14 (a) for 230 nm and 280 nm and Eq.4.5 and Eq.4.6 are for the freeze dried mucus in Figure 4.14 (b) at 230 nm and 280 nm. Figure 4.15 shows the corrected fluorescence intensity to fish mucus using equation 4.3 applied to Figure 4.15 (a); and equation 4.4 applied to Figure 4.15 (b) and is within range of TOC data in Figure 4.9 (max concentration is 3.45 mg L^{-1}).

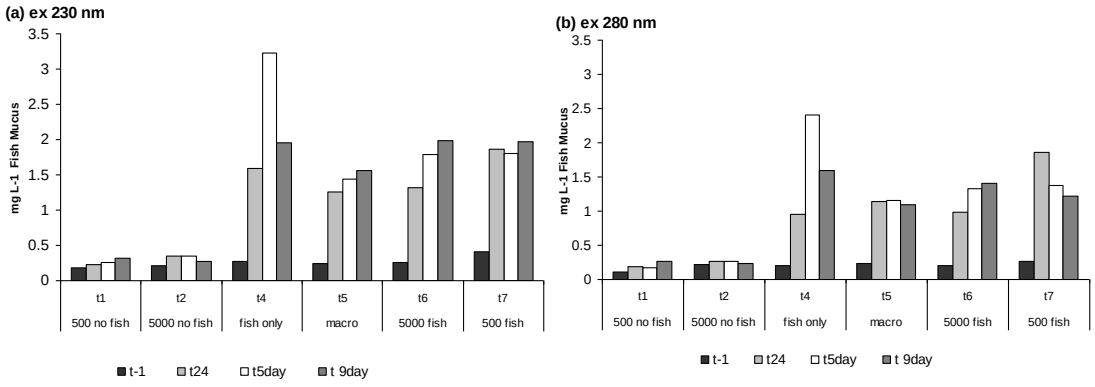

Figure 4.15 Fluorescence intensity corrected to mg L^{-1} fish mucus for (a) ex 230 nm and (b) ex 280 nm

Figure 4. 16 shows the fluorescence EEMs for the free dried mucus, at 5, 15, 20 and 80 mg l^{-1}. Compared to the EEMs in Figure 4.13 the fresh mucus, changes have occurred in the fluorescence resulting in considerable left shifting of the tryptophan-like peak to lower wavelengths and with the appearance of an additional peak at 310 nm.

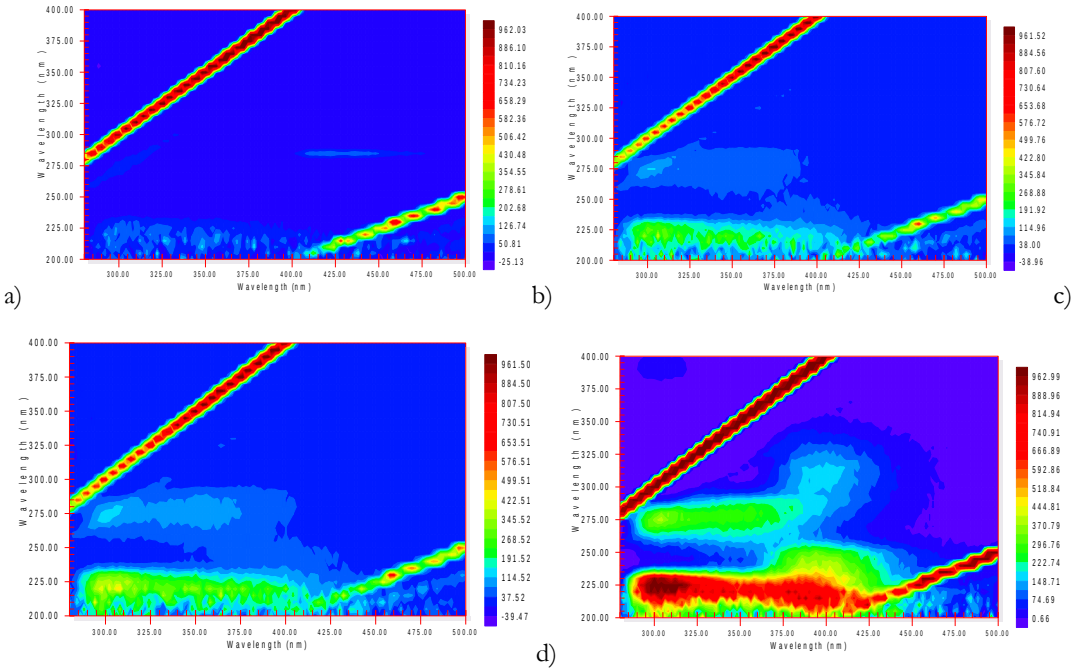

Figure 4. 16 Fluorescence EEMs for a) 5, b) 15, c) 20, d) 80 mg L^{-1} of the freeze dried mucus

4.4.3.1 Estimating the quantity of tryptophan-like compounds in the mucus

Standard curves of tryptophan, presented in Figure 4.17, Eq.4.7 and Eq.4.8 were also applied to establish the quantity of tryptophan residue in the mucus make up. Pure tryptophan is highly fluorescent at concentrations less than 1 mg L^{-1}.

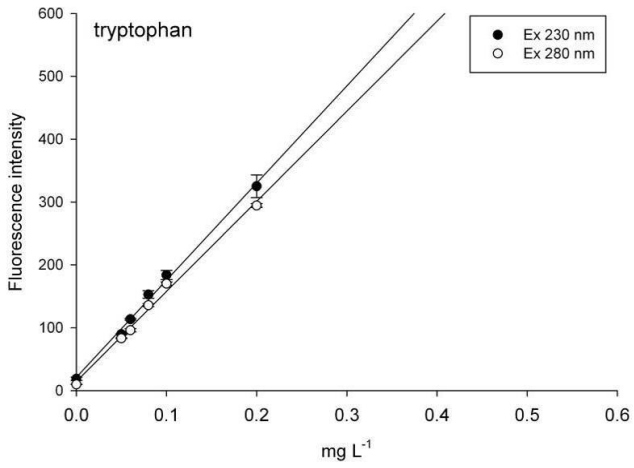

Figure 4. 17 Fluorescence intensity of pure tryptophan at a series of concentrations in pure water at Ex 230 nm and 280 nm.

$y = 1545.4x + 21.094$ $R^2 = 0.9955$, λ 230 nm

Eq.4.7

$y = 1432.7x + 14.622$ $R^2 = 0.9938$, λ 280 nm

Eq.4.8

Table 4-4 shows the calculated quantity of tryptophan in the fresh and freeze-dried mucus. The amount of tryptophan in both the fresh and freeze dried mucus can be estimated by the application of equations 4.3-4.6 and then using equation 4.7 or 4.8 to gain the amount of tryptophan present in 1 mg L^{-1} mucus, whereby the calculation is done by substituting one into the other. Excitation at 280 nm was less sensitive for fluorescence and hence the estimated tryptophan numbers are slightly different. It follows that there is 1-2% tryptophan present in mucus.

Table 4-4 calculated quantity tryptophan present in mucus per mass and as a percent

Mucus type	Excitation wavelength λ	mucus mass Mg/ L	fluorescence intensity a.u	calculated tryptophan mg Trypt/ 1 mg mucus	calculated tryptophan %
Fresh	230nm	1	53.53	0.02	1.89
	280nm	1	30.19	0.01	1.15
Freeze-Dried	230nm	1	37.54	0.01	0.93
	280nm	1	12.98	0	.0
	280nm	10	40.13	0.02	0.18

4.3.5 Fluorescence quenching of TiO_2 NPs with mucus

Both fluorescence quenching and enhancement were observed with the TiO_2 NPs in the presence of freeze-dried mucus (Figure 4.18). Where fluorescence quenching is the loss of fluorescence intensity (FI) from other chemicals or an effect of temperature (Manciulea *et al.*, 2009). Titanium dioxide NPs were mixed with the freeze dried mucus to establish the relationship between the NP and the natural fish exudate by means of fluorescence. The

freeze dried mucus was used to study the difference concentration effects. The extent of the quenching was not constant with the amount of quenching observed being dependant on the wavelength pairs analysed. Figure 4.18 shows fluorescence intensity results from the mixing of 0, 0.5 and 5 mg L^{-1} TiO_2 NPs with freeze dried mucus at 0, 5 and 20 mg L^{-1} mucus.

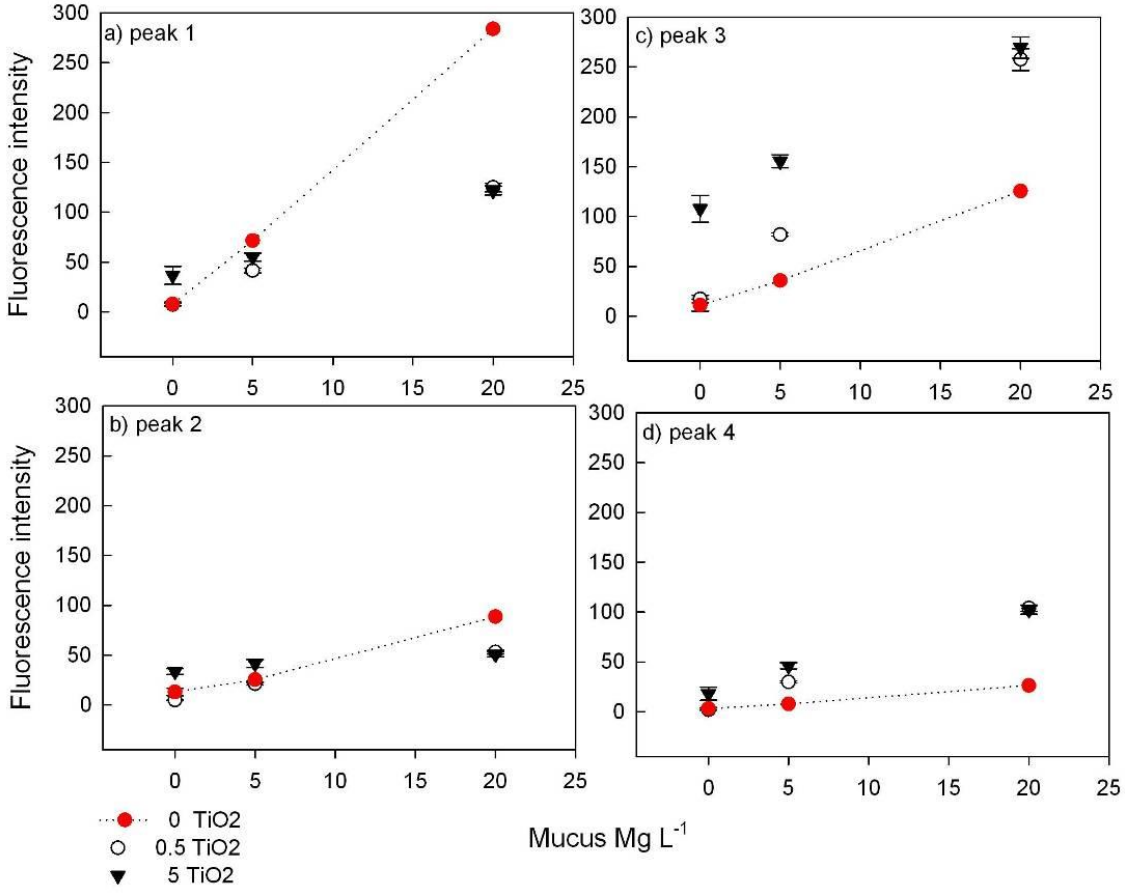

Figure 4.18 Titanium dioxide NPs and mucus with the dotted line represents the mucus only. Error bars represent the standard deviation of three samples for ex/ at a) 230 nm b) 280 nm c) 230/350 nm; d) 310

In Figure 4.18, the most mucus quenching is observed for peak 1 (a, Ex 230 nm), where the FI of the mucus decreases in the presence of TiO_2 NPs. For peak 2, mucus at 5 mg L^{-1} FI decreases in presence of 0.5 mg L^{-1} TiO_2 NPs, but FI increases for 5 mg L^{-1} TiO_2 NPs.

However, at 20 mg L^{-1} of mucus, FI decreases in the presence of TiO_2. For peak 3, (c, Ex/Em 230/350 nm) and peak 4 (d, Ex 310 nm), the FI of the mucus is enhanced at all TiO_2 concentrations. Peak 2 fluorescence intensity did not show much change with increased mucus concentration. This figure demonstrates that the suppression or enhancement of the fluorescence varies with the emission/excitation peak. Optical filters were applied during the scans to eliminate interference from secondary and tertiary scatter lines a result of internally refracted light. A number of samples were run using both methods and the peaks heights recorded (these are listed in Appendix 5). Comparisons between a particular sample analysed with and without the applied optical filters gave an overall error of less than 10 % over 72 measurements.

4.4 Discussion

4.4.1 Nanoparticle characterisation

Characterisation of the TiO_2 NPs by DLS and by XRD revealed a particle size between 75 and 220 nm (DLS =220nm), larger than the manufacturer's indicated size of 25-75 nm. The calculated size from BET, 68 nm, does however fit within the manufacturer's range. Other studies have also found discrepancies between the advertised particle size and actual particle size (Adams *et al.*, 2006) and this may simply be because the different sizing techniques employed are measuring different things such as primary particles, hydrodynamic diameter, crystal structure or aggregation and will depend whether it is a dry powder or in aqueous suspension. Furthermore, the fact that aggregated particles, particularly working near the pzc, plays a strong role in observed particle size in data from a number of techniques, even after sample sonication, will affect results (Dunphy Guzman *et al.*, 2006a). Redispersions of nanopowders are also likely to aggregate due to close proximity and charge effects, resulting in polydisperse suspensions. As very small changes in the NPs size, shape, charge, crystal

structure etc., can have large effects on its behaviour with itself and other chemistry. Full NP characterisation is an important prerequisite for understanding the mechanisms in toxicological or fate and behavioural studies (Jiang *et al.*, 2009).

4.4.2 Characterisation of NPs in the fish tanks

In general, particle size (here given as, DLS, H_d z-average) in the fish tanks appear to increase over the nine day exposure, although variations between tanks and large error bars in the data mean that there are no apparent trends. However, in tank 3 only with fish only present (no NPs) there was also an increase in particle size after day one, and this was attributed to a build up of biological exudates, but again, with large measurement error in the data conclusions are tentative and therefore further conclusions cannot be drawn.

For the tanks that contained fish and NPs, the effects of flocculation and sedimentation were observed by eye, and these sediments were selected for viewing with ESEM. These ESEM images showed interactions between the organic fish mucus, particulates and NPs, leaving only smaller particles in suspension. In this work, macro (bulk) TiO_2 dispersions showed smaller sizes than the nano TiO_2 and this may be due to either sedimentation out of suspension and more probably, that smaller NPs can form larger aggregates or the particles were inaccurately measured by DLS (Pettibone *et al.*, 2008). The former was demonstrated by Dunphy Guzman *et al.,* (2006a) who by using different measurement techniques, estimated that with a (XRD) primary particle, or crystal size, of 5-12 nm, TiO_2 formed aggregates consisting of between 8 and 4000 NPs, <150 nm (DLS). However work with NP exposure to more soluble NOM tends to increase the stability of NPs (Diegoli *et al.*, 2008).

Electrophoretic mobility results in this work exhibited negative values. The observed values were thus insufficient to maintain particle stability and no obvious trends were observed. In

the presence of fish, large flocculants of NPs were visible and identified by ESEM as TiO_2 NPs intimately bound to the fish exudates. The pzc of TiO_2 NPs reported in the literature are to be for pH values 4 to 5.2 (Domingos *et al.*, 2009b) the pH of the fish tanks in this study were pH 6.6-7.8 with electrolytes present, electrolytes may affect TiO_2 NPs stability (Dunphy Guzman *et al.*, 2006a). Domingos *et al.,* (2009b) found that stability of TiO_2 NPs generally decreased with increasing electrolyte concentration consistent with a decrease in the thickness of the electrical double layer and a consequent decrease in repulsive electrostatic interactions among the TiO_2 particles.

4.4.3 Fluorescence signals from the fish tank waters

Fluorescence signals were seen from both the NPs and from the presence of fish in the fish tanks. Tryptophan-like fluorophore intensities correlated with the TOC concentrations, which was then attributed to fish mucus production from the analysis of pure fish mucus. Tanks waters did not increase in TOC/fluorescence levels, probably due to sedimentation or from the water tank being changed every other day. Mucus production is a result of fish stress and is considered to act as a physical and chemical defence barrier against predators and pollution (Alexander and Ingram, 1992; Federici *et al.*, 2007). In this experiment amounts of mucus were produced by the fish in response to exposure to NPs and similar observations concerning excess mucus production with exposure to carbon nanotubes has been noted elsewhere (Federici *et al.*, 2007).

It is possible that the photocatalyic properties of the TiO_2 may have acted on the organics present in the tanks by degradation under the UV light producing an inorganic carbon by-product (Melnyk *et al.*, 2005). However, there was insufficient evidence to support this theory in the fluorescence data and further work is required here which would involve

exposure to UV light and timely fluorescence analysis. A slight increase in inorganic carbon from the fish tanks containing TiO_2 particles and fish was observed. Concentrations were lower for either the NPs only or fish only tanks. However, as tank waters were changed every other day this theory is inconclusive but could be considered a subject in further work.

4.4.4 NPs and mucus

From fluorescence analysis and additional experiments, mucus was found to contain a tryptophan-like residue of about 1-2%. Fluorescence quenching occurred on mixing the mucus with the NPs at excitation 230 nm and less for ex 280, but this was not observed with all Ex/Em fluorophores and at Ex 310 nm and Ex/Em 230/350 nm fluorescence enhancement was seen for mucus in the presence of the TiO_2 NPs. Work by Manciulea *et al.,* (2009) showed iron oxide nanoparticles with fulvic acid were more effective quenchers when in the aggregated state and metal and metal oxides are known to quench fluorescence (Ohno *et al.*, 2008). Otherwise, little work has been reported of the behaviour of fluorescence quenching of nanoparticles and NOM.

In some studies, it has been seen that toxicity was not simply due to the size of the primary particle (Pettibone *et al.*, 2008), but on its ability to form aggregates. Once formed, and depending on other external stabilising or destabilising factors, large aggregates may be unable to penetrate biota, resulting in little or no effect or harm (Warheit *et al.*, 2006). The fish here produced mucus, which in turn adhered to the NPs; and aggregation and sedimentation removed them from the water column. The fish themselves were not observed to be affected by the presence of the TiO_2 NPs over the nine day exposure (Johnston *et al.*, 2010).

4.5 Conclusion

Trout fish exposed to TiO_2 NPs produced skin mucus exudates, most likely as a defence mechanism against the added NPs. TiO_2 NPs were associated with fish mucus. The mucus increased flocculation of nanoparticles which sedimented to the bottom of the tank. This process has several implications, particularly for their detoxification and removal from surface waters. Compared to TOC results there was a notable decrease in fluorescence of the tanks waters containing the TiO_2 and the fish together. The decrease in fluorescence may be due to 1) sedimentation of NP-mucus aggregates 2) quenching of mucus fluorescence 3) degradation of mucus by TiO_2 NPs, 4) routine water removal during exposure or 5) reduction in mucus production.

This chapter has dealt with titania NPs and their interactions with fish exudates and has shown that there are biological materials that may aid removal of NPs out of suspension. The mucus produced by the fish was fluorescent and quantifiable both to the amount of tryptophan present in the mucus and to organic carbon concentration making it possible to quantify the amount of mucus produce in response to NP dose. Chapter 5 explores the aggregation of iron oxide NPs when exposed to different suspension conditions of natural organic matter and pH and examines the effect on particle size using field flow-field fractionation.

5

Iron oxide nanoparticles: Size effects from NOM and pH

Chapter Summary

Metal oxide nanoparticles are known to change their behaviour in response to environmental factors including pH, ionic strength and colloidal concentration such as natural organic matter (NOM). These factors may help to determine fate, transport and bioavailability of nanoparticles in the aquatic environment. This chapter investigates fully characterised uncoated iron oxide nanoparticles with a primary particle diameter of about 7 nm by examining their behaviour in the presence of fulvic and peat humic acids at low pH for F/FFF and all pH values for other analyses. The influence of polysaccharide material, often present in aquatic and terrestrial samples from microbial processes, was also investigated. NPs were found to increase in size both as a factor of pH and as a factor of NOM concentration. The amount of NOM also influenced the stability of the iron oxide. This work was presented in Chicago in October 2008, and has in part, been prepared as a manuscript for submission to the journal, *Science of the Total Environment*. Acknowledgements go to Peter Bomford for help with NP synthesis.

5.1 Introduction

Iron oxide nanoparticles (NPs) have many applications in industry as catalysts and in metallic paints, they also feature in medical imaging, drug delivery and in environmental sensors. Other uses of iron oxide NPs include water purification and magnetic nanoparticles for recording media and MRI imaging (DEFRA, 2005b; Luoma, 2008). Associated with their rising use is the potential that iron oxide NPs are reaching the environment, thus creating new forms of environmental risk. Iron oxides NPs have shown toxicity with an EC_{50} of 30 mg L^{-1} (Brunner *et al.*, 2006) and are able to translocate within organisms. For example, a study by Zhu *et al.,* (2008) demonstrated the ability of tissue translocation in pumpkin plants (*Curcubita maxima*), with 45%, of the administered NPs accumulating in the roots. Other research has considered environmental engineering to counteract global warming by using iron oxide NPs for CO_2 sequestration in the oceans. The iron oxide acts as nutrient for algae growth, the algae then take the CO_2 to the ocean floor upon dying, thus removing CO_2 from the atmosphere (Blain *et al.*, 2007; Pollard *et al.*, 2009).

More widely, the knowledge of fate and transport studies of ENPs in the environment is becoming increasingly important, as scientists are learning about the life cycle of products containing nanoparticles (Nowack and Bucheli, 2007) and how they may enter the environment and pass through the food chain. Some studies of natural (iron oxide) NPs have shown that they are able to transport contaminants (such as uranium, lead, arsenic and phosphorous) from mining sites over long distances in fresh waters (Wigginton *et al.*, 2007), and how this process may be aided by organic macromolecules (Stipp *et al.*, 2002; Waychunas *et al.*, 2005; Weng *et al.*, 2008). This may explain the strong DOC/Fe relationships in Welsh (UK) upland catchments found with increased stream DOC (Neal *et al.*, 2008). It has already been shown that Suwannee River-NOM can stabilise normally insoluble, hydrophobic carbon nanotubes (CNTs) (Hyung *et al.*, 2007), thereby indicating

there could be increased mobility of NPs through aquatic systems due to the presence of NOM.

Iron oxides vary according to their crystal structure. Figure 5. 1 shows the structure, and TEM image of naturally occurring heamatite (α-Fe_20_3). Other common crystal structures include goethite (α-FeO(OH)), ferrihydrite ($Fe(OH_3)$), magnetite (Fe_3O_4) and maghemite (γ-Fe_2O_3). These may be present in the nanoscale (Hochella *et al.*, 2008; Navrotsky *et al.*, 2008). Many iron oxides, such as haematite, can be synthesised in the laboratory at the nanoscale for experimental use. A study of particle size using synthetic NPs to investigate the influence of natural NPs may be informative of fate and behaviour of metal oxide NPs in the environment.

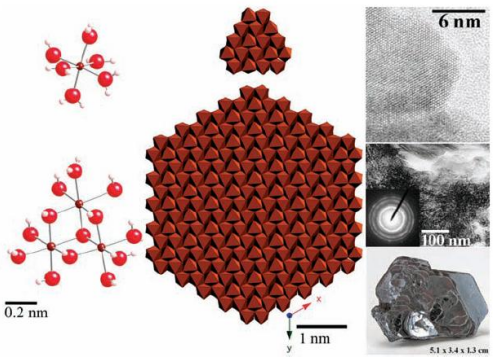

Figure 5. 1 Image showing structure of haematite and TEM images top, HR resolutions image of haematite, middle, image of an unorientated aggregate of 3-5 nm haematite crystals (stippled portion of the image) from an acid mine drainage site in Montana, USA) and bottom, photograph of macroscopic specular hematite. Taken from Hochella *et al.* (2008).

5.1.1 Chapter objectives and structure

To achieve the aim of a better understanding of iron oxide behaviour in the presence of NOM, the current chapter characterises iron oxides, establishes the change in particle size and charge due to pH and investigates the effects of NOM on the iron oxide at varying pH levels. To achieve these objectives the following techniques will be employed using

synthesised iron oxide nanoparticles on their own and with concentrations of NOM (Suwannee River Fulvic Acid (SRFA), a peat humic acid (PHA) and an exo-polysaccharide, succinoglycan (exo-PS)). The suspensions will be analysed by using the following techniques which were described more fully in chapter 3:

1) Sizing; flow field-flow fractionation (FFF), dynamic light scattering (DLS), transmission electron microscopy (TEM), x-ray diffraction crystallography (XRD)
2) Charge; electrophoretic mobility (EPM)

The section that follows describes the techniques that were employed in conducting this analysis in greater detail. The remainder of the chapter is then divided into two main results sections: the first examines the characterisation of the iron oxide NPs; and, the second reports the results of iron oxides with NOM. The chapter finishes with a discussion and conclusion about the effects of NOM on iron oxides.

5.2 Experimental details

Details on instrumentation and general methods are presented in chapter 3. The section below provides additional detail of the work carried out in this chapter.

5.2.1 Synthesis of iron oxide NPs

Iron oxide nanoparticles were synthesised by forced hydrolysis adapted from a method by Matijevic and Schiener (1978). Iron chloride was dissolved in HCl and poured into boiling HCl which immediately produced a dark red suspension. It was then stirred while boiling for a further 30mins. The details of the procedure and the chemicals are found in Appendix 6. The cooled nanoparticle suspension was filtered through a 0.1 μm membrane and stored in the dark at 4 ^{o}C before being used without further modification. A stable suspension at pH 2

was produced with iron concentration of about 1000 mg L^{-1}. All subsequent dilutions for sample preparation were made with pure water (Triple red, Nanopure).

5.2.2 Preparation of HS and polysaccharides

Two humic substances (HS), a Suwannee river fulvic acid (SRFA) and a peat humic acid (PHA), were obtained from the International Humic Substances Society (*IHSS, Colarado*). Both of these have been well characterised in the literature (Hosse and Wilkinson, 2001; IHSS, 2009; Lead *et al.*, 2003; Lead *et al.*, 2000a; Lead *et al.*, 2000b). Succinoglycan, a well – known bacterial exo-polysaccharide (PS) (*Carbomer Inc*), was also briefly examined for iron oxide size effects as PS also forms part of the NOM in aquatic systems (Balnois et al., 2000; Ridout et al., 1997). Stock suspensions of HS (SRFA and PHA) from freeze dried powders were made to a concentration of 400 mg L^{-1} (8 mg in 20 ml), by dissolving in pure water. PHA was suspended more readily first by adding a few drops of 1M NaOH (rapidly shaken before diluting and adjusting to prevent localised effects). The pH was adjusted to 7, with either 1M or 0.1M HNO_3 or NaOH solutions. Polysaccharide (PS), succinoglycan, stock suspension was prepared by suspending 20 mg, exo-PS, in 50 mL pure water which was then stirred for 24 hours to dissolve. The suspension was then filtered through a 0.2 μm membrane to remove the larger fraction, whereby the final concentration of 120 mg L^{-1} was calculated from the difference in filter paper weights.

The working samples containing the iron oxides NPs and NOM suspensions were prepared by diluting the stocks suspensions described above in pure water to concentration ranges of 0-25 mg L^{-1} NOM in a 5 mL polypropylene (PP) vial where all samples had an Fe concentration of 200 mg L^{-1}. Samples were then adjusted for pH for 24 hours to allow for equilibrium before fractionation. Separate sample batches were made for further

measurements by DLS. These working concentrations were chosen to represent the concentrations of NPs and humics typically found to reflect their relevant environmental chemistry. Additionally, due to the requirements of some analytical techniques, such as FlFFF, it was deemed necessary to optimise conditions resulting in usage of higher iron oxide NPs concentrations. These concentrations would not unreasonably be found in ground water remediation situations.

5.2.3 Iron dissolution

Sample preparation for both the iron dissolution studies and the XRD crystallography, were prepared via ultrafiltration, whereby the sample residue was kept and dried on the filter paper for XRD and the filtrates were kept and analysed for dissolved iron. Following the procedure in chapter 3 (Table 3-2) the iron oxide NPs (200 mg L^{-1}) suspension at pH 2, 3 4 and 5 was passed through a pre-washed (10% $HN0_3$, MilliQ water) 1 kDa (1-3 nm) membrane (*VWR*). Samples were subsequently readjusted to pH 2 and analysed at a wavelength of 304 nm with a UV-visible spectrophotometer (*wma, lightwave*) in a one cm pathway quartz cuvette (Steiner and Lazaroff, 1974) for iron chloride determination. Standards, 0-40 mg L^{-1} Fe were prepared from 1000 mg L^{-1} Fe, iron chloride solution ($FeCl_3.6H_20$ M.W.= 270, *Fisher scientific*) in 3.75 x 10^{-3} M HCl and diluted in 3.75 x 10^{-3} M HCl. Further details of the method and calibration curve are presented in chapter 3.

5.2.4 Analytical instrumentation

Prepared samples were analysed for particle size and surface charge using flow field-flow fractionation (F*l*FFF), dynamic light scattering (DLS), electrophoretic mobility (EPM), transmission electron microscopy (TEM) and x-ray diffraction (XRD). The theory and other details for these techniques are described more fully in chapter 3.

5.2.4.1 Flow Field- flow Fractionation

Experimental conditions are summarised in Table 3-3 in Chapter 3. Channel flow was set to 1 ml min^{-1} and the cross flow was set between 0.5 and 1 mL min^{-1} to obtain good separation of the void peak and sample peak. The membrane (1kDa, *Postnova*) was conditioned by repeated injections of concentrated (1000 mgL^{-1}) iron NPs to improve separation and reduce adsorption. The carrier solution was 10^{-4} M $NaNO_3$. The pH of the carrier solution was adjusted to the pH of the sample. Sample peaks were detected online with a UV/Vis spectrophotometer (*Varian*) at 254 nm. Peaks were baseline corrected with peak software and exported and calibrated to diffusion coefficients and hydrodynamic diameters using F/FFF theory in chapter 3 (Schimpf *et al.*, 2000).

5.2.4.2 Dynamic light scattering

Dynamic light scattering (DLS) measurements were carried out on a HPPS (*Malvern Instruments, UK*) in triplicate at 25 °C. Samples were not shaken and the aliquot was taken from the top part of the sample. Sample was injected by syringe into low volume disposable plastic cuvettes 1 cm pathway to avoid air bubbles. Z-average (nm) was taken as a mean of three measurements, where the z-average, as opposed to the volume or number average, is considered a more suitable measurement (chapter 3; section 3.2.3) where there is a mixture of aggregated and non aggregated particles present. Where visible aggregation had occurred in the sample, suspensions were not shaken, and the aliquot was taken from the top part of the sample.

5.2.4.3 Electrophoretic Mobility

Electrophoretic mobilities were analysed on a Zetamaster (*Malvern Instruments, UK*) at 25°C. The sample was injected into a quartz capillary cell and a mean was taken from five to ten

measurements. Due to rapid measurements and erroneous data, zero (machine error non-readings) measurements were ignored.

5.2.4.4 TEM

Samples for TEM were prepared on 300 holey carbon copper grids (Agar), where 50μL of the sample was dropped on and after 15 minutes, the excess liquid removed with a paper towel. The samples were examined on a Phillips Technai F20 and images were analysed by Gatan software.

5.2.4.5 X-ray diffraction crystallography (XRD)

X-ray diffraction (XRD) analysis was performed on a *Siemens D5000* by Professor Colin Greaves (School of Chemistry, University of Birmingham) from prepared dried iron oxide NPs at pH 2, 3 4 and 5 obtained by separation through a 1KDa UF membrane. NPs were dried on the UF paper then transferred and stored in glass vials. Particle size from XRD patterns were derived using Scherrer's formula (Patterson 1939) (chapter 3). Furthermore, NPs (pH 2) were aged at 800°C then analysed on XRD to confirm the crystal structure of the materials.

An earlier experiment had been conducted, aimed at obtaining powdered NP crystals for XRD analysis by freeze drying the suspension from a previously frozen sample. This proved to be unsatisfactory as the resulting material deliquesced, absorbing water almost immediately, probably due to the presence of chloride ions. The material around the lid edge had a bright yellow appearance, which was almost certainly hydrated iron oxide also known as iron (III) hydroxide ($Fe(OH)_3$).

5.3 Characterisation

This section reports on the characterisation of the iron oxides NPs on their own, using the techniques and methods outlined in the previous section. SRFA and PHA were also examined their own using F/FFF. The following section, 5.4, then goes on to examine the effects of NOM on the iron oxides NPs at different pH.

5.3.1 Characterisation of the iron oxide NPs

Transmission electron microscope (TEM) images, of produced iron oxide particles at pH 2, revealed a fairly monodisperse sample containing spherical to hexagonal particles of 6.73 nm ± 2.2 nm (n=50) (Figure 5.2 (a) and (b). The histogram in Figure 5.2 (c), measured manually using digital micrograph (Gatan software), from the calibrated TEM images, shows the distribution of these particles (n=50). The similarity between the mean, median (6.69 nm) and mode (6.78 nm) values indicates a normally distributed sample. This is in agreement with values from Baalousha *et al.* (2008) of 6.9 ± 3.85 nm (TEM), of 6.5 ± 2.49 nm (AFM) and an equivalent hydrodynamic diameter number average of 9.6 nm ± 1.72 (F/FFF) from a similar nanoparticle batch. DLS analysis revealed a larger, hydrodynamic, primary particle of 16 nm, probably weighted by the presence of a few larger particles.

(a) 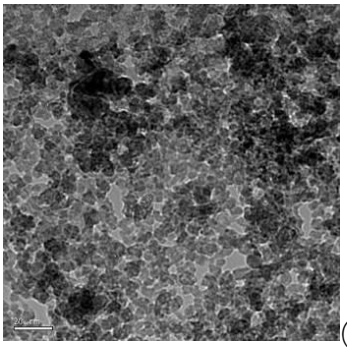 (b) 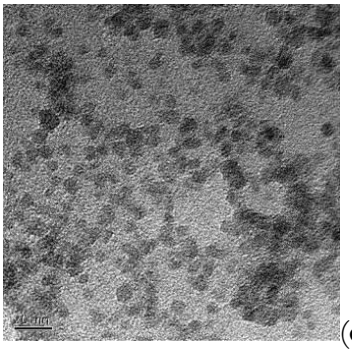 (c) 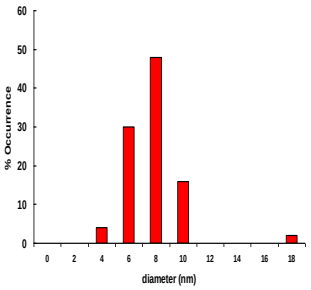

Figure 5.2 (a) TEM micrograph image of iron oxide nanoparticles at pH 2 from original supplied by Peter Bomford; (b) batch 2 synthesised by the author. Scale bar is 20 nm. (c) TEM histogram for particle size of iron oxide NPs derived from image (b).

5.3.1.1 XRD

X-ray crystallography patterns of the FeO NPs only, as shown in Figure 5. 3, revealed that no effect was observed with increasing pH, indicating that changing the pH of the NPs did not affect the crystal structure of the NPs. However, the high noise to signal relationship with low peaks indicated that the 5-7 nm NPs have no definitive crystal structure and are amorphous in nature. However, heating the sample (pH 2) to 800 ^{o}C revealed a structure similar to that of haematite where the haematite standard is shown as red bars (Figure 5.4). Heating the nanoparticles is this way is not expected to be detrimental to the original sample. Work by Waychunas (2005) has further indicated that raising the temperature does not change the crystalline structure of the iron oxides but may increase particle size. A particle size of the heated sample was determined to be 4 nm ± 1 nm was derived from peak width using Scherrer's formula (Patterson, 1939).

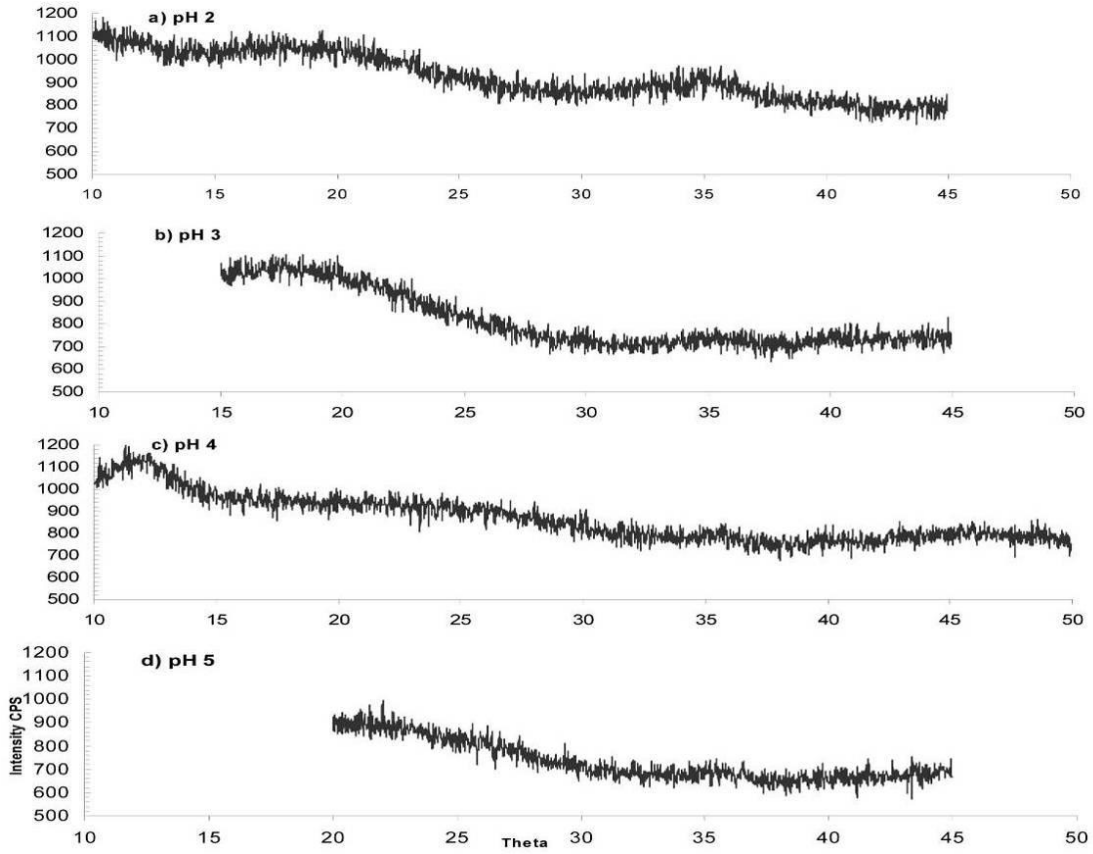

Figure 5. 3 XRD patterns for iron oxide nanoparticles at: a) pH 2; b) pH 3; c) pH 4; and d) pH 5

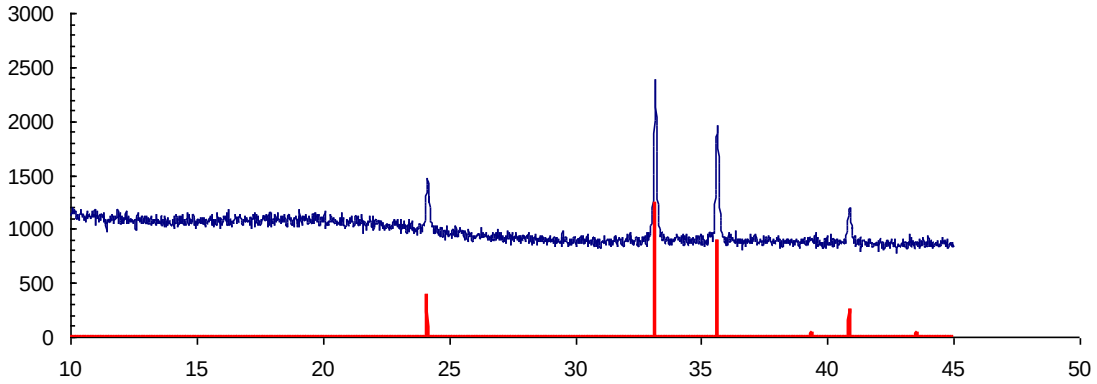

Figure 5. 4 XRD pattern (blue trace) showing original iron oxide NPs at pH 2 samples after heating to 800 degrees. Column markers (in red) indicate the positions of haematite peaks.

Table 5-1 provides a summary of the NP by all techniques used, TEM, FFF, XRD and DLS, and range from 4 to 16 nm. The size shows variation due to the different ways the particles are analysed with the largest size derived from dynamic light scattering.

Table 5-1 Summary of the iron oxide particle size from different instrument techniques:

	XRD	TEM	F*/*FFF	DLS(z-average)
Size (nm)	4	6.73	10	16
Standard deviation	*1*	*2.2*		*0.1*

5.3.2 Iron solubility

Dissolution values obtained though NP suspension separation using ultrafiltration though a 1 kDa UF membrane, shows that dissolved Fe^{3+} ions were present only in solutions at pH 2 and 3, 69.3 mg L^{-1} and 9.2 mg L^{-1} respectively (Figure 5.5). Above pH 4 no Fe ions were detected in solution below the detection limit (DL) of 0.16 mg L^{-1} (DL from 3 St dev blank). This indicates that at conditions above pH 4, dissolved Fe had either adsorbed directly onto existing surfaces of the iron oxide NPs or hydrolysed to form new oxides of haematite or

amorphous iron oxide (Stipp *et al.*, 2002). The dissolved iron was primarily present from the synthesis process, rather than from dissolution of the NPs. To examine behaviour under more realistic conditions, the particles were not cleaned to remove the chloride content but the presence of Cl^- may affect surface chemistry, such as charge (Cromieres *et al.*, 2002).

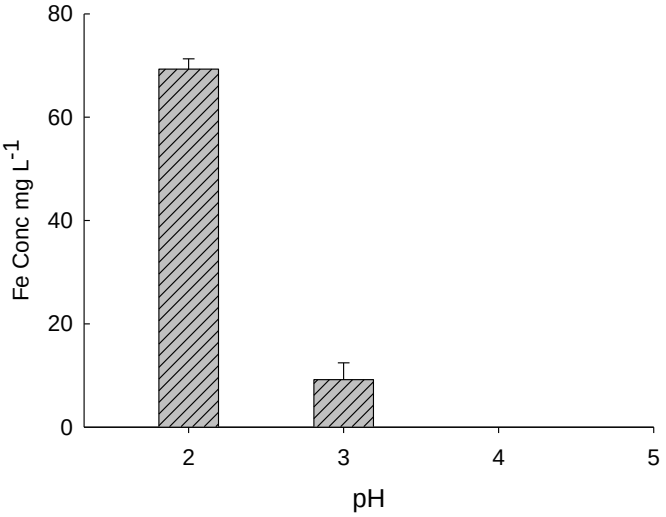

Figure 5.5 Free ion (as Fe^{3+}) concentrations present at pH 2-5: detected at 304 nm using UV-vis spectrometry. Standards were $FeCl_3$ in HCl measured at pH 2, values have been blank subtracted and error bars represent a standard deviation of three measurements.

5.3.3 The effect of pH on the iron oxides

5.3.3.1 Dynamic Light Scattering (DLS) and Electrophoretic mobilities (EPM)

Electrophoretic mobilities and z-average size of iron oxide suspensions between pH 2 and pH 12 are presented in Figure 5.6 (a) and (b). The point of zero charge (pzc) was calculated to be approximately pH 7.1 in Figure 5.6 (a), which fits within the range of reported values of pH 7-9 (Kosmulski, 2002). Mean NP size by DLS increases incrementally through pH 2-5 from 16 nm to 146 nm. Thereafter, as shown in Figure 5.6 (b), a sudden increase in particle size from pH 5.9 to pH 7 is observed with a maximum particle size of 8.3 μm. From pH 9 - 10 particle size decreases to 330 nm (data in Appendix 7).

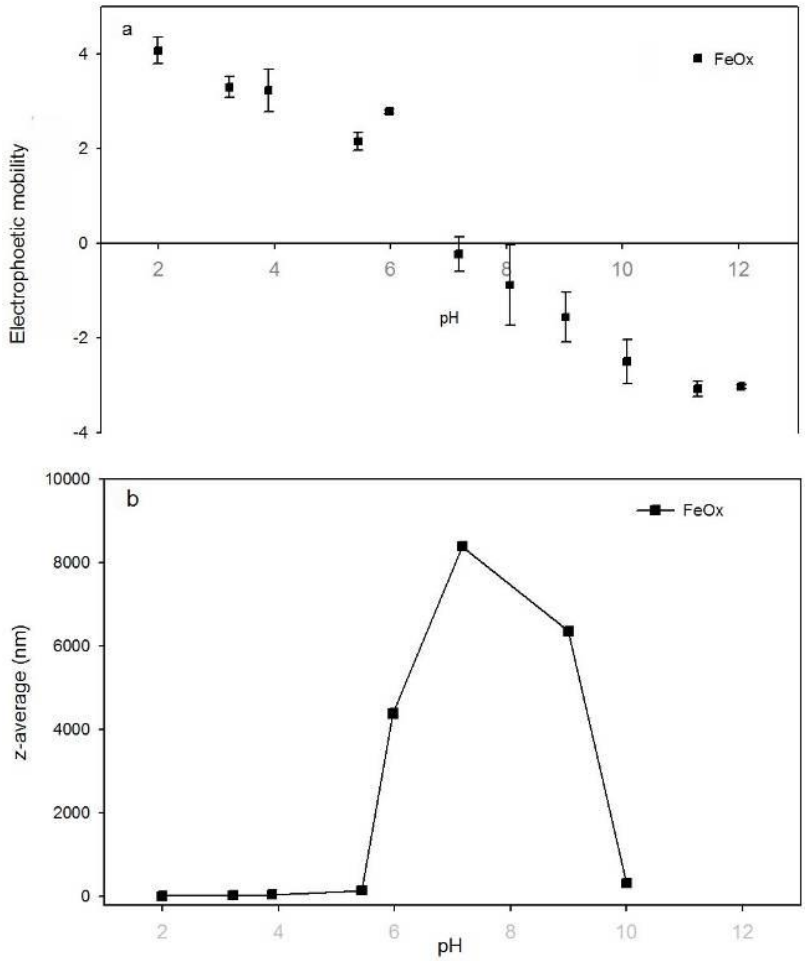

Figure 5.6 Iron oxide nanoparticles of diameter 5-7 nm: (a) electrophoretic mobilities 10^{-8} m^2 Vs (b) particle size by DLS, z-average, as a function of pH. Error bars are standard deviations of at least three measurements.

5.3.4 F*l*FFF characterisation of IHSS SRFA and PHA at pH 2-5

To examine the F*l*FFF separation behaviour, for hydrodynamic diameter (*Hd)* and diffusion coefficients (*D*) of the HS on their own, Suwannee River fulvic acid (SRFA) and peat humic acid (PHA) were separated under the same conditions as the iron oxide NPs and HS samples for each pH value 2-5. The data in Table 5-2 provide the diffusion coefficients and size for SRFA and PHA on their own obtained from F*l*FFF.

Table 5-2 Experimental conditions diffusion coefficients and hydrodynamic diameters for the peat and fulvic acids. Channel flow was 1 mL min^{-1}.

	Condition	Size H_d (nm)	*Diffusion Coefficients* D $m^2\ s^{-1}$	UV response a.u.	Cross flow mL min^{-1}	*Channel width, w* µm
PHA 100ppm	pH2	5.96	8.09E-11	268	1	224.76
	pH3	3.6	1.34E-10	631	1	224.76
	pH4	6.26 *	7.71E-11	946	0.5	228.84
	pH5	5.42	8.89E-11	3774	0.5	228.84
SRFA 100ppm	pH2	1.83	2.63E-10	450	1	228.84
	pH3	2.43	1.99E-10	829	1	228.84
	pH4	4.66	1.04E-10	612	0.5	232.66
	pH5	6.23	7.74E-11	4477	0.5	232.66

* denotes estimation in peak height which lies between 3 and 7 nm due to a broader peak maximum.

The fractograms that provided the sharpest and smoothest peaks were obtained from 100 mg L^{-1} HS, averaged from three runs, are given in Figure 5.7 at 100 mg L^{-1} HS. Fractograms were converted to *Hd* and *D*, using F*l*FFF theory presented in chapter 3, calibrated with standard beads (20, 33 and 50 nm), and fit within the reported values of 1-5 nm (Baalousha and Lead, 2007b; Lead *et al.*, 2000a; Schimpf and Petteys, 1997). Figure 5.7 (a) shows an increase in SRFA *Hd*, with an increase in pH from pH 2 to pH 4. In contrast, Figure 5.7 (b) shows no such trend for PHA under the same conditions. At pH 5 however, SRFA and PHA show fractograms with increased absorbance and an increased particle size range, up to 30 nm in size with a maximum peak height of 6 and 5 nm for SRFA and PHA respectively.

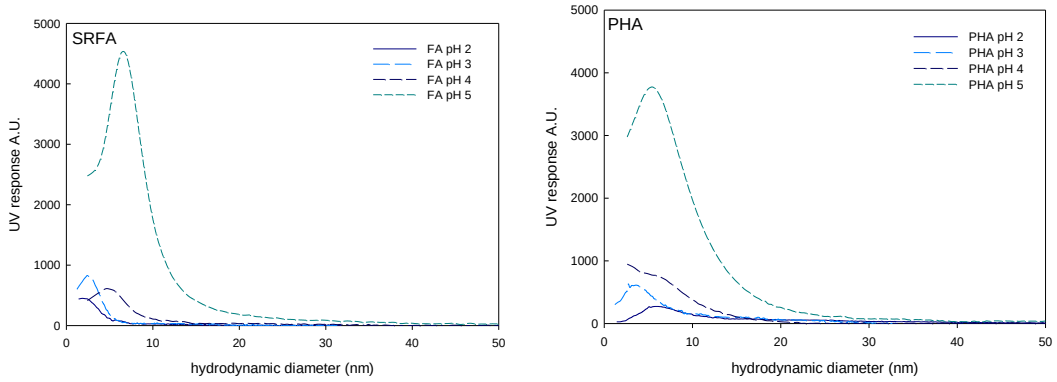

Figure 5.7 F/FFF fractograms for 100 mg L^{-1}: (a) Suwannee river fulvic acid (b) peat humic acid, for pH 2- 5. Fractograms are averaged from 3 separate fractionations.

5.4 Effect of NOM on nanoparticles

This section leads on from the iron oxide characterisation and examines, in terms of particle size and charge, the effect of SRFA, PHA or exo-PS on the iron oxide NPs at pH 2-5 by:

1) Providing the results of iron oxide NPs with NOM (SRFA, PHA and exo-PS) in turn
2) Applying the following techniques: F/FFF, (including analysis peak area) DLS and EPM.

5.4.1 Effect of the nanoparticles with fulvic acid

The size of iron oxide NPs increased with both an increase in pH (2-5) and with an increase in the concentration of SRFA (0-25 mg L^{-1}) when separated by F/FFF, see Figure 5.8 (a) to (d). Insets in Figure 5.8 provide an enlarged version of the fractionation. The greatest influence on the H_d sizes of the iron oxides, with and without SRFA, was pH. At pH 2, the F/FFF peak height maxima (most probable concentration, on a mass basis) shifted right showing an increase of H_d from 10 nm to 12 nm with SRFA concentration 0 to 25 mg L^{-1}.

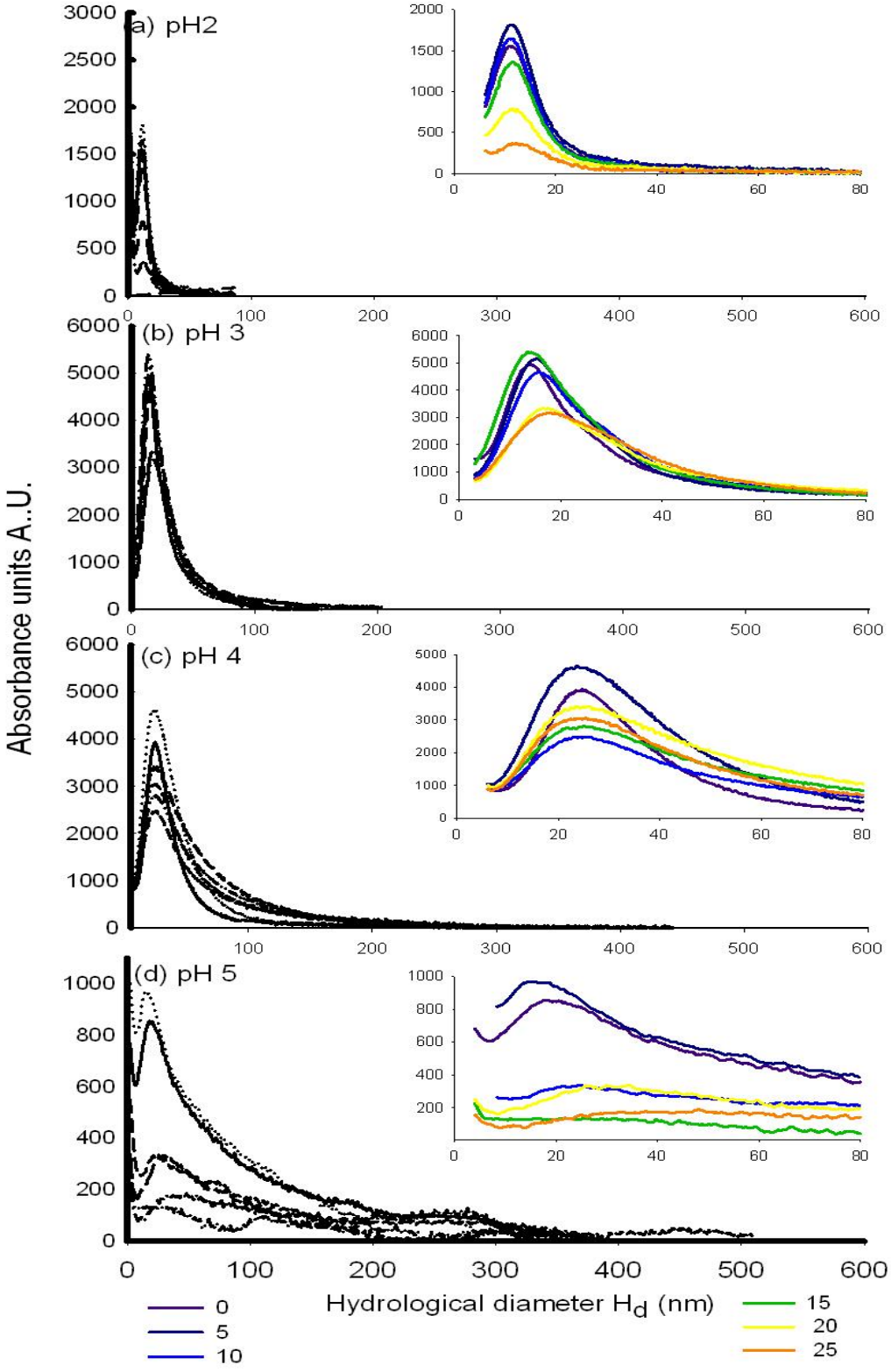

Figure 5.8 F/FFF Fractograms showing particle size (Hd) for suspensions containing 200 mg l^{-1} iron oxide NPs with 0-25 mg L^{-1} SRFA for conditions: (a) pH 2, (b) pH 3, (c) pH 4 and (d) pH 5

On raising the pH, peak height maxima H_d were 14.5-17.1 nm (pH 3), 23-26 nm (pH 4) and 16-48 nm (pH 5). As pH increased, there was an increase in long tailings of the fractograms from pH 2-5 and at pH 5 this extends to 500 nm. Peaks at pH 5 also show reduction in absorbance of peak maxima, indicating reduction in particle number. In general, as the pH is increased fractograms become right-shifted toward a larger particle size. Equivalent diffusion coefficients (from which the diameters are calculated via the Stokes' relationship) are given in Appendix 8.

5.4.1.1 Peak areas

In the fractionation process, two peaks are obtained, the first, the void peak is the elution of material containing some of the dissolved fraction, the position of which is used to calculate the channel volume. By examining its geometric content, sample losses can be calculated. Peaks areas (minus void peak) were calculated in *Sigmaplot* by the trapezium rule, and results are shown in Figure 5.9. Peak area shows an increase with increase in pH 2 to 4 with a decrease at pH 5. There is a reduction in peak area with increasing SRFA concentration at pH 2. At pH 5 there is a reduction in peak area, but no observed trend with SRFA concentration.

Some peak loss can be explained by examining the amount lost in the void peak. Figure 5.10 shows this loss as the difference between total peak area and the void peak in percentage terms. At pH 2, losses rise from 30% in the absence of SRFA to 60% at 25 mg L^{-1}, which could be due to the unbound (smallest) fraction. The loss of sample though the void peak at pH 5, with the exception of 15 mg L^{-1}, is similar to pH 3 and 4 and is probably accountable to aggregation.

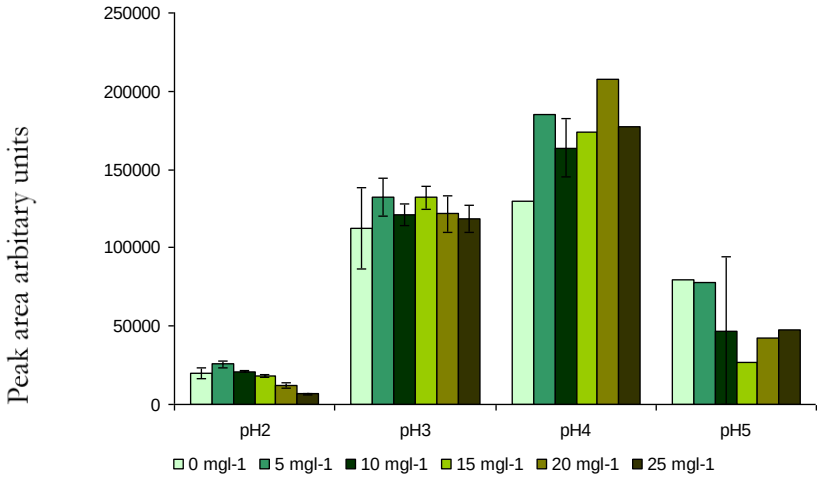

Figure 5.9 Calculated F/FFF fractogram peak areas (minus the void) for iron oxides NPs and SRFA for pH value 2-5 and for SRFA concentrations 0-25 mg L^{-1}. Y-axis is the peak area in arbitrary units. Error bars are the standard deviations of two measurements

F/FFF peak height maxima data and DLS z-average data are presented in Figure 5. 11 and Figure 5.12, respectively. Good agreement is observed between both data sets. Z-average data in Figure 5.12, shows larger increases in particle size than F/FFF. The relationships between the two data sets were compared, with a good correlation obtained for pH 2, pH 3, and pH 4 with r^2 values of 0.741, 0.690, 0.528 respectively (P= 0.05). However, at pH 5 there is no correlation between F/FFF and DLS data. These differences are due to differences in the way that the techniques deal with the presence of larger aggregated particles where the F/FFF peak height maximas represents the majority of a single size and the DLS is an average of the representative sizes present in the sample.

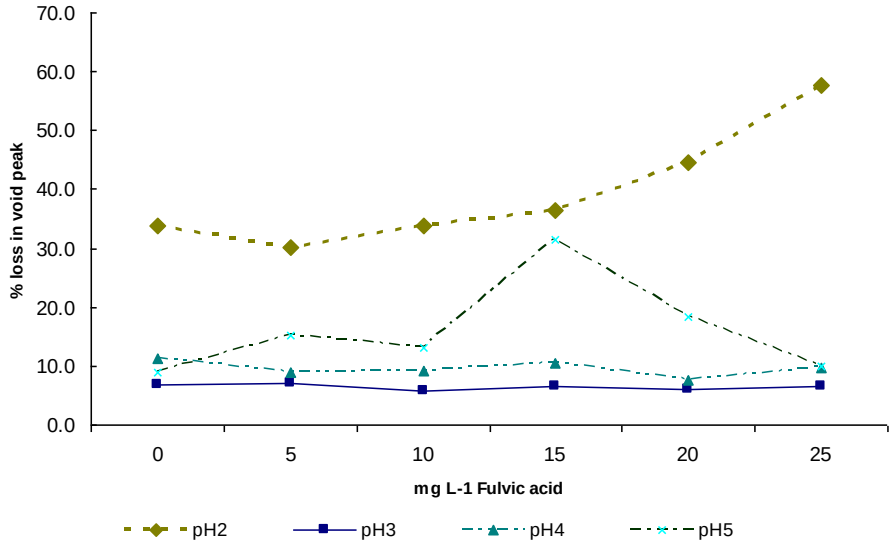

Figure 5.10 Percentage of material lost in the void peak from FÆFFF fractograms calculated as the difference between total peak areas and peaks areas minus the void peak

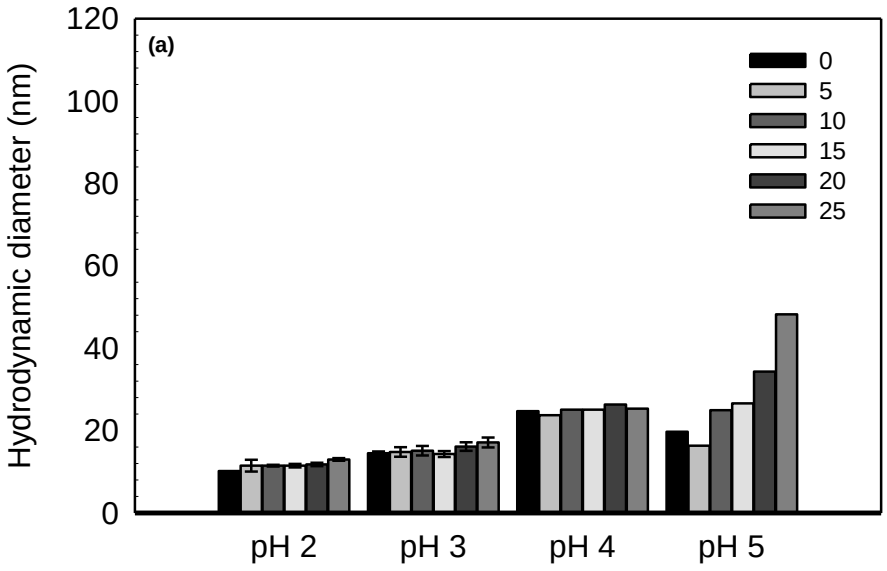

Figure 5. 11 Particle sizes of Iron iron oxide NPs and SRFA 0-25 mg L^{-1} maximum peak heights taken from FÆFFF fractograms as a function of pH error bars are standard deviations of two measurements for pH 2 and pH 3 whereas pH 4 and 5 were singular observations.

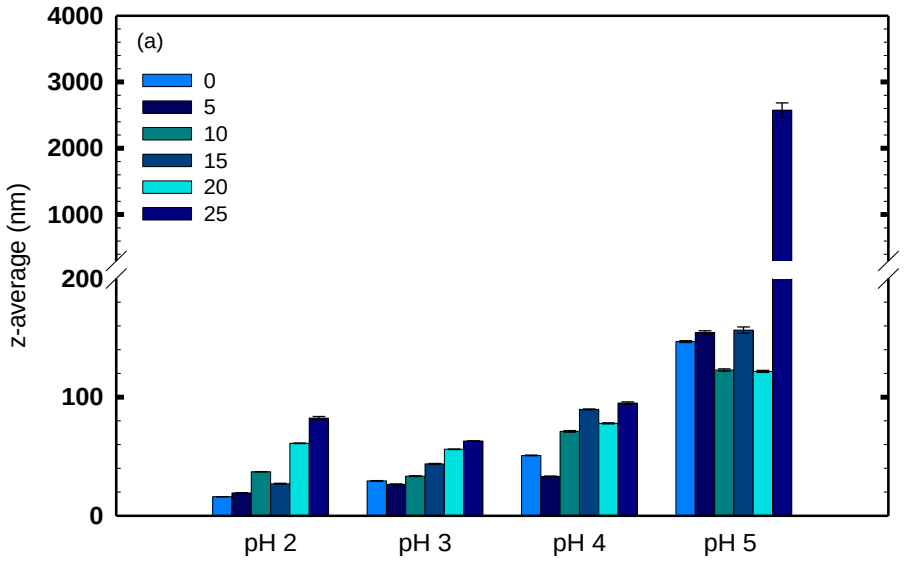

Figure 5.12 Dynamic light scattering, Z-average data for SRFA and iron oxide NPs pH 2-5 and SRFA concentration 0-25 mg L^{-1} . Error bars are standard deviations of three measurements

Figure 5.13 (a) and (b) below show the z-average (nm) and EPM data for iron oxide NPs and 0, 10 and 20 mg L^{-1} SRFA for pH 2 -10 (see Appendix 7 for all data). The addition of 10 mg L^{-1} of SRFA appeared to have little effect on charge, but the particle size increased greatly at pH 6 and 7. The results are as would be expected from EPM, the addition of SRFA at 20 mg L^{-1} has had the effect of only slightly reducing the zero point of charge, to approximately 6.5. Comparing the two figures, there is a left shift of increased particle size for 20 mg L^{-1} in concurrence with a lowered pzc. Samples were visible aggregated from pH 5.5 to pH 8. At pH 9 and above the particles were in suspension with no sediment.

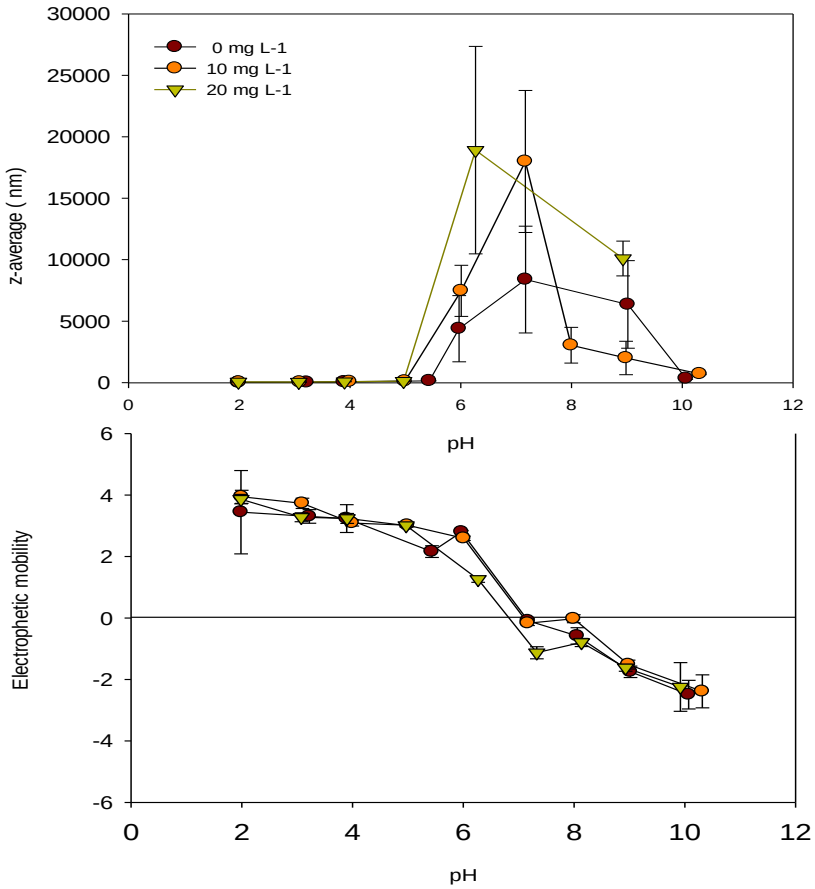

Figure 5.13 Fulvic acid (0, 10 and 20 mg L^{-1}) and iron oxide NPs as a function of pH: (a) z-average (nm) and (b) electrophoretic mobility for pH 2- 10 Error bars are the standard deviations of three measurements for DLS and five measurements for EPM.

5.4.2 Effect of the nanoparticles with peat humic acid

Iron oxide NPs (200 mg L^{-1}) were also mixed with a peat humic acid (PHA) of concentrations 0-25 mg L^{-1} (Figure 5.14 to Figure 5.19). As with the iron oxide mixed with SRFA, data shows that an increase in particle size is observed with both an increase in pH and an increase in SRFA concentration. Additionally samples were also analysed to pH 12 for size charge using DLS and EPM.

Figure 5.14 (a)-(d) shows the F*l*FFF fractograms of the iron oxide NPs with and without PHA at pH values between 2 and 5. Insets provide an enlarged version of the figure. In

general, as the pH increases, fractograms show right-shifted peaks towards a larger particle size. Peak maxima also right-shifts with an increase in PHA concentration. Increased tailing is observed with increase in pH. At pH 5, there is a difference between the iron oxide NPs on their own and with PHA, where the addition of PHA at all concentrations show less defined peaks with much longer tailing. At pH 2 values for peak maxima were 10-12 nm. On raising the pH, sizes ranges were 13-16 nm (pH 3), 19.9-21.7 nm (pH 4) and 29-57 nm (pH 5) for the range of HS added. At pH 5 flat lines are observed, but not for the iron oxide. Equivalent diffusion coefficients are provided in Appendix 8. Again, not all the increases are consistent, particularly at pH 4 and 5.

5.4.2.1 Peak areas

Calculated peaks areas (minus void peak), presented in Figure 5.15, show an increase in peak area with an increase in pH from 2 to 4, with a decrease at pH 5. There is a reduction in peak area with increasing PHA concentration at pH 2 and at pH 5. At pH 5 there is a reduction in peak area, but no observed trend with SRFA concentration.

At pH 2, losses shown in Figure 5.16, rise from 30% in the absence of PHA to 60% at 25 mg L^{-1}. This could be due to the unbound (smallest) fraction. The loss of sample though the void peak at pH 5, with the exception of 25 mg L^{-1} with a loss of 30 % material in the void peak, is similar to pH 3 and 4 and is probably accountable to aggregation. No overall pattern is observed but the data is similar compared to the iron oxides NPs with SRFA.

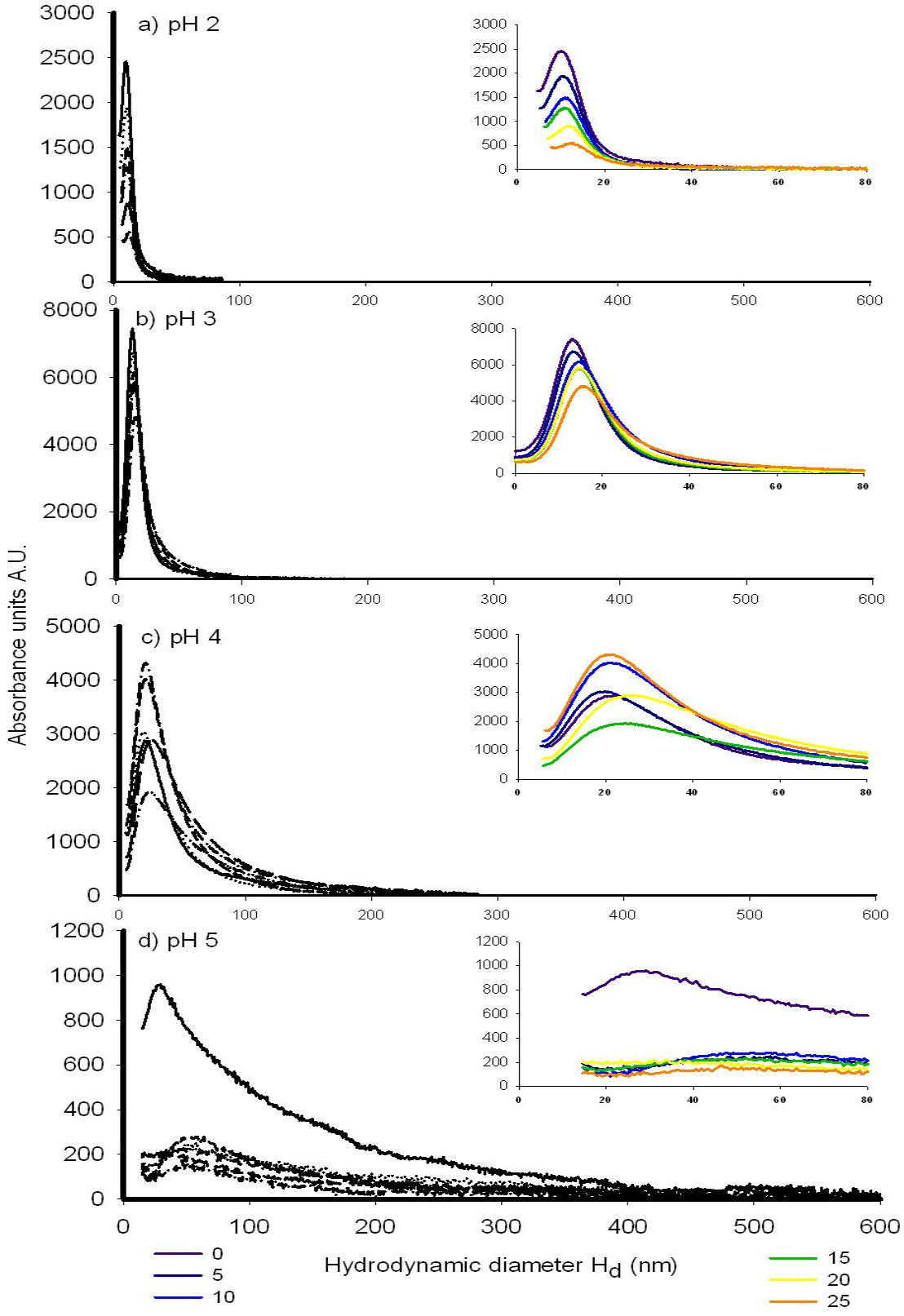

Figure 5.14 FlFFF fractograms for iron oxide nanoparticles and PHA 0-25 mg L^{-1}: a) pH 2; b) pH 3; c) pH 4; and d) pH 5

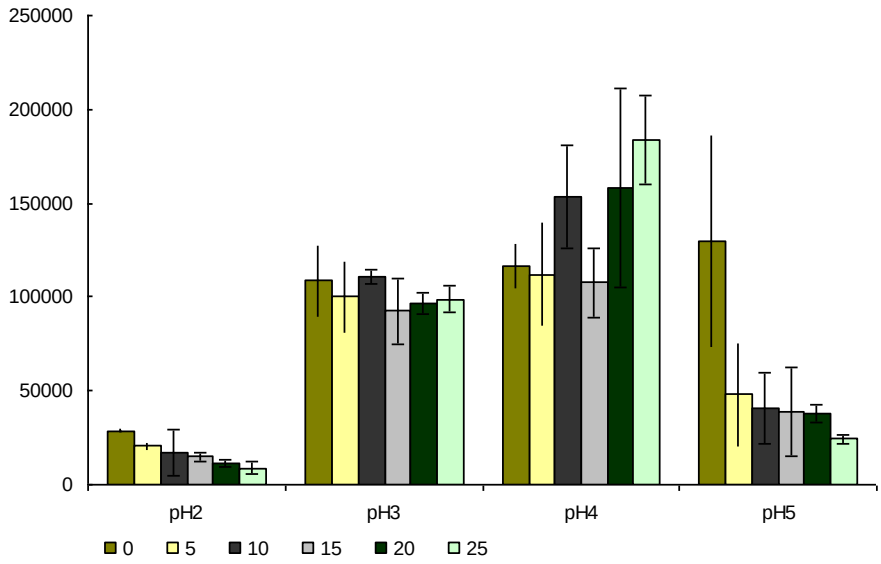

Figure 5.15 F/FFF peak areas for iron oxide nanoparticles and peat humic acid 0-25 mg L^{-1}, pH 2-5, the void peak subtracted

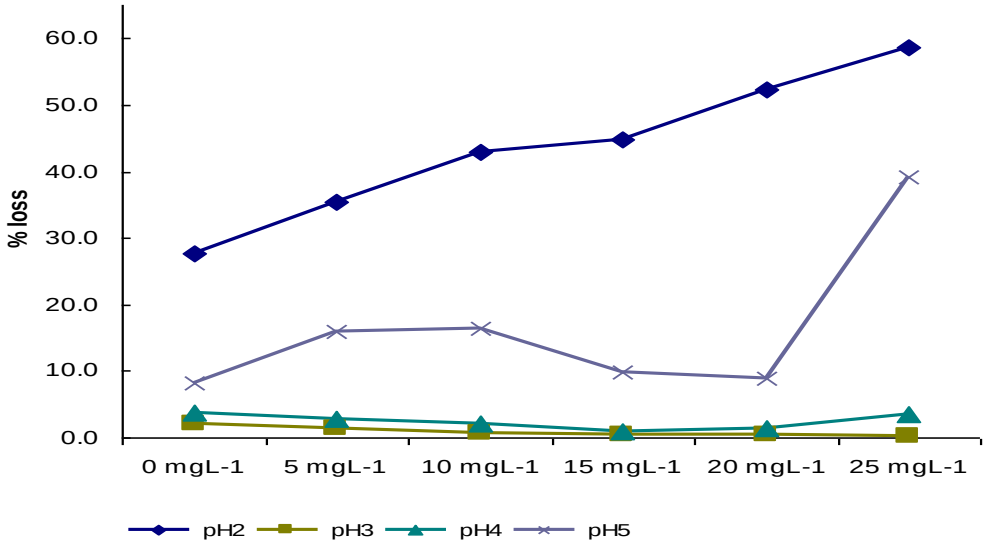

Figure 5.16 Percentage of material lost through the void peak, for iron oxide nanoparticle and peat humic acid 0- 25 mg L^{-1}, pH 2-5

Particle size increased with both an increase in PHA and in pH value from pH 2 to 5 and was seen when measured using dynamic light scattering and from F/FFF peak height

measurements. Figure 5.17 and Figure 5.18 show that there is good agreement between both data sets. The increase in the size of the error bars in both data sets at pH 5 shows variability in the samples, due to polydispersity and instability probably due to its near aggregated state. F*/*FFF data demonstrates incremental increases in hydrodynamic diameter of a few nanometres both for pH and for PHA concentration (Figure 5.17). Z-average data in Figure 5.18 shows larger step increases in particle size from pH 2-4. The relationships between the two data sets were compared, the correlation is good at pH 2, pH3, and pH 4 (pH 2, r^2 = 0.944; pH 3, r^2 = 0.833, pH 4 r^2 = 0.851). The correlation is less robust at pH 5 (r^2 = 0.4).

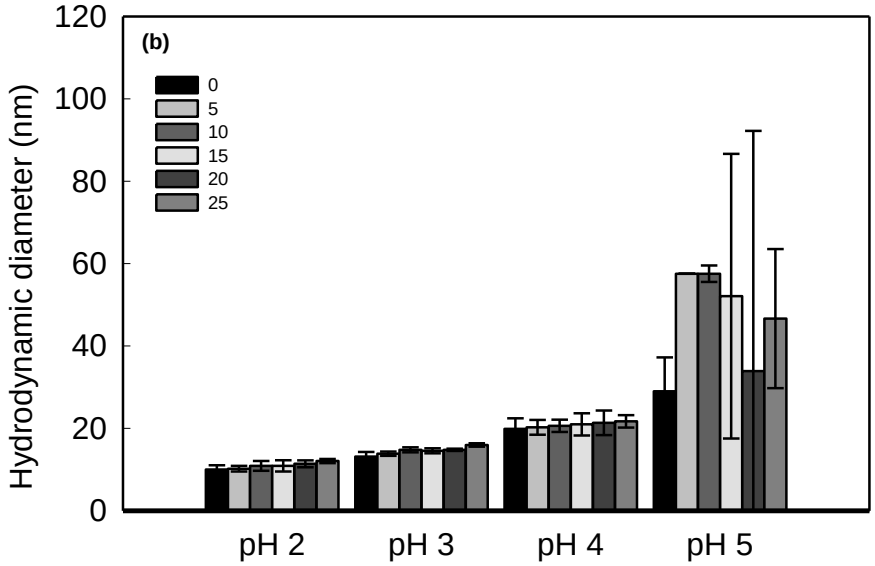

Figure 5.17 Particle sizes of iron oxide NPs and PHA 0-25 mg L^{-1} maximum peak heights taken from F*/*FFF fractograms as a function of pH

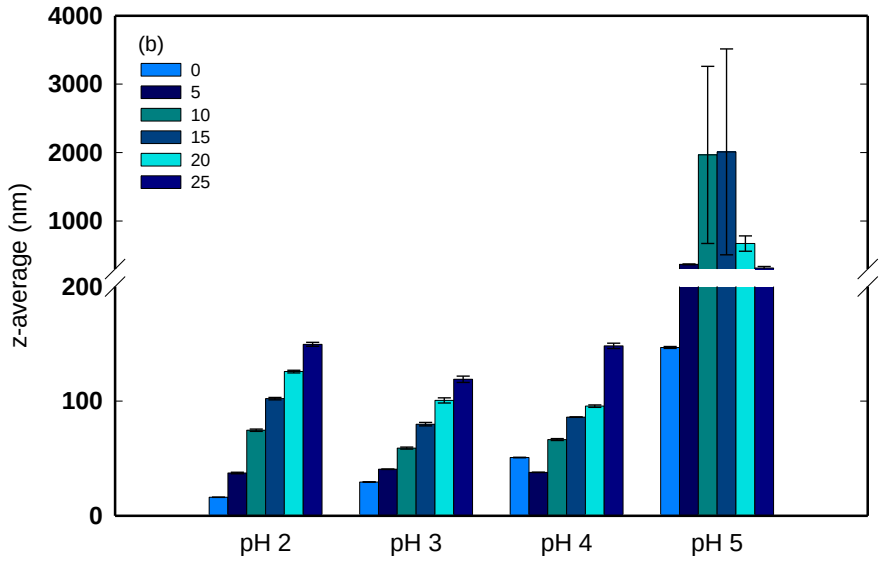

Figure 5.18 Dynamic light scattering, Z-average data for peat humic acid and iron oxide NPs pH 2-5 and SRFA PHA concentration 0-25 mg L^{-1}

Figure 5.19 a and b show the z-average and electrophoretic mobility data for iron oxide NPs and 0, 10 and 20 mg L^{-1} PHA for pH 2-10 (see Appendix 9 for all data). The addition of 10 or 20 mg L^{-1} of PHA had no measurable effect on point of zero charge on iron oxide NPs, so PHA was therefore unable to fully shield the effect of solution charge or there was a lack of iron oxide particle charge. Baalousha (2009) observed that a 10 mg L^{-1} dose of humic acid had no effect on the pzc of the iron oxide, but 100 mg L^{-1} shifted the pzc to low pH due to the higher overall negative surface charge from the humic acid. In this work, particle size greatly increased at pH 6 and 10, and samples were visibly aggregated from pH 5.5 to pH 8 but at pH 9 and above there was no visible sediment. Compared to SRFA in Figure 5.13, the maximum particle size is 20 μm for PHA at pH 8 and 19 μm for SRFA at pH 6. At pH 11 and 12, particle size is smaller than at circum-neutral pH.

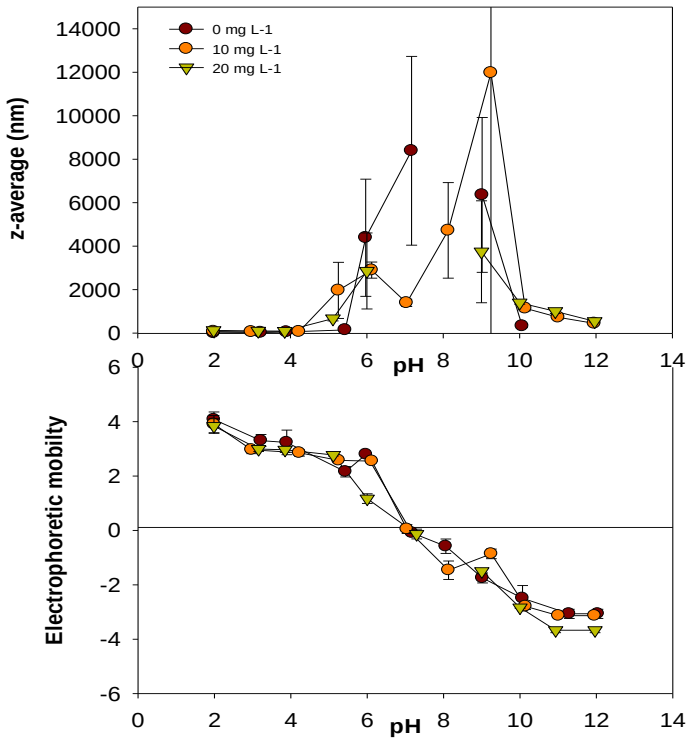

Figure 5.19 Iron oxide NPs with peat humic acid at 0, 10 and 20 mg L^{-1}: (a) z-average (above); and (b) electrophoretic mobilities (below). Continuous lines are there to guide the eye rather than to suggest absolute trends.

5.4.3 Effect of the nanoparticles with a polysaccharide

Polysaccharides also are present in the aquatic environment from bacterial and fungal exudates, so an experiment was conducted by mixing the iron oxide NPs (200 mg L^{-1}) with an exo-polysaccharide (exo-PS), succinoglycan, and fractionated through the F*l*FFF channel at a cross flow rate of 0.5 – 0.75 mL min^{-1}. Exo-PS contain long chains of flexible and rigid repeating carbohydrates, high molecular weight, negatively charge molecules and make up 30% of natural organic matter. Experiments were conducted at pH 2, 3 and 4 at doses of 0-25 mg L^{-1} succinoglycan and separated on the F*l*FFF. Results are shown in Figure 5.20, with inserts of the graphs showing the peaks at higher resolution. In Figure 5.21 peak heights ranged from 9.56 to 11.63 nm at pH 2; and 11.48 to 12.43 nm at pH 3; and 23.1 to 30.2 nm at pH 4.

The effect of polysaccharides on the iron oxide NPs was to increase particle size with increasing pH. From the fractograms in Figure 5.20, no discernible effect on particle size (peak heights) was shown as PS concentration increased at pH 2 and 3. However, an increase in particle size and aggregation was observed with increasing concentration at pH 4 (See also Figure 5.21 for peak heights).

5.5 Discussion

In general, results from DLS and F/FFF studies demonstrated the particle size of the iron oxide increased by increasing the pH of the suspension and by increasing the concentration of either the SRFA or the PHA. At the point of zero charge, aggregation, which onset immediately as the pH was raised, and sedimentation occurred. Further increase of the pH from 8 to 10 in SRFA and PHA reduced aggregate size and the particles were again stabilised with a negative charge, and at these pH values, OH^- ions dominated.

5.5.1 Influence of pH on particle size

F/FFF measurements generally showed a right–shift of the fractogram curves with increase in pH presented in Figure 5.9, Figure 5.14 and Figure 5. 20. Tailing of the fractograms peaks was observed at pH 4 and 5, indicating polydisperse and aggregated

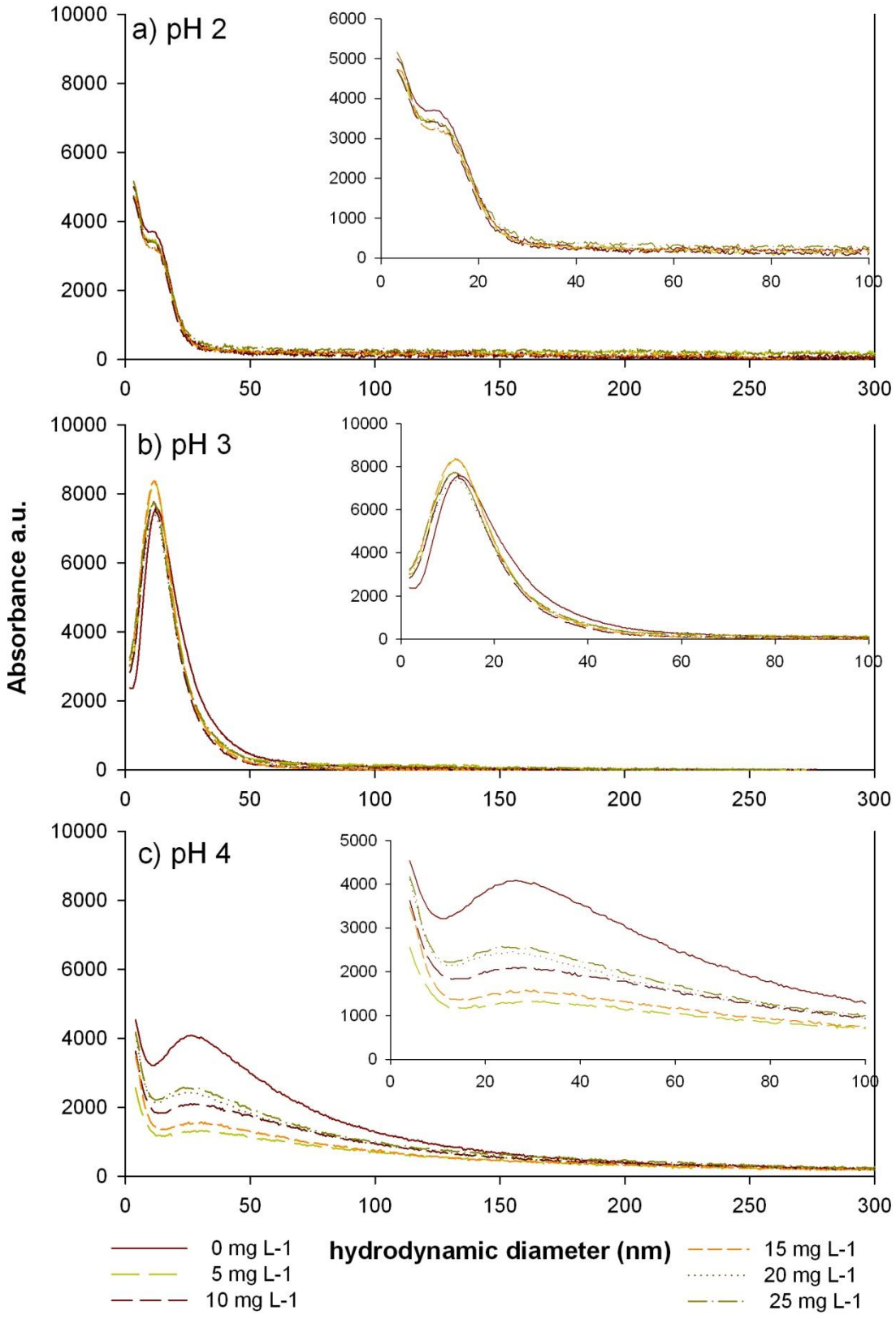

Figure 5. 20 Iron oxide and succinoglycan mixed with iron oxide NPS and fractionated on the F*f*FFF

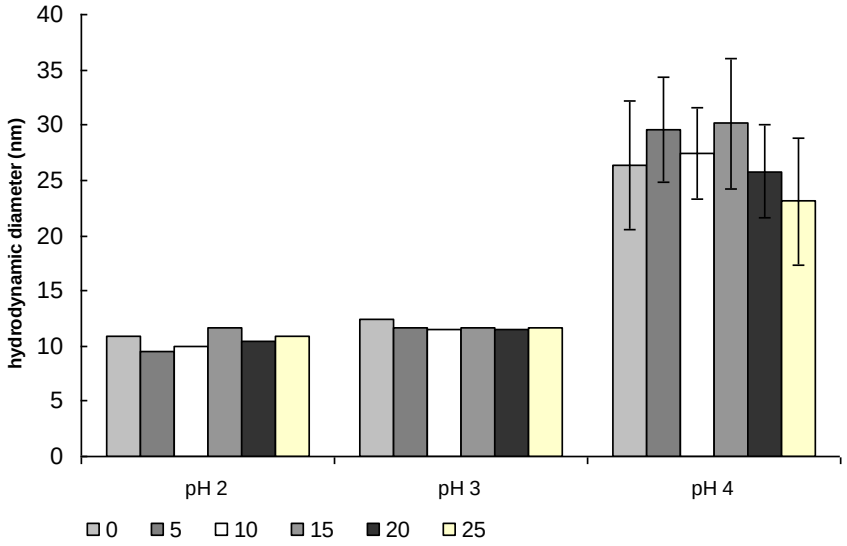

Figure 5.21 Particle size (*Hd*) of iron oxide and 0-25 mg L^{-1} PS obtained from FlFFF peak maxima fractograms for pH 2, 3 ad 4. Error bars are st dev of 3 measurements.

particles. Aggregation in the absence of HS is was minimal at pH values less than 5.5, and aggregation occurred between pH 5.5 and 8. The aggregated state of the samples made it unsuitable for separation in the F*l*FFF channel. However, DLS enabled measurement above pH 5 and revealed a maximum particle size at pH 8 of approx 8 μm (Figure 5.6b), which agrees with Cromieres *et al.,* (2002). Notably particle size was much larger in the presence of humics; however, in DLS the presence of aggregated humics can themselves contribute to the z-average and is therefore not particularly accurate in these conditions. Particle size closely follows the EPM charge data, where reduced charge leads to particle instability leading to aggregation and therefore aggregation can be explained by charge effects.

5.5.2 Effect of FA and PHA on the point of zero charge of iron oxide NPs

Particle size closely follows the EPM charge data, where reduced charge leads to particle instability leading to aggregation and therefore aggregation can be explained by charge effects. The point of zero charge of the iron oxide nanoparticles was calculated to be pH 7.1.

In theory, the addition of HS lowers the pzc due to electrostatic shielding from the humics (Illés and Tombácz, 2006). This lowering of the pzc as an effect of the presence of HS was not apparent from the results with PHA, and with SRFA the alteration was minimal. It is likely that, even at high concentrations of HS, incomplete coating by the NOM exposed some iron oxide surfaces, resulting in insufficient stabilisation. HS coating on iron oxide influences the surface charge of the NP, but this coating may change conformation at different pH and HS concentrations, not necessarily behaving as a coherent film under all conditions. Shift in pzc and aggregation are both pieces of evidence Indeed recently, Baalousha (2009) reported little change in the pzc of iron oxides (200 mg L^{-1}) NPs with humic acid at 10 mg L^{-1}, but the pzc was significantly lowered when humic acid was increased to 100 mg L^{-1}. This implies that, for complete NP stabilisation, there is an optimum ratio of HS to iron oxide (Filius *et al.*, 2000; Fuerstenau and Colic, 1999). Equally, a change in iron concentration would affect the pzc.

5.5.3 Influence of NOM concentration on particle size

The size increases of the iron oxides in the presence of NOM can be attributed to a surface coating at low pH (2 and 3). As the size increase (0.5 to 1.3 nm) was approximately the size of the SRFA molecule (Filius *et al.*, 2000), it was likely that it adhered to the surface in spherical conformation (Zhou *et al.*, 2001), thus increasing the hydrodynamic layer. This is consistent with previous observations (Baalousha *et al.*, 2008; Filius *et al.*, 2000). These size changes were largely consistent for all concentrations and pH values i.e. increased particle size as pH and SRFA concentration increased. Interestingly, low concentrations of added SRFA gave a higher, sharper peak for all pH values than when compared to that of the iron oxides alone. Further additions of SRFA of 20 and 25 mg L^{-1} gave broader peaks with

reduced uv absorbance particularly at pH 2 and 3 due to the presence of coalesced and aggregated particles.

At pH 4 and 5 the iron oxide NPs with 5 mg L^{-1} SRFA decreased the particle size and gave a higher, sharper peak. However, further additions of SRFA resulted in the particle size becoming much larger, with pronounced aggregation observed from increased tailing in the F/FFF fractograms. The unexpected decrease in size after addition of small amount of SRFA was repeatable and perhaps due to the influence of free SRFA not sorbed to the iron oxide. Where pH is also increased, the formation of additional iron oxide materials from hydrolysis is likely to be important at least up to pH 4. The increased aggregation at higher NOM concentrations is only partly consistent with charge neutralisation, and bridging mechanisms between NOM and iron oxide may be involved.

The effects of the PHA on iron oxides are very similar qualitatively to the effects of SRFA, with increased sizes due to the reasons discussed above; i.e. nanoscale surface film formation of NOM on the iron oxide NPs, bridging and hydrolysis of dissolved iron. Nevertheless, less consistency in trends is observed due to the complexity of the peat HA compared to the SRFA. The PHA with a higher molecular mass is more polydisperse and aggregates more readily, especially at this low pH, however, as it is more hydrophobic at these conditions it is more likely to bind readily to the iron oxide surface. PHA may also undergo several transformations as pH changes. Interestingly, both the SRFA and the PHA show vast increase in absorbance at pH 5. This observation is seen throughout the data set presented in this chapter.

Size increase of the FeO NPs in the presence of SRFA and PHA strongly indicates that NOM surface films were forming on the iron oxides. At higher pH, the size increase was

due to aggregation. Significantly, this was not as clear in experiments with the exo-PS conducted at pH 2, 3 and 4 (Figure 5. 20).

5.5.4 Effect of succinoglycan on the iron oxides

For the F*l*FFF separation experiment with iron oxides and succinoglycan, there was no major shift in particle size following the addition of PS. Only one notable difference was found at pH 4, where the hydrodynamic diameter decreased with increasing PS concentration. However, error bars are large at pH 4 indicating instability in particle size, so these results need to be viewed in that light. Exo-PS are also negatively charged macromolecules, but with a different (more fibular) molecular structure, and higher MW. Their binding properties and mechanisms may differ from HS, likely forming meshes due to its fibular structure encapsulating particles (Wilkinson *et al.*, 1999).

5.5.5 Examination of the peak areas

Peak area increase, seen with SRFA and PHA from raising the pH 2-4, can be better understood by looking at the amount of material that was present in the void peak estimated as a percentage of the whole fractogram represented in Figure 5.10 and Figure 5.16. The highest amount of material lost was at pH 2 which increased with higher concentrations of HS. This suggests that the loss of material in the void peak at pH 2 (and less at higher pH) is indicative of very small particles present and dissolved Fe^{3+} which probably contained both iron oxides and HS. No clear trend is observed with concentration of HS on actual peaks area, except at pH 2 where there is a reduction in peak area with increasing concentration of both FA and PHA.

5.5.6 The multi-method approach

Data from DLS gives a good estimation of the larger aggregates, whereas investigations using F/FFF reveal a more quantitative and accurate analysis of the primary particle size and smaller aggregates. By using a combination of these techniques (and others, such as TEM, XRD etc where possible) in a multi-method approach a more coherent and accurate picture can be obtained to inform studies on NP fate, behaviour and impacts. Without requisite data from a variety of techniques, partial understanding of transport and biological effects will result.

5.6 Conclusion

Iron oxide NPs were investigated for changes in particle size and surface charge when subject to changes in pH and with additions of different NOM (SRFA, PHA and a polysaccharide). Particle size increased with 1) an increase in pH when raised from pH 2 to 8; and 2) an increase in NOM concentration from 0-25 mg L^{-1} SRFA and PHA, with the exception of exo-PS where particle size either did not change or reduced with increased NOM concentration. In most cases, aggregation could be explained by charge effects. NOM was shown to interact with the NPs forming a surface film which increased stability at low NOM:NP ratios compared to NPs alone. However, at higher ratios, aggregation by bridging mechanisms resulted.

The introduction of large concentrations of iron oxides NPs into the environment would almost certainly aggregate and form sediments. The presence of NOM may allow some small aggregates to remain in suspension in even around pH 7. However, this work confirms that fate and effects of nanoparticles in the environment are critically dependent on interactions with natural organic macromolecules.

A variety of techniques have been used to examine the behaviour of NPs with and without NOM. Discrepancies in the data show that reliance on a single method distorts understanding and is to be avoided as each technique analyses different aspects of the sample. The following chapters explore the process by which nanoparticle size is controlled in the laboratory and the role of ligands; and applies these particles to environmental conditions with a more detailed study on the effect of counter-ions.

6

Silver nanoparticle synthesis with citrate

Chapter Summary

In this chapter the synthesis of silver NPs are investigated with a citrate stabiliser. The aim was to look at how silver NPs can be varied by certain methodological adjustments, with the ultimate aim of producing monodispersed silver NPs suspensions. Several experiments are presented that looked at the rate of reduction, the type of reductant, changes in citrate concentrations and the effects of heating and aging on NP suspensions. Monodispersed silver - citrate NPs (15 nm) were produced by aging at 100°C. These particles were subsequently used in chapter 7 for the investigation of size effects and environmental conditions.

6.1 Introduction

Developed from the classical 'Turkevich' bottom up method, the creation of Ag NPs from a silver nitrate reduction in the presence of tri-sodium citrate has been well documented (Doty *et al.*, 2005; Henglein and Giersig, 1999; Jana *et al.*, 2001; Morones and Frey, 2007; Sun and Xia, 2002). Citrate itself is well known to act as both a reducing and capping agent (ligand), which can control the size, shape and stability of Ag, Au and Cu nanoparticles (Henglein and Giersig, 1999; Pillai and Kamat, 2003). These ligands provide the important role of 'shielding' the particles and preventing coagulation. When silver nitrate is heated with sodium citrate alone, Ag NPs are produced, however, they are highly polydisperse and this is revealed in its wide absorbance surface plasmon resonance (SPR spectra) (Pillai and Kamat, 2003), for which silver has a maximum at 420 nm (Lee and Meisel, 1982; Rivas *et al.*, 2001). While other ligands can be used, the correct choice of capping agent is important as this affects the optical transmission and other properties of the final material (Link and El-Sayed, 2003). By introducing reducing agents such as sodium borohydride ($NaBH_4$), the rate of NP formation can be increased, typically resulting in spherical particles with SPR absorption maxima around 380−400 nm (Pillai and Kamat, 2003). Unlike NP formation using citrate only, this reaction is usually performed at or below room temperature (Van Hyning and Zukoski, 1998). Most recipes are reported in millimolar concentrations and are approximately equal concentrations of silver salt to ligand as larger concentrations may be unstable and largely polydisperse (Henglein and Giersig, 1999; Van Hyning *et al.*, 2001b). However, particle size tuning can be achieved by altering the ligand concentration (Henglein and Giersig, 1999; Rivas *et al.*, 2001). The reactivity of the $NaBH_4$ (i.e. using fresh solutions) also controls the nanoparticle formation.

The properties of the primary particle in the nanoparticle suspension are subject to changes post reduction (Mandal *et al.*, 2001; Matijevic and Scheiner, 1978; Scolan and Sanchez, 1998)

and may involve a secondary growth stage. Therefore, ageing and stability of the NP suspension is a necessary consideration in NP production. Controlling these processes of ageing and growth, is key in the way forward to producing monodisperse particles. Normally aged at room temperature (Henglein and Giersig, 1999), silver NPs have also been subjected to short durations of 10 minutes at temperatures above 60^{o}C (Mandal *et al.*, 2001). The importance of NP ageing was highlighted by Pal *et al.* (2007), who found the biocidal activity of silver NPs diminished with increased ageing time. However, little else is reported on aging of silver nanoparticles

As a result of using commercially available NPs, there have been reported size discrepancies between results when characterised in the laboratory and those stated for the product (Adams *et al.*, 2006). Appropriate in-house nanoparticle preparation followed by extensive NP characterisation has the advantages of potentially providing the researcher a choice of capping agent, particle size and stability, whilst eliminating the need for particle drying and thus preventing unnecessary aggregation. However, the advantages of NP materials supplied from manufacturers, is that they provide a more realistic testing agent comparable, perhaps to products released from industry. Although the synthesis techniques are generally straight forward, not all the above are easily achievable and NP properties are extremely sensitive to reaction conditions (Bronstein *et al.*, 1999).

Reaction conditions also include the concentrations of the reagents. The aims of most NP synthesis are to produce quality (size, shape and monodispersity) and quantity (a larger number of them) of NPs suitable for commercial production. Increasing the NP concentration has been found to increase the particle size range and promote aggregation and is thus a limitation remaining a challenge in the synthesis process. Working reagent concentrations were for this reason chosen from the published literature.

6.1.1 Aims, objectives and structure of chapter

The aims of this chapter are to produce stable monodisperse silver nanoparticles deemed suitable for use in nanoparticle experiments of fate, behaviour, transport and eco-toxicology. The ability to produce NP suspensions of distinct particle size ranges are also seen as desirable and thus are also included in the aims. To achieve these aims systematic investigation of reaction conditions can be done by: 1) changing the ratio of the reagents; 2) changing the temperature pre and post reaction 3) changing the presence and concentration of other reducing agents whilst checking for NP stability by measuring the particle size over time.

6.2 Materials and methods

6.2.1 Basic synthesis of silver citrate capped NPs

Silver nitrate was reduced by sodium borohydride in the presence of tri-sodium citrate to produce a NP suspension. Based on the method described by Jana *et al.* (2001) and Doty *et al.* (2005), the basic NP synthesis was conducted by the following procedure: a 200 mL solution containing 8.7 mg $AgNO_3$ and 14.5 mg citrate was stirred vigorously at 900 rpm, at room temperature allowing rapid contact of reagents. Six mL of the reducing agent, $NaBH_4$, of concentration 38 mg per 100 mL, was added to the $AgNO_3$ and sodium citrate solution. The resultant suspension was then stirred using a magnetic stirrer for a total of 30 minutes. Experimental variations on the above procedure to investigate the effect on particle size are explained below. Subsequent methods chilled the reagent solutions to below 18^{o}C before mixing to maintain temperature consistency. Details of the batches of silver nanoparticle produced that are referenced to in the text can be found in Table 6-1.

6.2.1.1 (a) Experiment to assess the rate of adding the reducing agent

The following experiment investigated the effect of altering the flow rate of the added reducing agent, sodium borohydride ($NaBH_4$) on Ag NP size and SPR. Six mL of a solution containing 38 mg $100mL^{-1}$ $NaBH_4$ was dispensed into the magnetically stirred $AgNO_3$-citrate solution through four different methods:

a) The $NaBH_4$ reagent was pipetted in two 3 mL additions (total 6 mL) in quick succession.

b) Fast addition: Six mL of $NaBH_4$ was placed into a hydrophobic plastic weigh boat and then quickly poured into the stirred citrate and silver nitrate solution.

c) Slow addition: Six mL of $NaBH_4$ was added drop wise over 10 minutes into the stirred citrate and $AgNO_3$ solution.

d) Medium speed of addition: A constant stream was achieved by using 2 pipettes (5 mL and 1 mL in each hand) and steadily injecting into the stirred $AgNO_3$-citrate solution.

All reagent solutions were stirred for 30 minutes, left overnight in a fume cupboard and filtered the next day at 0.1 μm, before storage at 4^oC in the dark.

Table 6- 1 Batch details of the silver nanoparticle solutions showing experimental conditions

Batch no.	$AgNO_3$: citrate ratio	Reductant	rate of reductant $	Ag NO_3 mg/ 200mL	Citrate* mg/ 200mL	$NaBH_4$ mg/ 100mL	Temperature °C	Notes	Section reference
#B1	1:1	$NaBH_4$	(a)two shots	8.7	14.7	37.8	20		6.3.1
#B2	1:1	$NaBH_4$	(b)fast	8.7	14.6	36.7	20		6.3.1
#B3	1:1	$NaBH_4$	(c)slow dropwise	8.7	14.6	36.7	20		6.3.1
#B4	1:5	$NaBH_4$	(d)medium	9.6	75.2	38.5	20	made in batches of 125 ML	6.3.2
#B4a-e	1:5	$NaBH_4$+ AA		9.6	75.2	38.5	20		6.3.2
#B5	1:1	$NaBH_4$	(d)medium	8.4	14.6	38	18	reduced cold, then refluxed for 2 hours.	6.3.4
#B6	1:1.25	$NaBH_4$	(d)medium	8.4	18.6	38	15		6.3.4
#B7	1:1.5	$NaBH_4$	(d)medium	8.7	22.7	38	15		6.3.4
#B8	1:1.75	$NaBH_4$	(d)medium	8.5	25.8	38	16		6.3.4
#B9	1:1.25	$NaBH_4$	(d)medium	8.5	18.6	38.2	17		6.3.5
#B10	1:2	$NaBH_4$	(d)medium	8.6	29.3	38.2	15		6.3.5
#B11	1:3	$NaBH_4$	(d)medium	8.6	44.4	38.2	13		6.3.5
#B12	1:5	$NaBH_4$	(d)medium	8.5	74	38.2	15		6.3.5
#B13	1:7.5	$NaBH_4$	(d)medium	8.4	110.7	38.3	15		6.3.5
#B14	1:10	$NaBH_4$	(d)medium	8.6	147.1	38.3	17		6.3.5
#B15	1:5	$NaBH_4$	(d) 3mL	4.3		36.7	20	Volume 100 mL	6.3.4

$ ((a) medium 3 mL + 3 mL; (b) fast, all at once; c) slow = dropwise over 10 minutes; (d) 5 mL followed by 1 mL

molecular weights	$AgNO_3$	Ag	Na	$TSC.2H_2O$	TSC	$NaBH_4$
MW	169.87	107.87	22.99	294.1	258	37.8

*Tri-sodium citrate (TSC) = $Na_3C_6H_5O_7$

.

6.2.1.2 (b) Experiment to assess the effect of adding ascorbic acid

Batch #B4, was prepared with a higher concentration of citrate (1:5 M ratio $AgNO_3$ to citrate) $NaBH_4$ reduction speed was by method (d), see details in Table 6-1. To four mL sub samples of batch #B4, one mL of ascorbic acid (AA) was added to make final concentrations of 0, 0.02, 0.05, 0.1, 0.15 and 0.2 M AA, and shaken, suspension details can be found in Appendix 10.

6.2.1.3 (c) Aging by heating the Ag NPs suspensions

Four Ag NPs batches #B5 to #B8, see Table 6-1, were made using different molar concentrations of tri-sodium citrate of 1:1 to 1:1.75 M, $AgNO_3$ to citrate (prepared as described in section 6.2.1 using method (d) to dispense the $NaBH_4$). Samples were spilt post reduction and subjected to different ageing treatments. The initial reaction temperature was below room temperature (15-18^{o}C) by using chilled reagents (30 minutes in the fridge) prior to mixing. The sample was split to study the effects of aging. Where 150 ml was transferred, 10 minutes post reduction, and heated, by refluxing, to 100^{o}C for a total of two hours, cooled to room temperature overnight before being placed in the fridge (see refluxing apparatus in Figure 6.1).

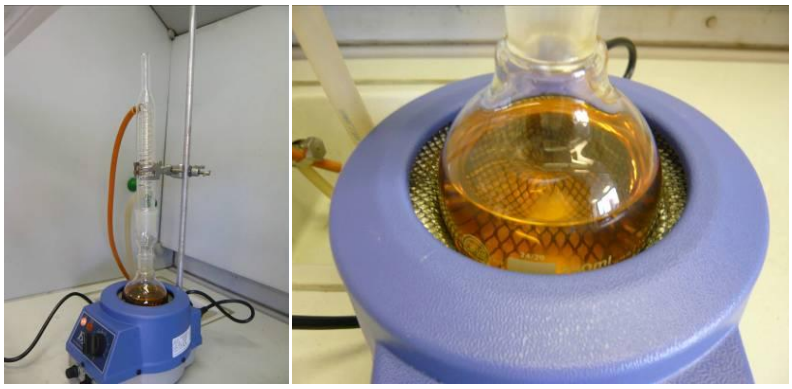

Figure 6. 1 Apparatus used for the refluxing of the reduced silver nanoparticles

The remaining unheated suspension continued stirring for a total of 30 minutes and this suspension was split, with 50 mL was transferred and stored at 4°C in the dark. The remaining 50 mL was left in the fume cupboard overnight then stored at 4°C in the dark. All suspensions were filtered at 0.1 μm the following day. The procedure is explained schematically in section 6.3.4.

6.2.2 Chemicals and materials

All glass and plastic (HDPE) were acid washed in 10% HNO_3 and triple rinsed with pure water (18.2 MΩ) ensuring no traces of acid remained. Chemicals (trisodium citrate, silver nitrate, sodium borohydride) were purchased from Sigma Aldrich and were the highest grade possible (99.9% purity), and stored in a desiccator. Silver nitrate was stored in a dark container to prevent photo oxidation. All reagents were freshly prepared in 'A' grade volumetric flasks and used within hours. Pure water was drawn from either a Barnsted, Nanopure system or a Milli Q system (when the former was out of order), both delivered at 18.2 MΩ. Nanoparticle suspensions were stored in new, acid washed, plastic HDPE bottles in the fridge at 4°C. Suspensions were pipetted using variable pipettes (Eppendorf), tested regularly on a 4-place balance (*Sartorius*). Suspensions were also prepared gravimetrically.

Reduction of silver salts was performed in a conical flask and transferred to a stirred mantle heater with 'quickfit' glassware (round bottomed flask fitted to a condensing column) used for refluxing. NPs were filtered with 0.1 μm cellulose nitrate filter paper under vacuum before analysis.

6.2.3 Instrumentation and analysis

Particle sizing was undertaken by dynamic light scattering (DLS) using a Nanosizer 5000 (*Malvern*) or an HPPS (*Malvern* instruments) Z-averages and the particle distributions graphs were presented here because from the synthesis of a monomodal NPs suspension is

considered an accurate and suitable way of presenting the size distribution data as discussed in chapter 3 section 3.2.3. surface plasmon resonance was measured with a UV absorbance spectrometer (*Lightwave*) and TEM imaging was performed on a Technai F20 (further details available in chapter 3). Sample preparation on TEM slides were by dropping 10 μL of the sample suspension onto 400 holey carbon film copper girds, and left to dry completely. Suspension pH was measured with a VWR gel filled probe, which minimised Cl^- interactions with the silver.

6.3 Results and discussion

The results presented in this section are a series of experiments that focus on the individual steps that are involved in the formation of silver nanoparticles. Collectively the section considers the type of reducing agent, the rate it is added, the ageing temperature, NP stability and the quantity of citrate. The principle objective is to determine whether any of these factors is influential in achieving monodispersity in AgNPs. An additional objective is to examine the physico-chemical properties of nanoparticles by investigating size, shape, colour and SPR of NPs during each stage. The remainder of this section focuses on the following topics in the order they are presented below:

a) nature of borohydride addition

b) nature of ascorbic acid

c) stability and aging

d) aging by heating

e) citrate concentrations

6.3.1 Nature of rate of $NaBH_4$ addition

In this sub-section, changes in the formation of silver nanoparticles are examined under different conditions by altering the rate at which the reducing agent (the borohydride) is added to the citrate and silver nitrate solution. To see the effect on NP size, uniformity, SPR and suspension colour. To demonstrate this, three batches of silver NPs were made for comparison (as described in section 6.2.1):

a) Ag NPs were reduced by adding $NaBH_4$ two shots of 3 mL and then 3 mL

b) Ag NPs were reduced by adding $NaBH_4$ all at once

c) Ag NPs were reduced by adding $NaBH_4$ drop-wise for 10 minutes

d) Ag NPs were reduced by adding $NaBH_4$ 5 ml then 1mL steadily or 'medium' rate using a pipette in each hand.

The effect of NaBH4 addition rate on nanoparticle size was examined, by using the procedure outlined in section 6.2.1.1 (a, b or c) according to speed. Where batch #B1, was reduced by method (a), batch #B2 by method (b), and batch #B3 by method (c).

Nanoparticle suspensions showed variation in particle size colour, SPR peak shape, and morphology depending on the rate at which the reducing agent, $NaBH_4$, was added. Particle size by DLS revealed differences between batches with z-averages of 16 ± 5 nm; for batch #B1, 6.6 ± 2 nm for batch #B2; and 14 ± 0.21 nm for batch #B3 and #B5 11.73 ± 0.5nm.

Figure 6.2 (a)-(c) are the TEM images for batches #B1 to #B2, batch #5 was not examined by TEM. Two images are presented for each batch. The micrographs show variation in morphology according to the method of reduction. Whereas the particles in batch #B1 were reasonable well defined, the particles in batch #B2 were assembled in a more linear fashion. Batch #B3 did not show any evidence of crystallinity.

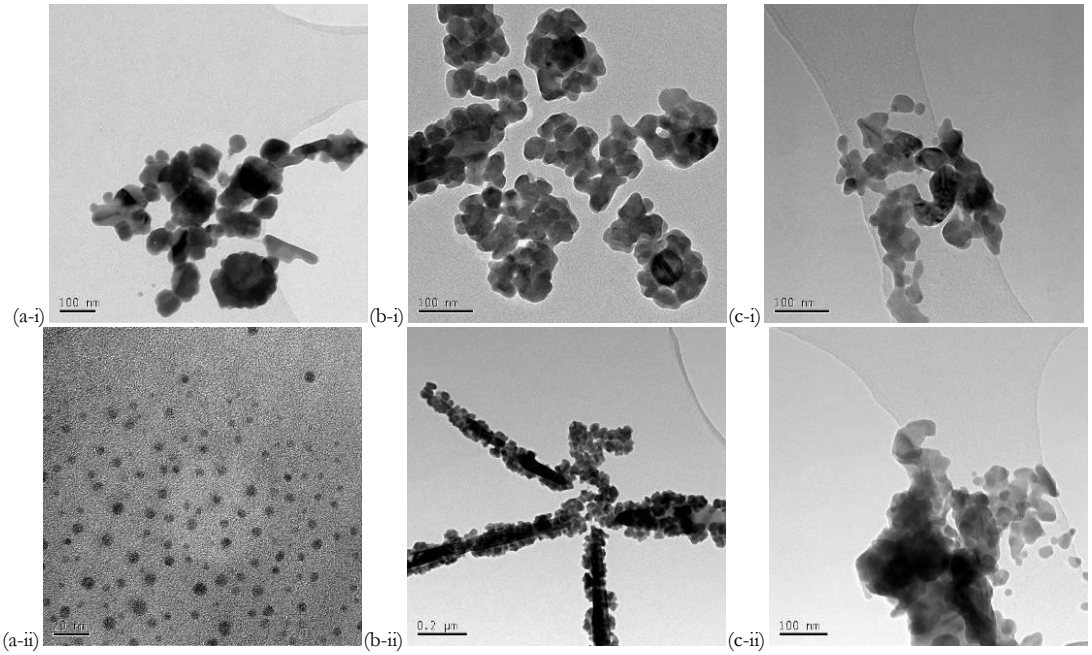

Figure 6.2 TEM micrographs of silver nanoparticles showing different rates of $NaBH_4$ additions: a-i and a-ii (batch #B1, 3ml plus 3ml), b-i and b-ii (batch #B2, all at once) and c-i and c-ii (batch #B3, drop-wise)

The Ag NP suspension was generally golden yellow in colour, which has been widely reported elsewhere (Pal *et al.*, 1997). However, batch #B2, where the $NaBH_4$ was added very quickly, resulted in a suspension that was dark green/brown in colour and was repeatable. Initially, the colour of batch #B1 went dark immediately on adding the $NaBH_4$ turning to yellow within seconds. This observed colour change from dark to yellow occurred throughout all subsequent batches. Van Hyning and Zukoski (1998) attributed the darker colour to the presence of larger particles, which agrees with TEM observations in Figure 6.2 (b-i and b-ii).

SPR peaks for batches #B1, #B2 and #B3 and #B5 are presented in Figure 6.3. Table 6-2 provides additional information on SPR peak height, width and wavelength. Together Figure 6.3 and Table 6-2 illustrate differences in peak shape and height. Batch #B5 had the most absorbance and batch #B2 displayed the broadest width at half peak maxima (WHPM) of 86 au. The narrowest width was batch #B5 with a WHPM of 38 au. The SPR pattern in Figure

6.3 shows some absorbance between 200-250 nm, which Van Hyning and Zukoski (1998) attributed to be a mixture of silver and borohydride and not NPs. Batch #B5 also showed the largest red-shift of any of the peaks. Peak shifting indicates a larger particle size with higher wavelengths. An increase in peak width highlights a polydisperse NP suspension. Z-average size by DLS showed some consistency with changes in SPR absorption (Figure 6.3) as SPR can be influenced by surface chemistry e.g. citrate loading, shape and aggregation. Extremely small (or very large) particles may not appear in the plasmon band as the SPR shows NPs that are approximately between 2 and 50 nm (Link and El-Sayed, 2003). DLS z-averages can be skewed towards a larger size measurement if aggregates are present.

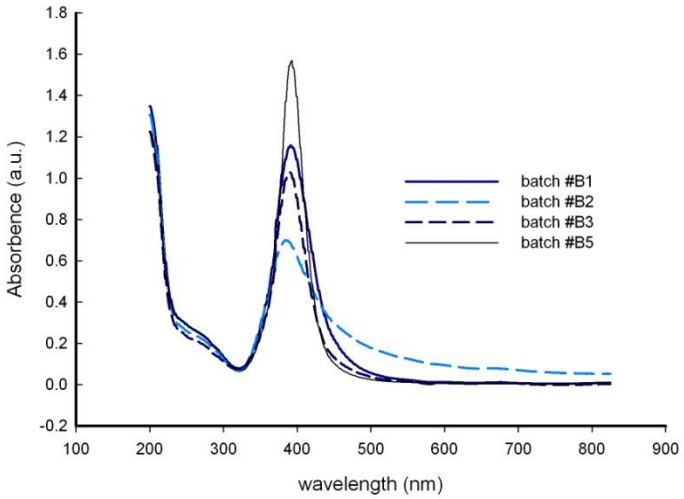

Figure 6.3 Absorbance spectra of the three nanoparticle suspensions made by adding the $NaBH_4$ at different rates: (a) batch #B1 (3ml plus 3ml), (b) batch #B2 (all at once) and (c) batch #B3 (drop-wise). Suspensions have been diluted by three times.

The result of simply changing the speed at which the reducing agent, $NaBH_4$, comes into contact with the reagents, citrate and $AgNO_3$, seems to affect the size, colour, SPR (see Figure 6.2) and morphology of the agglomerates of the finished silver NPs (see Figure 6.1). From these findings method (a), fast addition, produced the smallest but the most amorphous particles whereas method (c) the slow addition, the particles were more polydisperse. Obtaining the optimum particle size and dispersity by tuning in this way led to

choosing most appropriate method (d) which yielded 15 nm particles with the least polydispersity of the four methods tried. It therefore seems apparent from the experimental results that to gain the most defined NPs, the $NaBH_4$ has to be introduced to the stirring reagents at a steady rate or 'medium' method d).

Table 6-2 SPR data for batches *#B1, #B2 and #B3* for the wavelength (λ) peak maxima and the value for the width at half peak maxima (WHPM)

	batch #B1	*batch #B2*	*batch #B3*	*batch #5*
λ (nm) at full peak	391	386	389	393
Absorbance (a.u.) at full peak	1.16	0.70	1.03	1.57
Absorbance (a.u.) at half peak	0.58	0.35	0.51	0.79
λ (nm) at half peak (1)	366	354	368	368
λ (nm) at half peak (2)	424	440	416	412
WHPM (a.u.)	58	86	48	38

Altering other factors of the synthesis process could also change the nature of the resultant Ag NPs and changes to some of these are explored in the following sub-sections in this chapter. One such factor could be including the use of an additional reducing agent such as ascorbic acid, as has been suggested in the literature (Ledwith *et al.*, 2007; Sondi *et al.*, 2003). This provides the focus for section 6.3.2.

6.3.2 Effects on silver nanoparticles using ascorbic acid as a reductant

Ascorbic acid (AA) will also reduce silver nitrate to silver and provides an alternative or additional reducing agent to borohydride. Experiments in the literature have described a further reduction of Ag-citrate seeds to produce larger NPs using ascorbic acid often using a different capping agent of a higher molecular weight (Jana *et al.*, 2001; Ledwith *et al.*, 2007; Suber *et al.*, 2005). Here, an Ag NP batch, batch #B4 made with a higher citrate concentration was reduced further using AA. Immediate colour changes were observed, described in Table 6- 2 with further changes occurring over several days. As described in section 6.2.1, Batch #B4, with a $AgNO_3$ to citrate molar ratio of 1:5 was produced at room

temperature with the $NaBH_4$ dispensed using method (d). Sub-batches consisting of 4 ml aliquots of #B4 described in Table 6-2, had 1 mL of a suspension containing AA added to make a final concentration 0 to 0.2 M AA. All synthesis was performed at 20°C.

Particle colour, SPR, maximum peak absorbance, peak width at half peak maximum (WHPM) and particle size were all found to be affected by additions of AA. Colour ranged from yellow to dark red. Colour change described in Table 6-2, was generally unstable with increasing concentrations of AA and change occurred rapidly over a few hours. Analysis was performed four days after AA additions. However, analysis was not performed with EM in this instance.

Table 6- 2 Colour reactions of adding ascorbic acid to silver citrate NPs suspensions

AA conc (M)	On addition	1 hour	3 days
0	yellow	yellow	yellow
0.02	yellow	light yellow	yellow
0.05	yellow	yellow	pinky orange
0.1	orange/yellow to dark pink	red	pinky orange
0.15	pink to dark pink to cherry red	dark blue	olive green
0.2	pinky orange	pinky orange	yellow

Surface plasmon resonance SPR is presented in Figure 6.4 and shows the variation in peak shape. The WHPM (see Table 6-3) and wavelength at peak maxima (see Figure 6.4) show a red shift with increasing AA concentration until 0.1M after which a blue shift occurs with further increase until 0.2 M. Higher AA concentrations of 0.15M and 0.2 M caused further peaks at 600 nm, indicating presence of larger particles. This agrees with the larger particles obtained by (Velikov *et al.*, 2003) with increasing AA concentration. An additional peak is observed at 263 nm with concentrations greater than 0.05 M AA and can be accounted for the presence of AA.

Particle size, analysed on day 4 by DLS, ranged from 14 to 57 nm with the largest size resulting from the 0.1M AA addition (Figure 6.5). The particle size (DLS z-average) increased with increasing AA concentration until 0.1M AA. AA increases thereafter, resulted in a reduction in particle size. This was probably either due to sedimentation of

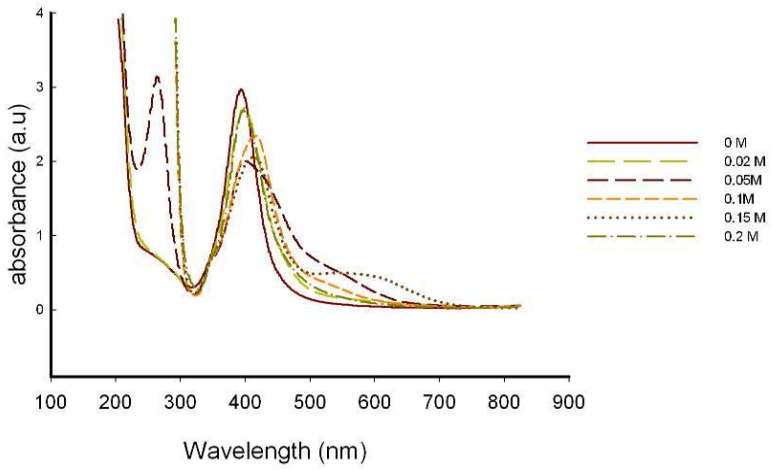

Figure 6.4 SPR UV spectra of 1:5 Molar ratio Ag-citrate NPs with, 0- to 0.2 M ascorbic acid added. Results are an average of three measurements.

Table 6-3 SPR data for λ at peak maxima absorbance intensity and width at half peak maximum (WHPM)

	0 M	**0.02 M**	**0.05M**	**0.1M**	**0.15 M**	**0.2 M**
λ (nm) at full peak	393	400	401	417	412	398
Absorbance (a.u.) at full peak	2.972	2.721	2.001	2.343	2.058	2.685
absorbance (a.u.) at half peak	1.486	1.360	1.000	1.172	1.029	1.342
λ (nm) at half peak (1)	365	366	366	370	366	370
λ (nm) at half peak (2)	423	435	474	452	454	434
WHPM (a.u.)	58	69	108	82	88	64

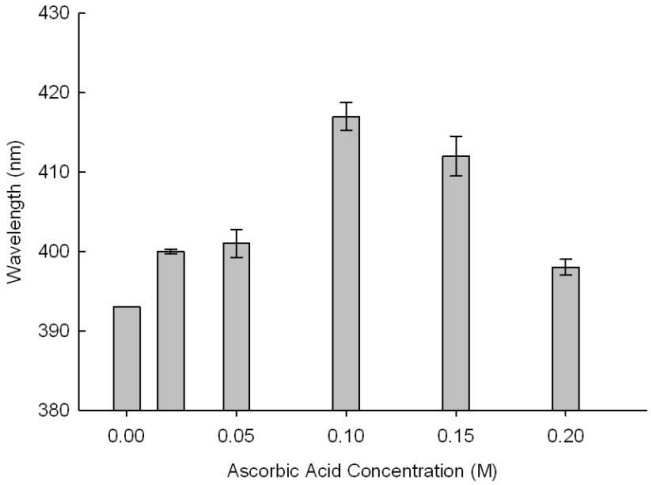

Figure 6.5 SPR maximum absorbance peak wavelength for suspensions with additions of ascorbic acid 0-0.2 M along the x-axis. Results are an average of three measurements and error bars are standard deviations.

aggregates (indicated by sample turbidity) or because dissolution occurred due to the presence of acid. There is a trend of increasing DLS particle size (Figure 6.6) with a shift of SPR peak maxima (Figure 6.5), but particle size and WHPM show no relationship.

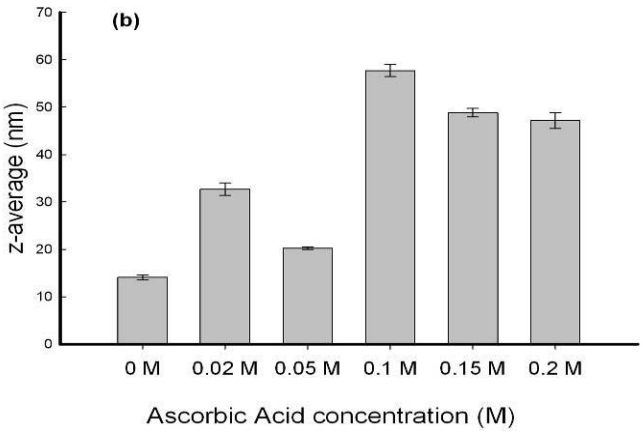

Figure 6. 6 DLS z-average (nm) for suspensions with additions of ascorbic acid 0-0.2 M and are an average of three measurements measured 4 days after addition

Instability of some suspensions was observed. This is likely to be due to the reaction of AA with Ag NO_3 to give two moles of HNO_3 (a strong oxidizer and acid) (Stathis, 1948), which can destabilise the freshly formed Ag NPs back to Ag^+. Tri-sodium citrate in this instance may not be a robust enough to shield the particles in the presence of the newly formed acid

(Suber *et al.*, 2005). More resilient capping agents, such as Daxad 19 (sodium salts of naphthalene sulphonate formaldehyde condensate (mol wt 8000), have been identified in the literature to stabilise silver NPs when reduced by AA providing spherical and pyramidal particles of 15 and 26 nm (Sondi *et al.*, 2003; Suber *et al.*, 2005). The presence of a peak at 250 nm in some SPRs (see Figure 6.3), indicate that not all the AA has been consumed during the reaction. If the reaction continues further, and produces more acid, then the Ag NPs may re-dissolve in acid condition.

6.3.3 Effect on Ag NPs particle size over time

Tri-sodium citrate is considered a good stabilising agent for silver nanoparticles (Henglein and Giersig, 1999). Stability was tested in batch #B2 by monitoring changes in SPR and z-average size intensively for a short period and an aliquot of batch #B1 was recorded at intervals over a 15 day period. In addition, batch #B2 was measured over a two day period every 23 minutes for 100 measurements at 25°C in the dark.

Figure 6.7 is the z-average taken from DLS every 23 minutes, fluctuation in size can be observed, which may be due to instrumental drift as fluctuations are less than 1 nm. However, the dip in particle size may be due to a period of settlement from aggregation followed by another period of growth. The fluctuations are insignificant as no net particle size change is observed – the average size was 6.64 ± 2 nm. This compares to an original size z-average of 5.8 nm taken on the day of synthesis.

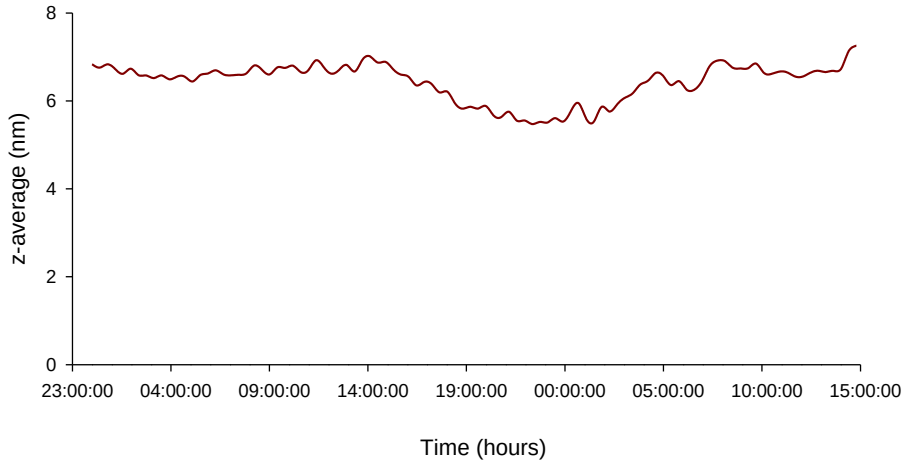

Figure 6.7 Batch #B2 DLS, z-average (nm) time series for 100 measurements over 44 hours at 25°C

The data presented in Figure 6.8 represent the particle size distribution of batch #B2 taken for the 1st, 10th 50th, 80th and 100th measurement. The graph shows a bimodal distribution for 1-3 nm with another size around 50-60 nm. This graph is a breakdown of the given z-average output, of about 6 nm. There is no actual peak at 6 nm and this demonstrates that the z-average value is an average of particle distribution size. According to the manufacturer (*Malvern*), the z-average is the most comparable number to measurements from other instruments.

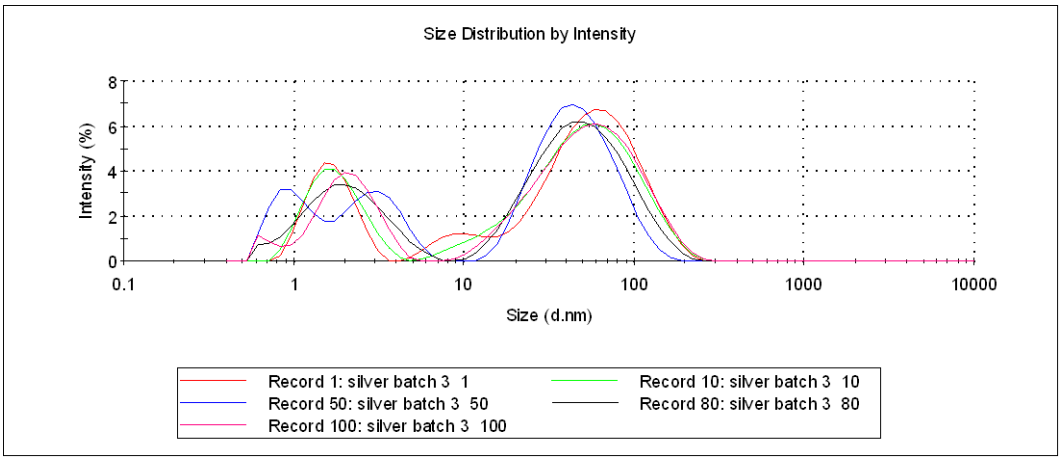

Figure 6.8 DLS size distribution by intensity for batch #B2 taken at intervals over a 44 hour period at 1, 10, 50, 80 and 100 for batch three

Figure 6.9 shows the variation in SPR from aliquots taken from batch #B1 (initial DLS measurement 15 ± 4.9 nm) taken over the first 15 days post synthesis. The samples were stored at 4°C in the dark after day 1. The SPR peak maxima gained height and red-shifted to a maximum peak absorbance, from day 1 to day 3, of 388 nm to 397 nm. Moreover, the WHPM reduces from 76 to 56 a.u. indicating from the peak narrowing that the NP suspension changes during this period (see Table 6-4). From day 3 to 15 little change is observed suggesting that NPs were stable over this time period.

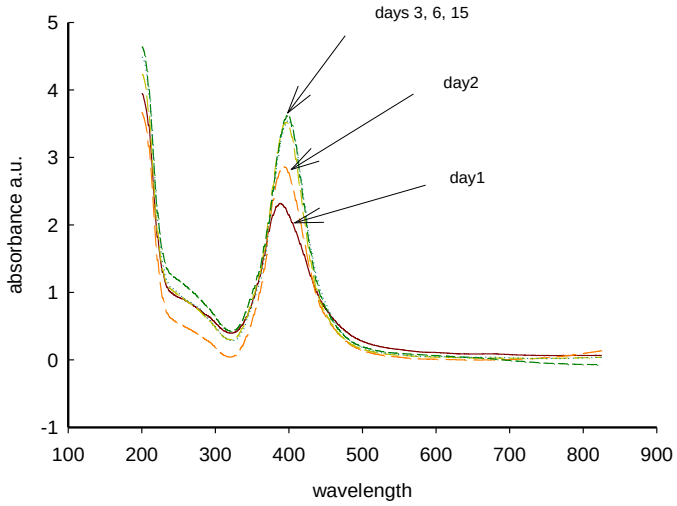

Figure 6.9 Absorbance spectra of Ag–citrate NPs, batch #B1 analysed at intervals for 15 days after synthesis

Table 6- 4 SPR data for λ at peak maxima absorbance intensity and width at half peak maximum (WHPM)

	Day 1	Day 2	Day 3	Day 6	Day 15
wavelength at full peak	388	393	397	397	389
absorbance at full peak	2.32	2.87	3.52	3.62	3.56
absorbance at half peak	1.16	1.43	1.76	1.81	1.78
wavelength at half peak (1)	357	368	369	369	370
wavelength at half peak (2)	433	427	425	426	427
WHPM	76	59	56	57	57

Particle size for batch #B1 (initial DLS measurement 15 ± 4.9 nm) was also measured by DLS at intervals over time when stored in the dark at 4°C, day 7 (9.91 ± 0.6 nm), day 14

(11.2 ± 0.6 nm), day 21 (11.3 ± 0.6 nm). However, stored at room temperature for day 21 it had increased to 31.2 ± 0.4 nm, showing that the light and temperature had an effect on particle size during storage.

This short study demonstrates that the silver nanoparticles undergo initial changes (or aging) post synthesis, but after 3 days of being stored in the dark at 4 ^{o}C changes are minimal and so the suspension is deemed stable. The mechanism for change, from observations in SPR, has been postulated by Van Hyning and Zukoski (1998), using the Drude model for dielectric properties, whereby Mie theory predicts that in the 6−10 nm particle size range the location of the surface plasmon peak does not change significantly but the absorption maximum grows. It is possible that as oligomeric species are lost, the silver particles grow (Van Hyning and Zukoski, 1998).

From measurement of batch #B1 over time particles show small variations, possibly because of particle ageing under different conditions. In section 6.3.4, ageing is exploited as a means of achieving monodisperse particles and examines in more detail particle size at different stages of the NP production. Moreover, other researchers have reported applying ageing times of 5-7 hours (Jana *et al.*, 2001; Mandal *et al.*, 2001), and change in particle shape (Suber *et al.*, 2005).

6.3.4 Effect of ageing from heating

The previous sub-section showed that silver nanoparticles were sensitive to storage conditions of light and temperature post reduction possibly due to silver's photosensitivity (Liz-Marzan and Lado-Tourino, 1996). This sub-section attempts to control NP aging over a short period at a high temperature of 100^{o}C with the aim of producing uniform NPs. The

synthesis procedure was as described in section 6.2.1.3 on four batches consisting of different silver to citrate molar ratios (see Table 6.5). NP heating has been reported as either part of the synthesis or ageing. Heating by refluxing immediately after synthesis however, has not been reported in detail. Heating, was performed in a stirred mantle heater with a condensing unit to minimise vapour loss, and refluxed for two hours, as shown in Figure 6.1. Preliminary tests on previous batches demonstrated that the boiling of freshly made NPs, reduced sample polydispersity. Figure 6.10 shows the pathways for the experiment.

Table 6- 5 Summary of batch conditions used in this section

	Ag : Citrate ratio	Reduction temperature
Batch #B5	1:1	15
Batch #B6	1:1.25	15
Batch #B7	1:1.5	16
Batch #B8	1:1.75	17

Suspension boiling affected particle size and increased monodispersity of Ag NPs compared to NPs suspension that had not been heated. Figure 6.11 shows the SPR peaks for the silver NPs for each of the four batches #B5 to #B8 (a-d) for the three different post synthesis treatments; fridge only (4°C in dark), room then fridge, and boiled-room then fridge. In every case where the particles had been boiled, the SPR peaks are higher and sharper than for the particles that underwent lower temperature ageing, indicating that the smaller particles not visible by SPR had grown to form larger particles that absorbed at approximately 400 nm. In Figure 6.11(b) there is some peak shift, which cannot be explained, but compared to DLS result in Figure 6.10 below batch #B6 also shows a larger particle size from boiling.

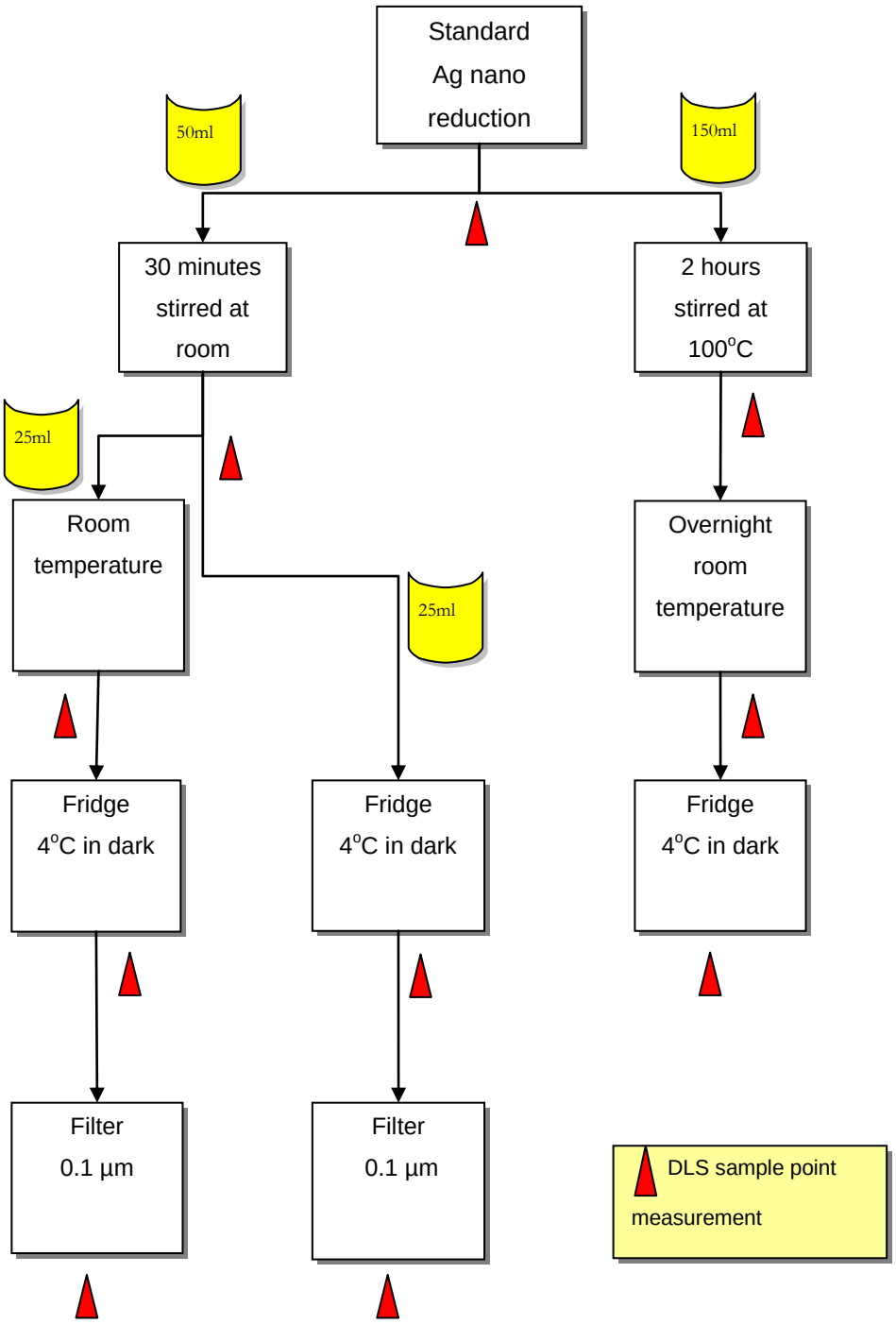

Figure 6. 10 Schematic diagram of ageing experiment showing pathways of different treatments of sub-samples with indicators where suspension aliquots were taken

The SPR results in Figure 6.11 demonstrate an increase in absorbance maxima as a result of boiling and agrees with those of Van Hyning *et al.*, (2001a), who reported NPs were produced from suspensions previously reduced at higher temperatures (2-60°C). Other studies of temperature effects on SPR (Ledwith *et al.*, 2007; Van Hyning *et al.*, 2001b) are nearly always with NP suspensions that have used a higher reduction temperature. In this study, the nucleation reduction was performed at low temperature, and then subjected to 100°C. At the higher temperatures, citrate acts as a reducing agent as well as a capping agent (Ledwith *et al.*, 2007). Furthermore, increased reaction temperature also increases borohydride consumption (Van Hyning *et al.*, 2001a) thus having an effect on formation of NPs.

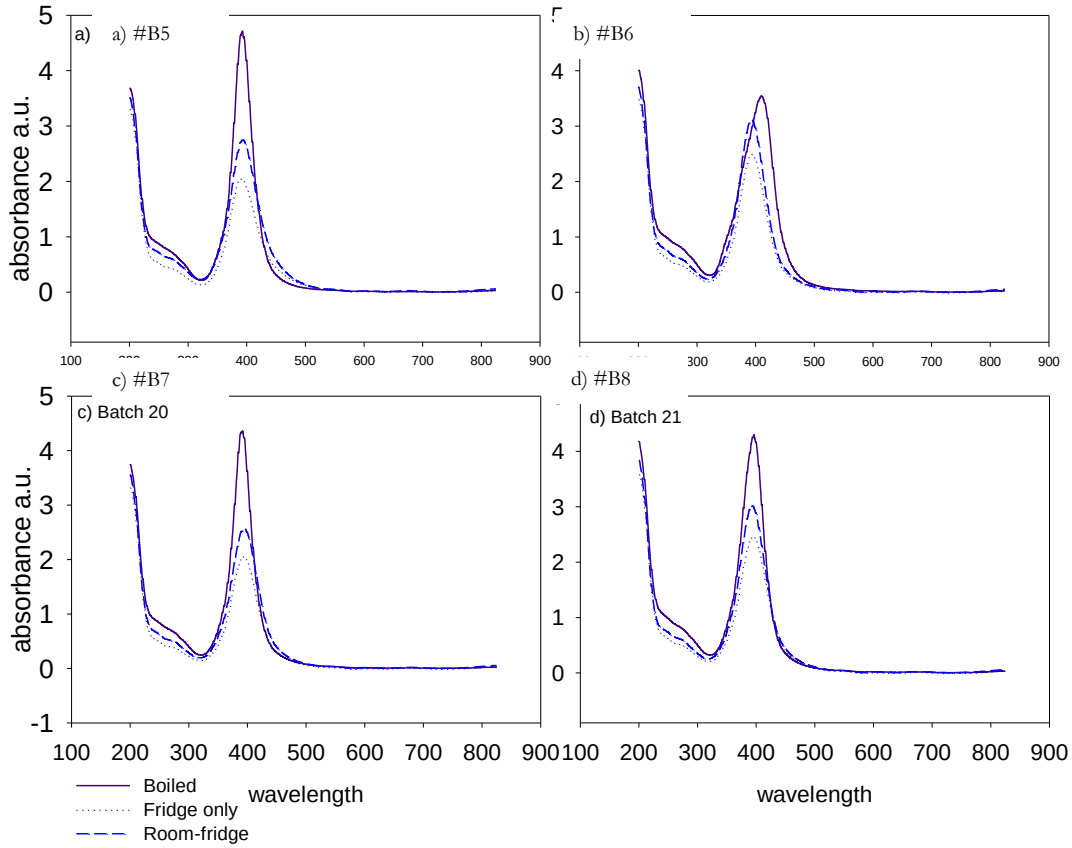

Figure 6.11 Result for batches #B5 – #B8 UV absorbance SPR taken for three different treatments post synthesis: 1) stored in the fridge only; 2) stored at room temp overnight, then in fridge; or 3) boiled, room then placed in the fridge

More detail can be learnt about NP formation from taking aliquots of the NP suspension at different times during the reaction. The following graphs, Figure 6.12 and Figure 6. 13, show that changes occur with time and between batches. Figure 6.12 shows that immediately after synthesis nucleation (3 minutes) samples revealed minimal polydispersity. When nucleation occurs, small NPs are produced which subsequently grow, but after boiling the size range is reduced and particle size increased. From comparison to aliquots taken at 3 and 15 minutes, the boiling of NP suspensions does not appear to reduce the polydispersity but rather prevented it from increasing (Figure 6.12). The exception is batch #B5 consisting of equal molar quantities of $AgNO_3$ and citrate where boiling appears to reduce the polydispersity. In most cases, average particle size increased from boiling with the exception of batch #B7 (Figure 6.12(c)). The differences in the sizes from DLS are presented in Appendix 11.

NP size for all batches did not alter much between 3 and 15 minutes indicating that the first stage of the reaction is complete within 3 minutes of adding the reducing agent (Figure 6.12). The initial size of the NP is about 10-13 nm and shows a mono-modal distribution. The period following up to 2 days, sees much alteration the NP suspension particularly according to treatment. Boiling alters the particle size range depending on the amount of citrate used with an increase in the average size and distribution.

The difference in the NP batches according to treatment post nucleation is shown in Figure 6. 13. Suspensions that had been boiled (3) were more monodisperse about 5-35 and 5-60 nm compared to suspensions that had been aged at room temperature or colder (1 and 2) which were bimodal with < 100 nm. The suspensions that had been transferred straight to the fridge (1) showed the greatest polydispersity and batches #B6 and #B7 show bi-modal distributions.

a)

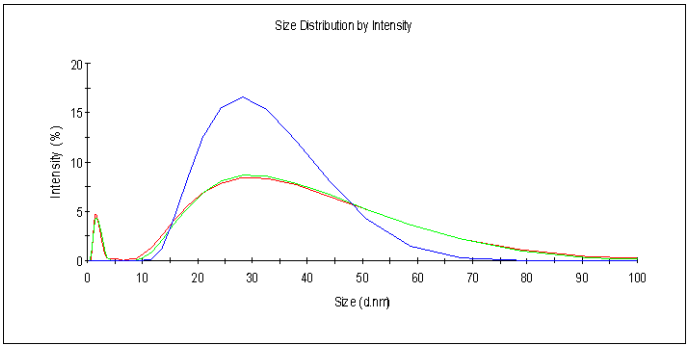

b)

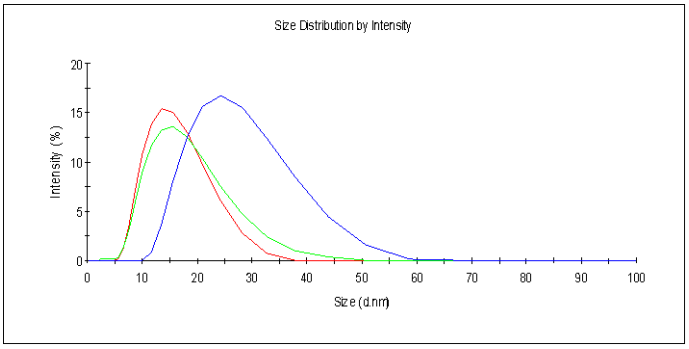

c)

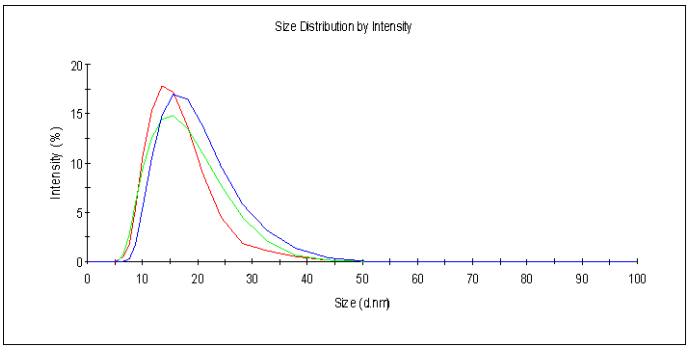

d)

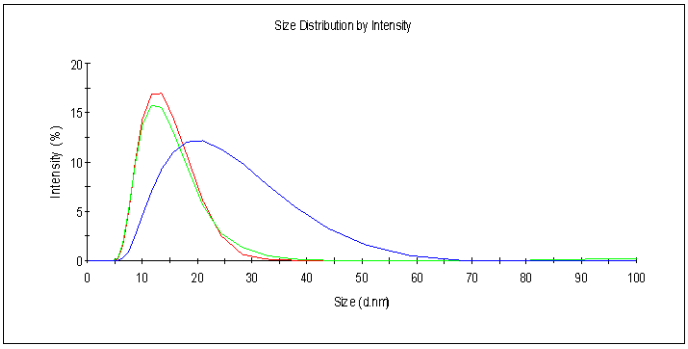

Figure 6.12 DLS size distribution by intensity for 3 (red), 15 minutes (green) and post boiling (blue) for a) batch #B5 1:1, b) batch #B6 1:1.25, c) batch #B7 1:1.5 and d) batch #B8 1:1.75. Averages are taken over three measurements.

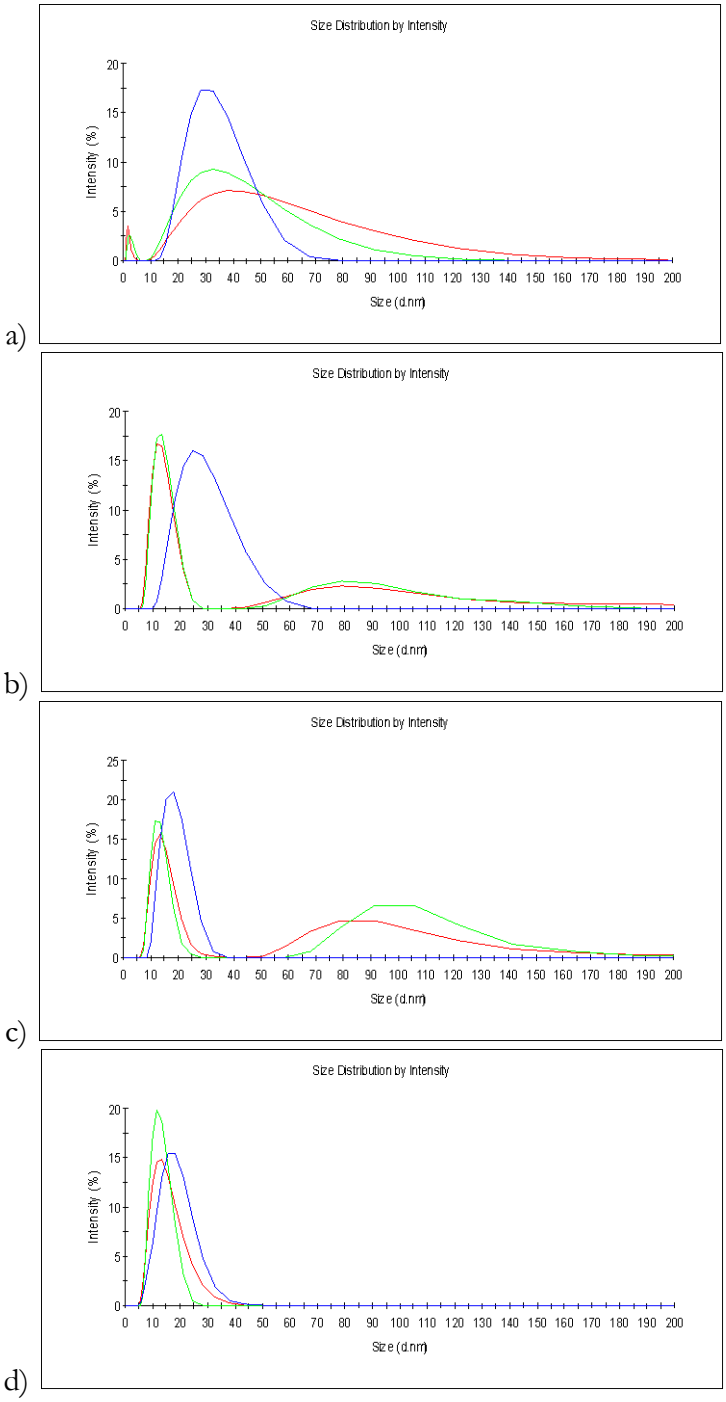

Figure 6. 13 Batch #B5-#B8 after day 3 for samples subject to fridge (red), room then fridge (green) and boil, room then fridge (blue) for: a) batch #B5, 1:1; b) batch #B6, 1:1.25; c) batch #B7, 1:1.5; and, d) batch #B8 1:1.75 where the ratio value is the concentration (M) of $AgNO_3$ to trisodium citrate. Each line is an average of three measurements.

Particle sizes for these suspensions are presented in Appendix 11. Only small changes were observed between day 2 and 3 and only the data for day 3 is shown here (Figure 6.13). By transferring the NPs straight to the fridge, particularly for batches #B5 and #B7, the NP

suspensions show more polydispersity than those that had spend a period at room temperature in the light.

The amount of citrate present controls the original particle size at synthesis. In addition, the particle size at 100°C with citrate present will change as the citrate chemically reduces the Ag NPs as well as stabilising them. Figure 6.14 shows that the particles are uniformly spherical as a result of heating the suspension post nucleation. Compared with the TEM image showing the particles of Batch 1, 2 and 3, that had not undergone heating (Figure 6.2), the particle shown in Figure 6.14 are more evenly distributed showing no agglomeration. Heating the NPs resulted in more rounded NPs shapes and agrees with the results of Ledwith *et al.,* (2007) and Mock *et al.*, (2002). However, the suspension of Mock *et al.*, (2002) went green and all suspensions in this experiment were yellow.

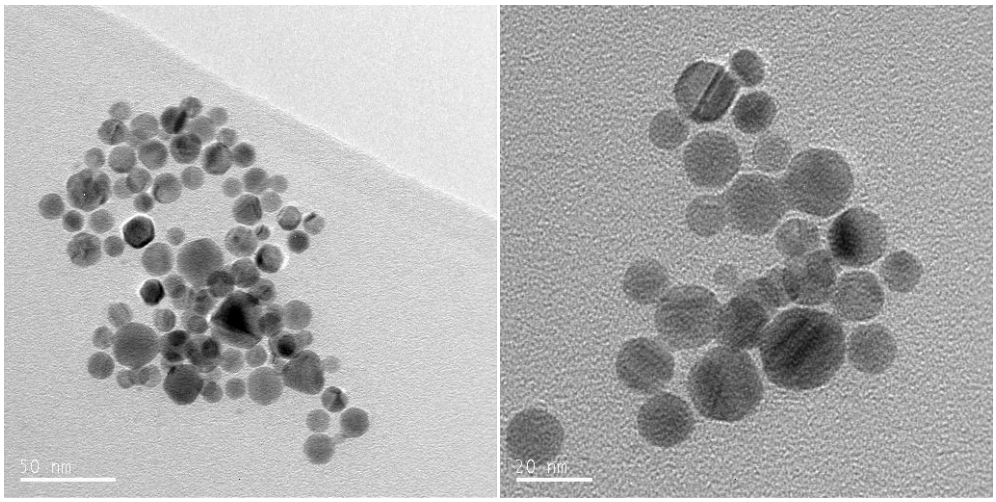

Figure 6. 14 Spherical or near-spherical particles achieved by boiling (images of batch #B9)

Figure 6.15 shows the DLS z-average of particle size according to post nucleation treatment. Batches that were not boiled showed a larger degree of variation in particle size than those that were boiled/heated, with the latter NPs remaining small and showing little variation throughout.

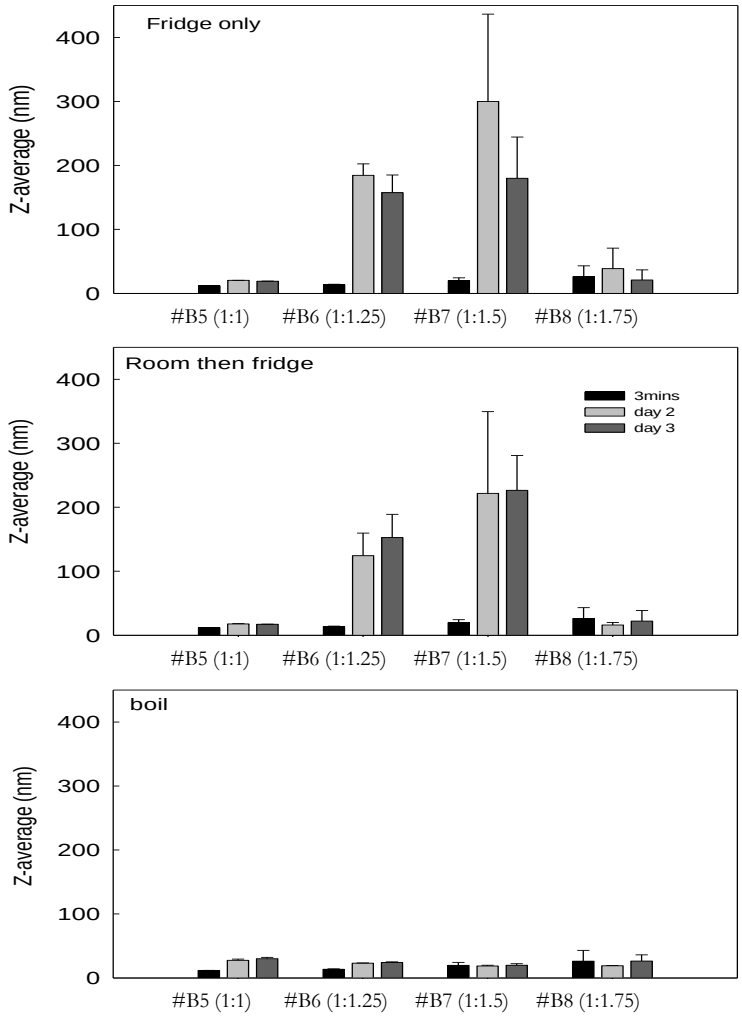

Figure 6.15 DLS z-average for batches #B5 to #B8 for measurements taken at 3 minutes, 2 days and 3 days post synthesis. Treatments post synthesis are for (a) placed immediately at 4°C in the dark; (b) left overnight, then in the cold and dark; and (c) boiled, cooled at room temperature overnight then at 4°C in the dark.

Exposure to UV light may also be responsible for NP ageing (An *et al.*, 2007). Figure 6.16 is of a sub sample of a batch #B15 containing 1:5 Ag:citrate left at room conditions in the light for two weeks. Its colour changed from yellow to green and the TEM image revealed large

particles well over 100 nm with smaller particles appended to them. This agrees with the colour changes with slow ageing of Sastry *et al.,* (1997) where colour is related to particle size (Ledwith *et al.*, 2007). On placing in the fridge, no further colour change was observed.

Figure 6.16 Silver-citrate of batch #B15 NPs left on the bench for 2 weeks. The initial colour was yellow, but turned green. TEM image of the suspension centrifuged onto the grid. The scale bar is 100 nm colour remained stable once placed in the fridge, where as others left out went on to be blue before eventually losing colour completely.

In one particular batch the particles remained small as a result of the heating process (#B7, Figure 6.15 (c)). It is possible that several mechanisms are (simultaneously) at work here. Pilli and Karmat (2003) postulated an initial formation mechanism by small clusters agglomerating to form larger stabilised capped nanoparticles, as shown in Figure 6.17, which probably occur during nucleation. It is likely that similar mechanisms could be operating here, for example, small particles can be seen attached to the outside of the larger particle in Figure 6.16.

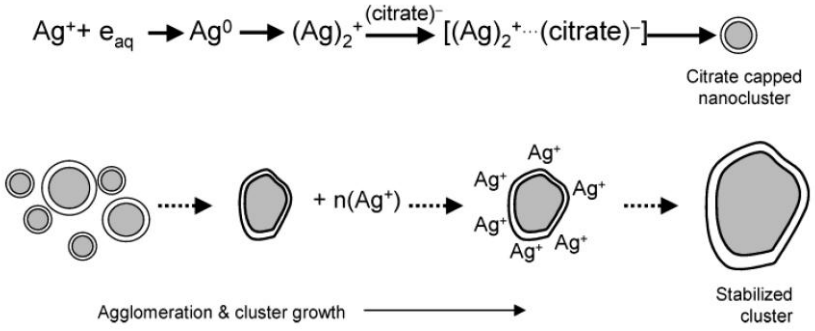

Figure 6.17 Primary and secondary growth in the formation of silver nano crystallites. Taken from Pilli and Karmat (2003)

In this work, the ageing process by heating, reduced the particle size range in the 1:1 M ratio (see Figures 6.12(a) and 6.13 (a)). The mechanism by which it reduced the number of larger particles, was probably by etching (removal of outside sharp bits), as proposed by An *et al.,* (2007) and illustrated in Figure 6.18. The boiling process resulted in the spherical particles shown in Figure 6. 14, which can be contrasted with the Ag NPs shown in Figure 6.2 that were not boiled. Therefore, the author postulates that the fragments from the etched particle during boiling would then agglomerate to form new particles.

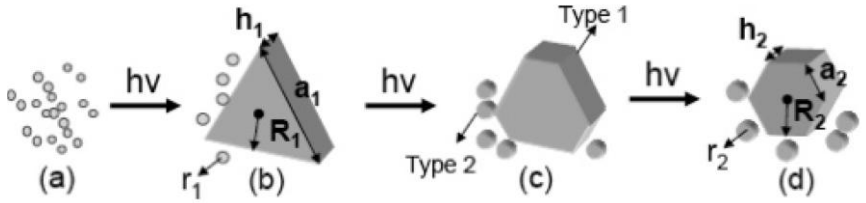

Figure 6.18 Schematic diagram of photo induced shape evolution of triangular to hexagonal silver nanoparticles. Taken from An *et al.,* (2007)

6.3.5 Effect of particle size on citrate concentrations

Altering the concentration or the molar ratio of the metal salt to the citrate ligand can produce particles of different shapes and sizes (Henglein and Giersig, 1999; Ledwith *et al.*,

2007). Nine NP suspensions were prepared with different citrate concentrations, the Ag NO_3 concentration was the same throughout. The data presented below in Figure 6.19 are Ag–citrate NP suspensions produced by the method in section 6.3.4. All nanoparticles were subject to boiling for 2 hours and left for 24 hours before measurement. Size was analysed by DLS and electrophoretic mobilities were also measured at the same time.

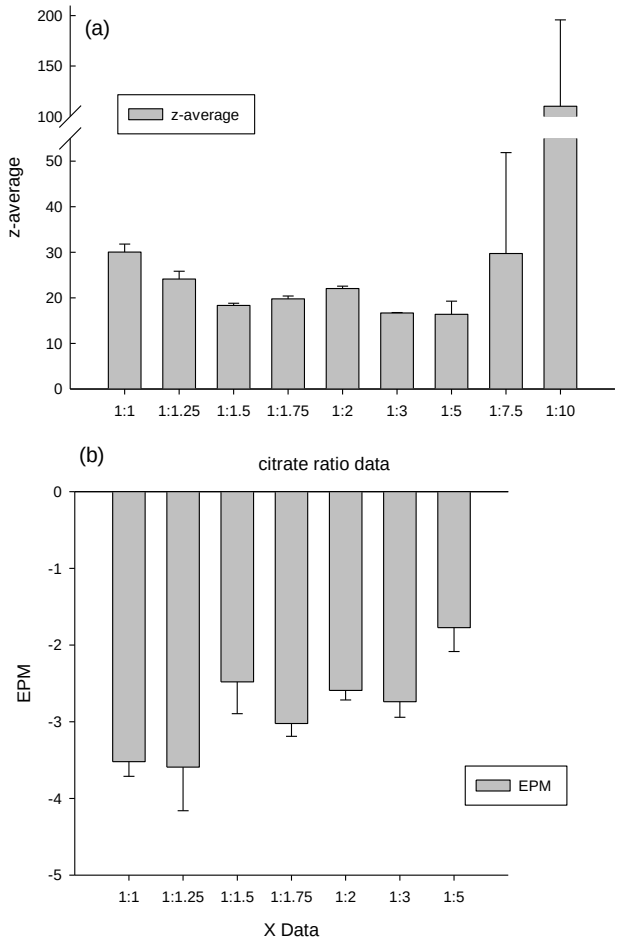

Figure 6. 19 shows (a) particle size as a function of citrate concentration shown as a ratio of Ag : citrate; (b) the electrophoretic mobilities for the same data. Data for 1:7.5 and 1:10 are absent.

Interestingly, the results are not linear, increasing the ratio of Ag NO_3 to citrate from 1:1 to 1:5 M reduced particle size with the lowest sizes at 1:3 and 1:5 ratio. At 1:7.5 particle size increases and as it does, so does the standard deviation which indicates increased polydispersity. Of further note is the behaviour of the electrophoretic mobilities. EPM decreases with increasing citrate concentration and particle size, and does not fit the

assumed relationship of low EPM and high particles size because of aggregation occurring from a low surface charge. Rivas *et al.* (2001) changed the citrate concentration without using a reducing agent and found that increasing the citrate concentration decreased the particle size and made them more monodisperse. The relationship with citrate is, however, complex (Henglein and Giersig, 1999). At low citrate concentration, the citrate layer is not so effectively built up around the Ag clusters and NPs are not fully protected from further reaction (Henglein and Giersig, 1999).

6.4 Conclusion

The factors determining nanoparticle shape and size in a standard borohydride reduction with silver nitrate in the presence of citrate is complex. However, by controlling one or more of these factors, monodisperse nanoparticles can be achieved. Ascorbic acid can also be used as a reducing agent on silver nanoparticles which will alter the size; however, this process is difficult to control even at low concentrations and is a slower reaction compared to $NaBH_4$. It was found that the rate of $NaBH_4$ addition, ageing temperature and the concentration of citrate were critical factors in the resultant particle size and monodispersity of the NP suspension. Changing the citrate concentration, for example, did not create linear results in terms of particle size due to coalescence at higher concentrations.

In the next chapter, chapter 7, particles from these experiments were cleaned and characterised further, then subjected to additions of NOM, Ca^{2+} and Na^{+} counter ions at pH 5 and pH8.

7

Behaviour of Ag NPs under environmentally relevant conditions

Chapter Summary

In Chapter 6, monodisperse silver nanoparticles (Ag NPs) were produced, in this chapter, Ag NPs were further characterised using field flow fractionation and investigated for changes in particle size under conditions of pH 5 and 8, humic substances and counter ions. Environmentally relevant fate and behaviour investigations such as these are essential to gain understanding towards bioavailability and toxicology. Results showed that the presence of HS improved stability of Ag NPs under these conditions by forming a surface coating, resulting in both steric and charge stabilisation. This implies that Ag NPs could have longer residence times in aquatic systems may be possible with HS, increasing bioavailability. Chapter 7 was published in *Chromatography A* (Cumberland and Lead, 2009).

7.1 Introduction

Silver NPs (Ag NPs) are the main NP type in use currently in consumer products (Luoma, 2008) as they have powerful anti-microbial properties (Sondi and Salopek-Sondi, 2004) and show potential in medicine and health-related areas. Silver toxicity to many organisms has long been known in the dissolved or ionic form (Reinfelder and Chang, 1999), with sources from discharges also occurring from the photographic industry and mining (Eckelman and Graedel, 2007). More recently, significant concerns have been expressed about the potential risk of Ag NPs, due to the current and projected high exposure (Luoma, 2008; Mueller and Nowack, 2008) and their likely high hazard and toxicity in the environment (Klaine *et al.*, 2008). Indeed, a number ecotoxicology studies of Ag NPs in algae, bacteria, invertebrates, fish and humans in both in vivo and in-vitro studies (Braydich-Stolle *et al.*, 2005; Carlson *et al.*, 2008; Gopinath *et al.*, 2008; Hwang *et al.*, 2008; Lubick, 2008; Soto *et al.*, 2005; Yoon *et al.*, 2008) have been conducted. Suggested mechanisms of action of toxicity include oxidative stress, binding to thiol groups on proteins, cell wall pitting, changes in membrane permeability and effects on the proton motive force and ATP generation (Choi and Hu, 2008; Lok *et al.*, 2006). In addition, lowest observed effect concentrations (LOECs) range from a few ng L^{-1} to tens of mg L^{-1}, with the differences due to a number of factors such as species differences and suspension conditions. However, one of the major uncertainties is in accurate dose measurement, appropriate characterisation and the use of commercially available nanoparticles which are polydisperse, heterogeneous and not easily dispersible.

This lack of data at environmentally realistic conditions, including relevant pH, ionic strength and accounting for the influence of natural organic macromolecules (NOM) such as humic substances (HS) is one of the major limitations on current NP ecotoxicological and environmental research. The presence of HS and suspension conditions such as pH, affect surface properties and gold and iron oxide NPs (Baalousha *et al.*, 2008; Diegoli *et al.*, 2008)

and aggregation of fullerenes and carbon nanotubes (Giasuddin *et al.*, 2007; Hyung *et al.*, 2007) and in the short term, bacterial toxicity of fullerene NPs is reduced (Li *et al.*, 2008).

7.1.1 Aims and objectives

The objective of the work reported here is to use well defined Ag NPs (batch #B12, chapter 6) to characterise them appropriately and to examine the change of size in relation to suspension conditions and washing procedures. To achieve these aims the silver nanoparticles were exposed to a variety of suspension conditions (pH 5 - 8; ion concentrations; Ca addition; presence and absence of humic substances (HS); presence of different HS types including Suwannee River humic acid (SRHA), SR fulvic acid (SRFA) and a peat humic acid (PHA). Changes in particle size were assessed using field-flow fractionation. The detailed analysis performed here is a fundamental requirement for further toxicology and transport studies.

7.2 Experimental

7.2.1 Silver synthesis and cleaning

Ag NPs were prepared from a standard reduction of the silver salt in sodium citrate (Doty *et al.*, 2005; Henglein and Giersig, 1999; Jana *et al.*, 2001), with minor adjustments, from work described in chapter 6 to prepare NPs which were both small and monodisperse. For purposes of instrument detection, trials were conducted with dilutions of the silver nanoparticles and a three times dilution was considered to give the best working peak detection. HS concentrations, at 10 mg per litre were chosen to reflect typical HS concentrations found in UK surface waters.

Briefly, 100 mL sodium citrate solutions (0.31 mM), 100 mL silver nitrate (0.25mM) and sodium borohydride (0.25 mM) were prepared in pure water and kept at 4°C in the dark for 30 minutes. The silver nitrate and sodium citrate solutions were mixed together in a conical flask and vigorously stirred. 6 mL of the sodium borohydride solution was added at once in a steady stream to produce a final Ag concentration of about 26 mg L^{-1}. After 10 minutes of stirring, the resultant suspension was heated slowly to boiling and heated in a stirred mantle heater with reflux apparatus for a further 90 minutes, left overnight and then cooled (4 °C, in the dark).

In this work, Ag NPs were cleaned to remove the excess citrate before use and compared to uncleaned Ag NPs at some conditions. As explained in chapter 3, suspensions were ultrafiltered (Amicon, 1 kDa regenerated cellulose membrane, Millipore) using a diafiltration method, by removing 70% of the solution and replacing with pure water to prevent drying of the particles. This process was repeated four times and measurements performed to ensure greater than 98% removal of free citrate. The final solution was replaced with $NaNO_3$ to give a final concentration of 10^{-3} M. For the uncleaned Ag NPs, the suspensions were used without further modification.

7.2.2 Sample preparation

From initial tests with flow field-flow fractionation (F*l*FFF), the final working Ag NPs suspension concentration that gave satisfactory separation and detection was approximately 8.5 mg L^{-1} (x3 dilution from original suspension). This high concentration was necessary due to the large dilution occurring in the F*l*FFF channel. Salt concentrations between 10^{-3} M and 10^{-2} M in either $Ca(NO_3)_2$ or $NaNO_3$ were used. Three types of IHSS HS including SRFA SRHA PHA (Hosse and Wilkinson, 2001; Lead *et al.*, 2003) were used to prepare stock suspensions, as described in chapter 3, and left overnight to dissolve. The hydrophobic,

PHA required a few drops of 1M NaOH to dissolve fully, and then the pH was subsequently readjusted. The HS was used at a final suspension concentration of 10 mg L^{-1}. The samples were prepared as detailed in the following. In an acid washed, ultra pure rinsed, 8 mL glass vial, silver suspensions (2.66 mL) followed by 0.8 mL HS (100mg L^{-1} stock suspension HA or water for HA = 0) were added together and then water (4.38 mL) and a salt solution (0.16 mL) to make 8 mL total. The ion concentration of the silver solution was accounted for in the calculations. Solution pH was adjusted using 0.1M HNO_3 or 0.1M NaOH, left for 24 hours to equilibrate and then pH re-measured and adjusted if necessary and again re-equilibrated without sonication or other mechanical stirring. The pH was measured using a 6mm VWR gel filled probe to avoid interference from KCl with a Thermo pH meter. No buffers were used to avoid possible complications in surface chemistry of the NPs.

7.2.3 Flow field-flow fractionation (F*l*FFF)

FlFFF analysis was carried out using a symmetrical flow-field flow fractionator (F*l*FFF) (F1000 Universal Fractionator, *Postnova Analytics*, Germany) and is described in chapter 3. The accumulation wall consisted of a 1 kDa regenerated cellulose membrane and was conditioned by repeated injections of concentrated (26 mg L^{-1}) silver NPs to improve separation and reduce adsorption, followed by washing to remove excess NPs. The eluent was adjusted to match the sample conditions for pH and ionic strength in order to prevent sample changes. Channel flow was set to 1 ml min^{-1} and the cross flow was set between 0.4 and 1 mL min^{-1} to obtain good separation of the void and sample peak.

The F*l*FFF was used as described in chapter 3 with the addition of a second UV detector. Detector 1 was set at 400 nm wavelength for detection of the Ag NPs and detector 2 was set at 254 nm for detection of the HS fraction. Initially it was assumed that that silver NPs did

not significantly absorb at 254 nm, but subsequent results from UV-vis scans showed that there was a contribution from the both the HS and the Ag NPs at 254nm. Data acquisition was via a Campbell CR23X datalogger using Loggernet software (v 3.3.1, Campbell scientific, Loughborough, UK). Data was baseline corrected and calculations made using FFF theory set out in chapter 3 (Schimpf *et al.*, 2000), with poly bead standards used as a further checks on accuracy of sizing. In all cases, 20 μL of sample was injected, at least three independent replicates were run per sample and the data averaged. Excellent agreement (peak heights differing by < 2%, in general) between replicates was observed.

7.2.4 TEM

Grids were prepared on Cu mesh 400 holey carbon film (Agar scientific). Suspensions were diluted approximately 10 times to achieve optimal surface coverage. About 10 μL of sample was dropped on and left to dry completely, without rinsing. Images were obtained from a Phillips Technai F20 and recorded using Gatan software.

7.2.5 DLS and zeta potential

Measurements were conducted with a Malvern Nanosizer 5000 in low volume disposable cuvettes and the mean of at least three measurements were taken. Electrophoretic mobility (EPM) measurements, in disposable zeta cells, were converted to zeta potential, were also performed using 5 replicates for each sample due to poorer reproducibility. Measurements were performed in the absence of HS to give a primary size distribution and some size and charge data collected from batch samples. Z-average from DLS was used to represent the particle size from DLS as it is considered suitable for both mono dispersed and aggregated particles.

7.2.6 Surface plasmon resonance and fluorescence spectrometry

Analysis was performed through a 1 cm pathway quartz cuvette (VWR) Spectral (UV) scans were obtained from a ultraviolet- visible spectrometer (Lightwave) in a 1 cm pathway quartz cuvette, the instrument was referenced with a sealed water cell and wavelengths were collected from 200 nm to 800 nm from at least three measurements and were blank corrected.

7.3 Results

7.3.1 Characterisation of Ag nanoparticles

Silver nanoparticle size derived from TEM images was 13.7 ± 6.2 nm (n = 266 particles) for cleaned particles and 13.6 ± 5.3 nm (n = 240 particles) for uncleaned Ag NPs and a representative image of both types are shown in Figure 7. 1 and their associated size distributions in Figure 7. 2.

a) 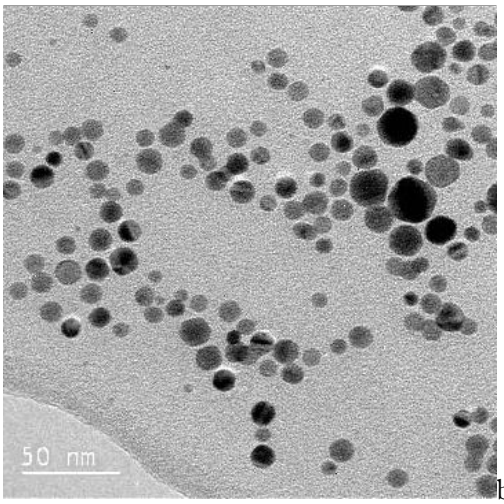

b) 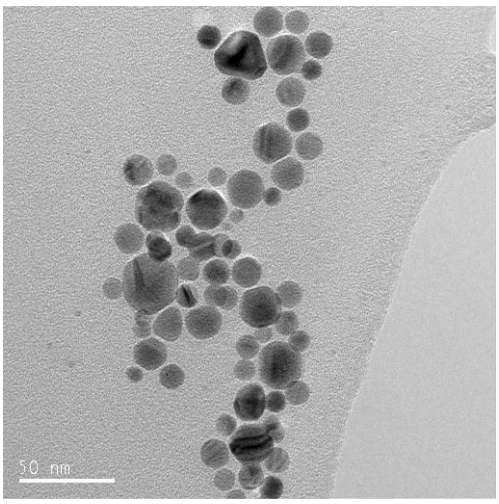

Figure 7. 1.Transmission electron microscope image of a) cleaned silver nanoparticles and b) uncleaned silver nanoparticles. Scale bars are 50 nm

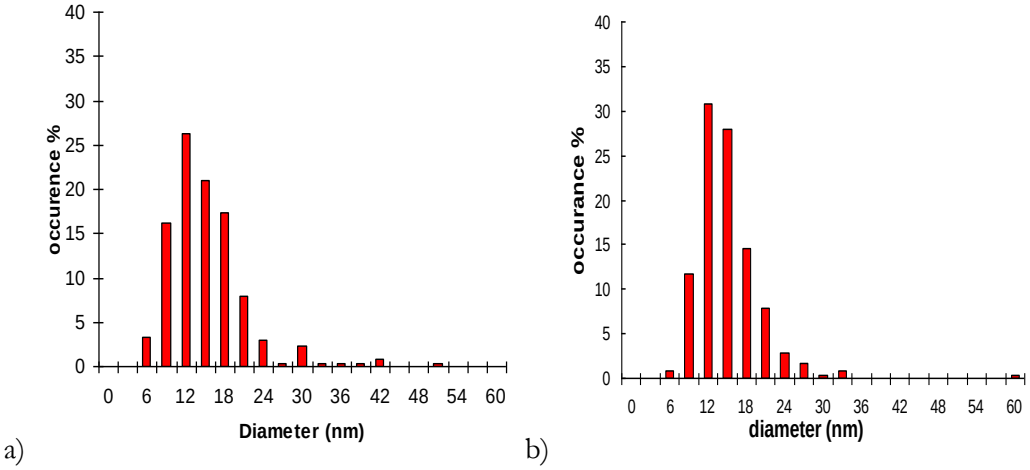

Figure 7. 2. Particle size distributions from TEM image on the a) cleaned Silver nanoparticles (n=266) b) uncleaned silver nanoparticles (n=240)

Particle size measured by DLS (z-average) was determined to be 25.0 ± 8.5 nm (pH 6) for the cleaned Ag NPs and 21.8 ± 0.1 nm (pH 6) for the uncleaned Ag NPs. However this disagrees with the distribution DLS data in figure 7.3 which shows more similarity to particle size from TEM of about 10 nm for the cleaned NP and about 15 nm for the uncleaned NP. This demonstrates that the z-average is influenced by any larger particles present within the suspension and reports its hydrodynamic size (Diegoli *et al.*, 2008).

Surface plasmon resonance peaks at 396 nm were observed as shown in Figure 7. 4 the peak is typical of a narrow particle distribution that occurs ± 400 nm for silver nanoparticles (Jana *et al.*, 2001) and UV scans showed some spectral shift (of 375-417nm), confirming the TEM and DLS data. Electrophoresis was negative across the pH range measured in the FFF experiments, with the point of zero charge lower than pH 2, due to the citrate stabiliser (data not shown). Zeta-potential (mV) was determined for the cleaned Ag NPs as -25.8 ± 5.0 (for combined pH 5 and 8, as no significant difference was observed between pH values) and for the uncleaned Ag NPs as -29.7 + 2.5 (pH 5 and 8 together).

a)

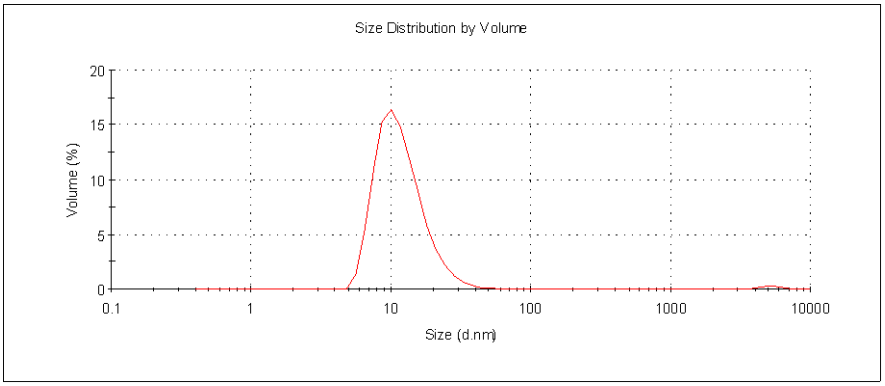

b)

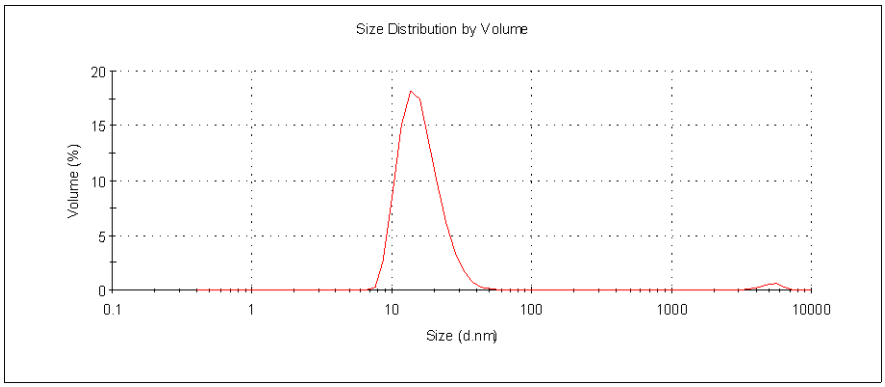

Figure 7.3. Dynamic light scattering size distribution graph of the a) cleaned silver nanoparticles and b) uncleaned silver nanoparticles, both by volume

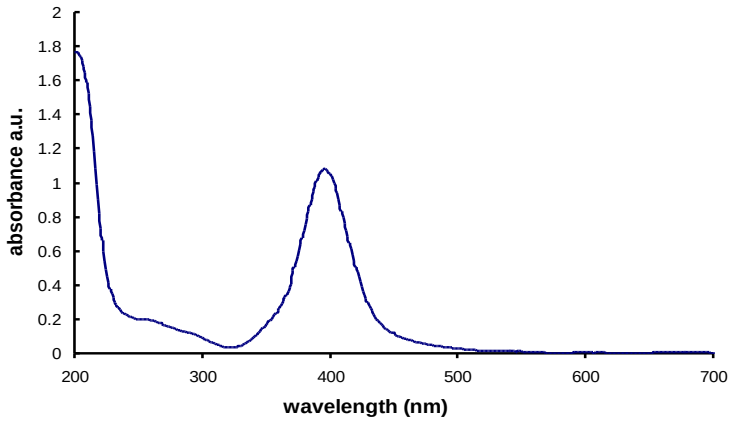

Figure 7. 4 UV surface plasmon resonance spectra for cleaned silver nanoparticles at pH 5 peak maximum occurs at 396 nm

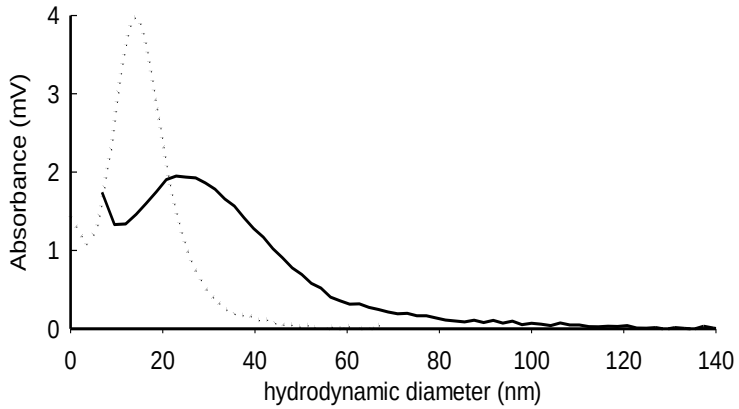

Figure 7. 5. Field flow fractionation of hydrodynamic size for the cleaned (solid line) and uncleaned (dotted line) silver nanoparticle without humics at pH 5.

Figure 7. 5 shows the FFF fractograms for the cleaned and uncleaned Ag NPs. For the uncleaned NPs the size was 13.7 nm in good agreement with the values from TEM, especially, and DLS for the same samples. However, upon cleaning i.e. removal of citrate, a new F*/*FFF size of 23.1 nm was observed, with longer tailing observed for the cleaned particles. Although, there is reasonable agreement between the DLS and TEM/F*/*FFF, in general DLS gives larger size distributions than F*/*FFF as shown in Table 1, which compares the size distributions given by FFF and DLS for the same samples. In all cases, the DLS sizes are larger than those for F*/*FFF by a factor of 2.5-4.0, and may be due to the slight bi-modal distribution as seen in figure 7.3 and agrees with that of Domingos *et al.,* (2009a).

Table 7- 2 A comparison of FFF median peak heights at maximum absorbance vs. DLS z-average values for set of conditions of pH 5 for the cleaned particles.

	FlFFF (nm)	*Stdev*	DLS (nm)	*Stdev*
Ag NPs	14		35.18	*8.9*
Ag NPs & SRFA	13.53	*1.5*	67.85	*7.18*
Ag NPs & PHA	15.26	*2.58*	63.46	*8.73*

7.3.2 The effect of suspension conditions on Ag NP size

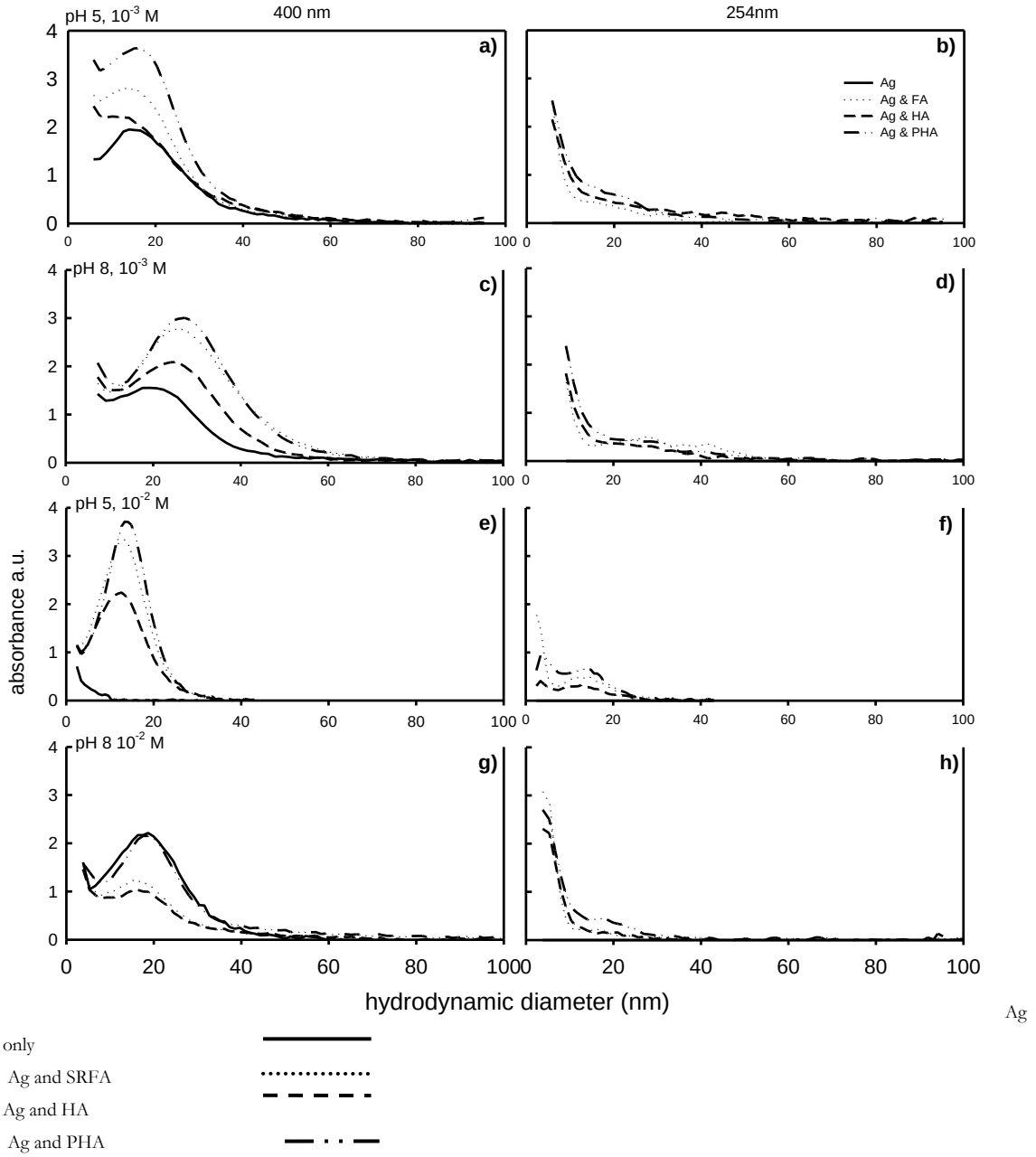

Figure 7.6; fractograms of silver nanoparticles with and without humics at ionic strength of 10^{-3} M, pH 5 and pH 8 (a-d) and at 10^{-2} M at pH 5 and pH 8 (e-h) a, c, e, g were observed at 400 nm and b, d, f, h at 254 nm. For $NaNO_3$

Figure 7.6 shows the FlFFF fractograms of cleaned NPs, at pH 5 and 8, at two ion concentrations and in the presence and absence of different types of HS. Figure 7. 7 shows the effects of Ca (at the lower of the two ionic strengths in Figure 7.6), pH and presence/absence different types of HS. Note that a) under some solution conditions such

as high Na, no fractogram was observed in the absence of HS, b) in the absence of HS, no fractogram trace was observed at the low Ca concentration and c) at higher ion concentrations of Ca, no F*/*FFF trace was observed, even in the presence of HS (see Discussion section 7.4 for explanation). Data is shown at 400 nm, which is the peak for Ag NPs and at 254, which is the peak value for HS.

It is clear from Figure 7.6 that there are only small consistent change in the fractogram due to pH (compare 6a with 6c and 6e with 6g), with peak heights increasing slightly at lower pH values, especially in the presence of HS and peaks are right shifted for each ionic strength condition. This is explained as an increase in ionic strength reduces hydrodynamic size (compare 6a with 6e and 6c with 6g) at both pH values from 25-30 to below 20 nm (see next section for discussion of this). At the lower pH value, the increase in ionic strength results in an almost complete loss of the fractogram signal of Ag NPs in the absence of HS.

The presence of HS clearly changes the fractogram signal, with greater absorbance values at 400 nm seen in general with HS present. In addition, in the absence of HS at pH 5, ionic strength 0.01 M, no fractogram is observed, while in the presence of all HS types, the signal is present, although the HS absorbs minimally at this wavelength (Diegoli *et al.*, 2008). At 254 nm, where HS absorbs light strongly, a peak is observed below 10 nm undistinguished from the void peak from the HS, but residual signal is also observed between 15 and 30 nm and is from the humics and the Ag NPs.

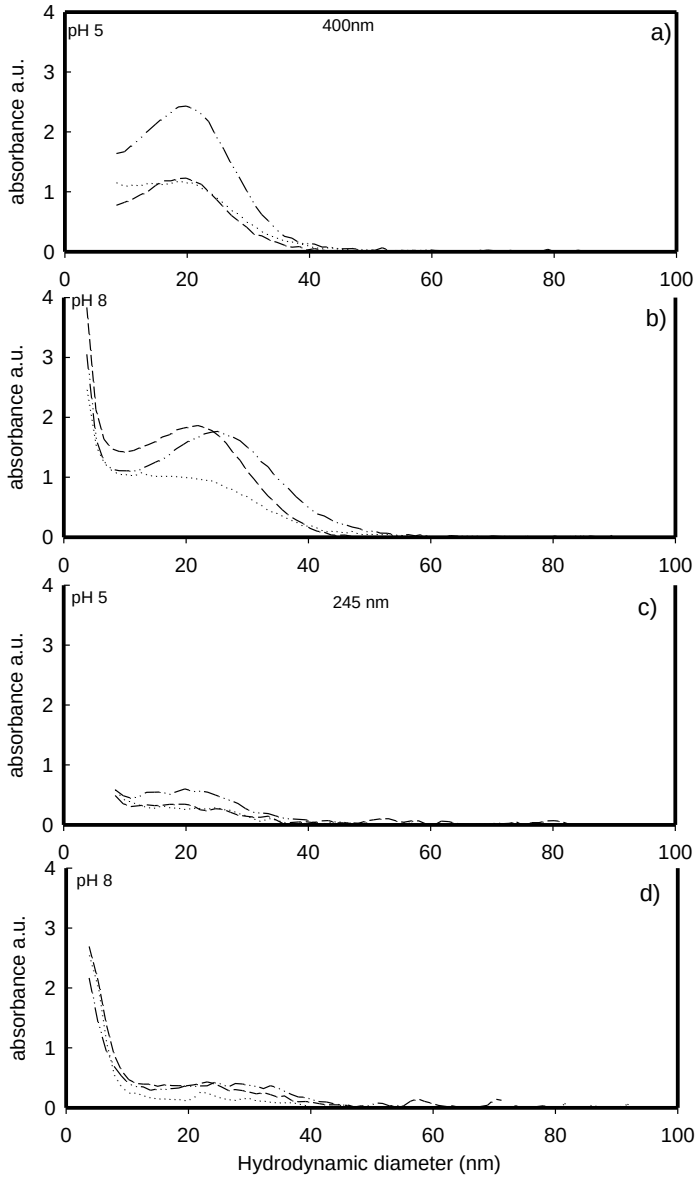

Figure 7. 7 Effect of calcium: fractograms of silver nanoparticles with and without humics at 10^{-3} M Ca, pH 5 (a and c); and pH 8 (b and d) a and b were observed at 400 nm and c and d, 254 nm.

The silver nanoparticles were also analysed by F*/*FFF in the presence of divalent, $Ca(NO_3)_2$ at ionic strengths equal to the lower of those in Figure 7.6. At the higher ion concentration with Ca^{2+} present, the sample turned red then colourless within minutes and precipitates/aggregates were observed in the bottom of the sample vessel. F*/*FFF fractionation was impossible and no traces were observed. Repeating at a lower ionic

strength (identical to those in Na), samples remained coloured and little aggregation was observed by eye, but fractograms were still unobtainable for the citrate stabilised Ag NPs only. The addition of HS to the Ag NP suspension, however, did produce fractograms at 400 nm for both pH 5 and pH 8 and the results are shown in Figure 7. 7. Ag NPs and humic suspensions fractionated at pH 5 size showed max peaks of 20 nm for all samples and the highest absorbance signal was from PHA. Fractograms observed at λ 254 nm were about 20 nm.

At pH 8 in Ca^{2+}, peaks have right shifted, and were marginally but significantly broader and flatter than at pH 5, particularly with SRFA present, with a maximum peak height between 14 and 18 nm. SRHA increased the peak sizes slightly more (ca 21 nm) and PHA to ca 25 nm. Peak heights at λ 254 nm ranged from 22 to 28 nm. For the Ag and HS, the PHA generally gave the largest peak with most absorbance, with SRHA providing the smallest peak with least absorbance.

7.4 Discussion

7.4.1 Characterisation

These NPs have been well characterised by a range of techniques including by size, surface chemistry and surface charge using TEM, DLS and F*l*FFF, surface plasmon resonance and zeta potential. Silver NPs have been reported to be poorly soluble based on previous work (Fabrega *et al.*, 2009a; Navarro *et al.*, 2008b) more recent reports suggests that the rate of the release of Ag^{+} is largely dependent on the size of the particle with a higher rate of release from smaller particles (Sotiriou and Pratsinis, 2010) and on solution conditions such as pH and temperature (Liu and Hurt, 2010). The measured sizes show the NPs are very monodisperse and this is indirectly confirmed by the surface plasmon resonance (Figure 7.

4) and the electrophoretic mobility data (not shown). In general, TEM sizes were smaller than but comparable to F*l*FFF sizes, while the DLS sizes were significantly larger than both Figure 7.3. The differences presumably reflect the fact that TEM measures a number based size distribution of the physical size only, not including citrate capping agent, while F*l*FFF measures a hydrodynamic volume or mass based size distribution (Baalousha and Lead, 2007a). However, DLS is very sensitive to small amounts of large particles either from aggregation or from contamination (Domingos *et al.*, 2009a) and this has the effect of shifting the DLS based measurements to larger sizes.

The effect of washing to remove excess free citrate on the TEM and DLS sizes was not significant, but there was a shift based on the F*l*FFF data, as shown if Figure 7. 2. and Figure 7.3 as compared with Figure 7. 5. The TEM sizes are not expected to change as the physical particle size is measured by this method. The increase in size on removal of excess citrate as measured by F*l*FFF might be expected as re-equilibration within the cleaned NPs would produce less surface-bound citrate, reducing stability and increasing size. This is compatible with the slightly lower zeta potentials measured for the cleaned NPs. Although mean particle sizes by DLS do not significantly change, it is also clear that the DLS size distributions are very slightly shifted to larger sizes (Figure 7.3). This indicates the effect is real, but that DLS is less sensitive to such changes compared to F*l*FFF.

7.4.2 Effect of suspension conditions from F*l*FFF data

Clearly, from the above discussion, F*l*FFF agrees well with the other techniques and appears to have some advantages over DLS particularly. In addition, the method is less time consuming than TEM and related microscopy methods but should be viewed as one very useful technique among many and is, in fact, highly complementary to microscopy methods (Baalousha and Lead, 2007a). The F*l*FFF was further used, with detection by uv-vis

absorbance measurements at both 400 nm for the Ag NPs and 254 nm for the HS. Inaccuracies due to losses to the F/FFF membrane or channel overloading are possible, but under our experimental conditions were minimised by charge repulsion between membrane and NPs and by using relatively dilute concentrations with low mass loadings.

At low (10^{-3} M) ionic strength in a non-specifically binding cation (sodium), without HS present, the Ag NPs are stable in suspension at both pH 5 and pH 8 (Figure 7.6). There is no clear and significant effect of pH here which is to be expected since there is no major change in citrate charge over this pH range, as shown by the zeta potentials measured in this work and agrees with previous studies on citrate stabilised gold (Diegoli *et al.*, 2008). The effect of increasing ionic strength to 10^{-2} M is that we were not able to observe a fractogram (pH 5), most likely due to aggregation and elution after longer times. This is expected following usual interpretation of DLVO theory; the ionic strength shields charges, reduces the diffuse layer size and allows NPs to come into contact sufficiently closely to produce aggregation. However, at pH 8, there is minimal change in size, presumably because the degree of charge reduction here is insufficient to cause aggregation at this higher pH value. In addition to being no trace at pH 5 and higher ion concentration, there are no traces at 254 nm, which is to be expected, in the absence of HS.

On addition of natural organic macromolecules of HS (SRFA, SRHA and PHA), a completely different picture emerged and at all ionic strengths using Na as a counter-ion, with well defined fractograms observed at 400 nm, indicating the presence of Ag NPs. The effect of increasing the ionic strength is different to that seen in the absence of HS. Peak areas can be used to assess the quantity of NPs that have not aggregated in the F/FFF channel at the higher ionic strength, the apparent size decreases, and peak area also changes. The smaller peak size indicates that the diffuse layer, including some of the HS, contracts to

give NPs with smaller hydrodynamic sizes, but unexpectedly in the absence of aggregation. Taken together, the results indicate a dual role for HS, with 1) aggregates being re-dispersed in the presence of HS and 2) changes due to contraction of the electric double layer when ion concentration in the presence of HS, due to non-charge i.e. steric, stabilisation (Diegoli *et al.*, 2008). A similar picture emerges at low ionic strengths of Ca, but at the higher Ca concentrations, no fractograms were observed even in the presence of HS due to aggregation and loss of material from suspension. Dispersion and aggregation appear to be dependent on the interplay of both HS type and concentration and Ca concentration. These results have potentially important implications for the fate and behaviour of Ag NPs in aquatic environments and thus exposure and ecotoxicology.

At 254 nm, fractograms show the presence of HS at sizes equivalent to the Ag NP size, indicating some association of the HS and NPs at less than 10 nm this is certainly the HS but at size greater than 20 nm this can be considered to be a combination of AgNPs and the HS. .The differences observed in peak height between the Ag-HS NPS indicate that the concentration of the Ag NPs have increased due to the increased stability from the coated Ag NPs with highest absorbance gained from the higher molecular mass PHA. Taken together with our previous results (Baalousha *et al.*, 2008; Diegoli *et al.*, 2008) and others (Sanchez-Cortes *et al.*, 1998) and the zeta potentials measured in this study, it is clear that the Ag NPs become coated with nanoscale HS surface films, which in general act to stabilise the NPs more fully than citrate alone. Both charge and steric stabilisation mechanisms are apparent (Diegoli *et al.*, 2008). In addition, it is likely that this nanoscale film forms when HS replaces the citrate, based on thermodynamic considerations (Diegoli *et al.*, 2008) and it is less likely that the citrate itself is overlain by HS. The behaviour of HS in this study is consistent with the literature showing that HS size changes with both changing electrolyte concentration and pH (Avena *et al.*, 1999; Schimpf and Petteys, 1997).

7.5 Conclusion

Citrate-stabilised and monodisperse silver nanoparticles were synthesised and appropriately characterised. The effect of adding sodium and calcium at relatively low (relevant to freshwater and estuarine systems) ion concentrations and circum-neutral pH values was to cause increased aggregation which in many cases prevented analysis by F/FFF. However, addition of low and environmentally relevant concentrations of HS stabilised the NPs and reduced losses by aggregation/sedimentation and permit F/FFF analysis. This stabilisation occurs at all but the highest Ca concentrations measured.

Ag NPs are known to be almost certainly entering the environment in large amounts (Luoma, 2008; Mueller and Nowack, 2008) and to be potentially hazardous. Understanding their size, dispersion and aggregation under environmentally conditions of pH, major ion concentration and HS concentration is essential in trying to determine their fate and behaviour using laboratory experiments. These laboratory experiments can be used to help to determine possible fate and behaviour processes such as aggregation and sedimentation. It is clear from this work that the standard conception of immediate and likely irreversible aggregation and loss from aquatic systems to the sediment may not be realistic, due to stabilisation with HS. Further questions remain, related to NP stabilisation mechanisms and how this might affect environmental behaviour and effects. For instance, how does HS interact with NPs when the capping agent is strongly (chemically) bound? Additionally, what are the kinetics of desorption of HS under environmentally and biologically relevant condition? More detailed answers to such questions will provide the requisite information to better understand environmental processes and behaviour of NPs.

At low ionic strength Ag NPs particle size increased from pH 5 to 8. However, changing the ionic strength from 10^{-3} M to 10^{-2} M Na increased instability of the Ag NPs, and loss of peak

at pH5 but in the presence of humic substance (HS), a reduction in NP size was seen, most likely due to a reduction in the diffuse layer. The presence of Ca^{2+} ions, at the higher ionic strengths caused complete loss of the suspension Ag NPs with or without HS, most likely due to aggregation. At the lower Ca^{2+} ion concentrations the Ag NPs were still unstable, but again, in the presence of HS the NPs were fully dispersed. The full published version of this work is available online at http://dx.doi.org/10.1016/j.chroma.2009.07.021 (Cumberland and Lead, 2009).

8

Synthesis of NOM capped silver nanoparticles

Chapter Summary

To date there have been many attempts to produce silver nanoparticles using a variety of stabilisers and capping agents. However, few studies have looked at natural organic matter (NOM). NOM provides one potential agent because of its negative charge, functional bonding groups and its stability under a wide range of pH values. Indeed humic substances (HS) have been shown to improve the stability of pre-existing manufactured nanoparticles and fullerenes under different conditions. Using NOM as the primary and only stabiliser during the synthesis phase has been rarely researched. This chapter therefore investigates the production of silver nanoparticles in the presence of four different commercially available NOM types (HA, FA, PHA and a polysaccharide) and two different reducing agents (sodium borohydride and ascorbic acid). Suspensions were analysed for colour, SPR, size (TEM and DLS) and charge (EPM). The main conclusions are that silver nanoparticles were synthesised from all NOM groups, and a large range of sizes were obtained but with no clear trends observed by reaction conditions.

8.1 Introduction

Achieving NP stability is possible through electrostatic repulsion (charge) or steric stabilisation (non-DLVO). In the former, stabilisation occurs purely though repulsion where outwardly facing groups are provided to prevent aggregation and particle growth (Christian *et al.*, 2008). In the latter, the particle surface is saturated with polymer layers (ligands) attached in loops and trains. The polymer thickness then acts as a barrier preventing particles approaching each other (Balnois *et al.*, 2007; Reinhardt, 2004). Stability of uncharged or slightly charged nanoparticles thus requires the presence of ligands to prevent weak, attractive van der Waals' forces causing aggregation. As discussed earlier in chapter 6 various organic compounds, such as the negatively charged tri-sodium citrate, are good stabilising capping agents for NPs (Henglein and Giersig, 1999; Pillai and Kamat, 2003). Additionally, polymers with a fibrillar string-like conformation, such as polyethylene glycol (PEG), polyacrylic acid (PAA), polyvinylpyrrolidone (PVP) and polyvinyl alcohol (PVA), have also been successfully used as ligands to stabilise silver, gold and other NPs (Ledwith *et al.*, 2007; Sun and Xia, 2002; Van Hyning and Zukoski, 1998). These are known to strongly adsorb to silver surfaces and provide excellent steric stabilisation (Spalla, 2002; Van Hyning and Zukoski, 1998).

Generally, NP capping and stabilisation occurs during synthesis, whereby the concentration of the capping ligand controls initial particle size and further particle growth and shape (Henglein and Giersig, 1999). Surface attachment mechanisms maybe covalent e.g. via carboxylic, thiol, or other groups, or non-covalent. To date, most capping agents used have been synthetically produced in laboratories. However, natural organic macromolecules, of plant and bacterial origin, are known to further stabilise engineered NPs (Baalousha, 2009; Gu *et al.*, 2002; Hyung *et al.*, 2007; Villalobos-Hernandez and Muller-Goymann, 2006).

To take this process a step further, a few studies have substituted synthetic ligands for natural and food grade products, as primary stabilisers in NP synthesis. This has been successful to the extent that Ag NPs have been formed inside the living cells of alfalfa sprouts (Gardea-Torresdey *et al.*, 2003). The range of reported natural ligands used to produce NPs are wide, however, the study of them in more detail is limited. Examples include the synthesis of 60-68 nm silver and gold nanoparticles using dried *Cinnamomum camphora* leaf (Huang *et al.*, 2007). Antibacterial wound dressings have been produced by impregnating silver NPs into exo-bacterial cellulose by a sodium borohydride reduction (Maneerung *et al.*, 2008). Additionally, antibacterial cleaning cloths have been produced from embedded silver NPs in fungal exudates (Duran *et al.*, 2007).

Using natural, non-toxic ligands may help further understand the toxicity mechanisms in cells and lower animals and its effects on daphnia (Glover and Wood, 2004). Such ligands may even prove to be better stabilisers. Humic substances (HS) have been found to be excellent stabilisers for coated nanoparticles, and gold nanoparticles have been produced by humic acid (Alvarez-Puebla *et al.*, 2007) and fulvic acid alone (dos Santos Jr *et al.*, 2005). Moreover, such products have shown potential as environmental sensors for herbicide detection (Dubasa and Pimpan, 2008). Silver ions have been shown to be reduced by HS (Jacobson *et al.*, 2005) probably by the hydroquinones and phenol groups present in the humics (Alvarez-Puebla *et al.*, 2007). Furthermore, silver has an affinity with thiol groups present in the humic molecules. In this chapter, the synthesis of silver NPs from natural organic matter (NOM) is presented and characterised using a range of techniques including colour, SPR, TEM, DLS and EPM. The results are also examined over time for signs of stability.

8.1.1 Aims, objectives and structure

The aim of the experiments reported in this chapter was to synthesise silver nanoparticles and assess their stability, size and size range under three different NOM concentrations and four different NOM types. Two different reducing agents were also compared; these were sodium borohydride ($NaBH_4$) and ascorbic acid (AA). The results are objectively assessed by using observational methods and the application of four analytical techniques: SPR, TEM, DLS and EPM. A basic statistical analysis is undertaken, comparisons are made between techniques and the stability of the NPs over time is examined.

The remainder of this chapter is presented in two key parts. In the first experimental section, the details of all the synthesis procedures are described. Furthermore, this section reports on the results of a pilot test which led to the design of the main experiment. In the second part, the results and discussion section, the outcome of the main synthesis are presented in the order of colour, SPR, TEM, DLS and EPM. For TEM the results include images, histograms, size tables and statistical assessments. DLS data is provided at 24 hours and 3 months post synthesis, and compared against TEM and EPM values. Finally, the results are drawn together in a brief concluding section.

As in chapters 6 and 7 the effect of the concentrations of the synthesis reagents, silver nitrate and capping agent, are important as both the resultant NP size and monodispersity are affected. Experiments here used the same Ag concentration, but the HS and PS were varied (1, 10 and 100 mg L^{-1}).

8.2 Experimental

8.2.1 Materials and methods

8.2.1.1 Materials and reagent preparation

IHSS Suwannee River fulvic acid (FA) and Suwannee River humic acid (HA) stock suspensions (400 mg L^{-1}) were prepared by weighing 0.01g of the freeze dried powder and dissolving it in pure water. The suspension was shaken by hand for one to two minutes and left to equilibrate without further preparation. IHSS peat humic acid (PHA) stock suspension was made as above, but suspended using a few drops of 1M NaOH, topped up with pure water. Acid was then added to produce a stable suspension at pH 7 and a final concentration of 400 mg L^{-1}. The exo-polysaccharide (PS), succinoglycan, was prepared by dissolving 50.6 mg of succinoglycan in 100 mL of pure water. The suspension was stirred for 24 hours in 100 mL screw topped glass bottle. After which, the suspension was filtered through 0.2 μm pre-weighed filter papers to remove aggregates. The overall mass was calculated gravimetrically, by subtracting the original filter paper weight from the dried filter papers, the resulting concentration of PS was 336 mg L^{-1}. The $AgNO_3$ was prepared from a stock solution of 100 mg L^{-1} Ag NO_3 and diluted to 8 mg L^{-1} in 20 mL in the synthesis solutions. $NaBH_4$ was prepared by dissolving 38 mg in 100 mL of pure water. Solution activity was noted by the presence of bubbles (H_2 gas) and ascorbic acid (0.01 M) ,where the concentration was based on the work in chapter 6 section 6.3.2, was prepared by dissolving 178.7 mg in 100 mL of pure water. Reducing reagent solutions were freshly prepared and used within hours as the reactivity of borohydride reduces in water as it converts, over time, to several non reductive borate species as the borohydride dissociates in water making it non-reactive (Van Hyning and Zukoski, 1998).

8.2.1.2 Overview of synthesis

Reagents were diluted in pure water in a 25 mL glass vial. Mixing then occurred by manual shaking for 2-3 minutes. The NOM and the silver nitrate were mixed together first and left for 24 hours. The next day, 1 mL of the reducing agent (AA or $NaBH_4$) solution by pipette, without altering the dispersion speed was added to the reagents and shaken by hand again for 2-3 minutes and colour changes noted.

8.2.1.3 Synthesis (I) for preliminary experiment with FA

Fulvic acid, FA was suspended and used at a concentration of 100 mg L^{-1}. Silver nitrate was then added to make a concentration of 8 mg L^{-1} in total volume of 12.5 mL in a 25 mL glass vial. The suspension was shaken and left in the fridge. After three weeks of no apparent colour change, 0.5 mL of a 37 mg/100 mL suspension of $NaBH_4$ was added and the suspension shaken. An immediate colour change from pale brown to bright yellow was observed.

8.2.1.4 Synthesis (II) and suspension preparation with NOM

In 20 mL volumes, each separate NOM (HA, FA, PHA or PS) suspension of either 1, 10 or 100 mg L^{-1} were placed in a glass vial (pre-acid washed and rinsed) and mixed with 1.6 mL of silver nitrate for a final concentration of 8 mg L^{-1}. The samples were left to equilibrate over night in the fridge. The following day, 1 mL of the reducing agent (either $NaBH_4$ or ascorbic acid (AA)) was pipetted into the vial and shaken well. The suspensions were kept at room temperature for the remainder of the day (~8 hours) then placed in the fridge before being analysed the following day.

8.2.1.5 Particle characterisation

Nanoparticles were characterised by TEM using a Technai F20. TEM grids were prepared from the NPs suspensions of 1, 10 or 100 mg L^{-1} NOM concentrations. TEM grids were prepared by dropping 10 µl of a NP suspension diluted ten times onto 400 holey carbon films (Agar) and left to dry completely. Images were representative of the sample looking widely across the grid with several images taken for each sample. Particle size distributions were produced from measured particles from calibrated TEM images manually deriving particle size using Gatan software and plotted using Excel. To minimise subjectivity all particles in the frame were included, unless they were either touching the edge of the frame or where a particle could not be distinguished from its neighbour.

Surface plasmon resonances (SPR) were measured using ultra violet–visible light absorbance, 200-800 nm (*Lightwave* instrument), in 1 cm pathway quartz cuvettes (VWR). Suspensions were diluted as required, generally by less than ten times. Particle size was analysed by DLS with a Malvern Nanosizer 5000 the sample was analysed in disposable low volume plastic cuvettes. The data for the z-average weighted mean (as opposed to number–weighted or volume–weighted) from DLS were presented as the most suitable size measurement in representing both mono and aggregated particle size distributions as discussed in chapter 3 section 3.4.2.3 Electrophoretic mobilities were measured using the same instrument using a disposable zeta cell.

8.2.1.6 Statistical analysis

TEM particle size data were analysed for both reducing agents ($NaBH_4$ and AA) using descriptive statistics (mean, mode, median, stdev, range and number). The results are presented in table 8-2 and 8-3. Table 8-4 presents the statistical outcome for all the particles

by reducing agent, NOM type and NOM concentration. In Table 8-5 the descriptive stats for TEM particle size are provided (standard error (SE), median, mode, stdev, variance, range distribution and the confidence interval). This contains all data, per reducing agent, and in more detail for each concentration and NOM type. Table 8-6 takes the particle size obtained from the DLS, z-average data and compares the data taken at 24 hours and 3 months to note any change in particle size over this time period. T-tests were performed, and Mann-Whitney tests were undertaken where data were not normally distributed, using Sigma Plot (Systat).

8.2.2 Results of preliminary experiment with silver nitrate and FA

A preliminary experiment was conducted using FA, $AgNO_3$ and $NaBH_4$ to assess the feasibility of NP production in the presence of a natural ligand. FA and HA have been known to reduce gold chloride to Au NPs (Alvarez-Puebla *et al.*, 2007; Alvarez-Puebla *et al.*, 2006). However, after an initial (3 week) period using just the FA and $AgNO_3$ there were no observable colour changes. The reducing agent $NaBH_4$ was added and an immediate colour change to yellow was noted. It was possible that while binding may have taken place between the Ag^+ and the FA, the absence of visible colour change meant that NPs were not formed spontaneously prior to adding the $NaBH_4$. Following the borohydride addition, hexagonal Ag NPs were formed which were greater than 100 nm with some smaller species visible (Figure 8.1). From the SPR chart in Figure 8.1, the width at half peak maximum (WHPM) was 103 a.u., with the wavelength at peak maximum recorded at 403 nm. The average size and standard deviation from DLS measurement was 72 ± 94 nm, demonstrating a large variability.

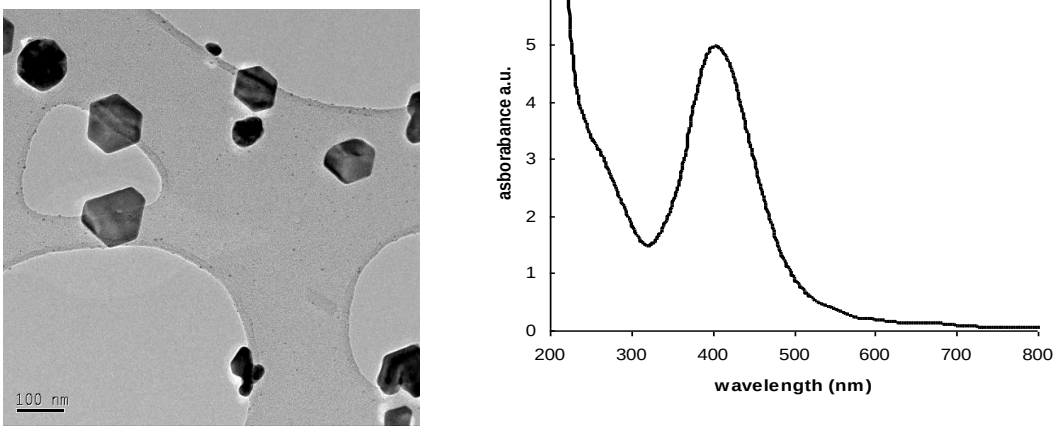

Figure 8.1 TEM graphs of silver nanoparticles synthesised with FA and sodium borohydride (scale bar 100 nm). On the right, SPR by UV absorbance (average of 3 measurements).

The initial study showed that NOM was capable of producing NPs, possibly of unusual structures, but that it was largely incapable of acting as a reductant. Further experiments were performed and this is detailed below. Further, the samples were assessed for colour, SPR, size (TEM and DLS) and charge.

8.3 Results and discussion

8.3.1 Synthesis of silver NPs using four NOM types

NOM-Ag interactions were studied more systematically. Four different types of commercially available IHSS NOM types (HA, FA, PHA, PS) were chosen as capping agents at three different concentrations (1, 10 and 100 mg L^{-1}) for the synthesis of silver nanoparticles. Additionally, two reducing compounds $NaBH_4$ and AA were compared. In all 24 reactions took place without replication. Reactions were performed in 25 ml glass vials, on 20 ml suspensions and were subsequently characterised with, SPR TEM, DLS and EPM. There was no suspension colour prior to synthesis for 1 and 10 mg L^{-1}, and for 100 mg L^{-1}

HA PHA, suspensions were slightly coloured (from the NOM), but the PS suspension was completely colourless.

8.3.2 Observations of suspension colour post reduction

Most suspensions containing silver nitrate and NOM underwent a colour change on adding the reducing agents. This strongly suggests that silver NPs were formed in the reaction. From the observations and photographs presented in Figure 8.2 (A to H) and Table 8- 1, the NOM/Ag NP suspensions showed a great deal of variation in suspension colour change with NOM concentration and reducing agent type. Colours ranged from colourless to yellows, browns, blacks and one blue suspension occurred. With the exception of the HA with AA, colour intensity increased with NOM concentration. PS suspensions were colourless with the exception of the 100 mg L^{-1} PS reduced with $NaBH_4$. Turbid suspensions were obtained from Ag/HA with AA, indicating larger particles had formed through aggregation. Blue silver NPs suspensions have in the literature been attributed to large particles or triangles (Ledwith *et al.*, 2007).

The AA was generally much slower to react than the $NaBH_4$, taking hours rather than minutes. Earlier experiments using AA and citrate have also shown that this reaction was difficult to control and was concentration dependent (see chapter 6). As a result larger aggregated particles were produced that later sedimented. Ledwith *et al.* (2007) has described this reaction as a slower growth process and they used it to grow NP seeds that had previously been produced through the $NaBH_4$ reduction. Other researchers have used AA to reduce Ag^+ in the presence of higher molecular weight capping agents (Ledwith *et al.*, 2007; Sondi *et al.*, 2003; Velikov *et al.*, 2003). The latter are more suited due to AA strong reducing capabilities (Suber *et al.*, 2005). The reaction of AA and $AgNO_3$ is shown in Eq8.1.

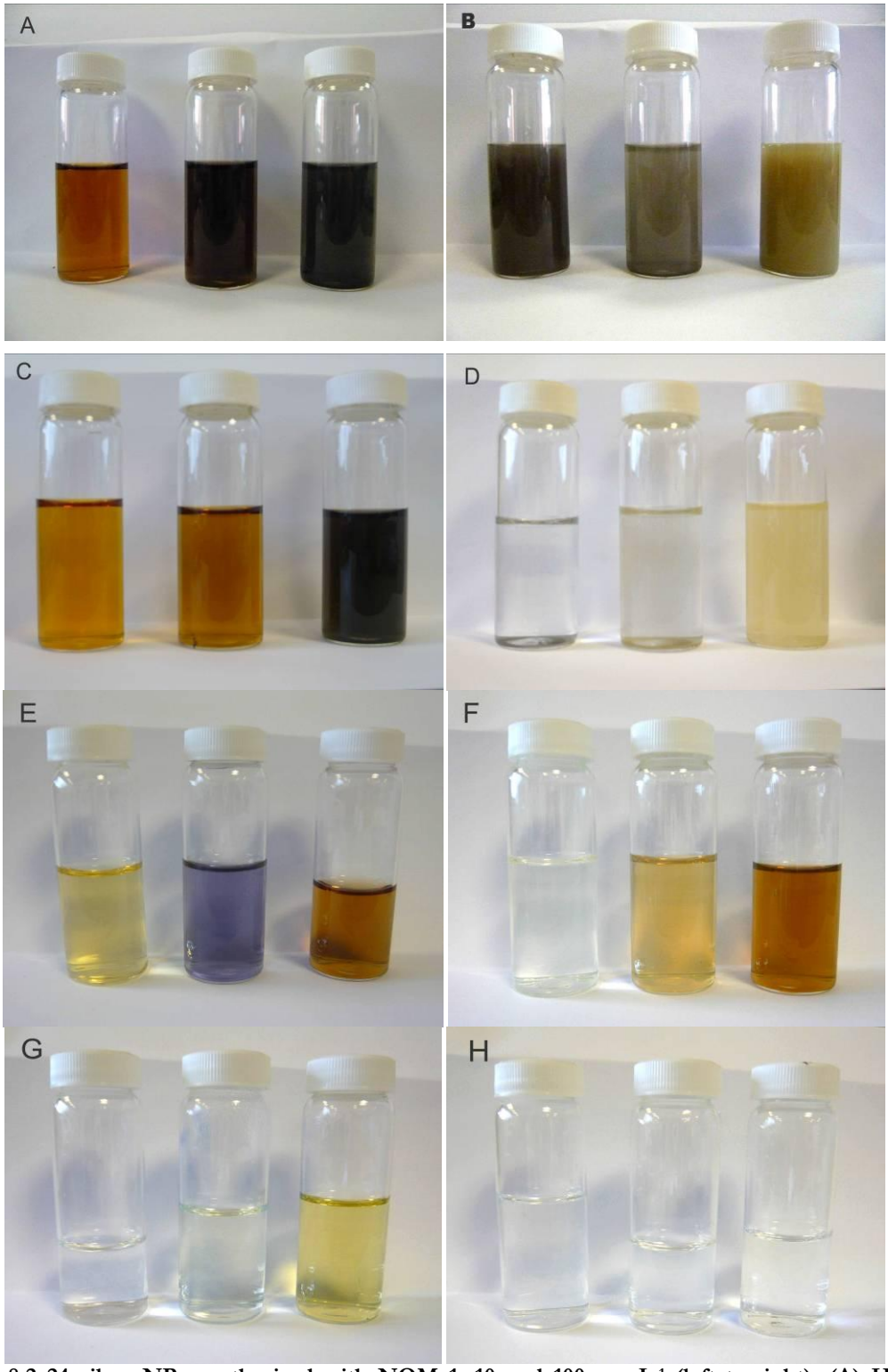

Figure 8.2 24 silver NPs synthesised with NOM 1, 10 and 100 mg L^{-1} (left to right): (A) HA and $NaBH_4$; (B) HA with ascorbic acid; (C) FA with $NaBH_4$; (D) FA with ascorbic acid; (E) PHA with $NaBH_4$; (F) PHA with ascorbic acid; (G) PS with $NaBH_4$; (H) PS with ascorbic acid. Photos were taken with a digital camera, Panasonic Lumix FX 33.

Table 8- 1 Observations of suspension colour during and after synthesis of Ag/NOM using ascorbic acid and sodium borohydride

Reducing agent	NOM	Concentration Mg L^{-1}	Prior to adding reducing agent	Immediately after adding reducing agent	Observation at 2 hours	Observation at 6 hours
$NaBH_4$	FA	1	colourless	dark grey	black	
		10	v. pale yellow	d. brown	brown	
		100	pale yellow	d. brown/ grey	brown	
	HA	1	colourless	black		turbid grey
		10	very light brown	very dark brown		dark brown
		100	pale brown	darker brown		light brown
	PHA	1	colourless	colourless yellow	yellow	
		10	mid / pale brown	light brown to paler	blue suspension	
		100	dark	mid brown	brown	
	PS	1	colourless	darker brown	colourless	
		10	colourless	pale yellow/ brown	pale yellow/ brown	
		100	colourless	no change	yellow	
Ascorbic acid	FA	1	colourless	colourless	cloudy	
		10	very pale yellow	very pale yellow	cloudy	
		100	pale yellow	pale yellow	yellow and cloudy	
	HA	1	colourless	turbid brown		turbid yellow
		10	very light brown	turbid		turbid grey
		100	pale brown	no change		turbid brown/grey
	PHA	1	colourless	no change	pale yellow	
		10	mid / pale brown	no change	turbid	
		100	dark	no change	turbid	
	PS	1	colourless	colourless	colourless	colourless
		10	colourless	colourless	colourless	colourless
		100	colourless	colourless	colourless	colourless

Described initially by Stathis (1948) it demonstrates that two moles of nitric acid are produced.

$$2AgNO_3 + C_6H_8O_6 \rightarrow 2Ag + C_6H_6O_6 + 2HNO_3$$

(After Stathis 1948)

Eq 8.1

The amount of nitric acid, a strong oxidizer, resulting from the above reaction, can be quite large. If large concentrations are used then the HNO_3 will cause the freshly formed silver NPs to re-dissolve, particularly at higher temperatures (Suber *et al.*, 2005). However, due to lack of pH data this reaction was not confirmed.

The exact nature of the reaction with borohydride is unclear as borohydride dissociates in water prior to contact with the silver ion (Van Hyning and Zukoski, 1998). If left uncapped other boro-species produced from this reaction may produce further aggregation of the silver NPs (Van Hyning and Zukoski, 1998).

8.3.3 Characterisation of SPR using UV absorption

Surface plasmon resonance (UV absorbance λ 200-800 nm) of the suspensions were analysed on aged samples at 24 hours and 3 months post synthesis. The results taken at 24 hours are presented in Figure 8.3. They show that, like suspension colour (Figure 8.2), variation exists between samples. Yellow and light brown suspensions show absorbency at 400 nm (Ag/FA 1 and 10 mg L^{-1}, Ag/PHA 1 mg L^{-1}, Ag/PS 100 mg L^{-1} and all Ag/HA). This was also found with Ag-citrate NPs. The blue suspension of Ag/PHA 10 mg L^{-1} showed some absorbance at 600 nm, probably due to the presence of hexagons in the sample. Ledwith *et al* (2007) found that their blue suspensions absorbed at 600 nm where triangles were present.

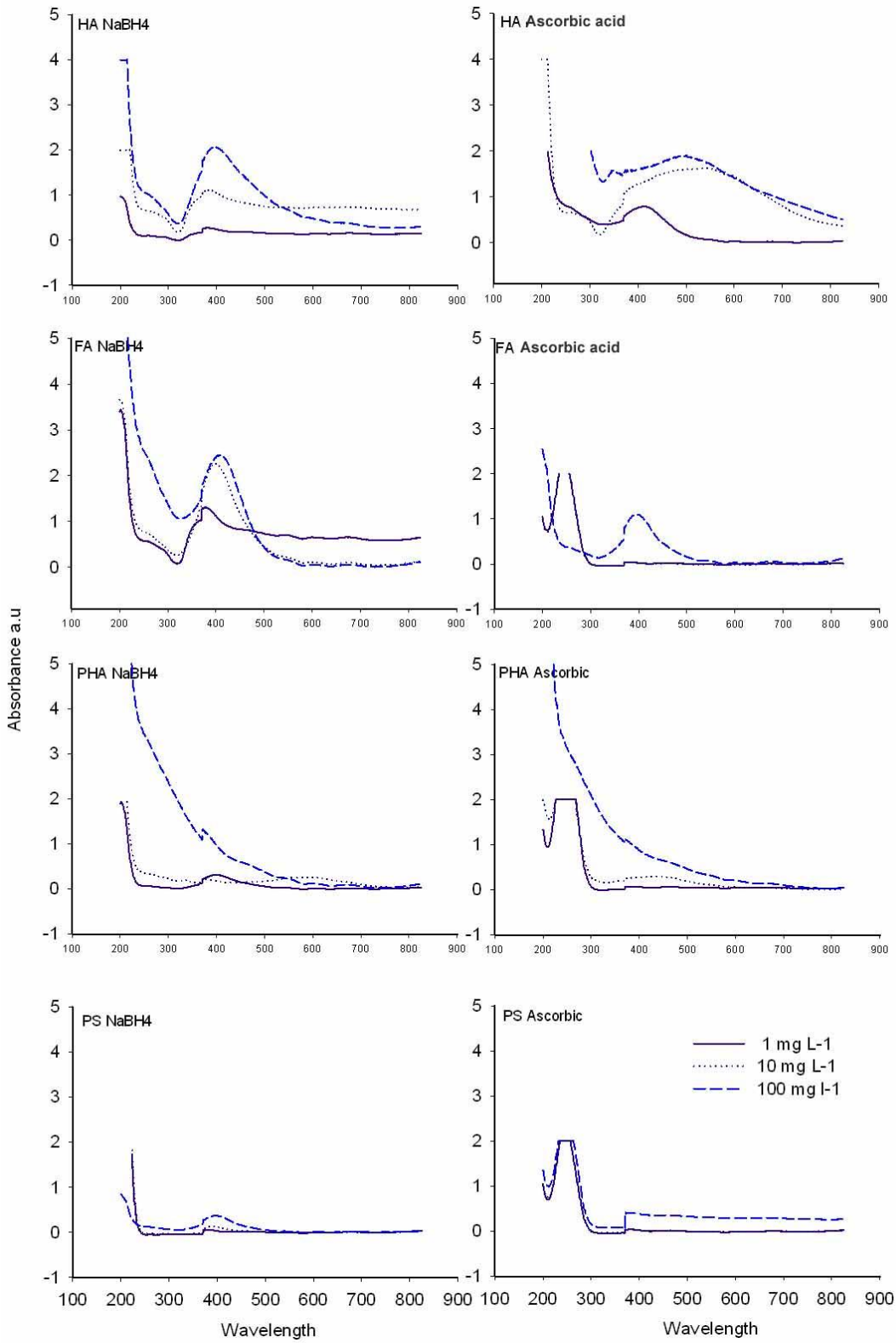

Figure 8.3 SPR UV absorbance spectra for Ag/NOM, using humic acid (HA), fulvic acid (FA) peat humic acid (PHA) or polysaccharide (PS) NP suspensions reduced with NaBH4 or ascorbic acid. Samples were analysed about 24 hours post synthesis.

In general, Figure 8.3 shows greater SPRs at higher NOM concentrations for all NOM types with both reductants. In most cases absorbance values appear similar for 1 mg L^{-1} and 10 mg L^{-1} NOM suspensions, with the exception of Ag/HA. Only a few SPRs showed strong peak absorbency around λ400 nm, indicating that very small, non-spherical or large aggregated NPs were present in the solution. Ag/HA and Ag/FA gave sharp peak maximas at 100 mg L^{-1}. However, Ag/PHA at 100 mg L^{-1} gave a stronger, broader absorbance pattern. Weaker SPRs at 400 nm or 600 nm are observed for Ag/PHA at 1 and 10 mg L^{-1} showing very small peaks. The flatter SPR patterns may also be due to the interference of the NOM to the particles' surface. This was also observed by Dos Santos *et al.,* (2005) with Au and FA.

As shown in Figure 8.3, Ag suspensions that had been reduced using $NaBH_4$ gave stronger SPRs than those using AA in general. Figure 8.4 shows the absorbance pattern for the reducing agents, $NaBH_4$ and AA alone. Little absorbance is seen for $NaBH_4$, but the AA produces a peak maxima at 250 nm. This absorbance is also observed in the samples in Figure 8.3.

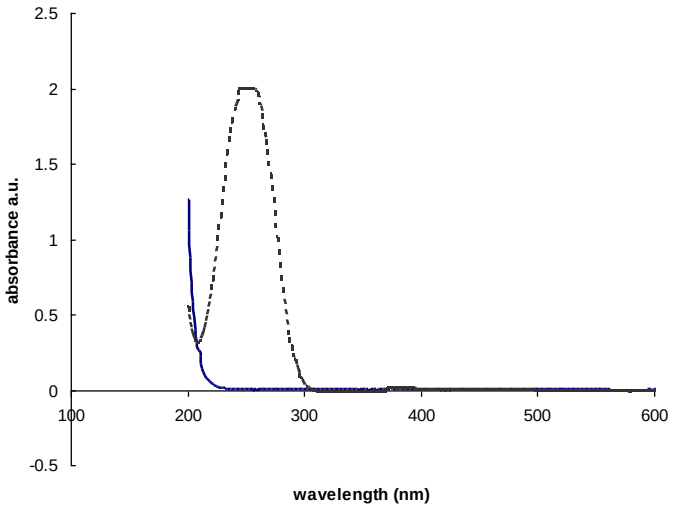

Figure 8.4 Absorbance spectra of suspensions of NaBH4 (undiluted) solid line, and ascorbic acid (x30) dotted line

Peak truncations seen in figure 8.3 are due to instrument maxima attained from undiluted samples, sample dilution was performed if necessary. The lack of AA peak in figure 8.3 probably indicates that the reaction was more completed and little or no AA was left in the sample.

Figure 8.5 are the SPR patterns for all the Ag/NOM samples analysed again at three months to check for stability. Compared with the samples at 24 hours (Figure 8.3), most SPR peak maxima were smaller after being left for 3 months. The exception was the Ag/HA 100 with $NaBH_4$ sample, where the peak width became narrower and the peak tip more rounded. The absorbance at 250 nm for the samples containing AA, showed peaks present at 24 hours which were notably reduced or absent after 3 months. The loss of this absorbance indicates that the reduction of silver by AA (Eq 8.1) continued after 24 hours.

Silver nanoparticles are known to produce SPRs with distinctive peak maximas around 400 nm, as has been observed in this thesis and elsewhere. Despite the poorly shaped and absent peaks in this particular experiment (see Figure 8.5), the TEM analysis below shows that NPs were present in all suspensions. Other work on gold NPs suggest that sorption of the HS may well influence surface properties such as dielectric constant on the surface of the nanoparticles, and thus their optical spectra (Diegoli *et al.*, 2008). It is likely that the presence of HS distorted some of these plasmon bands.

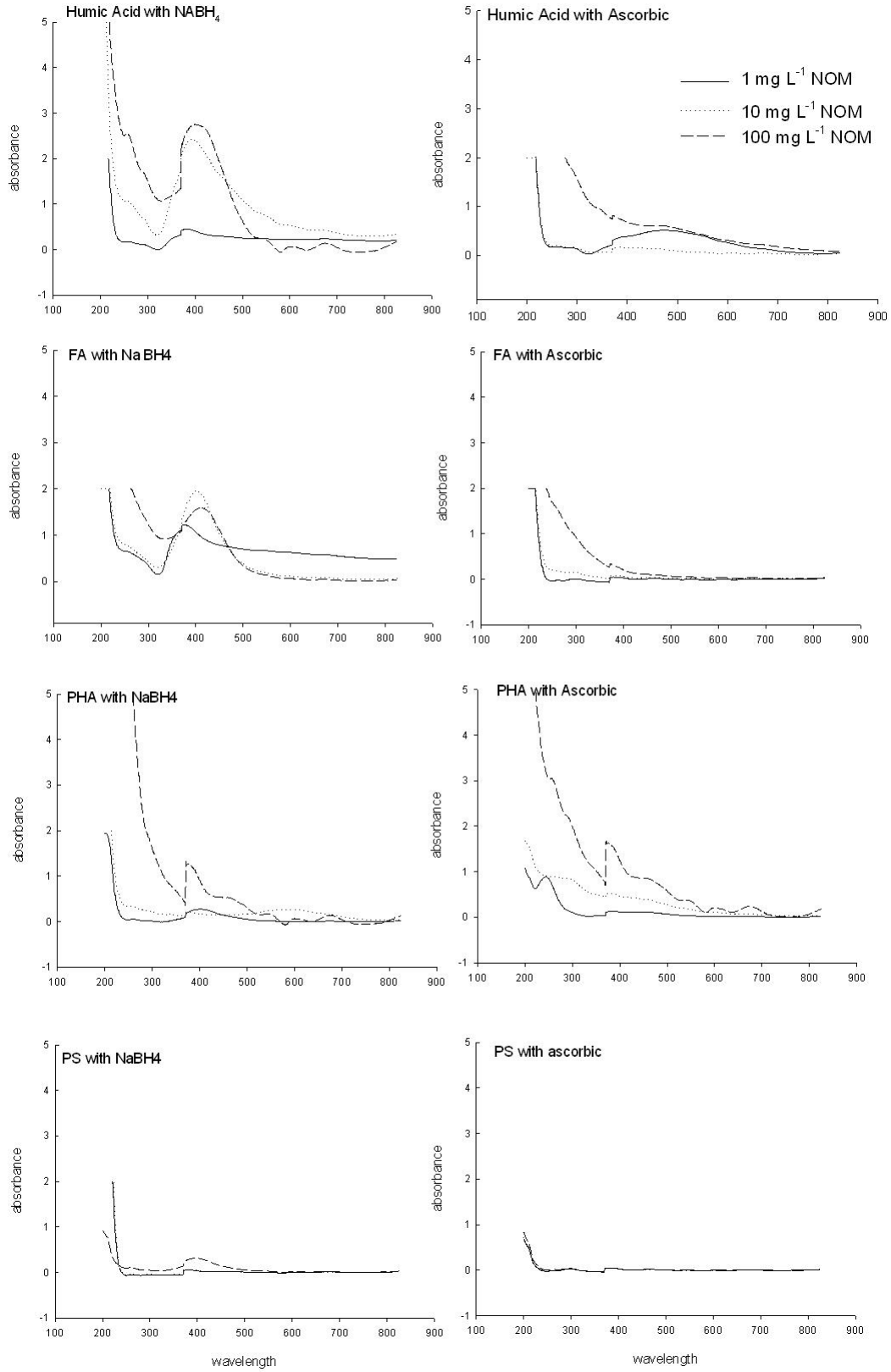

Figure 8.5 SPR UV absorbance spectra for Ag/NOM, using humic acid (HA), fulvic acid (FA) peat humic acid (PHA) or polysaccharide (PS) NP suspensions reduced with $NaBH_4$ or ascorbic acid. Samples were analysed 3 months post synthesis.

8.3.4 Characterisation with TEM

This sub-section looks at the information obtained from TEM analysis, first presenting the TEM images themselves with the suspensions reduced by borohydride. Histograms and tables of TEM particle diameter and descriptive statistics are also presented. The same results are then presented for AA. The TEM images reveal that in all cases, including the colourless samples, that silver nanoparticles were formed.

8.3.4.1 TEM images for Ag/NOM suspension reduced with borohydride

TEM images of the Ag/NOM samples are presented in Figure 8.6 to Figure 8.9. Ag/FA NPs reduced with $NaBH_4$ (Figure 8.6 (a) to (c)), show a range of single and agglomerated structures. An appearance of a surface film, likely FA, is also evident observed surrounding the NPs. At 1 mg L^{-1}, the particles show well defined structures, sometimes joined or 'bridged' together by fulvic acid. At closer magnification, banding is seen on the Ag NPs. This is considered to be an imperfection in the Ag lattice by some authors (Henglein and Giersig, 1999). Aggregated particles in dense groups are seen with a concentration of 10 mg L^{-1} FA and at 100 mg L^{-1} FA, rounded triangular particles are observed. The high resolution image in (c) shows the FA bridging two particles together.

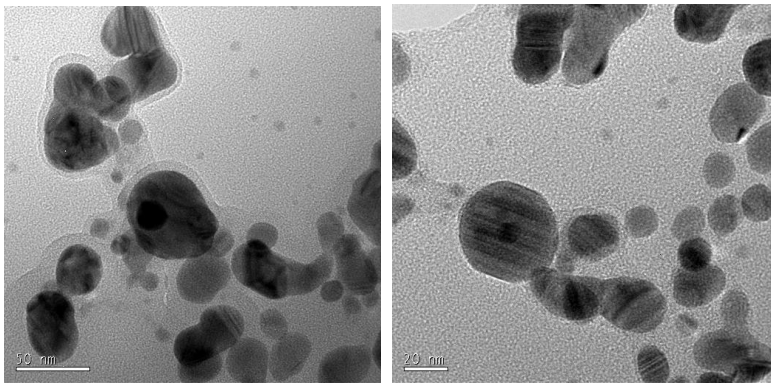

(a) TEM images of Ag NPs in Fulvic acid at 1 mg L^{-1} reduced with $NaBH_4$

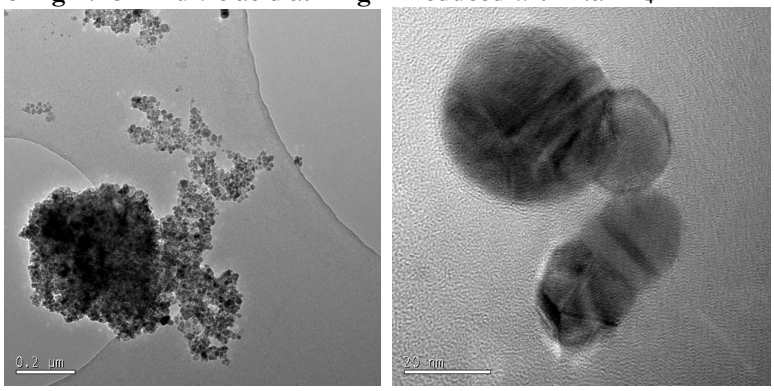

(b) Ag/FA 10 mg L^{-1} reduced with $NaBH_4$

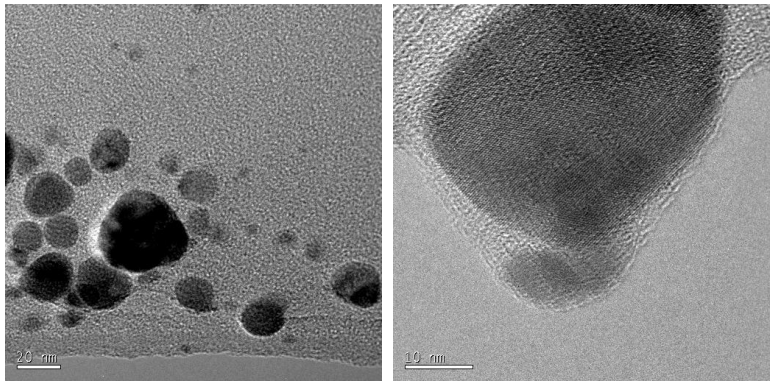

(c) Ag/FA 100 mg L^{-1} reduced with $NaBH_4$

Figure 8.6 TEM images of typically observed Ag /FA nanoparticles reduced with $NaBH_4$ for three different FA concentrations: (a) 1, (b) 10 and (c) 100 mg L^{-1}. Shown at two different magnifications.

The particles in Figure 8.7 show a range of structures and aggregates. For 1 mg L^{-1} HA, the particles have coalesced (see (a)). At higher magnification, the particles are seen surrounded by a HA film. The particles in (b) show more separation and mostly rounded, morphologies are observed. At the highest concentration, 100 mg L^{-1} HA, the excess HA is strongly present as a gel-like matrix resembling frog-spawn (see (c)).

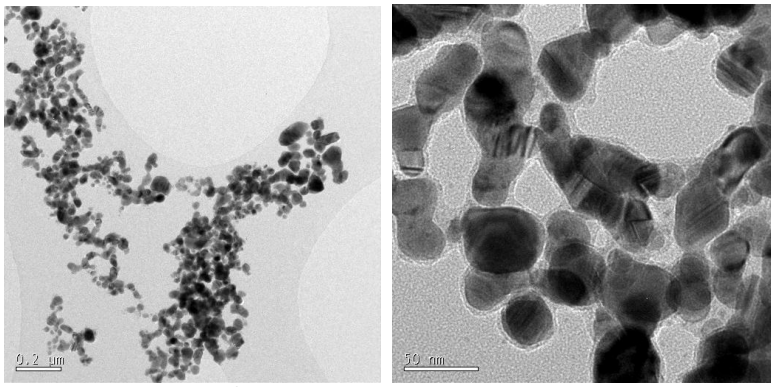

(a) Ag/HA NPs, Humic acid 1 mg L^{-1} reduced with $NaBH_4$

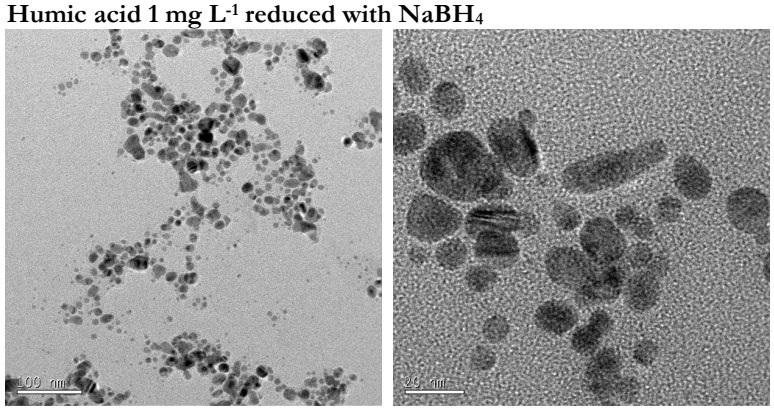

(b) Ag/HA NPs, Humic acid 10 mg L^{-1} reduced with $NaBH_4$

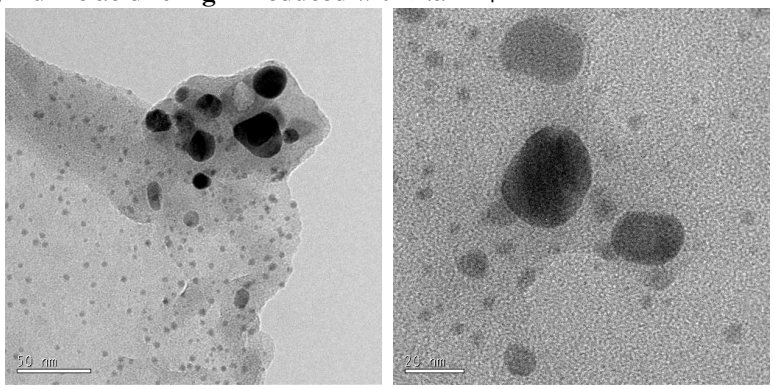

(c) Ag/HA NPs, Humic acid 100 mg L^{-1} reduced with $NaBH_4$

Figure 8.7 TEM images of Ag/HA NPs reduced with $NaBH_4$ for three different HA concentrations: (a) 1, (b) 10 and (c) 100 mg L^{-1}. Shown at two different magnifications.

TEM images in Figure 8.8 (a) to (c) for the Ag/PHA particles show a range of particle sizes and morphologies. Films of PHA can be seen surrounding the NPs in (a), with a more evenly dispersed sample shown in (b) and more polydispersity in (c). At 1 mg L^{-1}, groups of particles of varying sizes are observed surrounded by the PHA, which is not apparent in (b) and (c).

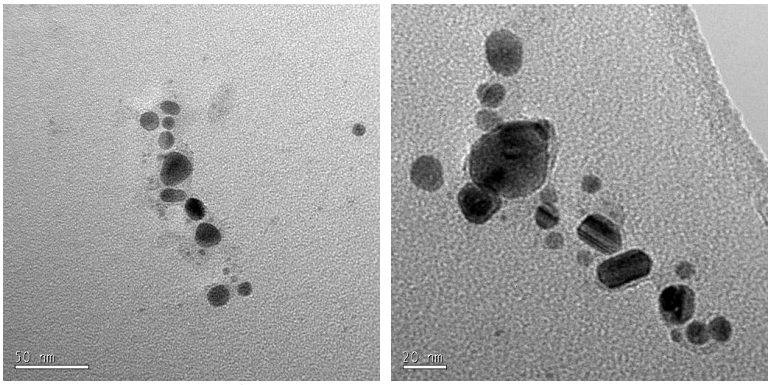

(a) Ag/PHA; Peat humic acid 1 mg L^{-1} reduced with $NaBH_4$

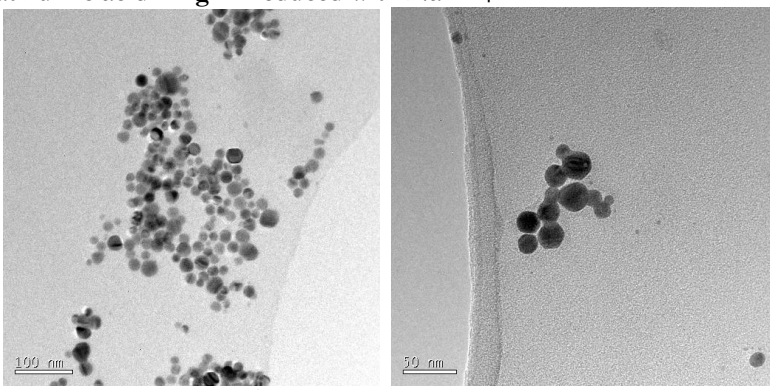

(b) Ag/PHA; Peat humic acid 10 mg L^{-1} reduced with $NaBH_4$

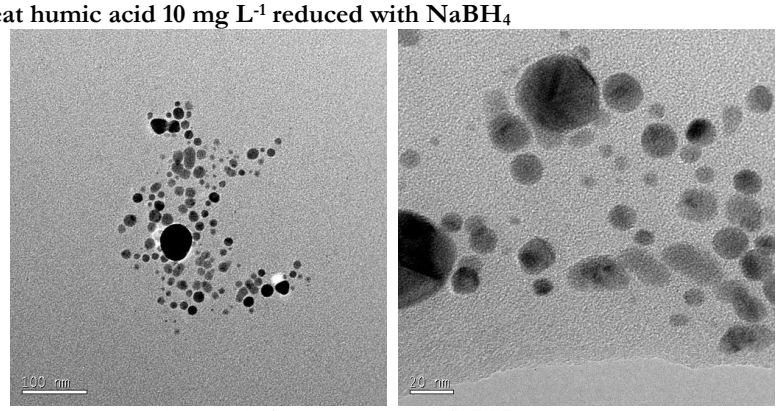

(c) Ag/PHA; Peat humic acid 100 mg L^{-1} reduced with $NaBH_4$

Figure 8.8 TEM images of Ag/PHA nanoparticles reduced with $NaBH_4$ for three different PHA concentrations: (a) 1, (b) 10 and (c) 100 mg L^{-1}. Shown at two different magnifications.

The Ag/PS TEM images in Figure 8.9 (a) to (c) appear as a bi-modal population of particle sizes and aggregates. In Figure 8.9 (a) numerous small particles appear to be embedded in a 'mesh' of PS. The PS is different structurally to the other HS being fibrillar and is likely to behave as other polymers. However, the larger Ag particles are seen surrounded by the PS. Particle aggregation is observed in (b) and (c).

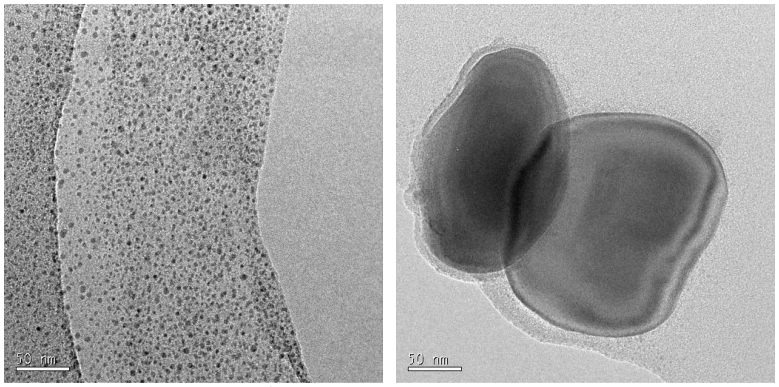

(a) Ag/PS NPs; Polysaccharide, 1 mg L^{-1} reduced with $NaBH_4$

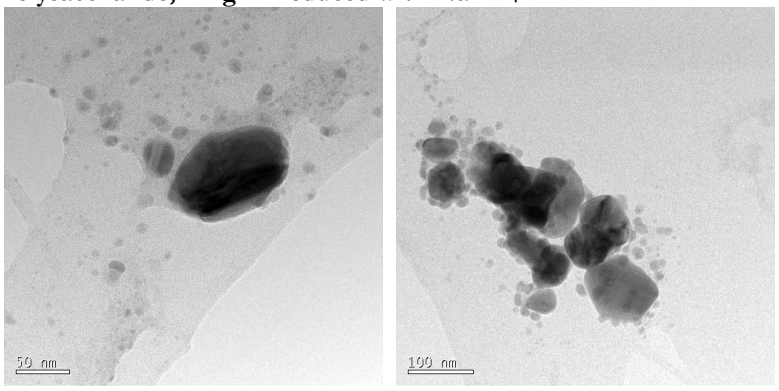

(b) Ag/PS NPs; Polysaccharide, 10 mg L^{-1} reduced with $NaBH_4$

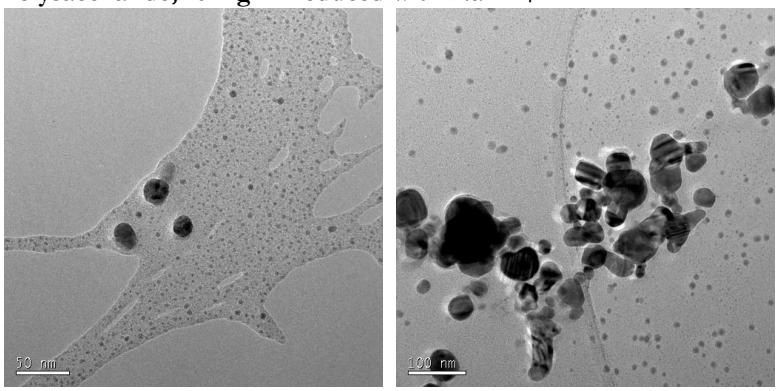

(c) Ag/PS NPs; Polysaccharide, 100 mg L^{-1} reduced with $NaBH_4$

Figure 8.9 PS TEM images of Ag/PS nanoparticles reduced with $NaBH_4$ for three different PS concentrations: 1, 10 and 100 mg L^{-1}. Shown at two different magnifications.

Figure 8.10 and Figure 8.11 are the histograms for Ag particle size derived from TEM images of Ag/FA and Ag/HA, and for Ag/PHA and Ag/PS. In all cases the samples were reduced with $NaBH_4$. This data is also presented in Table 8-2. Histograms mostly show a normal particle size distribution with most particles less than 100 nm. The most monodispersed are for HA at 10 mg L^{-1}, with a mean 9.7 ($\pm$3.4), mode of 10, a median of

9.7 and a particle range of 2 - 23 nm. With both sets of data below (FA and HA), the spread of the sizes reduces with increasing concentration of HS.

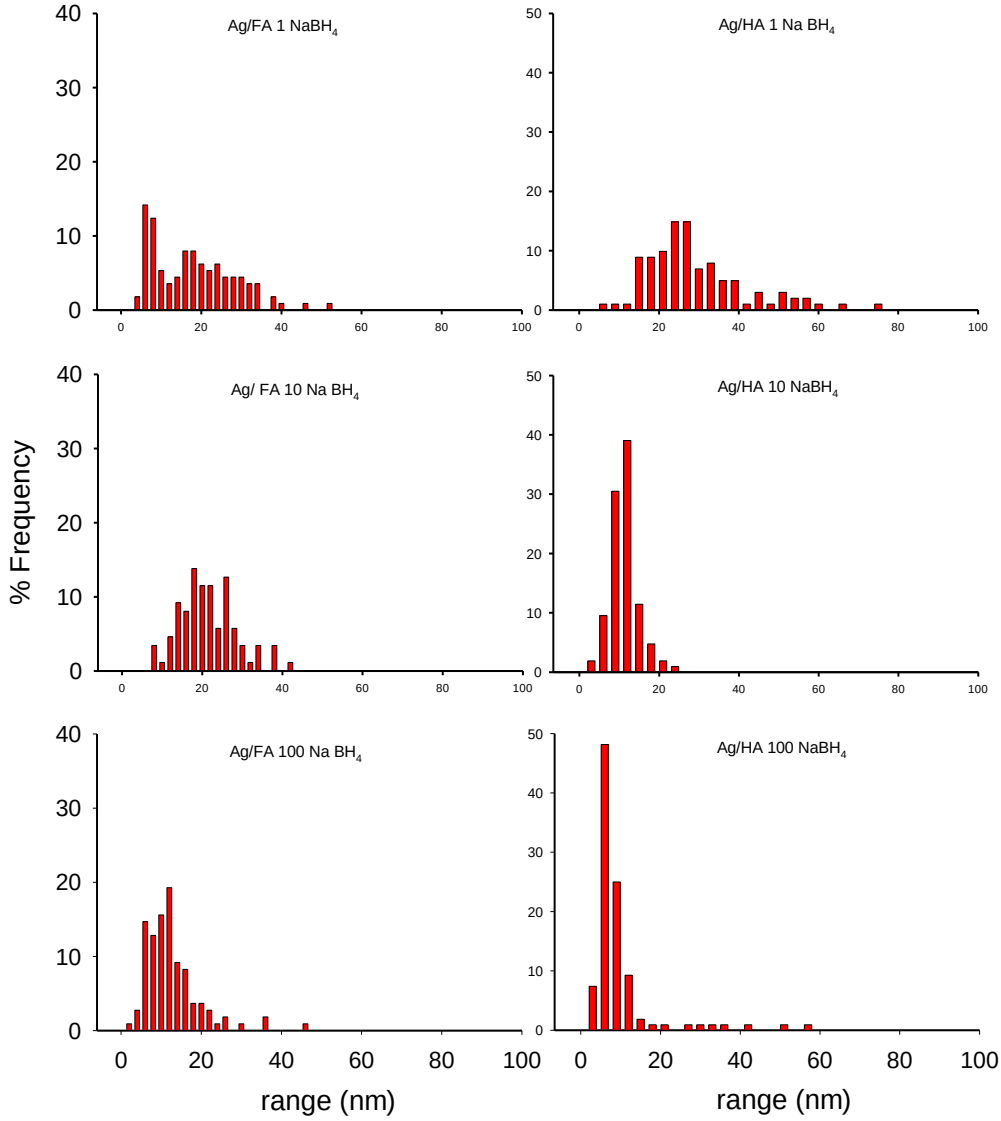

Figure 8.10 Ag/FA (left) and Ag/HA (right) histograms derived from TEM images for particle size range (nm) all samples were reduced with $NaBH_4$

In comparison to Figure 8.10 above, the PS on the right in Figure 8.11 show more spread towards the higher sizes from 1 mg L^{-1} to 100 mg L^{-1}. Contrary to the PS, the particle size range of the PHA reduces as the concentration increases.

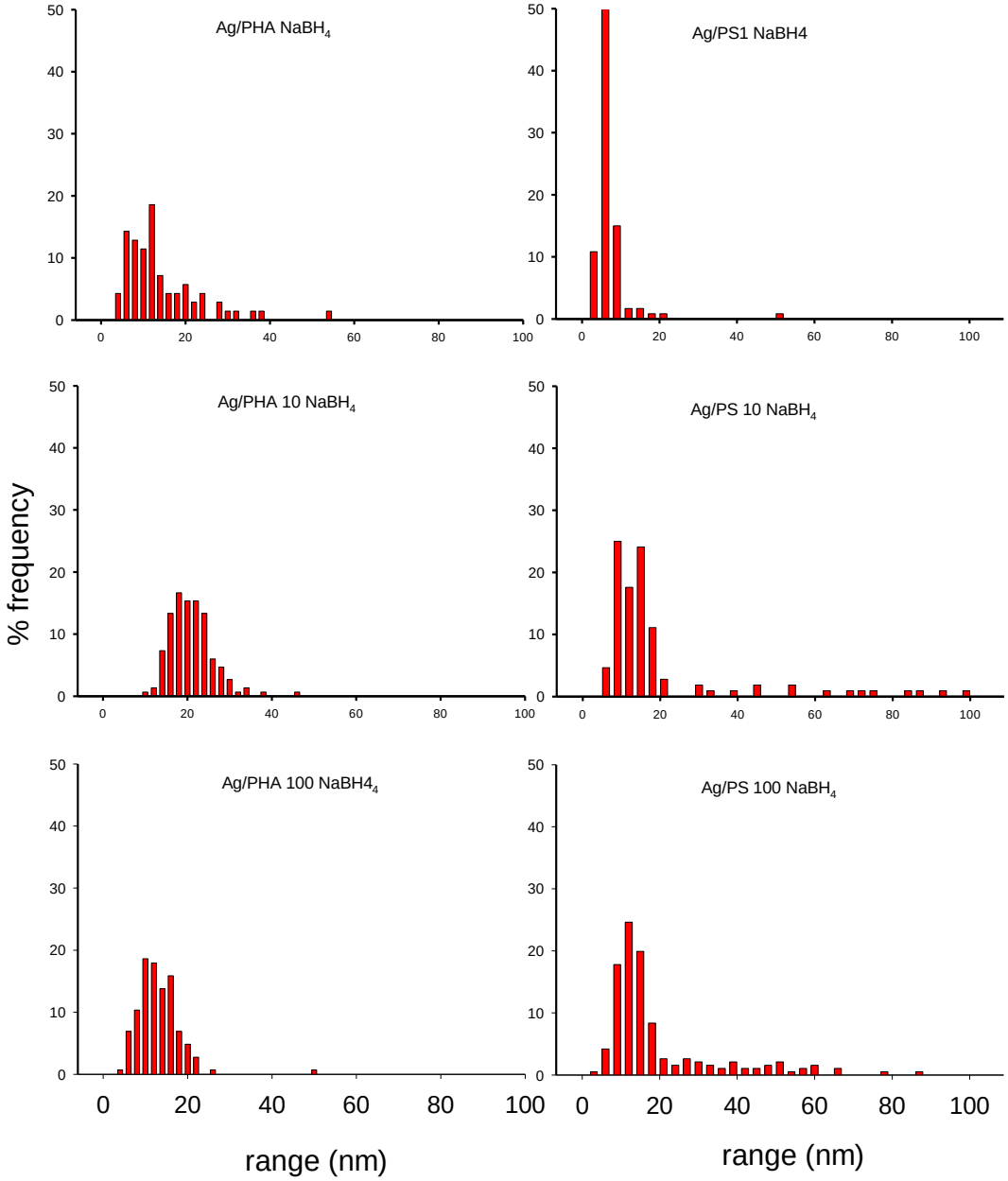

Figure 8.11 Histograms derived from TEM images for particle size ranges for PHA and PS reduced with $NaBH_4$

Table 8-3 is a summary of the TEM size data with some descriptive statistics (excel) for silver and NOM samples reduced with $NaBH_4$. Particle size ranged from 2 - 99 nm for all samples. The sample with the smallest size range was Ag/HA 10 and the samples with the largest particle ranges were FA 10, PS 10 and PS 100, which gave mean particle sizes of 23 and 18 nm respectively. HA 1 also gave a wide range in particle size distribution.

Table 8- 2 Descriptive statistics for Ag /NOM particle size (nm) obtained from TEM images for Ag with HA, FA, PHA and PS reduction using sodium borohydride

HA type	HS mg L^{-1}	Mean (nm)	Stdev (nm)	Range (nm) min	Range (nm) max	Mode (nm)	Median (nm)	Number
Humic	1	27.8	*12.6*	3.9	72.3	34.3	25.3	101
	10	9.7	*3.4*	2.4	23.1	10.0	9.7	105
	100	8.3	*8.8*	2.3	54.7	5.5	5.7	108
Fulvic	1	15.3	*10.3*	3.0	51.8	6.5	13.4	163
	10	22.5	*13.4*	6.2	95.9	17.5	20.0	90
	100	11.5	*6.9*	2.0	44.1	4.2	10.3	109
Peat	1	13.3	*9.1*	3.6	53.1	5.7	10.7	70
	10	20.0	*5.3*	8.5	44.9	19.2	19.2	150
	100	12.1	*5.1*	4.0	48.9	8.2	11.4	145
PS	1	5.6	*4.8*	2.3	50.2	6.8	5.0	120
	10	18.4	*19.5*	4.3	98.6	13.3	12.4	108
	100	17.9	*15.0*	2.0	84.8	9.1	12.4	191

8.3.4.2 TEM images for Ag/NOM suspension reduced with ascorbic acid

The TEM images of Ag/NOM suspensions that were reduced with AA are presented in Figures 8.12 – 8.15. The figures show an array of NPs which are different to those reduced with $NaBH_4$. Figure 8.12 (a) to (c) are for the Ag/FA and show particles that range from very small in (a), to agglomerates in (b) and large polygons in (c).

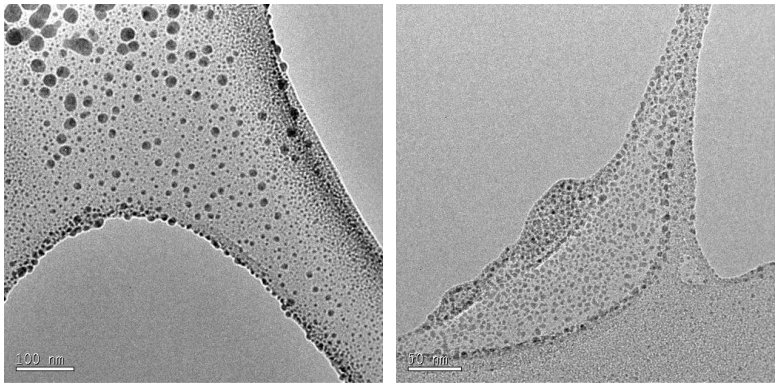

(a) Ag/FA NPs; Fulvic acid 1 mg L^{-1} reduced with ascorbic acid

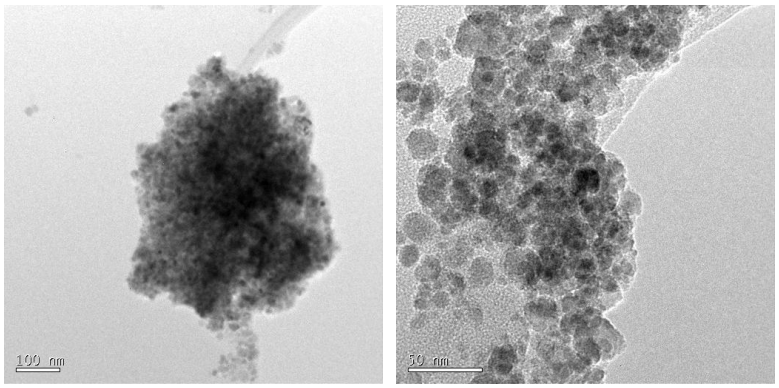

(b) Ag/FA NPs; Fulvic acid 10 mg L^{-1} reduced with ascorbic acid

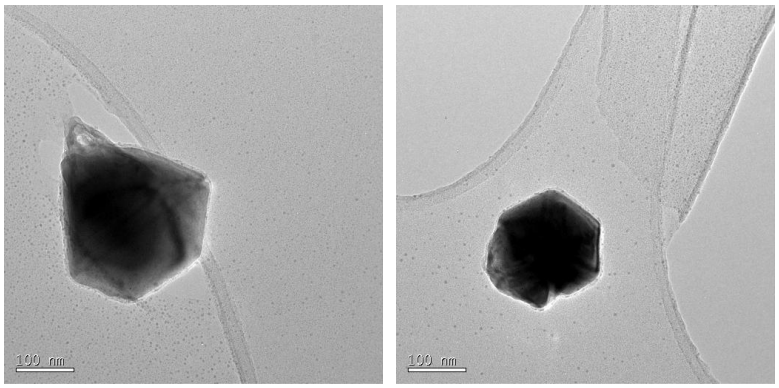

(c) Ag/FA NPs; Fulvic acid 100 mg L^{-1} reduced with ascorbic acid

Figure 8.12 Ag/FA NPs reduced with ascorbic acid at 1, 10 and 100 mg L-1 FA

The Ag/HA NPs show different structures compared to other NPs (see Figure 8.13). The particles in Figure 8.13 (a) (HA 1 mg L^{-1}) appear to be large, tightly packed aggregates of 100-200 nm consisting of many smaller spherical NPs with remarkable regularity. These aggregates appear like large particles with the HA forming an integral part of the structure as

well as a surface layer. In (b) and (c) the Ag NPs are 50-100 nm. In (c) the HA film surrounds the NPs, but appears not to bind them closely together.

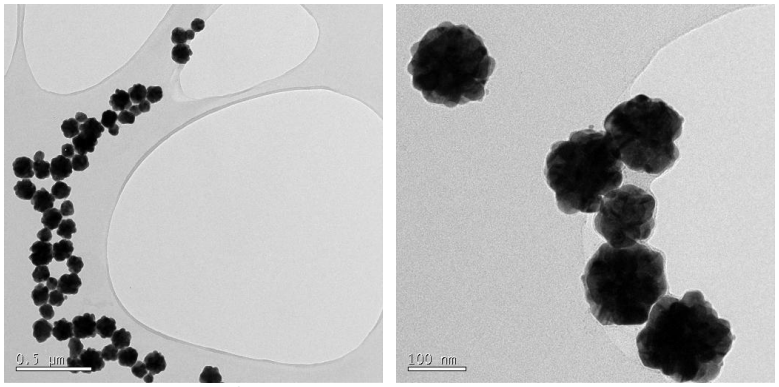

(a) Ag/HA NPs; Humic acid 1 mg L^{-1} reduced with ascorbic acid

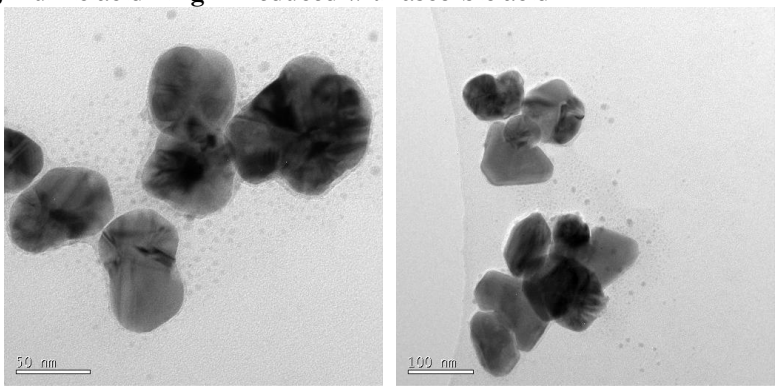

(b) Ag/HA NPs; Humic acid 10 mg L^{-1} reduced with ascorbic acid

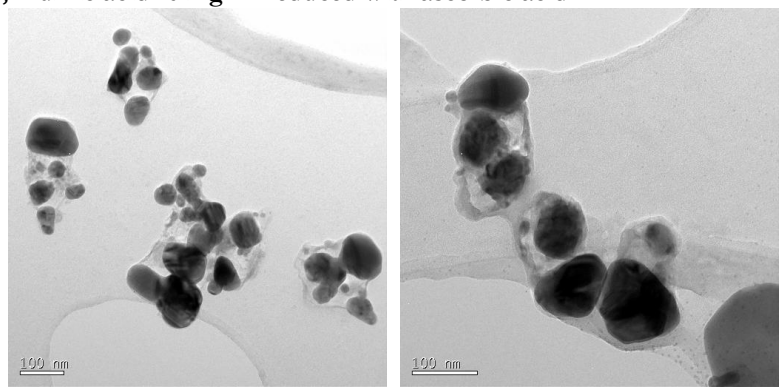

(c) Ag/HA NPs; Humic acid 100 mg L^{-1} reduced with ascorbic acid

Figure 8.13 Ag/HA NPs reduced with ascorbic acid at 1, 10 and 100 mg L^{-1} HA

Ag/PHA NPs (Figure 8.14), like Ag/FA, show individual particles at the lowest concentration, but at 10 and 100 mg L^{-1} PHA the particles have coalesced, and again show a NOM matrix encasing them.

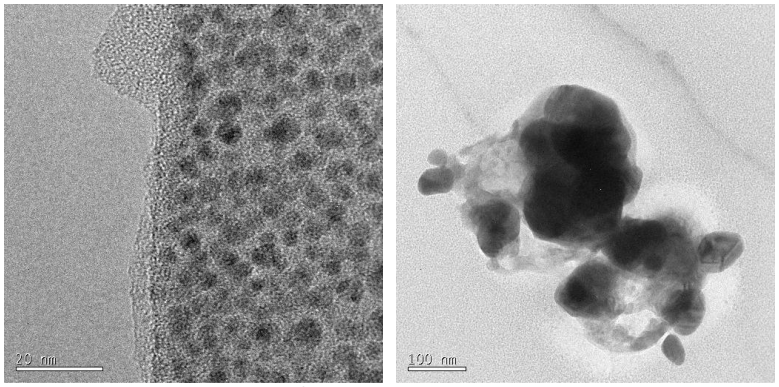

(a) Ag/PHA NPs; Peat humic acid 1 mg L^{-1} reduced with ascorbic acid

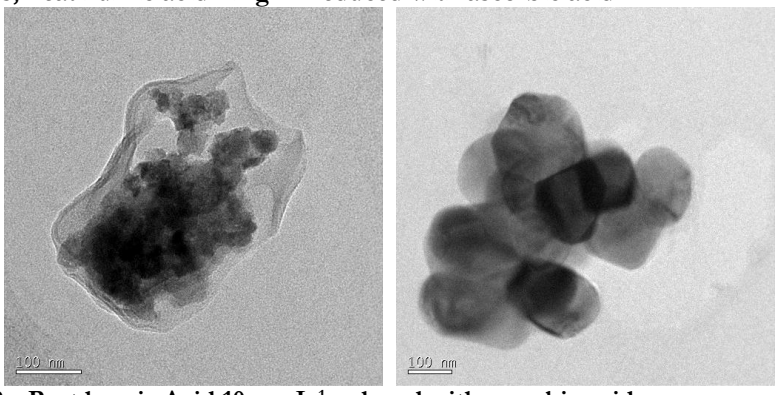

(b) Ag/PHA NPs; Peat humic Acid 10 mg L^{-1} reduced with ascorbic acid

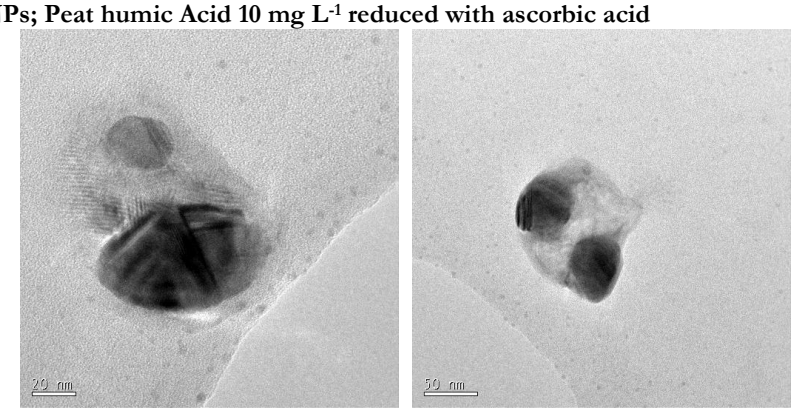

(c) Ag/PHA NPs; Peat humic Acid 100 mg L^{-1} reduced with ascorbic acid

Figure 8.14 Ag/PHA NPs reduced with ascorbic acid for PHA concentrations 1, 10 and 10 mg L-1

For Ag/PS, the images again show small individual particles for both 10 and 100 mg L^{-1} (Figure 8. 15 (a) and (b)). There was no image taken for the 1 mg L^{-1} PS.

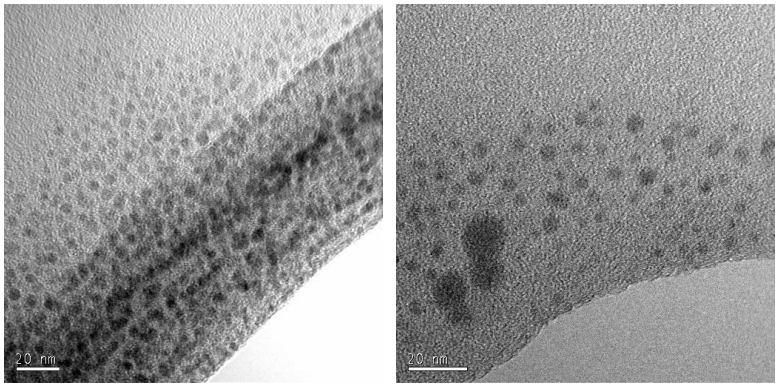

(a) Ag/PS NPs; Polysaccharide 10 mg L^{-1} with ascorbic acid. Scale bars are 20 nm

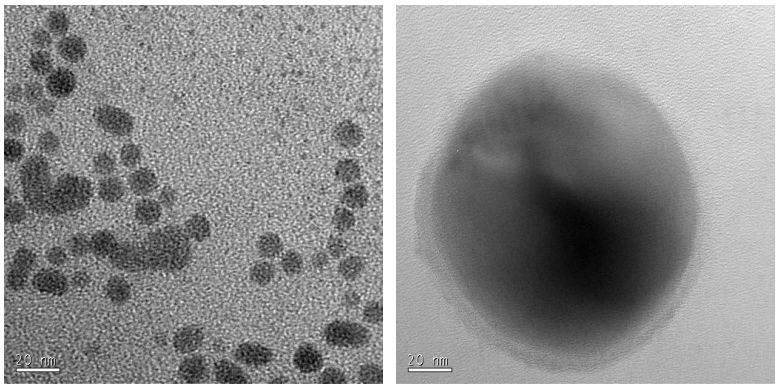

(b) Ag/PS NPs; Polysaccharide 100 mg L^{-1} with ascorbic acid. Scale bars are 20 nm

Figure 8. 15 Ag/PS NPs reduced with ascorbic acid. Polysaccharide concentrations of 10 and 10 mg L^{-1}.

The histograms of Ag/FA and Ag/HA represent distribution of particle size derived from TEM images (Figures 8.16 and 8.17) under the different NOM conditions reduced with AA. Ag/FA particles are smaller (10-30 nm) than Ag/HA particles (24-122 nm) and show a smaller size range for FA 1 and FA 10 only, than Ag/HA which all span greater than 100 nm. The unusual clusters observed in Figure 8.13 (a) for HA 1 (120 nm) show the large particle size and distribution.

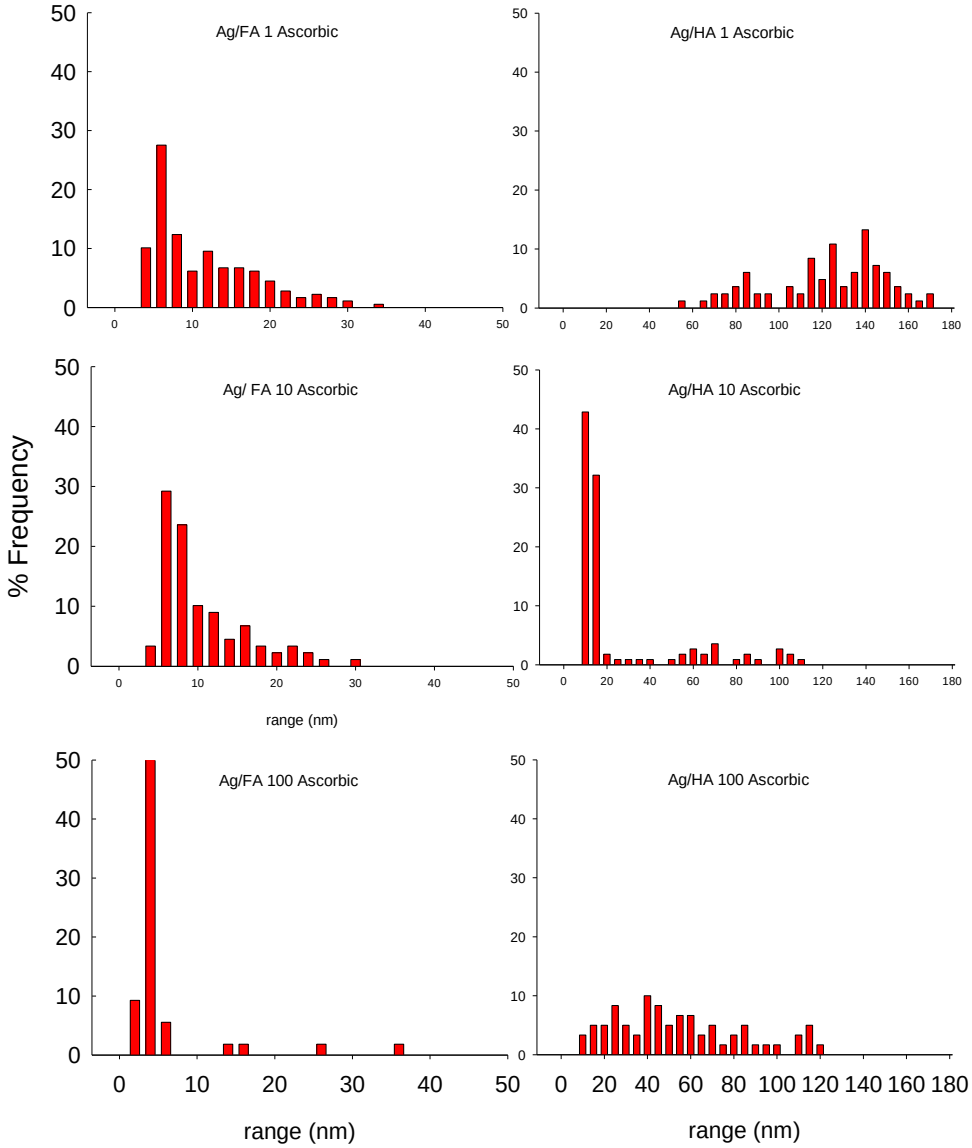

Figure 8. 16 Histograms from TEM images for Ag/fulvic acid and Ag/humic acid reduced with ascorbic acid

Figure 8. 17 are the histograms for Ag/PHA and Ag/PS reduced with AA. In general, the Ag/PS suspensions on the right demonstrate the very small (6-12 nm) showing a particle range of 13 and 16 nm respectively for the PS 10 and PS 100 suspensions. On the other hand the suspensions of Ag/PHA are poorly distributed and show a large size range of 16, 204, 302 nm respectively for the PHA 1, PHA 10 and PHA 100 Ag suspensions.

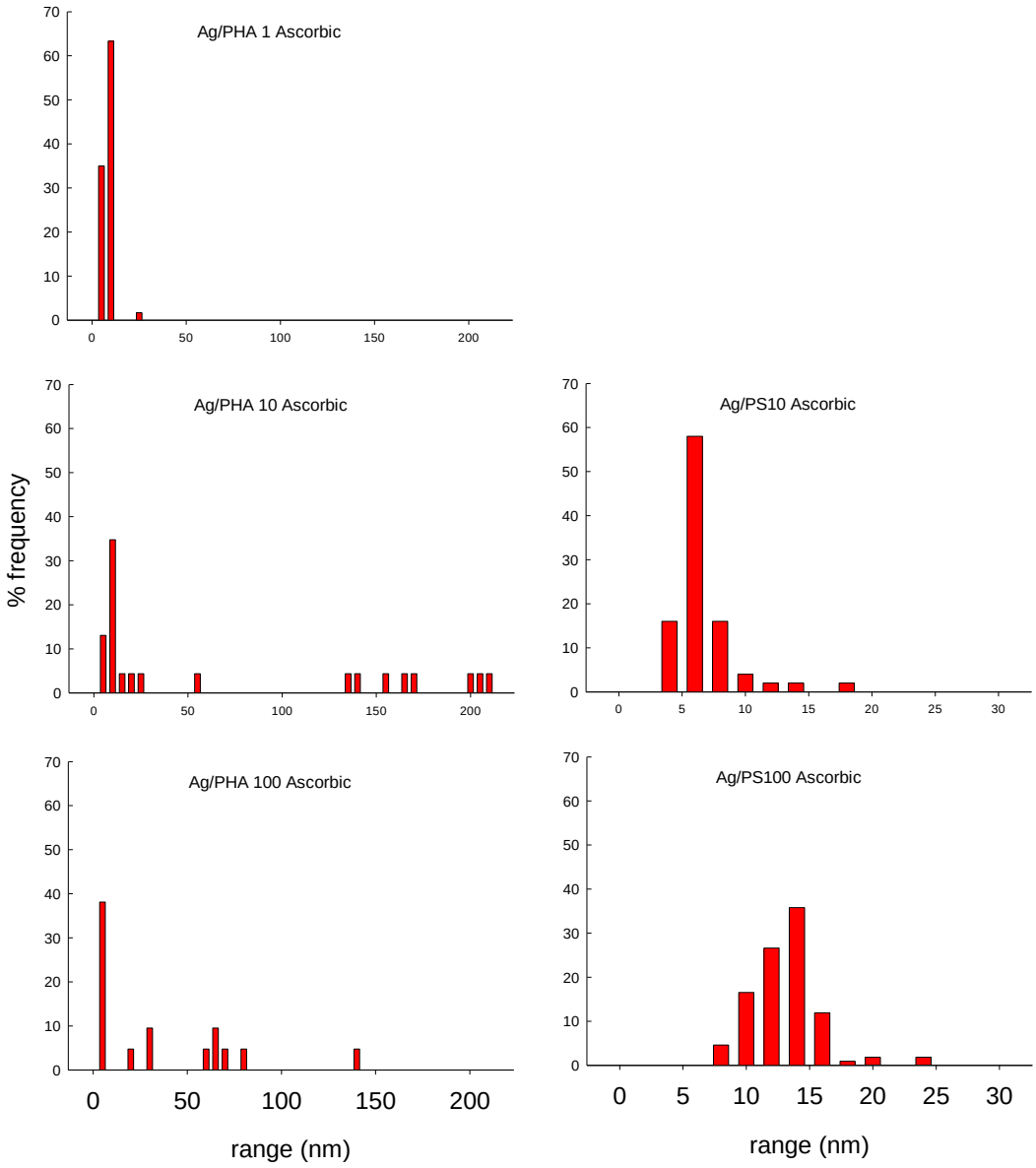

Figure 8. 17 Histograms from TEM images for Ag/PHA (left) nanoparticles for 1, 10 and 100mg L^{-1} and Ag/PS (right) nanoparticles for 10 and 100 mg L^{-1}

Table 8-3 is a summary of the TEM size data with some descriptive statistics for silver and NOM samples reduced with AA. Particle size ranged from 1-320 nm for all samples. The sample with the smallest size range was Ag/PS 10 and the samples with the largest particle ranges were Ag/PHA 10, Ag/PHA 100 and Ag/FA 100, which gave mean particle sizes of 66, 77 and 31 nm respectively.

Table 8- 3 Descriptive statistics for Ag/NOM particle size (nm) **obtained from TEM images for Ag with HA, FA, PHA and PS and for reduction using ascorbic acid**

HA type	HS mg L^{-1}	Mean (nm)	Stdev	Range (nm) min	Range (nm) max	Mode (nm)	Median (nm)	Number
Humic	1	121.7	*28.6*	53.3	188.4	137.5	124	83
	10	23.6	*27.3*	5.7	109.6	11.0	10.9	112
	100	52.6	*29.8*	9.0	118.9	#N/A	47.5	60
Fulvic	1	10.6	*6.8*	2.3	32.7	5.3	8.1	179
	10	10.1	*7.9*	2.4	63.4	6.1	7.4	90
	100	31.2	*72.0*	1.3	320.0	3.3	3.3	67
Peat	1	5.8	*2.2*	3.9	20.6	4.6	5.3	60
	10	66.3	*80.0*	3.7	208.0	#N/A	10.1	23
	100	77.4	*100.0*	3.9	307.0	#N/A	27.6	21
PS	1	*	*	*	*	*	*	*
	10	5.8	*2.4*	3.2	16.3	4.9	5.1	50
	100	12.1	*2.8*	6.8	22.9	10.4	12.2	109

*donates no data

Statistical tests performed on the TEM size data for variation by reaction conditions were not significant (Table 8-4). Tests were performed by reaction variable, reducing agent (AA vs. NaBH4), NOM type (HA vs. FA vs. PS vs. PHA) and NOM concentration, mg L^{-1} (1 vs. 10 vs. 100). That none of the tests were significant indicates that particle size was by chance.

Table 8- 4 Statistical outcome for TEM particle size

Parameter	Statistical test	Outcome P < 0.050?
Reducing agent	Whitney rank sum test	Not significant
NOM type	Whitney rank sum test	Not significant
Concentration	Whitney rank sum test	Not significant

Table 8-5 presents all the descriptive statistics (performed with Excel) for all the TEM data together, by NOM type and by reductant type, describing the skewness, the measurement of the distribution symmetry or shape of the peak and kurtosis, the measurement of the uniformity of a sample distribution or the sharpness of a peak. For a normal distribution, kurtosis is a value nearest three and the skewness to a value nearest zero (see (Borchert *et al.*, 2005)). The one distinctive sample that can be drawn out of the data is the HA 10 ($NaBH_4$) with a particle size of 9.7 nm a sample range of 20 nm (std dev = 3.4, median = 9.7, mode = 10). Additionally, kurtosis (2.2) and skewness (0.9) suggest a normal distribution of particle size to a confidence level of 0.7 ($p = 0.05$). Another sample with a small particle range also demonstrating a normal distribution, though less strongly, was the Ag/PS 100 reduced by AA. In this case the mean particle size was 12 nm (std dev = 2.8, median = 12, mode = 10) with a confidence in the mean of 0.5 ($p= 0.05$). The samples which performed least well statistically was the PHA 10 (with AA), which had a mean particle size of 66 nm and a range of 204 nm. The confidence interval was 34.6 ($p < 0.05$) and the variance was 6391. The confidence interval (nm) at 95 % is defined by 'Excel' as the mean, $\bar{x}$, $\pm$ 1.96 $\times$ (st dev / sq root of the sample size). That this sample gave a kurtosis value of 22.2 indicates that particle size distribution was more uniform than normally distributed (i.e. equal numbers of each particle size). Interestingly, the samples that conform to the most normal size distributions are those between 10-20 nm, as has been seen in chapter 6 with the citrate synthesis. The particles that were the most mono-morphological were the aggregates of Ag/HA 1 reduced with AA.

Table 8-5 The descriptive statistics (Excel) for all the TEM size data showing the peak shape and distribution information

For all data: Mean = 20.8nm; SE=0.6; Median= 11.6 nm; Mode=10.4; St Dev=31.2 nm; Variance=971.5; Kurtosis=23.3; Skewness = 4.2; Range =318.7nm, n=2314

		HA			FA			PHA			PS		
NOM concentration	**All data**	**1**	**10**	**100**	**1**	**10**	**100**	**1**	**10**	**100**	**1**	**10**	**100**
Borohydride													
Mean (nm)	**15.2**	**27.8**	**9.7**	**8.3**	**15.3**	**22.5**	**11.5**	**13.3**	**19.9**	**12.1**	**5.6**	**18.4**	**17.9**
Standard error	0.3	1.2	0.3	0.8	0.8	1.4	0.7	1.1	0.4	0.4	0.4	1.9	1.1
Median (nm)	12.2	25.3	9.7	5.7	13.4	20.0	10.3	10.7	19.2	11.4	5.0	12.4	12.4
Mode (nm)	13.3	34.3	10.0	5.5	6.5	17.5	4.2	5.7	19.2	8.2	6.8	13.3	9.1
Standard deviation (nm)	12.1	12.6	3.4	8.8	10.3	13.4	6.9	9.1	5.2	5.1	4.7	19.5	14.9
Sample variance	145.3	157.8	11.6	76.6	105.6	179.3	47.2	82.0	27.4	26.5	22.5	381.5	223.5
Kurtosis	**9.4**	**1.4**	**2.2**	**13.8**	**0.0**	**14.8**	**5.9**	**5.0**	**3.2**	**17.1**	**66.4**	**6.2**	**4.0**
Skewness	**2.5**	**1.1**	**0.9**	**3.6**	**0.8**	**3.4**	**2.0**	**1.9**	**1.2**	**2.7**	**7.4**	**2.6**	**2.1**
Range (nm)	96.6	68.4	20.7	52.4	48.8	89.7	42.1	49.5	36.4	44.9	48.0	94.3	82.8
Confidence interval (95.0%)		2.5	0.7	1.7	1.6	2.8	1.3	2.2	0.8	0.8	0.9	3.7	2.1
Ascorbic acid													
Mean (nm)	**30.3**	**121.7**	**23.6**	**52.6**	**10.6**	**10.1**	**31.2**	**5.8**	**66.3**	**77.4**		**5.8**	**12.1**
Standard error	1.6	3.1	2.6	3.8	0.5	0.8	8.8	0.3	16.7	21.8		0.3	0.3
Median (nm)	10.5	123.8	10.9	47.5	8.1	7.4	3.3	5.3	10.1	27.6		5.1	12.2
Mode (nm)	10.4	137.5	11.0	#N/A	5.3	6.1	3.3	4.6	#N/A	#N/A		4.9	10.4
Standard deviation (nm)	47.3	28.6	27.3	29.8	6.8	7.9	72.0	2.2	79.9	99.8		2.4	2.8
Sample variance	2241.8	820.0	747.1	887.3	45.8	62.9	5179.4	4.8	6391.6	9952.9		5.8	7.8
Kurtosis	**8.0**	**-0.3**	**1.9**	**-0.5**	**0.3**	**22.2**	**9.1**	**37.0**	**-1.2**	**0.5**		**8.2**	**2.7**
Skewness	**2.6**	**-0.3**	**1.8**	**0.6**	**1.0**	**3.8**	**3.1**	**5.5**	**0.8**	**1.4**		**2.6**	**1.0**
Range (nm)	318.7	135.1	103.9	109.9	30.4	61.1	318.7	16.7	204.0	302.6		13.2	16.1
Confidence interval (95.0%)		6.3	5.1	7.7	1.0	1.7	17.6	0.6	34.6	45.4		0.7	0.5

The presence and action of NOM can easily be seen either attached to the nanoparticle surface as a thick coating or as a bridge connecting other particles together. Silver nanoparticles are also observed encapsulated by a mesh of NOM. One interesting structure is that of humic acid at 1 mg L^{-1} reduced by AA. Figure 8.13(b), shows the presence of tight, spherical aggregates possibly as an intricate matrix of silver and humics. At HA 10 mg L^{-1} particles become denser and more crystalline than with 1 mg L^{-1}. Interestingly, and quite the opposite, is the structure observed with the PS where the silver nanoparticles are supported between the fibrillar, web-like structure. Similarly, this behaviour has been reported in the environmental context by Buffle *et al.,* (1998) and Balnois et al (2000) from AFM measurements of naturally produced inorganic colloids with natural organic macromolecules.

The graph shown in Figure 8.18 is the plotted mean values derived from TEM images that have been presented in Table 8-5. Standard deviations are also included in Figure 8.18. Comparisons between NOM concentrations for $NaBH_4$ show that the largest particle size for a single NOM type is at 10 mg L^{-1} and NOM concentrations 1 or 100 mg L^{-1} are smaller. The exception is Ag/HA where the lowest concentration, 1 mg L^{-1}, has the largest size. The greater the concentration, the greater the thickness of the NOM films, which may prevent particle interaction and therefore limit particle growth at nucleation. No trends in size were observed between the different NOM types. Comparison between reductant types (Table 8-5) showed that the mean particle size for Ag/NOM when $NaBH_4$ was used was smaller (15.2 nm) than when AA (30.3 nm) was used as a reducing agent. A test-test (Sigmaplot Systat) was applied ($NaBH_4$ vs. AA), which showed that there was no statistically significant difference ($P = 0.05$) between reducing agents.

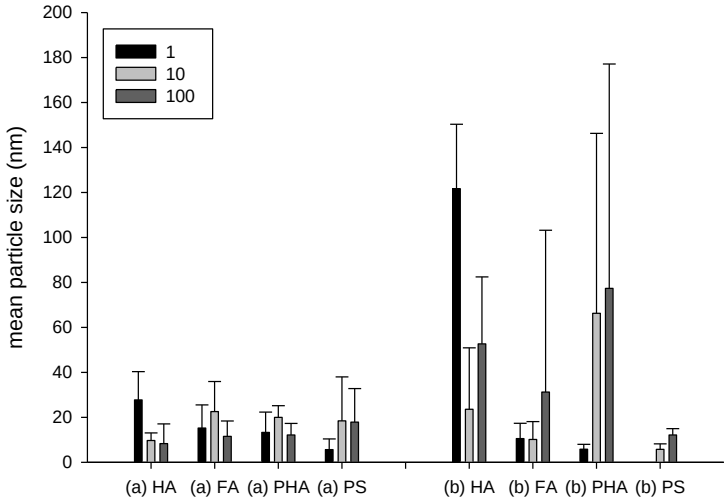

Figure 8.18 Ag/NOM mean particle size from TEM images for Ag/HA, Ag/FA, Ag/PHA and Ag/PS for (a) reduction with $NaBH_4$ and (b) ascorbic acid. Error bars are standard deviations.

8.3.5 Characterisation of particle size using dynamic light scattering

Table 8-6 presents the size data for the silver/NOM nanoparticle suspensions analysed by DLS at 24 hours and at 3 months post synthesis. Particle size is generally more variable than TEM and some samples show large standard deviations, indicating polydispersity and or an unstable sample at the point of measurement. Over time, most samples showed a statistical difference in sample change between measurement at 24 hours and three months. However, a few samples did not show any change (Ag/HA 10; Ag/PHA 1; Ag/PHA 10 and Ag/PHA 100 - all reduced by $NaBH_4$). Others samples also showed no change but with a high variability (Ag/FA 100 $NaBH_4$; Ag/FA 100 AA and Ag/PS 100 $NaBH_4$). In addition, some samples showed little change but were statistically different over time (FA 10 (14 nm to 18 nm) and PHA 10 (18 to 25 nm) with $NaBH_4$ and Ag/HA 1 (102 to 98 nm); Ag/HA 10 (172 to 162 nm) and Ag/HA 100 (83 to 79 nm) with AA).

Table 8-6 DLS Z-average sample means data for Ag/NOM nanoparticle suspensions at 24 hours and at three months post synthesis, standard deviations are from three measurements t-test (sigma plot – Systat) applied and Mann-Whitney test applied where marked.

For all data: Mean = 272 nm; SE = 40; Median = 146 nm; Mode = 272 nm; St Dev = 452; Variance = 203,138; Kurtosis = 12; Skewness = 3 Range = 2346; n= 126 (Excel).

Sodium borohydride							Ascorbic acid						
NOM concentration		24 hrs nm	24 hrs StDev(nm)	3 months nm	3 months StDev(nm)	Sample difference **t-test**			24 hrs nm	24 hrs StDev(nm)	3 months nm	3 months StDev(nm)	Sample difference **t-test**
1	HA	285.4	*13.4*	106.2	*1.6*	Yes (P=0.002)	1	HA	102.7	*1.1*	98.5	*1.4*	Yes (P=0.015)
	FA	63.8	*28.1*	25.1	*0.1*	Yes (P=<0.001)		FA	500.7	*119.3*	286.7	*90.7*	Yes (P=0.017)
	PHA	39.7	*14.5*	33.0	*2.0*	No (P=0.473)		PHA			136.9	*0.9*	
	PS	2129	*167.8*	702.2	*3.9*	Yes (P= <0.001)		PS			353.8	*100.6*	
10							10						
	HA	19.6	*0.8*	20.0	*0.6*	No (P=0.533)		HA	177.5	*1.9*	162.8	*1.2*	Yes (P= <0.001)
	FA	13.6	*175.0*	17.8	*0.5*	Yes (P=<0.001)		FA	276.4	*58.5*	150.5	*5.2*	Yes (P= <0.001)
	PHA	18	*0.2*	25.1	*0.0*	Yes (P=<0.001)		PHA			43.5	*1.2*	
	PS	428.9	*19.8*	387.8	*63.4*	No (P=0.168)*		PS			211.6	*23.6*	
100							100						
	HA	246.9	*22*	70.2	*22.5*	Yes (P=0.024)$		HA	83.8	*0.7*	79.2	*0.3*	Yes (P= <0.001)
	FA	309.3	*161.5*	31.4	*14.8*	No (P=0.1)$*		FA	169.6	*2.1*	130.2	*0.5*	No (P =0.1)$*
	PHA	159.8	*21.7*	128.6	*10.9*	No (P=0.131)		PHA			52.0	*0.5*	
	PS	200.7	*26.3*	173.6	*2.4*	No (P=0.211)*		PS			104	*2.9*	

$ Mann-Whitney test performed

* Variability in sample

For the data in both tables, again the sample that is the most stable is the Ag/HA10 with $NaBH_4$, in both measurement the particle size is 20 nm (standard deviation of the measurement = 0.6). This agrees with the TEM data (10 nm), but is double the size.

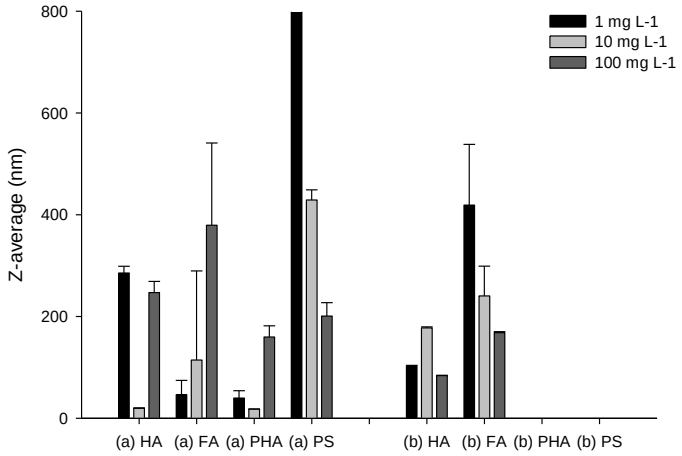

Figure 8.19 Dynamic light scattering results for the HA/Ag NPs reduced with $NaBH_4$ (a) or ascorbic acid (b). Data is missing for PHA and PS with ascorbic acid. Error bars are standard deviations from three measurements. The out of range value is 2129 nm.

8.3.6 Comparison particle size of DLS with TEM

Differences between DLS and TEM are mainly due to the fact that TEM is measuring the electron dense Ag core of the particle and DLS records the hydrodynamic diameter, including the capping agent. Nevertheless, as seen from the TEM images there is a certain amount of NOM material of varying thicknesses surrounding groups of NPs (not included in the physical measurements), probably contributing to particle size measurement in DLS. It is probable that artefacts were created under the electron beam in the UHV, which humics are sensitive to. Moreover, the presence of larger particles will scatter more light in DLS recording a larger particle size. For this reason, precision can be improved by using TEM images to assess the size of particle cores. However, there was no correlation between means

observed by TEM and DLS (r^2 = 0.04). For example, a notable larger particle size was obtained for the Ag/PS (cira 200–2000 nm) than was obtained though TEM, (20-60nm). This difference is probably due to interference from PS aggregates themselves.

The lack of correlation is likely due to the different measurement principles and presence of artifacts mentioned above. Diegoli *et al.,* (2008) also noted differences for citrate stabilised gold NPs. They gave two reasons for the differences between TEM and DLS sizes. First, the organic stabiliser is transparent to electrons, and therefore does not contribute to the diameter obtained by TEM. Second, the DLS method is sensitive to the double layer surrounding the gold nanoparticles in dispersion and is expected to overestimate the particles diameter.

8.3.7 Characterisation of particle size using electrophoretic mobility

EPMs for the Ag/NOM NP suspensions are reported in Figure 6.20 and in Table 6-7 and these data indicate that no relationships can be found with this EPM data when comparisons are made for NOM type, reductant type or NOM concentration. However, some relationships can be found and there is a weak correlation between particle size and surface charge for Ag/NOM with AA (r^2 = 0.5). This relationship does not exist with TEM particle size data or with DLS and Ag/NOM sample with $NaBH_4$. The EPM values for 80 mg L^{-1} PS only were -4.2 ± 1.4 10^{-8} m^2 V^{-1} s^{-1} (n = 5).

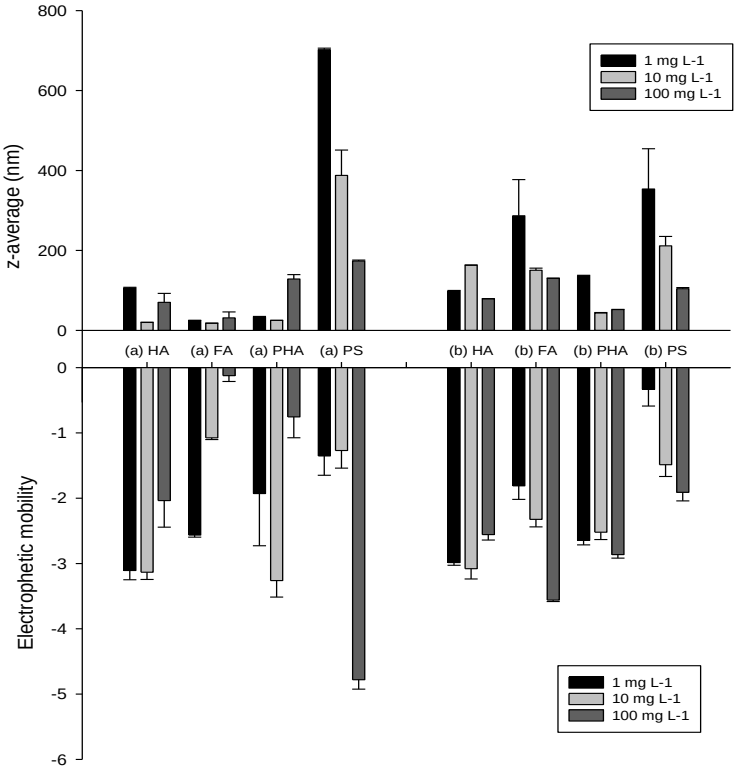

Figure 8.20 DLS and electrophoretic mobility (10^{-8} m^2 V^{-1} s^{-1}) for the samples error bars are the standard deviation from at least three measurements for size and five measurements for the EPM

Table 8-7 The electrophoretic mobilities (EPM) 10^{-8} m^2 V^{-1} s^{-1} for Ag/NOM NPs for conditions of NOM concentration 1, 10 and 100 mg L^{-1} and reductant type $NaBH_4$ and ascorbic acid for four different NOM types HA, FA, PHA and PS and area mean of five measurements

Sample type	NOM concentrations					
	1 mg L^{-1}	Standard deviation	10 mg L^{-1}	Standard deviation	100 mg L^{-1}	Standard deviation
Sodium borohydride						
Ag/HA	-3.11	*0.14*	-3.13	*0.11*	-2.04	*0.41*
Ag/FA	-2.56	*0.03*	-1.08	*0.03*	-0.12	*0.09*
Ag/PHA	-1.93	*0.80*	-3.26	*0.25*	-0.76	*0.32*
Ag/PS	-1.35	*0.30*	-1.27	*0.27*	-4.78	*0.14*
Ascorbic acid						
Ag/HA	-2.99	*0.04*	-3.08	*0.16*	-2.56	*0.08*
Ag/FA	-1.81	*0.21*	-2.32	*0.12*	-3.56	*0.02*
Ag/PHA	-2.64	*0.07*	-2.52	*0.11*	-2.86	*0.06*
Ag/PS	-0.33	*0.26*	-1.49	*0.18*	-1.91	*0.13*

For Ag/PS the EPM values varied from -0.3 to -4.8 10^{-8} m^2 V^{-1} s^{-1} for the Ag/PS 100 with $NaBH_4$. The PS with $NaBH_4$ had a greater negative charge *per se* than the same PS concentrations suspensions reduced with AA. Reduced negativity may be due to the HNO_3 (donating protons) generated from the Ag – AA reduction (see equation 8.1). The Ag/PS also showed a weak relationship (r^2 = 0.2) with a gradient of 54 with DLS particle size and charge, whereby, a reduced charge had a larger particle size and vice versa. This Ag/PS and AA relationship with DLS became stronger (r^2 = 0.9) with a gradient of 150 (and only three data points) when just the PS/AA data was compared. This also appeared to be true for the other Ag/NOM samples.

Generally, a high negative surface charge as indicated by the EPM data, demonstrates the stability of the NP suspension. The particles are prevented from aggregation through electrostatic mechanisms due to the thickness of the ligand. In this study only a weak relationship was found between particle size (DLS or TEM) and EPM suggests here particle size is independent to that of its EPM, and may be due to NOM, having a lack of a well defined slipping plane in terms of EPM measurements (Pelley and Tufenkji, 2008).

8.4 Conclusions

In this chapter, it has been demonstrated that Ag NPs can be formed and stabilised in the presence of NOM. Initial experiments, shown in section 8.3.1, demonstrated that silver nitrate and FA when mixed together did not spontaneously form NPs, even after several weeks. However, when reduced with $NaBH_4$, hexagonal NPs were produced. In comparison to the initial experiment, the Ag/FA samples in the main experiment did not show well defined hexagons (section 8.3.2). This suggests that some pre-reduction reactions may have occurred prior to adding in the reducing agent. In contrast, the work of dos Santos, Alvarez-

Puebla and co-workers (Alvarez-Puebla *et al.*, 2007; dos Santos Jr *et al.*, 2005) showed that the formation of gold or silver NPs happened spontaneously (and at 50 ^{o}C) in the presence of humic and fulvic acid without other reductants.

TEM images revealed some evidence of surface films on the surface of the Ag NPs from NOM, as has been seen in recent work (Baalousha, 2009; Baalousha *et al.*, 2008; Diegoli *et al.*, 2008; Pelley and Tufenkji, 2008). Ag NP formation with humics and fulvic acids also showed several structures observed of NP encapsulated by humics.

1) Rounded or spherical (nm) NPs were held together loosely encased in a web or net of NOM (e.g. Figures 8.13 and 8.14);

2) Dense aggregates of 100-200 nm were seen with silver-humic acid at 1 mg L^{-1} reduced with borohydride, probably as a complex of Ag NPs and humic acid (Figure 8.13 (a));

3) NPs were set within a gel-like matrix as was seen with HA (Figure 8.7 (c)) and a mesh containing NPs which formed from the polysaccharide fibrillar structures containing small NPs of about 10-20 nm (Figure 8.9).

The polysaccharide fibrillar structures containing particles were discussed by Buffle *et al.,* (1998), as a condition that may exist in the natural aquatic environment with other colloidal material.

Results showed that comparison of data from individual techniques did not always agree. In many cases this highlights differences in the way particles are measured, e.g. hydrodynamic diameter for DLS versus physical core measurement from TEM. It is likely that the amount and the matrix structure of the NOM influenced the actual measurement particularly in SPR. TEM images revealed NPs had formed even when there was no suspension colour and may be due to the NOM matrix absorbing the emitted light from the NPs. It is clear, therefore,

that from using one technique alone, a definitive assessment of NP size and structure cannot be made, and preference is towards a multi-method approach.

No definitive patterns or trends were observed in the 24 samples in suspension conditions by NOM type, by NOM concentration or by reducing agent. However, of the 24 suspensions analysed, one suspension in particular, the Ag/Ha 10 mg L^{-1} with $NaBH_4$, showed the least variability with TEM, DLS and over time, with a particle size of 10 nm (TEM) (or 20 nm by DLS). Nevertheless, this study did reveal that all of the NOM types chosen as suitable capping showed the possibility of making NPs. The study further showed that NOM is capable of forming mesh-like binding structures with NPs.

The next chapter, chapter 9, draws together the conclusions from this and previous chapters and discusses future possible research areas stemming from this thesis.

9

Discussion and further work

Chapter Summary

Nanoparticles are likely to become an intrinsic part of our society and while there are many potential benefits, risks from NPs towards environmental and human health cannot be ignored. For this reason NP synthesis, fate and interactions with natural aquatic materials are issues that are explored in this thesis. In this final chapter, the results from chapters 4 to 8 are integrated, along with previously published work. Conclusions are drawn about NP characterisation, eco-toxicology and NP transport in biological media. Continuing to contribute to this body of knowledge is essential both scientifically and to inform policy-makers and regulators, and as such future research priorities in this field are identified. .

9.1 Introduction

Engineered NPs (ENPs) produced from industry are reaching the natural environment from sources such as industrial waste effluents, domestic wastewaters, weathered painted surfaces and eventual product breakdown (Kaegi *et al.*, 2008; Nowack and Bucheli, 2007). Many of these substances have been found to cause adverse effects and toxicity to cells, human cells and fish (Handy *et al.*, 2008b; Sayes *et al.*, 2006). NP themselves may also be subject to modification from the conditions encountered in the environment, such as the presence of HS. Consequently, the release of ENPs is of great concern not only because of their bioavailability, but also their potential for modification post-discharge. The third aspect is the relationship between these two possibilities (Alvarez *et al.*, 2009). The work in this thesis has investigated the interactions of natural NPs, such as NOM, with engineered NPs of silver, iron oxide and titanium dioxide. The ENPs were chosen because of their high usage in industry, their consequential release and their potential toxicity subject to different environmental conditions of pH and ionic strength. In this work, silver and iron oxide NPs were synthesised in-house as monodispersed particles, while the titanium dioxide nanopowder was purchased from commercial suppliers.

9.2. Outcomes of the research

Results showed that interactions occurred between ENPs and NOM. This was seen with the TiO_2 nanoparticles and fish mucus, which led to NP and mucus aggregation (chapter 4). Iron oxide aggregation was found to be pH dependent and also dependent on the concentration of SRFA, PHA and PS (chapter 5). Iron oxide NP stabilisation occurred at low NOM concentrations and increased aggregation at higher NOM concentrations, which was entirely explainable by charge interactions. With the citrate stabilised silver nanoparticles, NOM provided enhanced stability for all conditions, except at the highest

Ca^{2+} concentrations. Furthermore, NOM was able to stabilise silver nanoparticles in the absence of other capping agents during synthesis (chapter 8). These results all indicate that NOM should play a crucial role in the fate and behaviour of NPs in natural systems.

Characterisation of the commercially available TiO_2 NP powder, nominally 25-75 nm (Sigma Aldrich), revealed a crystal structure containing a mixture of rutile and anatase, ranging from 75 to 110 nm (chapter 4). This powder had a tendency to form small agglomerates which were shown by DLS to be around 220 nm. Sizes were derived from several techniques and revealed that these particles had formed larger agglomerates than advertised. When these TiO_2 NPs were exposed to trout fish over a nine day period the particles aggregated and sedimented very quickly after interaction with mucus shed by the fish, presumably as a defence mechanism. Fluorescence analysis revealed that the mucus contained a tryptophan-like residue of about 1% and could be related to the quantity of mucus produced. The immediate response of the fish to the nanoparticles was the release of skin mucus, which subsequently associated with TiO_2 NPs and settled to the bottom. Suggesting that in the environment, rapid loss of NPs from the water column may occur because of NP interactions with biological material, followed by sedimentation. Nevertheless, the permanence of TiO_2 NP removal from suspension needs to be explored as remobilisation may be significant.

In bare iron oxide (5-7 nm) nanoparticle suspensions, the presence of NOM and its concentration (chapter 5) proved to be important as it altered the pH value where aggregation occurred. Without humics present, the electrostatically stabilised iron oxide NPs aggregated close to the point of zero charge (ca pH 7) and were several microns in size. These results were similar to that of Baalousha *et al.,* (2008). This implies that these nanoparticles would not generally stay in suspension under normal environmental pH

conditions (pH 6-8). In this study, the FA and PHA at 5 mg L^{-1} stabilised the iron oxide NPs up to pH 5. This indicates that the presence of low NOM concentrations in the aquatic environment, may improve the stability of metal oxide NPs. Beyond pH 8 (pH 8-12), the particle aggregate size decreased due to an increasingly negative surface charge, and greater stability.

The conclusions drawn in the above paragraph are in agreement with Cromieres *et al.,* (2002), who found the maximum aggregation of iron oxide occurred at pH 7. Furthermore, the conclusions demonstrate that under these conditions a fraction of iron oxide NPs could remain in suspension at the lower or higher pH environmental conditions (e.g. pH $\leq$5.5 or $\geq$ 8), thus allowing for NP transportation. It is further possible that not all NPs would sediment under mid-range pH conditions and that some may be small enough to remain in suspension (Baalousha, 2009). Furthermore, Baalousha (2009) found that aggregated iron oxide NPs were able to disaggregate, and thus potentially become re-mobilised, after the addition of 100 mg L^{-1} HA. NOM, which has an affinity for Fe, has also been found to transport Fe ions and natural Fe NPs in meromictic lakes (Lyven *et al.*, 2003; Taillefert *et al.*, 2000). However, at very high NOM concentrations the iron oxides would cause removal of the NOM fraction via aggregation, again being pH dependent.

Silver NPs are widely produced and are of economic importance due to silver's bactericidal properties. This makes Ag NPs a suitable NP for environment fate and behaviour studies. For such work, the ideal NP suspension consists of a mono-modal, monodisperse population. Several methods exist for the synthesis of silver NPs using citrate but true monodispersity is difficult to achieve. In this project, further investigation of NP production was undertaken (chapter 6). Using tri-sodium citrate to stabilise silver NPs, experimental results highlighted that there are several factors responsible for determining particle size

during the synthesis process. These factors are the reaction rate, temperature levels and the concentration of the citrate. After examining these reaction variables, it was found that monodispesrse stable nanoparticles could be produced by boiling soon after nucleation.

Chapter 8 investigated the synthesis of Ag NPs with NOM and showed that synthesis could occur in the presence of HS and in most cases could provide stabilising conditions without visible signs of sedimentation. However, from this and other experiments with citrate in chapter 6, the type of reducing agent was found to have an influence on nanoparticle formation and stability. The first reducing agent, sodium borohydride, formed a more stable NP through a rapid nucleation. In contrast, ascorbic acid was slower and harder to control, and demonstrated that a stronger capping agent was required to resist the nitric acid by-product. Where nitric acid is produced in excess, then weakly capped NPs could result in dissolution. In smaller quantities, AA may protonate capping agents, for example HS, thus reducing the charge and promoting aggregation.

Citrate coated 15 nm Ag NPs were found to behave differently to the iron oxides (chapter 7). The citrate ligand provided a negative charge on uncharged Ag clusters and was stable due to its negative zeta potential at all pH values greater than 2. With the addition of an HS, further stabilisation was achieved even in the present of Ca^{2+} ions. The latter in solution are normally responsible for destabilisation due to their bivalency and bridging effects. HS were able to shield the Ag NPs from these charges through steric stabilisation. Furthermore, depending on the molecular weight and hydrophobic behaviour of the HS, particle size was reduced (pH 5 and a higher ion solution concentration). This can be attributed to compression of the hydrodynamic layer and the NOM/citrate covering, lying closer to the particles' surface.

The differences in behaviour, as a function of pH and concentration, between the silver and iron oxide NPs, can be attributed to differences in surface charge. The citrate coated silver was negatively charged above pH 2, whereas the uncoated iron oxides were positively charged at low pH and negatively charged at high pH, with a pzc at about pH 7. Citrate stabilised silver NPs (8 mg L^{-1}) were further stabilised by 10 mg L^{-1} of HS whereas the more concentrated iron oxide only required small amounts of HS as a stabiliser (~200 mg L^{-1} iron to 5 mg L^{-1} HS) and the higher concentration of iron promoted aggregation sooner, closer to the pzc.

Silver NPs, absent of other capping agents, were found to be stabilised by bound HS that had attached at NP formation. This binding is probably via functional groups (e.g. thiols) and hydrophobic attachment to the NP surface (Pelley and Tufenkji, 2008). With the bare FeO NPs, the HS sorbed to the surfaces and the nanoscale layer that formed increased in thickness with increasing HS concentration. Nevertheless, no definitive data is provided to suggest whether citrate is replaced or overlain by HS, although Diegoli et al (2008) have suggested the former. The potential loss of stabilisers from the surface of ENPs in the environment and their subsequent replacement by pollutant chemicals, NOM or both, has also been questioned in the literature (Handy *et al.*, 2008c).

9.2.1 Nanoparticle characterisation

It is apparent that from the work undertaken in this thesis that when analysing NPs different techniques report different aspects about the nanoparticles' characteristics, thus they do not always agree, particularly on NP size. The reporting of only one or two techniques is insufficient when describing the nanoparticles alone and when subjected to different conditions. This leads to the conclusion that several types of data (e.g. surface area , size, charge, crystal structure) from various techniques (e.g. BET, TEM, EPM, XRD) are required

to provide full NP characterisation, indicating the need for a multi-method approach (Lead and Wilkinson, 2006; Tiede *et al.*, 2009). For example, TEM and F/FFF mostly agree on particle size. F/FFF data though, report the equivalent spherical hydrodynamic diameter calculated from directly measured diffusion coefficients. TEM on the other hand provides a two dimensional image of electron dense inorganic core material and particle size is often smaller for this reason.

DLS records a hydrodynamic measurement tracking movement in relation to particle size. However, comparisons to F/FFF were poor unless the sample was monodisperse, in which case the correlation was good, but DLS reported a larger size. Both F/FFF and DLS techniques can provide information on the dispersity of the sample. Whereby DLS is particularly sensitive to the presence of large aggregates, thus tends to provide a larger size value than F/FFF. TEM has many tools, such as PEELS and EDX, and direct particle measurement though observation can be achieved, but can be time consuming and expensive.

Surface plasmon resonance (SPR) is defined by Link and El-Sayed (2003) as "the electric field of an incoming light wave which induces a polarization of the electrons with respect to the much heavier ionic core of a spherical nanoparticle". SPR is easily and rapidly measured by UV absorbance and peak widths and can indicate particle size and distribution from band widths and the λ peak maxima absorbance. This phenomenon complies with Mie's theory for spherical particles. This method, however, has a narrow working size range of 2-20 nm, although the upper limit could be as large as 50-80 nm (Link and El-Sayed, 2003; Van Hyning and Zukoski, 1998). These techniques all provide a snapshot of nanoparticle characteristics. By using many complimentary techniques in a multi-method approach, greater information is provided and bias is reduced.

9.3 Wider implications

The work in this thesis has demonstrated that interaction occurs between ENPs and natural nanoparticles. This has been achieved by taking commercially available humic substances, polysaccharides and other biological (fish) material and mixing with ENPs of silver, iron oxide and titanium dioxide. To put these types of studies into the wider context, it will be probable that NPs will be mobile within the aquatic environment due to stabilisation from NOM. Evidence of NP mobility in the literature supports this, for example, TiO_2 NPs can start their journey into the drainage system from washing off a painted façade (Kaegi *et al.*, 2008). Urban drainage often leads into the municipal sewage treatment and the studies of Kiser *et al.* (2009) and Jarvie *et al.,* (2009) showed that NPs could pass through sewage treatment works possibly aided by OM or end up in sludge (Brar *et al.*, 2010). Silver NPs may also have a similar fate once released from textiles during washing and therefore enter the environment via waste waters (Benn and Westerhoff, 2008; Geranio *et al.*, 2009). Detecting ENPs in these systems or more widely in the environment is a challenge, and success will depend on the environmental background levels analogous to the NPs core material. This will be more challenging for iron and iron oxides given their widespread abundance. In a relative sense, silver should therefore be easier, though background levels of Ag ions have been recorded (Bell and Kramer, 1999; Ratte, 1999). Robust and reliable techniques of rapidly detecting manufactured nanoparticles in the natural environment have not been developed (Tiede *et al.*, 2009), but are urgently needed to properly inform knowledge of fate and behaviour.

9.3 Recommendations and further work

The investigative work into the TiO_2, FeO and Ag NP interactions with natural NOM covered in this thesis has shown effects on NP stability. The results shown here are suggestive, not definitive, and further research questions present themselves.

How would the behaviour of NPs differ to raw and untreated natural waters and HS? For example, the IHSS NOM used in this study is significantly altered from its original form. Unaltered or raw NOM may contain significant amounts of other material (non-organic particles, microorganisms, complex mixtures of major ions). Further work on these interactions is required under a wide range of relevant conditions, in particular to inform generic NP fate models. Working with raw waters and HS would almost certainly require experimenting with NPs not normally present in background concentrations.

What would the role of trace metals (Cd, Cu, Zn etc) have on NP behaviour and how might NPs affect the transportation of trace metals? In order to understand some of this it would be necessary to work with trace metals, as well as trace metals with IHSS NOM, before committing to environmental samples of a greater deal of complexity.

What is the role of sediments in providing stability towards aggregated and non aggregated nanoparticles and how might they become available to other benthic and non benthic feeding organisms? Additional experiments within the water column would also be necessary, as would exploring the benthic nature of NPs in sediments, to understand fate of resultant aggregated NPs and their longevity in that situation. While field studies may pose unethical release of ENPs, the use of artificially removed mesocosms for study in NP pathway experiments may provide answers, but caution must be adhered to as soil disturbances promote mineralization

(Kristensen *et al.*, 2000) and would require periods of settlement. These would parameterise fate/exposure models which inform bioavailability/toxicity models.

Finally, what would the effect of NP stability from HS with photocatalytic NPs such as TiO_2 and ZnO? Further investigation into the photocatalytic effects from NPs, such as TiO_2, on humic acid would be useful as this may be responsible for bringing the NPs back into suspension. The effects of metals, particles and sediments in estuarial brackish waters on sedimented NPs may introduce further chemistry that may result in the subsequent remobilisation of NPs

Appendix 1

Particle size distributions of silver nanoparticles at environmentally relevant conditions

Susan A. Cumberland and Jamie R. Lead

Journal of Chromatography A

Volume 1216, Issue 52, 25 December 2009, Pages 9099-9105

Abstract

Silver nanoparticles (Ag NPs) are becoming increasingly popular as antimicrobial agents in consumer goods with consequent risk to environmental health from discharges. Environmentally relevant fate and transport investigations are limited but essential to gain understanding towards bioavailability and toxicology. In this study, monodisperse 15 nm citrate-stabilised Ag NPs were synthesised, characterised and then fractionated by flow field-flow fractionation (FlFFF) at environmentally relevant conditions (pH 5 or 8, presence of natural organic macromolecules (NOM) and presence of sodium or calcium). At low ionic strength, Ag NPs particle size increased as pH increased from 5 to 8. However, changing the ionic strength from 10^{-3} to 10^{-2} M Na increased instability of the Ag NPs, and loss of peak at pH 5 but in the presence of humic substance (HS), a reduction in NP size was seen, most likely due to a reduction in the diffuse layer. The presence of Ca^{2+} ions, at the higher ionic strengths caused complete loss of the solution Ag NPs with or without HS, most likely due to aggregation. At the lower Ca^{2+} ionic strength the Ag NPs were still unstable, but again, in the presence of HS the NPs were largely dispersed. The presence of HS improved stability of Ag NPs under these conditions by forming a surface coating resulting in both steric and charge stabilisation. This work implies that Ag NPs could have long residence times in aquatic systems in the presence of HS potentially resulting in increased bioavailability.

Keywords: Flow field-flow fractionation; FFF; Silver nanoparticles; Humic substances; Natural organic matter (NOM)

Available online 17 July 2009

doi:10.1016/j.chroma.2009.07.021

Appendix 2

Bioavailability of Nanoscale Metal Oxides TiO_2, CeO_2, and ZnO to Fish

Blair D. Johnston, Tessa M. Scown, Julian Moger, Susan A. Cumberland, Mohamed Baalousha, Kathryn Linge, Ronny van Aerle, Kym Jarvis, Jamie R. Lead and Charles R. Tyler

Environ. Sci. Technol., 2010, 44 (3), pp 1144–1151

Abstract

Nanoparticles (NPs) are reported to be a potential environmental health hazard. For organisms living in the aquatic environment, there is uncertainty on exposure because of a lack of understanding and data regarding the fate, behavior, and bioavailability of the nanomaterials in the water column. This paper reports on a series of integrative biological and physicochemical studies on the uptake of unmodified commercial nanoscale metal oxides, zinc oxide (ZnO), cerium dioxide (CeO_2), and titanium dioxide (TiO_2), from the water and diet to determine their potential ecotoxicological impacts on fish as a function of concentration. Particle characterizations were performed and tissue concentrations were measured by a wide range of analytical methods. Definitive uptake from the water column and localization of TiO_2 NPs in gills was demonstrated for the first time by use of coherent anti-Stokes Raman scattering (CARS) microscopy. Significant uptake of nanomaterials was found only for cerium in the liver of zebrafish exposed via the water and ionic titanium in the gut of trout exposed via the diet. For the aqueous exposures undertaken, formation of large NP aggregates (up to 3 μm) occurred and it is likely that this resulted in limited bioavailability of the unmodified metal oxide NPs in fish.

DOI: 10.1021/es901971a

Publication Date (Web): January 5, 2010

* Corresponding author e-mail: c.r.tyler@exeter.ac.uk.,

http://pubs.acs.org/doi/abs/10.1021/es901971a

Appendix 3

Aggregation and surface properties of iron oxide nanoparticles: Influence of ph and natural organic matter

Mohammed Baalousha; Adriana Manciulea[1] Susan Cumberland[1] Kevin Kendall[2] Jamie R. Lead[1]

Environmental Toxicology and Chemistry

Volume 27, Issue 9, September 2008, pages 1875–1882

Abstract

The interactions between unpurified manufactured nanoparticles (NPs; iron oxide NPs, ~7 nm) and standard Suwannee River humic acid (SRHA) were investigated under a range of environmentally relevant conditions. At low pH, approximately 35% of the total iron was in the dissolved phase (<1 kDa), present from the initial synthesis, whereas at pH more than 4, this concentration was negligible because of the formation of new particles via hydrolysis. Dynamic light scattering results indicated that extensive aggregation of NPs began at approximately pH 5 to 6 and reached a maximum at approximately pH 8.5, whereas with added SRHA, aggregation was shifted to lower pH values of 4 to 5 and was affected by SRHA concentration. Aggregation could be explained mainly by charge neutralization. Further, more detailed investigations by flow field-flow fractionation and transmission-electron microscopy were performed under a more restricted set of conditions (pH 2–6) to examine the aggregation process. Results indicated the formation of SRHA surface coating on iron oxide NPs of approximately 1 nm and the increase in thickness of this coating with the increase of SRHA concentration. Iron oxide NPs were shown to form increasingly large aggregates with increases in both pH (from 2 to 6) and SRHA concentration (from 0 to 25 mg/L). The structure and aggregation mechanism of these aggregates were found to be both pH and SRHA concentration dependent, with open, porous aggregates in the absence of SRHA and compact aggregates in the presence of SRHA.

Keywords: Iron oxide; Nanoparticles; Solubility; Surface coating; Aggregation

Article first published online: 9 DEC 2009

DOI:10.1897/07-559.1

Appendix 4

High Doses of Intravenously Administered Titanium Dioxide Nanoparticles Accumulate in the Kidneys of Rainbow Trout but with no Observable Impairment of Renal Function

Tessa M. Scown, Ronny van Aerle, Blair D. Johnston, Susan Cumberland, Jamie R. Lead, Richard Owen, and Charles R. Tyler

TOXICOLOGICAL SCIENCES 109(2), 372–380 (2009)

Abstract

Our recent work suggests limited uptake of unstabilized metal oxide nanoparticles via water into fish, however, some other studies have indicated such exposures can induce oxidative stress. To investigate tissue distribution and toxicity of titanium dioxide (TiO_2) nanoparticles that may enter into fish, we conducted a series of injection studies. Rainbow trout (*Oncorhynchus mykiss*) were intravenously injected with 100 μg TiO_2 nanoparticles and the content of titanium in blood, brain, gills, liver, and kidney quantified at time points between 6 h and 90 days using inductively coupled plasma optical emission spectroscopy. Injected Ti was concentrated in the kidneys and remained there up to 21 days, however, there was evidence of clearance of TiO_2 at 90 days. Ti accumulation in the liver was 15 times lower than in the kidney with no apparent clearance. Using TEM we showed nanoparticles were localized in tissue vesicles surrounding the kidney tubules. In a second injection study, rainbow trout were injected with 100 μg TiO_2 and plasma samples from individual fish analyzed for total protein and creatinine content at time points between 6 h and 21 days to assess for possible effects on kidney function. No effect of TiO_2 on total plasma protein content or creatinine concentrations were found indicating that neither urine production nor glomerular filtration rate were affected. We conclude that in trout upon a single high dose exposure of TiO_2 nanoparticles via the bloodstream, TiO_2 accumulates in the kidneys but has minimal effect on kidney function.

Key words: titanium dioxide; rainbow trout; lipid peroxidation; intravenous injection; nanoparticles; nanotoxicology

DOI: 10.1093/toxsci/kfp064
Advance Access publication March 30, 2009

http://toxsci.oxfordjournals.org/content/109/2/372.short

Received December 10, 2008.

Accepted March 25, 2009.

Appendix 5

The difference in fluorescence with and without the optical filter applied

		With filters	Without ex 230	%
		peak 1	**peak 1**	
5	0.1	92.78	92.8	100
5	1	78.33	79.1	99
5	10	95.82	70.0	137
20	0.1	303.42	304.9	100
20	1	265.40	230.4	115
20	10	276.05	277.6	99
80	0.1	760.46	760.5	100
80	1	760.46	760.5	100
80	10	755.13	753.6	100
		peak 2	**ex280**	**peak 2**
5	0.1	21.29	21.3	100
5	1	19.77	38.0	52
5	10	15.97	16.0	100
20	0.1	73.00	93.5	78
20	1	66.92	91.3	73
20	10	60.08	83.7	72
80	0.1	239.54	263.9	91
80	1	257.03	272.2	94
80	10	234.22	245.6	95
		peak 3		**peak 3**
5	0.1	86.69	71.48	121
5	1	63.12	79.1	80
5	10	81.37	88.2	92
20	0.1	248.7	247.9	100
20	1	247.1	244.1	101
20	10	238.8	238.8	100
80	0.1	758.2	758.9	100
80	1	760.5	760.5	100
80	10	758.2	758.9	100
		peak 4		**peak 4**
5	0.1	19.77	18.3	108
5	1	36.50	19.0	192
5	10	27.38	20.5	133
20	0.1	78.33	78.3	100
20	1	84.41	84.4	100
20	10	75.29	75.6	100
80	0.1	296.58	292.0	102
80	1	309.51	308.7	100
80	10	312.55	313.3	100

Appendix 6

Iron Nanoparticles Synthesis

Protocol for synthesising iron oxide nanoparticles by Forced Hydrolysis

Equipment

$FeCl_3$.6H20 MW= 270

10-3 M HCl

Heating plate

1 litre conical flask*

Plastic vial

Thermometer

HDPE plastic storage container

500 ml volumetric flask

Preparation of solution

To prepare the HCl solution; make up 1 Molar solution of HCl take 1.875 ml of 1 Molar HCl into 500 ml ultra pure (MilliQ) water to give 3.75 x 10^{-3} M HCl (0.00375 M)

Method

Weigh 2.43g of $FeCl_3$.6H20 into plastic vial or beaker Add 12.5 ml of the 3.75 x 10^{-3} M HCl to the iron chloride and shake until dissolved Preheat the remaining 487.5 ml 3.75 x 10^{-3} M HCl to 100 ^{o}C – so that it is visibly boiling. Quickly add the dissolved iron chloride, whilst rapidly stirring# (manually) Continue stirring for 30 mins at 100 ^{o}C to gain particles of about 5 nm with a concentration of about 1000 ppm Fe.

*using a conical flask instead of a beaker helps the suspension reflux rather than evaporate during boiling.

the use of magnetic stirrers may result in a different nanoparticle i.e. magnetite instead of haematite

The second (and subsequent batches) were synthesised by myself. The only difference was vessel type, firstly and secondly in a large beaker and there after in conical flasks batches viewed by TEM were identical in size (Figure 5.2 (a)). Iron NPs were synthesised by forced hydrolysis (Kendall and Kosseva, 2005) from an iron chloride salt in dilute hydrochloric acid (3 mM) Briefly, 2.43g $FeCl_3$.6H20 was pre-dissolved in 12.5 ml of 3.75 mM HCl and quickly added to 487.5 ml boiling HCl solution and stirred for 30 mins at 100^{o}C.

Appendix 7

Dynamic light scattering, electrophoretic and zeta potential (calculated from instrument) for iron oxides and Fulvic acid see also Figure 5.

pH	FA mg L-1	measured pH	DLS z-average	Stdev	Electrophoretic Mobility	stdev	Zeta Potential	stdev
2	0	1.987	16.07	0.10	3.44	1.35	45.79	18.03
	5	1.995	19.21	0.21	3.94	0.36	52.15	6.07
	10	1.997	37.08	0.09	3.94	0.21	50.51	2.68
	15	1.994	26.93	0.38	4.01	0.34	52.49	5.39
	20	1.988	61.05	0.24	3.87	0.15	49.25	1.88
	25	1.977	82.24	1.41	3.88	0.10	49.02	1.15
3	0	3.221	29.41	0.19	3.30	0.22	44.98	6.33
	5	3.073	26.52	0.30	3.22	0.22	41.58	2.81
	10	3.097	33.40	0.25	3.73	0.17	47.97	2.10
	15	3.082	43.72	0.29	3.63	0.15	46.41	1.94
	20	3.077	56.02	0.14	3.28	0.14	41.86	1.85
	25	3.076	62.99	0.12	3.18	0.07	40.57	0.81
4								
	0	3.894	50.81	0.27	3.23	0.45	44.15	6.14
	5	4.00	40.77	0.31	2.53	0.56	33.19	7.33
	10	3.995	71.12	0.71	3.09	0.09	40.34	1.24
	15	4.046	89.66	0.37	3.18	0.09	41.09	1.11
	20	3.903	77.91	0.41	3.24	0.16	41.42	2.05
	25	4.050	95.02	1.01	3.11	0.06	39.49	0.73
5	0	5.435	146.8	0.8	2.16	0.19	27.86	2.45
	5	5.283	154.6	1.3	2.86	0.03	36.56	0.33
	10	4.991	122.8	0.9	3.02	0.05	38.39	0.62
	15	4.911	156.5	2.7	2.90	0.04	36.80	0.41
	20	4.971	121.7	0.9	3.01	0.04	38.09	0.52
	25	5.091	2575.0	110.0	2.70	0.02	34.06	0.28

Continued

pH	FA mg L-1	measured pH	DLS z-average	Stdev	Electrophoetic Mobility	stdev	Zeta Potential	stdev
6	0	5.973	4388.3	2695.7	2.80	0.05	37.71	5.92
	5	5.958	3686.7	1032.8	2.69	0.01	34.43	0.15
	10	6.011	7467.3	2078.8	2.59	0.07	33.01	0.88
	15	6.226	12482.7	4957.4	1.97	0.25	25.90	3.27
	20	6.269	18913.3	8441.7	1.26	0.10	15.87	1.23
	25	6.397	14870.0	1410.7	2.01	0.11	25.42	1.43
7	0	7.173	8385.3	4341.2	-0.09	0.06	-1.10	0.70
	5	6.996	10428.7	9686.8	-0.14	0.09	-1.73	1.18
	10	7.167	17993.3	5776.2	-0.17	0.08	-2.07	0.98
	15	6.982	2816.0	2700.8	-0.58	0.25	-7.13	3.06
	20	7.328			-1.13	0.20	-13.88	2.38
	25	7.295	1377.3	375.0	-0.69	0.21	-8.41	2.54
8	0	8.058	*	*	-0.58	0.27	-7.35	3.32
	5	7.923	*	*	-0.13	0.16	-1.57	2.01
	10	7.994	3040.3	1453.3	-0.02	0.13	-0.30	1.64
	15	7.976	*	*	-0.41	0.15	-5.22	1.93
	20	8.134	*	*	-0.80	0.13	-10.08	1.67
	25	7.826	*	*	-0.86	0.21	-10.88	2.67
9	0	9.019	6357.6	3562.0	-1.75	0.19	-23.27	2.44
	5	3.039	1556.3	653.8	-1.03	0.24	-13.44	3.11
	10	8.983	2001.0	1364.0	-1.52	0.14	-19.32	1.82
	15	8.985	4768.7	2955.0	-1.50	0.21	-18.92	2.64
	20	8.933	10102.0	1417.4	-1.62	0.11	-20.17	1.39
	25	9.900	856.4	324.6	-1.07	0.28	-13.22	3.52
10	0	10.07	330.4	70.9	-2.49	0.47	-30.55	5.69
	5	10.021	1058.7	208.6	-1.45	0.91	-17.59	11.07
	10	10.319	711.0	65.3	-2.39	0.54	-28.93	6.50
	15	9.939	988.4	158.8	-1.09	0.58	-13.14	6.96
	20	9.921	*	*	-2.24	0.79	-27.10	9.56
	25	10.245	326.9	63.1	-2.94	0.19	-35.48	2.30

Appendix 8

Diffusion coefficients *D,* m^2 s^{-1}, obtained from the F*I*FFF fractograms for (a) iron oxide with fulvic acid (FA) 0-25 mg L-

Conc. FA mg L^{-1}	pH 2 *D* (m^2 s^{-1})	pH 3 *D* (m^2 s^{-1})	pH 4 *D* (m^2 s^{-1})	pH 5 *D* (m^2 s^{-1})
0	4.50E-11	3.65E-11	1.79E-11	1.90E-11
5	4.27E-11	3.29E-11	1.86E-11	2.13E-11
10	4.41E-11	3.16E-11	2.16E-11	1.72E-11
15	4.33E-11	3.23E-11	2.07E-11	2.50E-11
20	4.32E-11	2.97E-11	1.78E-11	1.23E-11
25	3.83E-11	2.85E-11	1.75E-11	8.67E-12

Diffusion coefficients *D,* m^2 s^{-1}, obtained from the F*I*FFF fractograms for iron oxide with peat humic acid (PHA) 0-25 mg L^{-1}

Conc. PHA mg L^{-1}	pH 2 *D* (m^2 s^{-1})	pH 3 *D* (m^2 s^{-1})	pH 4 *D* (m^2 s^{-1})	pH 5 *D* (m^2 s^{-1})
0	4.59E-11	3.67E-11	2.44E-11	1.69E-11
5	4.38E-11	3.48E-11	2.44E-11	8.52E-12
10	4.14E-11	3.26E-11	2.31E-11	8.52E-12
15	4.21E-11	3.31E-11	1.89E-11	9.41E-12
20	3.89E-11	3.26E-11	1.89E-11	1.45E-11
25	3.71E-11	3.02E-11	2.31E-11	1.05E-11

Diffusion coefficients *D,* m^2 s^{-1}, obtained from the F*I*FFF fractograms for iron oxide with Succinglycan (exo-PS) 0-25 mg L^{-1}

concentration Succinglycan mg L^{-1}	pH 2 *D* (m^2 s^{-1})	pH 3 *D* (m^2 s^{-1})	pH 4 *D* (m^2 s^{-1})
0	4.53E-11	3.95E-11	1.83E-11
5	5.13E-11	4.19E-11	1.63E-11
10	4.91E-11	4.27E-11	1.76E-11
15	4.22E-11	4.19E-11	1.6E-11
20	4.71E-11	4.27E-11	1.87E-11
25	4.53E-11	4.19E-11	2.09E-11

Appendix 9

Dynamic light scattering, electrophoretic mobility and zeta potential (calculated from instrument) for iron oxides and peat humic acid

pH	PHA mg L^{-1}	measured pH	DLS z-average	stdev	Electrophoetic Mobility	stdev	Zeta Potential	stdev
2	0	1.987	16.07	*0.10*	4.08	*0.28*	54.65	*3.81*
	5	1.987	37.26	*0.65*	3.6	*0.3*	47.5	*2.9*
	10	1.987	74.63	*1.02*	3.9	*0.3*	48.9	*2.9*
	15	1.987	102.20	*1.06*	3.8	*0.2*	48.9	*2.9*
	20	1.987	125.77	*1.19*	3.8	*0.3*	49.1	*3.4*
	25	1.987	149.57	*1.75*	3.9	*0.3*	49.4	*3.5*
3	0	3.221	29.41	*0.19*	3.30	*0.22*	44.98	*6.33*
	5	3.074	40.56	*0.13*	2.9	*0.1*	38.8	*1.9*
	10	2.974	59.00	*0.86*	3.0	*0.1*	39.4	*1.9*
	15	3.027	79.85	*1.50*	3.0	*0.1*	39.8	*1.8*
	20	3.156	100.63	*2.26*	3.0	*0.1*	39.1	*1.1*
	25	2.948	119.03	*2.80*	3.0	*0.1*	40.0	*1.5*
4	0	3.894	50.81	*0.27*	3.23	*0.45*	44.15	*6.14*
	5	4.115	37.85	*0.16*	2.8	*0.1*	36.5	*1.4*
	10	1.225	66.46	*0.84*	2.9	*0.1*	36.5	*1.5*
	15	4.006	86.06	*0.20*	2.9	*0.2*	36.7	*2.6*
	20	3.852	95.63	*1.07*	3.0	*0.1*	37.1	*1.2*
	25	4.113	148.20	*2.31*	2.7	*0.0*	36.1	*0.3*
	0	5.435	146.80	*0.82*	2.16	*0.19*	27.86	*2.45*
5	5	5.042	367.93	*6.27*	2.8	*0.0*	36.5	*0.5*
	10	5.255	1966.67	*1294.18*	2.6	*0.0*	33.6	*0.1*
	15	5.223	2010.67	*1503.32*	2.6	*0.0*	33.0	*0.4*
	20	5.112	671.13	*112.13*	2.8	*0.0*	35.2	*0.5*
	25	5.026	314.00	*22.17*	2.8	*0.0*	35.0	*0.6*
	0	5.973	4388.33	*2695.67*	2.80	*0.05*	37.71	*5.92*
6	5	5.910	1507.00	*90.15*	1.60	*0.07*	21.34	*1.16*
	10	6.125	2898.00	*371.25*	2.55	*0.01*	33.70	*0.17*
	15	6.600	2919.33	*616.14*	1.50	*0.11*	19.38	*1.38*
	20	6.000	2857.67	*1749.60*	1.17	*0.18*	15.10	*2.30*
	25	6.026	4188.67	*1397.54*	2.68	*0.67*	34.46	*8.65*

Continued…

pH	PHA mg L^{-1}	measured pH	DLS z-average	*stdev*	Electro-phoetic Mobility	*stdev*	Zeta Potential	*stdev*
7	0	7.173	8385.33	*4341.16*	-0.09	*0.06*	-1.10	*0.70*
	5	7.145	546.90	*0.00*	-2.79	*0.20*	-34.38	*2.35*
	10	7.042	1390.00	*166.56*	0.05	*0.16*	0.62	*2.12*
	15	7.332	1386.33	*452.17*	1.11	*0.04*	13.68	*0.42*
	20	7.295	*	*	-0.13	*0.18*	-1.74	*2.33*
	25	7.061	4102.00	*704.21*	0.57	*0.11*	7.40	*1.40*
8	0	8.058	*	*	-0.58	*0.27*	-7.35	*3.32*
	5	8.243	20018.33	*25826.54*	0.18	*0.28*	2.36	*3.67*
	10	8.133	4725.33	*2196.85*	-1.46	*0.34*	-17.90	*4.15*
	15	7.945	12362.00	*6170.19*	-0.14	*0.06*	-1.72	*0.77*
	20							
	25	8.007	*	*	-1.61	*0.05*	-20.97	*0.63*
9	0	9.019	6357.60	*3562.01*	-1.75	*0.19*	-23.27	*2.44*
	5	9.164	3110.67	*509.37*	-2.30	*0.07*	-28.16	*0.87*
	10	9.249	11975.33	*14493.66*	-0.87	*0.18*	-11.30	*2.29*
	15	9.233	4721.33	*2313.33*	-1.69	*0.06*	-20.69	*0.78*
	20	9.003	3745.67	*2344.63*	-1.50	*0.09*	-19.36	*1.10*
	25	9.201	830.87	*130.85*	-1.22	*0.20*	-15.17	*2.51*
10	0	10.070	330.43	*70.86*	-2.49	*0.47*	-30.55	*5.69*
	5	10.021	933.13	*82.29*	-3.15	*0.03*	-38.42	*0.36*
	10	10.148	1144.33	*117.62*	-2.80	*0.12*	-36.04	*1.50*
	15	10.082	1132.27	*174.46*	-2.84	*0.03*	-36.45	*0.35*
	20	10.000	1400.67	*70.57*	-2.84	*0.03*	-36.45	*0.35*
	25	10.416	476.07	*3.40*	-3.51	*0.06*	-42.88	*0.70*
	25	9.985	665.13	*12.56*				
11	0	11.290	*	*	-3.07	*0.17*	-40.32	*2.18*
	5	11.023	574.73	*147.28*	-3.59	*0.09*	-43.83	*1.08*
	10	11.012	730.17	*79.08*	-3.14	*0.02*	-42.06	*0.29*
	15	10.917	181.93	*7.27*	-3.15	*0.03*	-40.34	*0.39*
	20	10.935	1006.30	*100.20*	-3.67	*0.09*	-44.85	*1.09*
	25	11.063	658.40	*45.45*	-3.15	*0.03*	-41.95	*0.47*
12	0	12.041	*	*	-3.07	*0.17*	-40.32	*2.18*
	5	12.031	*	*	-3.59	*0.09*	-43.83	*1.08*
	10	11.958	447.47	*2.10*	-3.14	*0.02*	-42.06	*0.29*
	15	11.976	277.30	*7.98*	-3.15	*0.03*	-40.34	*0.39*
	20	11.967	540.80	*31.40*	-3.67	*0.09*	-44.85	*1.09*
	25	11.921	136.30	*0.36*	-3.15	*0.03*	-41.95	*0.47*

Appendix 10

Volumes of 1M ascorbic acid used to add to Ag NPs to study the effect of size

Using 1M solution

vol of Ag NPs (mL)	volume of 1 M ascorbic acid (mL)	volume of water (mL)	Final AA concentration (M)
4	0	1	0
4	0.1	0.9	0.02
4	0.25	0.75	0.05
4	0.5	0.5	0.1
4	0.75	0.25	0.15
4	1	0	0.2

* 1M ascorbic acid = 176.13 g L^{-1}

Appendix 11

Comparison of size (DLS z-average) of Ag–citrate NP suspensions post reduction at three minutes, 15 minutes and after boiling DLS z-average results pre and post boil brackets donate standard deviation of at least three measurements

Batch no	Ag:TSC M ratio	Post reduction 3 minutes	Post reduction 15 minutes	Post boil
#B5	1:1	11.73 (± 0.55)	11.82 (± 0.1)	27.51(± 0.25)
#B6	1:1.25	13.64 (± 0.58)	14.77 (± 0.55)	23.15 (± 0.33)
#B7	1:1.5	19.64 (± 4.63)	14.04 (± 0.22)	17.02 (± 0.04)
#B8	1:1.75	26.24 (± 16.88)	24.77 (± 19.53)	25.02 (± 7.07)

Size for batches #B13 and #B14, citrate to silver ratio in brackets, taken at intervals of 3 minutes, 15 minute after boiling and at 24 hours

Batch no	3 minutes	15 minutes	Post boil	24 hours
#B13 (1:7.5)	355.30 (±537.10)	229.5 (±40.85)	38.67 (±27.03)	29.74 (±22.14)
#B14 (1:10)	56.72 (±40.74)	95.9 (±79.06)	59.97 (±73.39)	110.1 (±85.57)

Data for batches 18 to 25 all post boiling for DLS size, zeta potential, EPM and conductivity (Cond) with standard deviations in brackets of at least three measurements

Batch no	Ag:TSC M ratio	DLS nm	DLS stdev	Zeta mV	zp stdev	EPM 10^{-8} m^2 V^{-1} s^{-1}	EPM stdev	Cond	Cond stdev
#B5	1:1	30.05	(±1.75)	-44.90	(±2.45)	-3.52	(±0.19)	0.11	(±0.00)
#B6	1.25	23.84	(±0.77)	-50.90	(±5.09)	-3.99	(±0.40	0.13	(±0.00
#B7	1.1.5	18.34	(±0.47)	-31.60	(±5.29)	-2.48	(±0.41)	0.10	(±0.05)
#B8	1.75	19.78	(±0.63)	-38.60	(±2.14)	-3.02	(±0.17)	0.17	(±0.00)
#B9	1.25	24.43	(±2.65)	-40.80	(±9.42)	-3.20	(±0.74)	0.13	(±0.00)
#B10	2	22.04	(±0.53)	-33.00	(±1.56)	-2.59	(±0.12)	0.21	(±0.00)
#B11	3	16.68	(±0.10)	-34.90	(±2.58)	-2.74	(±0.20)	0.27	(±0.01)
#B12	5	16.39	(±2.88)	-22.60	(±3.97)	-1.77	(±0.31)	0.45	(±0.02)

Stdev = standard deviation of three measurements

References

Adams, L. K., Lyon, D. Y. and Alvarez, P. J. J. (2006). Comparative eco-toxicity of nanoscale TiO_2, SiO_2, and ZnO water suspensions. *Water research* 40 (**19**) pp 3527.

Aiken, G. R., McKnight, D. M., Wershaw, R. L. and MacCarthy, P., Eds. (1985). *Humic Substances in Soil, Sediment and Water*. Geochemistry, Isolation and Characterisation, John Wiley & Sons

Aitken, R. J., Chaudhry, M. Q., Boxall, A. B. A. and Hull, M. (2006). Manufacture and use of nanomaterials: current status in the UK and global trends. *Occup Med (Lond)* 56 (**5**) pp 300-306.

Alexander, J. B. and Ingram, G. A. (1992). Noncellular nonspecific defence mechanisms of fish. *Annual Review of Fish Diseases* 2 pp 249-279.

Allen, T. (1997). *Particle Size Measurement ,Volume 2, Surface area and pore size determination*, T.J. Press (Padstow) Ltd., Padstow. Cornwall.

Alvarez-Puebla, R. A., dos Santos Jr. , D. S. and Aroca, R. F. (2007). SERS detection of environmental pollutants in humic acid–gold nanoparticle composite materials. *The Analyst* 132 pp 1210-1214.

Alvarez-Puebla, R. A., Valenzuela-Calahorrob, C. and Garrido, J. J. (2006). Theoretical study on fulvic acid structure, conformation and aggregation: A molecular modelling approach. *Science of The Total Environment* 358 (**1-3**) pp 243-254.

Alvarez, P. J. J., Colvin, V., Lead, J. and Stone, V. (2009). Research Priorities to Advance Eco-Responsible Nanotechnology. . *ACS Nano* 3 (**7**) pp 1616-1619.

Amal, R., Raper, J. A. and Waite, T. D. (1990). Fractal structure of hematite aggregates. *Journal of Colloid and interface Science* 140 (**1**) pp 158.

An, J., Tang, B., Ning, X., Zhou, J., Xu, W., Zhao, B., Xu, W., Corredor, C. and Lombardi, J. R. (2007). Photoinduced Shape Evolution: From Triangular to Hexagonal Silver Nanoplates. *J. Phys. Chem. C* 111 (**49**) pp 18055-18059.

Arnall, A. and Parr, D. (2005). Moving the nanoscience and technology (NST) debate forwards: short-term impacts, long-term uncertainty and the social constitution. *Technology in Society* 27 (**1**) pp 23-38.

Assemi, S., Newcombe, G., Hepplewhite, C. and Beckett, R. (2004). Characterization of natural organic matter fractions separated by ultrafiltration using flow field-flow fractionation. *Water research* 38 (**6**) pp 1467.

Auffan, M., Rose, J., Bottero, J.-Y., Lowry, G. V., Jolivet, J.-P. and Wiesner, M. R. (2009). Towards a definition of inorganic nanoparticles from an environmental, health and safety perspective. *Nature Nanotechnology* 4 (**10**) pp 634-641.

Auffan, M., Rose, J., Proux, O., Borschneck, D., Masion, A., Chaurand, P., Hazemann, J. L., Chaneac, C., Jolivet, J. P., Wiesner, M. R., VanGeen, A. and Bottero, J. Y. (2008). Enhanced Adsorption of Arsenic onto Maghemites Nanoparticles: As(III) as a Probe of the Surface Structure and Heterogeneity. *Langmuir*.

Avena, M. J., Vermeer, A. W. P. and Koopal, L. K. (1999). Volume and structure of humic acids studied by viscometry: pH and electrolyte concentration effects. *Colloids and Surfaces A: Physicochemical and Engineering Aspects* 151 (**1-2**) pp 213.

Avouris, P., Chen, Z. and Perebeinos, V. (2007). Carbon-based electronics. *Nature Nanotechnology* 2 (**10**) pp 605-615.

Baalousha, M. (2009). Aggregation and disaggregation of iron oxide nanoparticles: Influence of particle concentration, pH and natural organic matter. *Science of The Total Environment* 407 (**6**) pp 2093-2101.

Baalousha, M., Kammer, F. V. D., Motelica-Heino, M. and Le Coustumer, P. (2005). Natural sample fractionation by F1FFF-MALLS-TEM: Sample stabilization, preparation,

pre-concentration and fractionation. *Journal Of Chromatography A* 1093 (**1-2**) pp 156-166.

Baalousha, M. and Lead, J. R. (2007a). Characterization of Natural Aquatic Colloids (<5 nm) by Flow-Field Flow Fractionation and Atomic Force Microscopy. *Environ. Sci. Technol.* 41 (**4**) pp 1111-1117.

Baalousha, M. and Lead, J. R. (2007b). Size fractionation and characterization of natural aquatic colloids and nanoparticles. *Science of The Total Environment* 386 (**1-3**) pp 93-102.

Baalousha, M., Lead, J. R., von der Kammer, F. and Hofmann, T. (2009). Natural Colloids and Nanoparticles in Aquatic And Terrestrial Environments. *Environmental and Human Health Impacts of Nanotechnology*. J. R. Lead and E. Smith. Chichester, Wiley & Sons.

Baalousha, M., Maniculea, A., Cumberland, S., Lead, J. and Kendall, K. (2008). Aggregation and Surface Properties of Iron Oxide Nanoparticles: Influence of pH and Natural Organic Matter. *Environmental Toxicology and Chemistry* 9 (**29**) pp 1875-1882.

Baalousha, M., Von der Kammer, F., Motelica-Heino, M., Baborowski, M., Hofmeister, C. and Coustumer, P. L. (2006). Size-Based Speciation of Natural Colloidal Particles by Flow Field Flow Fractionation, Inductively Coupled Plasma-Mass Spectroscopy and Transmission Electron Microscopy/X-ray Energy Dispersive Spectroscopy: Colloids- Trace Element Interaction. *Environmental Science and Technology* 40 pp 2156-2162.

Bae, T.-H. and Tak, T.-M. (2005). Effect of TiO_2 nanoparticles on fouling mitigation of ultrafiltration membranes for activated sludge filtration. *Journal of Membrane Science* 249 (**1-2**) pp 1-8.

Baker, A. (2002). Spectrophotometric discrimination of river dissolved organic matter. *Hydrological Processes* 16 (**16**) pp 3203-3213.

Baker, A. and Inverarity, R. (2004). Protein-like fluorescence intensity as a possible tool for determining river water quality. *Hydrological Processes* 18 (**15**) pp 2927-2945.

Ball, P. (2001). Roll up for the revolution. *Nature* 414 (**6860**) pp 142-144.

Balnois, E., Papastavrou, G. and Wilkinson, K. J. (2007). Force Microscopy and Force Measurements of Environmental Colloids. *Environmental Colloids and Particles Behaviour Separation and Characterisation*. K. J. Wilkinson and J. R. Lead, John Wiley & Sons. **10** 406-467.

Balnois, E., Stoll, S., Wilkinson, K. J., Buffle, J., Rinaudo, M. and Milas, M. (2000). Conformations of Succinoglycan as Observed by Atomic Force Microscopy. *Macromolecules* 33 (**20**) pp 7440-7447.

Baun, A., Hartmann, N. B., Grieger, K. and Kusk, K. O. (2008). Ecotoxicity of engineered nanoparticles to aquatic invertebrates: a brief review and recommendations for future toxicity testing. *Ecotoxicology* 17 (**5**) pp 387-395.

Beckett, R., Wood, F. J. and Dixon, D. R. (1992). Size and chemical characterization of pulp and paper-mill effluents by flow field-flow fractionation and resin adsorption techniques. *Environmental Technology* 13 (**12**) pp 1129-1140.

Bell, R. A. and Kramer, J. R. (1999). Structural Chemistry and Geochemistry of Silver–Sulfur Compounds: Critical Review. *Environmental Toxicology and Chemistry* 18 (**1**) pp 9-22

Benedetti, M. F., Ranville, J. F., Allard, T., Bednar, A. J. and Menguy, N. (2003). The iron status in colloidal matter from the Rio Negro, Brasil. *Colloids and Surfaces A: Physicochemical and Engineering Aspects* 217 (**1-3**) pp 1.

Benn, T. M. and Westerhoff, P. (2008). Nanoparticle Silver Released into Water from Commercially Available Sock Fabrics. *Environ. Sci. Technol.* 42 (**11**) pp 4133-4139.

Bigg, T. and Judd, S. J. (2000). Zero-valent iron for water treatment. *Environmental Technology* 21 (**6**) pp 661-670.

Biswas, P. and Wu, C. Y. (2005). Critical Review: Nanoparticles and the environment. *Journal Of The Air & Waste Management Association* 55 (**6**) pp 708-746.

Blain, S., Quéguiner, B., Armand, L., Belviso, S., Bombled, B., Bopp, L., Bowie, A., Brunet, C., Brussaard, C., Carlotti, F., Christaki, U., Corbière, A., Durand, I., Ebersbach, F., Fuda, J.-L., Garcia, N., Gerringa, L., Griffiths, B., Guigue, C., Guillerm, C., Jacquet, S., Jeandel, C., Laan, P., Lefèvre, D., Monaco, C. L., Malits, A., Mosseri, J., Obernosterer, I., Park, Y.-H., Picheral, M., Pondaven, P., Remenyi, T., Sandroni, V., Sarthou, G., Savoye, N., Scouarnec, L., Souhaut, M., Thuiller, D., Timmermans, K., Trull, T., Uitz, J., Beek, P. v., Veldhuis, M., Vincent, D., Viollier, E., Vong, L. and Wagener, T. (2007). Effect of natural iron fertilization on carbon sequestration in the Southern Ocean. *Nature* 446 pp 1070-1074.

Blaser, S. A., Scheringer, M., MacLeod, M. and Hungerbühler, K. (2008). Estimation of cumulative aquatic exposure and risk due to silver: Contribution of nano-functionalized plastics and textiles. *Science of The Total Environment* 390 (**2-3**) pp 396-409.

Borchert, H., Shevchenko, E. V., Robert, A., Mekis, I., Kornowski, A., Grubel, G. and Weller, H. (2005). Determination of Nanocrystal Sizes: A Comparison of TEM, SAXS, and XRD Studies of Highly Monodisperse $CoPt_3$ Particles. *Langmuir* 21 (**5**) pp 1931-1936.

Borm, P., Robbins, D., Haubold, S., Kuhlbusch, T., Fissan, H., Donaldson, K., Schins, R., Stone, V., Kreyling, W., Lademann, J., Krutmann, J., Warheit, D. and Oberdorster, E. (2006). The potential risks of nanomaterials: a review carried out for ECETOC. *Particle and Fibre Toxicology* 3 (**1**) pp 11.

Brar, S. K., Verma, M., Tyagi, R. D. and Surampalli, R. Y. (2010). Engineered nanoparticles in wastewater and wastewater sludge - Evidence and impacts. *Waste Management* 30 (**3**) pp 504-520.

Braun, J. H., Baidins, A. and Marganski, R. (1992). TiO2 pigment technology: a review. *Progress in organic coatings* 20 pp 105-138.

Braydich-Stolle, L., Hussain, S., Schlager, J. J. and Hofmann, M.-C. (2005). In Vitro Cytotoxicity of Nanoparticles in Mammalian Germline Stem Cells. *Toxicological Sciences* 88 (**2**) pp 412-419.

Bronstein, L. M., Sidorov, S. N., Valetsky, P. M., Hartmann, J., Colfen, H. and Antonietti, M. (1999). Induced Micellization by Interaction of Poly(2-vinylpyridine)-block-poly(ethylene oxide) with Metal Compounds. Micelle Characteristics and Metal Nanoparticle Formation. *Langmuir* 15 (**19**) pp 6256-6262.

Brunauer, S., Emmett, P. H. and Teller, E. (1938). Adsorption of Gases in Multimolecular Layers. *Journal Of The American Chemical Society* 60 (**2**) pp 309-319.

Brunner, T. J., Wick, P., Manser, P., Spohn, P., Grass, R. N., Limbach, L. K., Bruinink, A. and Stark, W. J. (2006). In Vitro Cytotoxicity of Oxide Nanoparticles: Comparison to Asbestos, Silica, and the Effect of Particle Solubility. *Environmental Science & Technology* 40 (**14**) pp 4374-4381.

Buffle, J. and Leppard, G. G. (1995a). Characterization Of Aquatic Colloids And Macromolecules .2. Key Role Of Physical Structures On Analytical Results. *Environmental Science & Technology* 29 (**9**) pp 2176-2184.

Buffle, J. and Leppard, G. G. (1995b). Characterization of Aquatic Colloids and Macromolecules. 1. Structure and Behavior of Colloidal Material. *Environmental Science & Technology* 29 (**9**) pp 2169-2175.

Buffle, J., Wilkinson, K. J., Stoll, S., Filella, M. and Zhang, J. (1998). A Generalized Description of Aquatic Colloidal Interactions: The Three-colloidal Component Approach. *Environmental Science & Technology* 32 (**19**) pp 2887-2899.

Buseck, P. R. (2002). Geological fullerenes: review and analysis. *Earth and Planetary Science Letters* 203 (**3-4**) pp 781-792.

Cai, W., Zhang, L., Zhong, H. and He, G. (1998). Annealing of mesoporous silica loaded with silver nanoparticles within its pores from isothermal sorption. *Journal of MAterials Research* 13 (**10**) pp 2888-2895.

Caldwell, K. D., Brimhall, S. L., Gao, Y. and Giddings, J. C. (1988). Sample overloading effects in polymer characterization by field-flow fractionation. *Journal of Applied Polymer Science* 36 (**3**) pp 703 - 719.

Cantrell, K. J., Kaplan, D. I. and Wietsma, T. W. (1995). Zero-Valent Iron For The In-Situ Remediation Of Selected Metals In Groundwater. *Journal Of Hazardous Materials* 42 (**2**) pp 201-212.

Carlson, C., Hussain, S. M., Schrand, A. M., K. Braydich-Stolle, L., Hess, K. L., Jones, R. L. and Schlager, J. J. (2008). Unique Cellular Interaction of Silver Nanoparticles: Size-Dependent Generation of Reactive Oxygen Species. *The Journal of Physical Chemistry B* 112 (**43**) pp 13608-13619.

CBEN. (2010). Theme 3: Nanoparticles and the Environment. *Center for Biological and Environmental Nanotechnology* Retrieved 01.01.10, from: http://cben.rice.edu/research/theme3.aspx.

Chen, K. L. and Elimelech, M. (2006). Aggregation and Deposition Kinetics of Fullerene (C60) Nanoparticles. *Langmuir* 22 (**26**) pp 10994-11001.

Chen, K. L. and Elimelech, M. (2007). Influence of humic acid on the aggregation kinetics of fullerene (C60) nanoparticles in monovalent and divalent electrolyte solutions. *Journal of Colloid and interface Science* 309 (**1**) pp 126.

Chenu, C. (1989). Influence of a fungal polysaccharide, scleroglucan, on clay microstructures. *Soil Biology and Biochemistry* 21 (**2**) pp 299.

Choi, O., Deng, K. K., Kim, N.-J., Ross Jr, L., Surampalli, R. Y. and Hu, Z. (2008). The inhibitory effects of silver nanoparticles, silver ions, and silver chloride colloids on microbial growth. *Water research* 42 (**12**) pp 3066-3074.

Choi, O. and Hu, Z. (2008). Size Dependent and Reactive Oxygen Species Related Nanosilver Toxicity to Nitrifying Bacteria. *Environmental Science & Technology* 42 (**12**) pp 4583-4588.

Christian, P. (2009). Nanomaterials: Properties, Preparation and Applications. *Environmental and Human Health Impacts of Nanotechnology*. J. R. Lead and E. Smith 31-77.

Christian, P., Von der Kammer, F., Baalousha, M. and Hofmann, T. (2008). Nanoparticles: structure, properties, preparation and behaviour in environmental media. *Ecotoxicology* 17 (**5**) pp 326-343.

Colvin, V. L. (2003). The Potential Environmental Impact of Engineered Nanoparticles. *Nature* 21 (**10**) pp 1166-1170.

Connor, E. E., Mwamuka, J., Gole, A., Murphy, C. J. and Wyatt, M. D. (2005). Gold Nanoparticles Are Taken Up by Human Cells but Do Not Cause Acute Cytotoxicity13. *Small* 1 (**3**) pp 325-327.

Corbett, J., McKeown, P. A., Peggs, G. N. and Whatmore, R. (2000). Nanotechnology: International Developments and Emerging Products. *CIRP Annals - Manufacturing Technology* 49 (**2**) pp 523-545.

Cromieres, L., Moulin, V., Fourest, B. and Giffaut, E. (2002). Physico-chemical characterization of the colloidal hematite/water interface: experimentation and modelling. *Colloids And Surfaces A-Physicochemical And Engineering Aspects* 202 (**1**) pp 101-115.

Crosera, M., Bovenzi, M., Maina, G., Adami, G., Zanette, C., Florio, C. and Filon Larese, F. (2009). Nanoparticle dermal absorption and toxicity: a review of the literature. *International Archives of Occupational and Environmental Health* 82 (**9**) pp 1043-1055.

Cumberland, S. A. and Baker, A. (2007). The freshwater dissolved organic matter fluorescence-total organic carbon relationship. *Hydrological Processes* 21 (**16**) pp 2093-2099.

Cumberland, S. A. and Lead, J. R. (2009). Particle size distributions of silver nanoparticles at environmentally relevant conditions. *Chromatograhy A* 1216 pp 9099-9105.

DEFRA (2005a).Characterising the potential risks posed by engineered nanoparticles. DEFRA pp 60.

DEFRA (2005b).A scoping study into the manufacture and use of nanomaterials in the UK. CB01070 DEFRA Downloaded from: http://www.defra.gov.uk/environment/quality/nanotech/policy.htm.

Derjaguin, B. and Landau, L. (1941). Theory of the stability of strongly charged lyophobic sols and of the adhesion of strongly charged particles in solutions of electrolytes. *Progress in Surface Science* 43 (**1-4**) pp 30-59.

Diallo, M. S., Christie, S., Swaminathan, P., Johnson, J. H. and III, W. A. G. (2005). Dendrimer Enhanced Ultrafiltration. 1. Recovery of Cu(II) from Aqueous Solutions Using PAMAM Dendrimers with Ethylene Diamine Core and Terminal NH_2 Groups. *Environmental Science and Technology* 39 (**5**) pp 1366 -1377.

Diegoli, S., Manciulea, A. L., Begum, S., Jones, I. P., Lead, J. R. and Preece, J. A. (2008). Interaction between manufactured gold nanoparticles and naturally occurring organic macromolecules. *Science of The Total Environment* 402 (**1**) pp 51-61.

Domingos, R. F., Baalousha, M. A., Ju-Nam, Y., Reid, M., Tufenkji, N., Lead, J. R., Leppard, G. G. and Wilkinson, K. J. (2009a). Characterizing manufactured nanoparticles in the environment - multimethod determination of particle sizes. *Environmental Science and Technology* 43 (**19**) pp 7277-7284.

Domingos, R. F., Tufenkji, N. and Wilkinson, K. J. (2009b). Aggregation of Titanium Dioxide Nanoparticles: Role of a Fulvic Acid. *Environ. Sci. Technol.* 43 (**5**) pp 1282-1286.

dos Santos Jr, D. S., Alvarez-Puebla, R. A., Oliveira Jr, O. N. and Aroca, R. F. (2005). Controlling the size and shape of gold nanoparticles in fulvic acid colloidal solutions and their optical characterization using SERS. *Journal of Materials Chemistry* 15 (**29**) pp 3045-3049.

Doty, R. C., Tshikhudo, T. R., Brust, M. and Fernig, D. G. (2005). Extremely Stable Water-Soluble Ag Nanoparticles. *Chem. Mater.* 17 (**18**) pp 4630-4635.

Dubasa, S. T. and Pimpan, V. (2008). Humic acid assisted synthesis of silver nanoparticles and its application to herbicide detection. *Materials Letters* 62 (**17-18**) pp 2661-2663.

Dunens, O. M., MacKenzie, K. J. and Harris, A. T. (2009). Synthesis of Multiwalled Carbon Nanotubes on Fly Ash Derived Catalysts. *Environmental Science & Technology* 43 (**20**) pp 7889-7894.

Dunphy Guzman, K. A., Finnegan, M. P. and Banfield, J. F. (2006a). Influence of Surface Potential on Aggregation and Transport of Titania Nanoparticles. *Environmental Science & Technology* 40 (**24**) pp 7688-7693.

Dunphy Guzman, K. A., Taylor, M. R. and Banfield, J. F. (2006b). Environmental risks of nanotechnology: National nanotechnology initiative funding, 2000-2004. *Environmental Science & Technology* 40 (**5**) pp 1401-1407.

Duran, N., Marcato, P. D., De Souza, G. I. H., Alves, O. L. and Esposito, E. (2007). Antibacterial effect of silver nanoparticles produced by fungal process on textile fabrics and their effluent treatment. *Journal Of Biomedical Nanotechnology* 3 (**2**) pp 203-208.

Duval, J. F. L. (2007). Electrophoresis of Soft Colloids: Basic Principles and Applications. *Environmental Colloids and Particles*. K. J. Wilkinson and J. R. Lead 315-344.

Dycus, P. J. M., Healy, K. D., Stearman, G. K. and Wells, M. J. M. (1995). Diffusion Coefficients and Molecular Weight Distributions of Humic and Fulvic Acids Determined by Flow Field-Flow Fractionation *Separation Science and Technology* 30 (**7 - 9**) pp 1435 - 1453

Eckelman, M. J. and Graedel, T. E. (2007). Silver emissions and their environmental Impacts: A multilevel assessment. *Environ. Sci. Technol.* 41 (**17**) pp 6283-6289.
El-Ansary, A. and Al-Daihan, S. (2009). On the toxicity of therapeutically used nanoparticles. *Journal of Toxicology* pp 9.
EWG. (2009). Skin Deep Cosmetic Safety Database. Retrieved 26th October 2009, from: http://www.cosmeticsdatabase.com/index.php.
Fabrega, J., Fawcett, S. R., Renshaw, J. C. and Lead, J. R. (2009a). Silver nanoparticle impact on bacterial growth: effect of pH, concentration and organic matter. *Environmental Science and Technology* 43 (**19**) pp 7285–7290.
Fabrega, J., Renshaw, J. C. and Lead, J. R. (2009b). Interactions of Silver Nanoparticles with Pseudomonas putida Biofilms. *Environmental Science & Technology* 43 (**23**) pp 9004-9009.
Faraday, M. (1857). The Bakerian lecture: Experimental Relations of Gold (and Other Metals) to Light. *Philosophical Transactions of the Royal Society of London* 147 pp 145-181.
Farkas, J., Christian, P., Gallego-Urrea, J. A., Roos, N., Hassellöv, M., Tollefsen, K. E. and Thomas, K. V. (2010). Effects of silver and gold nanoparticles on rainbow trout (Oncorhynchus mykiss) hepatocytes. *Aquatic Toxicology* 96 (**1**) pp 44-52
Federici, G., Shaw, B. J. and Handy, R. D. (2007). Toxicity of titanium dioxide nanoparticles to rainbow trout (Oncorhynchus mykiss): Gill injury, oxidative stress, and other physiological effects. *Aquatic Toxicology* 84 (**4**) pp 415-430.
Feynman, R. P. (1960). There's plenty of room at the bottom. *Engineering and Science* XXIII (**5**).
Filella, M., Zhang, J., Newman, M. E. and Buffle, J. (1997). Analytical applications of photon correlation spectroscopy for size distribution measurements of natural colloidal suspensions: capabilities and limitations. *Colloids and Surfaces A: Physicochemical and Engineering Aspects* 120 (**1-3**) pp 27.
Filius, J. D., Lumsdon, D. G., Meeussen, J. C. L., Hiemstra, T. and Van Riemsdijk, W. H. (2000). Adsorption of fulvic acid on goethite. *Geochimica et Cosmochimica Acta* 64 (**1**) pp 51-60.
Fuerstenau, D. W. and Colic, M. (1999). Self-association and reverse hemimicelle formation at solid-water interfaces in dilute surfactant solutions. *Colloids and Surfaces A: Physicochemical and Engineering Aspects* 146 (**1-3**) pp 33-47.
Gao, J., Bonzongo, J. C. J., Bitton, G., Li, Y. and Wu, C. Y. (2008). Nanowastes and the environment: Using mercury as an example pollutant to assess the environmental fate of chemicals adsorbed onto manufactured nanomaterials. *Environmental Toxicology and Chemistry* 27 (**4**) pp 808-810.
Gardea-Torresdey, J. L., Gomez, E., Peralta-Videa, J. R., Parsons, J. G., Troiani, H. and Jose-Yacaman, M. (2003). Alfalfa Sprouts: A Natural Source for the Synthesis of Silver Nanoparticles. *Langmuir* 19 (**4**) pp 1357-1361.
Geim, A. K. (2009). Graphene: Status and Prospects. *Science* 324 (**5934**) pp 1530-1534.
Geranio, L., Heuberger, M. and Nowack, B. (2009). The Behavior of Silver Nanotextiles during Washing. *Environmental Science & Technology* 43 (**21**) pp 8113-8118.
Giasuddin, A. B. M., Kanel, S. R. and Choi, H. (2007). Adsorption of Humic Acid onto Nanoscale Zerovalent Iron and Its Effect on Arsenic Removal. *Environmental Science & Technology* 41 (**6**) pp 2022-2027.
Gibson, C. T., Turner, I. J., Roberts, C. J. and Lead, J. R. (2007). Quantifying the Dimensions of Nanoscale Organic Surface Layers in Natural Waters. *Environmental Science & Technology* 41 (**4**) pp 1339-1344.
Giddings, J. C. (1993). Field-Flow Fractionation:Analyis of Macromolecular, Colloidal and Particulate Materials. *Science* 260 pp 1456-1464.

Giddings, J. C., Williams, P. S. and Benincasa, M. A. (1992). Rapid breakthrough measurement of void volume for field-flow fractionation channels. *Journal of Chromatography* 627 pp 23-35.

Gimbert, L. J., Hamon, R. E., Casey, P. S. and Worsfold, P. J. (2007). Partitioning and stability of engineered ZnO nanoparticles in soil suspensions using flow field-flow fractionation. *Environmental Chemistry* 4 (**1**) pp 8-10.

Gimbert, L. J., Haygarth, P. M., Beckett, R. and Worsfold, P. J. (2006). The Influence of Sample Preparation on Observed Particle Size Distributions for Contrasting Soil Suspensions using Flow Field-Flow Fractionation. *Environmental Chemistry* 3 (**3**) pp 184-191.

Glover, C. N. and Wood, C. M. (2004). Physiological interactions of silver and humic substances in Daphnia magna: effects on reproduction and silver accumulation following an acute silver challenge. *Comparative Biochemistry and Physiology Part C: Toxicology & Pharmacology* 139 (**4**) pp 273.

Gopinath, P., Sonit Kumar, G., Arun, C. and Siddhartha Sankar, G. (2008). Implications of silver nanoparticle induced cell apoptosis for in vitro gene therapy. *Nanotechnology* (**7**) pp 075104.

Gottschalk, F., Sonderer, T., Scholz, R. W. and Nowack, B. (2009). Modeled Environmental Concentrations of Engineered Nanomaterials (TiO2, ZnO, Ag, CNT, Fullerenes) for Different Regions. *Environmental Science & Technology* 43 (**24**) pp 9216-9222.

Grassian, V. H., O'Shaughnessy, P. T., Adamcakova-Dodd, A., Pettibone, J. M. and Thorne, P. S. (2007). Inhalation Exposure Study of Titanium Dioxide Nanoparticles with a Primary Particle Size of 2 to 5 nm *Environmental Health Perspectives* 115 (**3**) pp 397-402.

Gu, B., Watson, D. B., Wu, L., Phillips, D. H., White, D. C. and Zhou, J. (2002). Microbiological characteristics in a zero-valent iron reactive barrier. *Environmental Monitoring and Assessment* 77 (**3**) pp 293.

Guo, L. and Santschi, P. H. (2007). Ultrafiltration and its Applications to Sampling and Characterisation of Aquatic Colloids. *Environmental Colloids and Particles*. K. J. Wilkinson and J. R. Lead 159-221.

Handy, R., Ramsden, C., Smith, T. and Shaw, B. (2008a). Toxicology of dietary titanium dioxide nanoparticles to rainbow trout (Oncorhynchus mykiss). *Comparative Biochemistry and Physiology - Part A: Molecular and Integrative Physiology* 150 (**3**) pp S60-S61.

Handy, R. D., Henry, T. B., Scown, T. M., Johnston, B. D. and Tyler, C. R. (2008b). Manufactured nanoparticles: Their uptake and effects on fish - A mechanistic analysis. *Ecotoxicology* 17 (**5**) pp 396-409.

Handy, R. D., von der Kammer, F., Lead, J. R., Hassellov, M., Owen, R. and Crane, M. (2008c). The ecotoxicology and chemistry of manufactured nanoparticles. *Ecotoxicology* 17 (**4**) pp 287-314.

Hao, E. and Schatz, G. C. (2004). Electromagnetic fields around silver nanoparticles and dimers. *The Journal of Chemical Physics* 120 (**1**) pp 357-366.

Hassellov, M. (2005). Relative molar mass distributions of chromophoric colloidal organic matter in coastal seawater determined by Flow Field-Flow Fractionation with UV absorbance and fluorescence detection. *Marine Chemistry* 94 (**1-4**) pp 111-123.

Hassellov, M. and Kaegi, R. (2009). Analysis and Characterisation of manufactured NPs in Aquatic Environments. *Environmental and Human Health Impacts of Nanotechnology*. J. R. Lead and E. Smith.

He, Y. T., Wan, J. and Tokmaga, T. (2008). Kinetic stability of hematite nanoparticles: the effect of particle sizes. *Journal of Nanoparticle Research* 10 pp 321–332.

Henglein, A. and Giersig, M. (1999). Formation of colloidal silver nanoparticles: Capping action of citrate. *Journal of Physical Chemistry B* 103 (**44**) pp 9533-9539.

Hochella, M. F. (2002). There's plenty of room at the bottom: Nanoscience in geochemistry. *Geochimica and Cosmochimica Acta* 66 (**5**) pp 735-743.
Hochella, M. F., Lower, S. K., Maurice, P. A., Penn, L., Sahai, N., Sparks, D. L. and Twining, B. S. (2008). Nanominerals, Mineral Particles and Earth Systems. *Science* 319.
Hochella, M. F. and Madden, A. S. (2005). Earth's nano-compartment for toxic metals. *Elements* 1 (**4**) pp 199-203.
Holister, P. (2002). Nanotech the tiny revolution. CMP Científica. Downloaded from: www.cientifica.com.
Hosse, M. and Wilkinson, K. J. (2001). Determination of electrophoretic mobilities and hydrodynamic radii of three humic substances as a function of pH and ionic strength. *Environmental Science & Technology* 35 (**21**) pp 4301-4306.
Howard, A. G. (2005). *Aquatic Environmental Chemistry*. Oxford, Oxford University Press.
Huang, J., Li, Q., Sun, D., Lu, Y., Su, Y., Yang, X., Wang, H., Wang, Y., Shao, W., He, N., Hong, J. and Chen, C. (2007). Biosynthesis of silver and gold nanoparticles by novel sundried Cinnamomum camphora leaf. *Nanotechnology* 18 (**10**) pp 105104.
Huang, Z., Maness, P.-C., Blake, D. M., Wolfrum, E. J., Smolinski, S. L. and Jacoby, W. A. (2000). Bactericidal mode of titanium dioxide photocatalysis. *Journal of Photochemistry and Photobiology A: Chemistry* 130 (**2-3**) pp 163-170.
Hund-Rinke, K. and Simon, M. (2006). Ecotoxic Effect of Photocatalytic Active Nanoparticles (TiO_2) on Algae and Daphnids. *Environmental Science and Pollution Research* 13 (**4**) pp 225-232.
Hwang, E. T., Lee, J. H., Chae, Y. J., Kim, Y. S., Kim, B. C., Sang, B.-I. and Gu, M. B. (2008). Analysis of the Toxic Mode of Action of Silver Nanoparticles Using Stress-Specific Bioluminescent Bacteria. *Small* 4 (**6**) pp 746-750.
Hyett, G., Green, M. and Parkin, I. P. (2006). X-ray Diffraction Area Mapping of Preferred Orientation and Phase Change in TiO_2 Thin Films Deposited by Chemical Vapor Deposition. *Journal Of The American Chemical Society* 128 (**37**) pp 12147-12155.
Hyung, H., Fortner, J. D., Hughes, J. B. and Kim, J. H. (2007). Natural Organic Matter Stabilizes Carbon Nanotubes in the Aqueous Phase. *Environmental Science & Technology* 41 (**1**) pp 179-184.
IHSS. (2009). International Humic Substances Society. Retrieved 18/11/2009, from: http://ihss.gatech.edu/ihss2/.
Iijima, S. (1991). Helical microtubules of graphitic carbon. *Nature* 354 (**6348**) pp 56-58.
Illés, E. and Tombácz, E. (2006). The effect of humic acid adsorption on pH-dependent surface charging and aggregation of magnetite nanoparticles. *Journal of Colloid and interface Science* 295 (**1**) pp 115-123.
Jacobson, A. R., Martinez, C. E., Spagnuolo, M., McBride, M. B. and Baveye, P. (2005). Reduction of silver solubility by humic acid and thiol ligands during acanthite ([beta]-Ag2S) dissolution. *Environmental Pollution* 135 (**1**) pp 1.
Jana, N. R., Gearheart, L. and Murphy, C. J. (2001). Wet chemical synthesis of silver nanorods and nanowires of controllable aspect ratio *Chemical Communications* 7 pp 617-618.
Janz, A., Kockritz, A., Yao, L. and Martin, A. (2010). Fundamental Calculations on the Surface Area Determination of Supported Gold Nanoparticles by Alkanethiol Adsorption. *Langmuir* 26 (**9**) pp 6783-6789.
Jarvie, H. P., Al-Obaidi, H., King, S. M., Bowes, M. J., Lawrence, M. J., Drake, A. F., Green, M. A. and Dobson, P. J. (2009). Fate of Silica Nanoparticles in Simulated Primary Wastewater Treatment. *Environmental Science & Technology* 43 (**22**) pp 8622-8628.
Jeng, H. A. and Swanson, J. (2006). Toxicity of metal oxide nanoparticles in mammalian cells. *Journal Of Environmental Science And Health Part A-Toxic/Hazardous Substances & Environmental Engineering* 41 (**12**) pp 2699-2711.

Jiang, J., Oberdörster, G. and Biswas, P. (2009). Characterization of size, surface charge, and agglomeration state of nanoparticle dispersions for toxicological studies. *Journal of Nanoparticle Research* 11 (**1**) pp 77-89.

Johnston, B. D., Scown, T. M., Moger, J., Cumberland, S. A., Baalousha, M., Linge, K., van Aerle, R., Jarvis, K., Lead, J. R. and Tyler, C. R. (2010). Bioavailability of nanoscale metal oxides, TiO_2, CeO_2, and ZnO to fish. *Environmental Science and Technology* (in press).

Ju-Nam, Y. and Lead, J. R. (2008). Manufactured nanoparticles: An overview of their chemistry, interactions and potential environmental implications. *Science of The Total Environment* 400 (**1-3**) pp 396-414.

Kaegi, R., Ulrich, A., Sinnet, B., Vonbank, R., Wichser, A., Zuleeg, S., Simmler, H., Brunner, S., Vonmont, H., Burkhardt, M. and Boller, M. (2008). Synthetic TiO_2 Nanoparticle Emission From Exterior Facades Into the Aquatic Environment. *Environmental Pollution* 156 (**2**) pp 233-239.

Kallay, N. and Zalac, S. (2002). Stability of Nanodispersions: A Model for Kinetics of Aggregation of Nanoparticles. *Journal of Colloid and interface Science* 253 (**1**) pp 70-76.

Kaszuba, M., McKnight, D., Connah, M., McNeil-Watson, F. and Nobbmann, U. (2008). Measuring sub nanometre sizes using dynamic light scattering. *Journal of Nanoparticle Research* 10 (**5**) pp 823-829.

Kendall, K. and Kosseva, M. R. (2005). Adhesion of nanoparticles fouling glass surfaces. *Journal Of Adhesion* 81 (**10-11**) pp 1017.

Kerker, M. (1985). The optics of colloidal silver: something old and something new. *Journal of Colloid and interface Science* 105 (**2**) pp 297.

Kim, J., Davies, S. H. R., Baumann, M. J., Tarabara, V. V. and Masten, S. J. (2008). Effect of ozone dosage and hydrodynamic conditions on the permeate flux in a hybrid ozonation–ceramic ultrafiltration system treating natural waters. *Journal of Membrane Science* 311 pp 165-172.

Kim, J., Shan, W., Davies, S. H. R., Baumann, M. J., Masten, S. J. and Tarabara, V. V. (2009). Interactions of Aqueous NOM with Nanoscale TiO_2: Implications for Ceramic Membrane Filtration-Ozonation Hybrid Process. *Environmental Science & Technology* 43 (**14**) pp 5488–5494.

Kiser, M. A., Westerhoff, P., Benn, T., Wang, Y., PeÌ□ rez-Rivera, J. and Hristovski, K. (2009). Titanium Nanomaterial Removal and Release from Wastewater Treatment Plants. *Environmental Science & Technology*.

Klaine, S. J., Alvarez, P. J. J., Batley, G. E., Fernandes, T. F., Handy, R. D., Lyon, D. Y., Mahendra, S., McLaughlin, M. J. and Lead, J. R. (2008). Nanomaterials in the Enviornment: Behavior, Fate, Bioavailability, and Effects. *Environmental Toxicology and Chemistry* 27 (**9**) pp 1825-1851.

Koparde, V. N. and Cummings, P. T. (2007). Molecular dynamics study of water adsorption on TiO2 nanoparticles. *Journal Of Physical Chemistry C* 111 (**19**) pp 6920-6926.

Kosmulski, M. (2002). The pH-dependent surface charging and the points of zero charge. *Journal of Colloid and interface Science* 253 (**1**) pp 77-87.

Kovalevski, V. V., Prikhodko, A. V. and Buseck, P. R. (2005). Diamagnetism of natural fullerene-like carbon. *Carbon* 43 (**2**) pp 401-405.

Kristensen, H. L., McCarty, G. W. and Meisinger, J. J. (2000). Effects of Soil Structure Disturbance on Mineralization of Organic Soil Nitrogen. *Soil Sci. Soc. Am. J.* 64 pp 371-378.

Kroto, H. W., Heath, J. R., O'Brien, S. C., Curl, R. F. and Smalley, R. E. (1985). C60: Buckminsterfullerene. *Nature* 318 (**6042**) pp 162.

Langford, J. I. and Wilson, A. J. C. (1978). Seherrer after Sixty Years: A Survey and Some New Results in the Determinatio of Crystallite Size. *Journal of Applied Crystallography* 11 pp 102-113.

Lead, J. R., Hamilton-Taylor, J., Davison, W. and Harper, M. (1999). Trace metal sorption by natural particles and coarse colloids. *Geochimica et Cosmochimica Acta* 63 (**11-12**) pp 1661.

Lead, J. R., Muirhead, D. and Gibson, C. T. (2005). Characterization of freshwater natural aquatic colloids by atomic force microscopy (AFM). *Environmental Science & Technology* 39 (**18**) pp 6930-6936.

Lead, J. R., Starchev, K. and Wilkinson, K. J. (2003). Diffusion coefficients of humic substances in agarose gel and in water. *Environmental Science & Technology* 37 (**3**) pp 482-487.

Lead, J. R. and Wilkinson, K. J. (2006). Aquatic Colloids and Nanoparticles: Current Knowledge and Future Trends. *Environmental Chemistry* 3 (**3**) pp 159-171.

Lead, J. R. and Wilkinson, K. J. (2007). Environmental Colloids and Particles: Current Knowledge and Future Developments. *Environmental Colloids and Particles; Behaviour, Separation and Characterisation*. K. J. Wilkinson and J. R. Lead, John Wiley & Sons 1-15.

Lead, J. R., Wilkinson, K. J., Balnois, E., Cutak, B. J., Larive, C. K., Assemi, S. and Beckett, R. (2000a). Diffusion coefficients and polydispersities of the Suwannee River fulvic acid: Comparison of fluorescence correlation spectroscopy, pulsed-field gradient nuclear magnetic resonance, and flow field-flow fractionation. *Environmental Science & Technology* 34 (**16**) pp 3508-3513.

Lead, J. R., Wilkinson, K. J., Starchev, K., Canonica, S. and Buffle, J. (2000b). Determination of diffusion coefficients of humic substances by fluorescence correlation spectroscopy: Role of solution conditions. *Environmental Science & Technology* 34 (**7**) pp 1365-1369.

Ledwith, D. M., Whelan, A. M. and Kelly, J. M. (2007). A rapid, straight-forward method for controlling the morphology of stable silver nanoparticles. *Journal of Materials Chemistry* 17 (**23**) pp 2459-2464.

Lee, P. C. and Meisel, D. (1982). Adsorption and surface-enhanced Raman of dyes on silver and gold sols. *Journal of Physical Chemistry* 86 (**17**) pp 3391-3395.

Leenheer, J. A., Brown, G. K., MacCarthy, P. and Cabaniss, S. E. (1998). Models of metal binding structures in fulvic acid from the Suwannee River, Georgia. *Environmental Science & Technology* 32 (**16**) pp 2410-2416.

Leppard, G. G. (1992). Size, morphology and composition of particulates in aquatic ecosystems: solving speciation problems by correlative electron microscopy. *Analyst* 117 pp 595 - 603.

Lesher, E. K., Ranville, J. F. and Honeyman, B. D. (2009). Analysis of pH Dependent Uranium(VI) Sorption to Nanoparticulate Hematite by Flow Field-Flow Fractionation - Inductively Coupled Plasma Mass Spectrometry. *Environmental Science & Technology* 43 (**14**) pp 5403–5409.

Lewinski, N., Colvin, V. and Drezek, R. (2008). Cytotoxicity of Nanoparticles. *Small* 4 (**1**) pp 26-49.

Li, D., Lyon, D. Y., Li, Q. and Alvarez, P. J. J. (2008). Effect of Soil Sorption and Aquatic Natural Organic Matter on the Antibacterial Activity of a Fullerene Water Suspension. *Environmental Toxicology and Chemistry* 27 (**9**) pp 1888–1894.

Li, L., Fan, M. H., Brown, R. C., Van Leeuwen, J. H., Wang, J. J., Wang, W. H., Song, Y. H. and Zhang, P. Y. (2006). Synthesis, properties, and environmental applications of nanoscale iron-based materials: A review. *Critical Reviews In Environmental Science And Technology* 36 (**5**) pp 405-431.

Li, N., Sioutas, C., Cho, A., Schmitz, D., Misra, C., Sempf, J., Wang, M., Oberley, T., Froines, J. and Nel, A. (2003). Ultrafine Particulate Pollutants Induce Oxidative Stress and Mitochondrial Damage *Environmental Health Perspectives* 111 (**4**) pp 455-460

Li, Q., Xie, R., Li, Y. W., Mintz, E. A. and Shang, J. K. (2007). Enhanced Visible-Light-Induced Photocatalytic Disinfection of E. coli by Carbon-Sensitized Nitrogen-Doped Titanium Oxide. *Environ. Sci. Technol.* 41 (**14**) pp 5050-5056.

Limbach, L. K., Wick, P., Manser, P., Grass, R. N., Bruinink, A. and Stark, W. J. (2007). Exposure of Engineered Nanoparticles to Human Lung Epithelial Cells:â€‰ Influence of Chemical Composition and Catalytic Activity on Oxidative Stress. *Environmental Science & Technology* 41 (**11**) pp 4158-4163.

Lin, C.-C., Chen, S.-J., Huang, K.-L., Lee, W.-J., Lin, W.-Y., Liao, C.-J., Chaung, H.-C. and Chiu, C.-H. (2007). Water-soluble ions in nano/ultrafine/fine/coarse particles collected near a busy road and at a rural site. *Environmental Pollution* 145 (**2**) pp 562.

Link, S. and El-Sayed, M. A. (2003). Optical Properties and Ultrafast Dynamics of Metallic Nanocrystals. *Annual Review of Physical Chemistry* 54 (**1**) pp 331-366.

Liu, J. and Hurt, R. H. (2010). Ion Release Kinetics and Particle Persistence in Aqueous Nano-Silver Colloids. *Environmental Science & Technology* 44 (**6**) pp 2169-2175.

Liz-Marzan, L. M. and Lado-Tourino, I. (1996). Reduction and Stabilization of Silver Nanoparticles in Ethanol by Nonionic Surfactants. *Langmuir* 12 (**15**) pp 3585-3589.

Lok, C.-N., Ho, C.-M., Chen, R., He, Q.-Y., Yu, W.-Y., Sun, H., Tam, P. K.-H., Chiu, J.-F. and Che, C.-M. (2006). Proteomic Analysis of the Mode of Antibacterial Action of Silver Nanoparticles. *Journal of Proteome Research* 5 (**4**) pp 916-924.

Lomer, M. C. E., Thompson, R. P. H., Commisso, J., LKeen, C. and Powell, J. J. (2000). Determination of titanium dioxide in foods using inductively coupled plasma optical emission spectrometry. *Analyst* 125 (**12**) pp 2339-2343.

Long, T. C., Saleh, N., Tilton, R. D., Lowry, G. V. and Veronesi, B. (2006). Titanium Dioxide (P25) Produces Reactive Oxygen Species in Immortalized Brain Microglia (BV2): Implications for Nanoparticle Neurotoxicity. *Environ. Sci. Technol.* 40 (**14**) pp 4346-4352.

Loux, N. and Savage, N. (2008). An Assessment of the Fate of Metal Oxide Nanomaterials in Porous Media. *Water, Air, & Soil Pollution* 194 (**1**) pp 227-241.

Lovern, S. B. and Klaper, R. (2006). Daphnia magna mortality when exposed to titanium dioxide and fullerene (C-60) nanoparticles. *Environmental Toxicology and Chemistry* 25 (**4**) pp 1132-1137.

Lubick, N. (2008). Nanosilver toxicity: ions, nanoparticles;or both? *Environmental Science & Technology* 42 (**23**) pp 8617-8617.

Luoma, S. L. (2008).PEN report: Silver Nanotechnologies and the Environment Old problems or new challenges? W. W. I. C. f. S. a. T. P. C. Trusts Downloaded from: http://www.nanotechproject.org/publications/.

Lyven, B., Hassellov, M., Turner, D. R., Haraldsson, C. and Andersson, K. (2003). Competition between iron- and carbon-based colloidal carriers for trace metals in a freshwater assessed using flow field-flow fractionation coupled to ICPMS. *Geochimica et Cosmochimica Acta* 67 (**20**) pp 3791.

Madden, A. S. and Hochella, M. F. (2005). A test of geochemical reactivity as a function of mineral size: Manganese oxidation promoted by hematite nanoparticles. *Geochimica and Cosmochimica Acta* 69 (**2**) pp 389-398.

Mahmoodi, N. M., Arami, M., Limaee, N. Y., Gharanjig, K. and Nourmohammadian, F. (2007). Nanophotocatalysis using immobilized titanium dioxide nanoparticle: Degradation and mineralization of water containing organic pollutant: Case study of Butachlor. *Materials Research Bulletin* 42 (**5**) pp 797.

Malam, Y., Loizidou, M. and Seifalian, A. M. (2009). Liposomes and nanoparticles: nanosized vehicles for drug delivery in cancer. *Trends in Pharmacological Sciences* 30 (**11**) pp 592-599.

Malcolm, R. L. (1985). Geochemistry of Stream Fulvic and Humic Acids. *Humic Substance in soil, sediment and water: Geochemistry, Isolation and Characterization*. G. R. Aiken, D. M. McKnight, R. L. Wershaw and P. MacCarthy, John Wiley 692.

Manciulea, A., Baker, A. and Lead, J. R. (2009). A fluorescence quenching study of the interaction of Suwannee River fulvic acid with iron oxide nanoparticles. *Chemosphere* 76 (**8**) pp 1023-1027.

Mandal, S., Gole, A., Lala, N., Gonnade, R., Ganvir, V. and Sastry, M. (2001). Studies on the Reversible Aggregation of Cysteine-Capped Colloidal Silver Particles Interconnected via Hydrogen Bonds. *Langmuir* 17 (**20**) pp 6262-6268.

Maneerung, T., Tokura, S. and Rujiravanit, R. (2008). Impregnation of silver nanoparticles into bacterial cellulose for antimicrobial wound dressing. *Carbohydrate Polymers* 72 (**1**) pp 43-51.

Matijevic, E. and Scheiner, P. (1978). Ferric Hydrous Oxide Sols .3. Preparation of Uniform Particles by Hydrolysis of Fe(III)-Chloride, Fe(III)-Nitrate, and Fe(III)-Perchlorate Solutions. *Journal of Colloid and interface Science* 63 (**3**) pp 509-524.

Melnyk, V., Shymanovska, V., Puchkovska, G., Bezrodna, T. and Klishevich, G. (2005). Low-temperature luminescence of different TiO_2 modifications. *Journal Of Molecular Structure* 744 pp 573-576.

Miller, M. M. and Lazarides, A. A. (2006). Sensitivity of metal nanoparticle plasmon resonance band position to the dielectric environment as observed in scattering. *Journal of Optics A: Pure and Applied Optics* (**4**) pp S239.

Mobed, J. J., Hemmingsen, S. L., Autry, J. L. and McGown, L. B. (1996). Fluorescence Characterization of IHSS Humic Substances: Total Luminescence Spectra with Absorbance Correction. *Environmental Science & Technology* 30 pp 3061-3065.

Mock, J. J., Barbic, M., Smith, D. R., Schultz, D. A. and Schultz, S. (2002). Shape effects in plasmon resonance of individual colloidal silver nanoparticles. *The Journal of Chemical Physics* 116 (**15**) pp 6755-6759.

Monthioux, M. and Kuznetsov, V. L. (2006). Who should be given the credit for the discovery of carbon nanotubes? *Carbon* 44 (**9**) pp 1621-1623.

Moore, M. N. (2006). Do nanoparticles present ecotoxicological risks for the health of the aquatic environment? *Environment International* 32 (**8**) pp 967-976.

Mor, G. K., Shankar, K., Paulose, M., Varghese, O. K. and Grimes, C. A. (2006). Use of Highly-Ordered TiO_2 Nanotube Arrays in Dye-Sensitized Solar Cells. *Nano Letters* 6 (**2**) pp 215-218.

Morones, J. R., Elechiguerra, J. L., Camacho, A., Holt, K., Kouri, J. B., Ramírez, J. T. and Yacaman, M. J. (2005). The bactericidal effect of silver nanoparticles. *Nanotechnology* 16 pp 2346-2353.

Morones, J. R. and Frey, W. (2007). Environmentally sensitive silver nanoparticles of controlled size synthesized with PNIPAM as a nucleating and capping agent. *Langmuir* 23 (**15**) pp 8180-8186.

Mueller, N. C. and Nowack, B. (2008). Exposure modelling of engineered nanoparticles in the environment. *Environmental Science & Technology* 42 (**12**) pp 4447-4453.

Mühling, M., Bradford, A., Readman, J. W., Somerfield, P. J. and Handy, R. D. (2009). An investigation into the effects of silver nanoparticles on antibiotic resistance of naturally occurring bacteria in an estuarine sediment. *Marine Environmental Research* 68 (**5**) pp 278-283.

Navarro, E., Baun, A., Behra, R., Hartmann, N. B., Filser, J., Miao, A. J., Quigg, A., Santschi, P. H. and Sigg, L. (2008a). Environmental behavior and ecotoxicity of engineered nanoparticles to algae, plants, and fungi. *Ecotoxicology* 17 (**5**) pp 372-386.

Navarro, E., Piccapietra, F., Wagner, B., Marconi, F., Kaegi, R., Odzak, N., Sigg, L. and Behra, R. (2008b). Toxicity of Silver Nanoparticles to Chlamydomonas reinhardtii. *Environmental Science & Technology* 42 (**23**) pp 8959-8964.

Navrotsky, A., Mazeina, L. and Majzlan, J. (2008). Size-Driven Structural and Thermodynamic Complexity in the Iron Oxides. *Science* 319 (**5870**) pp 1635-1638.
Neal, C., Lofts, S., Evans, C., Reynolds, B., Tipping, E. and Neal, M. (2008). Increasing Iron Concentrations in UK Upland Waters. *Aquatic Geochemistry* 14 (**3**) pp 263-288.
Nel, A., Xia, T., Madler, L. and Li, N. (2006). Toxic Potential of Materials at the Nanolevel. *Science* 311 (**5761**) pp 622-627.
Nikolakis, V. (2006). Understanding the effect of specific surface area and surface reactions on silicalite-1 nucleation and growth. *Microporous and Mesoporous Materials* 93 (**1-3**) pp 101-110.
NNI (2007). The National Nanotechnology Initiative: Research and Development Leading to a Relvolution in Technology and Industry. *Supplement to the President's 2008 Budget* NSTC CT NSET, pp 48.
Nowack, B. (2009). Environmental behavior and effects of engineered metal and metal oxide nanoparticles. *In:Heavy Metals in the Environment*. J. P. C. Lawrence K. Wang, Yung-Tse Hung and Nazih K. Shammas, Taylor and Francis & CRC Press pp. 63-87.
Nowack, B. and Bucheli, T. D. (2007). Occurrence, behavior and effects of nanoparticles in the environment *Environmental Pollution* 150 (**1**) pp 5-22.
Nyberg, L., Turco, R. F. and Nies, L. (2008). Assessing the Impact of Nanomaterials on Anaerobic Microbial Communities. *Environ. Sci. Technol.*
Oberdorster, E. (2004). Manufactured Nanomaterials (Fullerenes, C_{60}) Induce Oxidative Stress in the Brain of Juvenile Largemouth Bass. *Environmental Health Perspectives* 112 (**10**) pp 1058-1062.
Oberdorster, G., Oberdorster, E. and Oberdorster, J. (2005). Nanotoxicology: An emerging discipline evolving from studies of ultrafine particles. *Environmental Health Perspectives* 113 (**7**) pp 823-839.
OECD (2009).Current Developments/ Activities on the Safety of Manufactured Nanomaterials. Downloaded from: http://www.olis.oecd.org/olis/2009doc.nsf/LinkTo/NT000049A2/$FILE/JT03267889.PDF.
Ohbo, Y., Fukuzako, H., Takeuchi, K. and Takigawa, M. (1996). Argyria and Convulsive Seizures Caused by Ingestion of Silver in a Patient with Schizophrenia. *Psychiaty and Clinical Neurosciences* 50 pp 89-90.
Ohno, T., Amirbahman, A. and Bro, R. (2008). Parallel factor analysis of excitation-emission matrix fluorescence spectra of water soluble soil organic matter as basis for the determination of conditional metal binding parameters. *Environmental Science & Technology* 42 (**1**) pp 186-192.
Owen, R. and Depledge, M. (2005). Nanotechnology and the environment: Risks and rewards. *Marine Pollution Bulletin* 50 (**6**) pp 609-612.
Oxonica. (2009). Envirox ™ -Diesel Fuel Additive. Retrieved 26-10-2009, from: http://www.oxonica.com/energy/energy_envirox_product_information.php.
Padovani, S., Sada, C., Mazzoldi, P., Brunetti, B., Borgia, I., Sgamellotti, A., Giulivi, A., Acapito, F. D. and Battaglin, G. (2003). Copper in glazes of Renaissance luster pottery: Nanoparticles, ions, and local environment. *Journal Of Applied Physics* 93 (**12**) pp 10058-10063.
Pal, S., Tak, Y. K. and Song, J. M. (2007). Does the Antibacterial Activity of Silver Nanoparticles Depend on the Shape of the Nanoparticle? A Study of the Gram-Negative Bacterium Escherichia coli. *Appl. Environ. Microbiol.* 73 (**6**) pp 1712-1720.
Pal, T., Sau, T. K. and Jana, N. R. (1997). Reversible formation and dissolution of silver nanoparticles in aqueous surfactant media *Langmuir* 13 (**6**) pp 1481-1485.
Patterson, A. L. (1939). The Scherrer Formula for X-ray Particle Size Determination. *Physical Review* 56 pp 978-982.

Paz, Y., Luo, Z., Rabenberg, L. and Heller, A. (1995). Photooxidative self-cleaning transparent titanium dioxide films on glass. *Journal of MAterials Research* 10 (**11**) pp 2842-2848.

Pelley, A. J. and Tufenkji, N. (2008). Effect of particle size and natural organic matter on the migration of nano- and microscale latex particles in saturated porous media. *Journal of Colloid and interface Science* 321 (**1**) pp 74-83.

Pettibone, J. M., Cwiertny, D. M., Scherer, M. and Grassian, V. H. (2008). Adsorption of Organic Acids on TiO2 Nanoparticles: Effects of pH, Nanoparticle Size, and Nanoparticle Aggregation. *Langmuir* 24 (**13**) pp 6659-6667.

Pillai, Z. S. and Kamat, P. V. (2003). What Factors Control the Size and Shape of Silver Nanoparticles in the Citrate Ion Reduction Method? *Journal of Physical Chemistry B* 108 (**3**) pp 945-951.

Pollard, R. T., Salter, I., Sanders, R. J., Lucas, M. I., Moore, C. M., Mills, R. A., Statham, P. J., Allen, J. T., Baker, A. R., Bakker, D. C. E., Charette, M. A., Fielding, S., Fones, G. R., French, M., Hickman, A. E., Holland, R. J., Hughes, J. A., Jickells, T. D., Lampitt, R. S., Morris, P. J., Nédélec, F. H., Nielsdóttir, M., Planquette, H., Popova, E. E., Poulton, A. J., Read, J. F., Seeyave, S., Smith, T., Stinchcombe, M., Taylor, S., Thomalla, S., Venables, H. J., Williamson, R. and Zubkov, M. V. (2009). Southern Ocean deep-water carbon export enhanced by natural iron fertilization. *Nature* 457 pp 577-580.

Ponder, S. M., Darab, J. G., Bucher, J., Caulder, D., Craig, I., Davis, L., Edelstein, N., Lukens, W., Nitsche, H., Rao, L., Shuh, D. K. and Mallouk, T. E. (2001). Surface Chemistry and Electrochemistry of Supported Zerovalent Iron Nanoparticles in the Remediation of Aqueous Metal Contaminants. *Chemical Materials* 13 (**2**) pp 485.

Ratte, H. T. (1999). Bioaccumulation and toxicity of silver compounds: A review. *Environmental Toxicology and Chemistry* 18 (**1**) pp 89-108.

Reinfelder, J. R. and Chang, S. I. (1999). Speciation and Microalgal Bioavailability of Inorganic Silver. *Environ. Sci. Technol.* 33 (**11**) pp 1860-1863.

Reinhardt, A. (2004). Contrasting Roles of Natural Organic Matter on Colloidal Stabilization and Flocculation in Freshwaters. *PhD Thesis*. Universite de Geneve,Geneva 120 pages.

Rickerby, D. G. and Morrison, M. (2007). Nanotechnology and the environment: A European perspective. *Science and Technology of Advanced Materials* 8 (**1-2**) pp 19.

Ridout, M. J., Brownsey, G. J., York, G. M., Walker, G. C. and Morris, V. J. (1997). Effect of o-acyl substituents on the functional behaviour of Rhizobium meliloti succinoglycan. *International Journal of Biological Macromolecules* 20 (**1**) pp 1.

Rivas, L., Sanchez-Cortes, S., Garcia-Ramos, J. V. and Morcillo, G. (2001). Growth of silver colloidal particles obtained by citrate reduction to increase the Raman enhancement factor. *Langmuir* 17 (**3**) pp 574-577.

Roco, M. C. (2005). Environmentally Responsible Development of Nanotechnology. *Environmental Science & Technology* 39 (**5**) pp 106A-112A.

Ross, J. M. and Sherrell, R. M. (1999). The role of colloids in tracemetal transport and adsorption behavior in New Jersey Pinelands streams. *Limnology And Oceanography* 44 (**4**) pp 1019-1034.

RS/RAEng (2004).Nanoscience and nanotechnologies: opportunities and uncertainties. Royal Society and Royal Academy of Engineering pp 127. Downloaded from: http://www.nanotec.org.uk/finalReport.htm.

Sanchez-Cortes, S., Francioso, O., Ciavatta, C., Garcia-Ramos, J. V. and Gessa, C. (1998). pH-Dependent Adsorption of Fractionated Peat Humic Substances on Different Silver Colloids Studied by Surface-Enhanced Raman Spectroscopy. *Journal of Colloid and interface Science* 198 (**2**) pp 308.

Sandler, R. (2009).PEN report 16: Nanotechnology:The Social and Ethical Issues. Woodrow Wilson International Center for Scholars and The Pew Charitable Trusts pp 63. Downloaded from: http://www.nanotechproject.org/publications/.

Sastry, M., Mayya, K. S. and Bandyopadhyay, K. (1997). pH Dependent changes in the optical properties of carboxylic acid derivatized silver colloidal particles. *Colloids and Surfaces A: Physicochemical and Engineering Aspects* 127 (**1-3**) pp 221.

Savage, N. and Diallo, M. S. (2005). Nanomaterials and water purification: Opportunities and challenges. *Journal of Nanoparticle Research* 7 pp 331-342.

Sayes, C. M., Wahi, R., Kurian, P. A., Liu, Y., West, J. L., Ausman, K. D., Warheit, D. B. and Colvin, V. L. (2006). Correlating Nanoscale Titania Structure with Toxicity: A Cytotoxicity and Inflammatory Response Study with Human Dermal Fibroblasts and Human Lung Epithelial Cells. *Toxicological Sciences* 92 (**1**) pp 174-185.

Scherer, M. M., Richter, S., Valentine, R. L. and Alvarez, P. J. J. (2000). Chemistry and microbiology of permeable reactive barriers for in situ groundwater clean up. *Critical Reviews In Microbiology* 26 (**4**) pp 221-264.

Schimpf, M., Caldwell, K. and Giddings, J. C., Eds. (2000). *Field-Flow Fractionation Handbook*. New York, Wiley -Interscience.

Schimpf, M. E. and Petteys, M. P. (1997). Characterization of humic materials by flow field-flow fractionation. *Colloids and Surfaces A: Physicochemical and Engineering Aspects* 120 (**1-3**) pp 87-100.

Schmid, K. and Riediker, M. (2008). Use of Nanoparticles in Swiss Industry: A Targeted Survey. *Environmental Science and Technology* 42 (**7**) pp 2253-2260.

Scolan, E. and Sanchez, C. (1998). Synthesis and characterization of surface-protected nanocrystalline titania particles. *Chemistry Of Materials* 10 (**10**) pp 3217-3223.

Scown, T. M., van Aerle, R., Johnston, B. D., Cumberland, S., Lead, J. R., Owen, R. and Tyler, C. R. (2009). High doses of intravenously administered titanium dioxide nanoparticles accumulate in the kidneys of rainbow trout but with no observable impairment of renal function. *Toxicological Sciences* pp kfp064.

Seo, D. J., Park, S. B., Kang, Y. C. and Choy, K. L. (2003). Formation of ZnO, MgO and NiO Nanoparticles from Aqueous Droplets in Flame Reactor. *Journal of Nanoparticle Research* V5 (**3**) pp 199.

Serpone, N., Dondi, D. and Albini, A. (2007). Inorganic and organic UV filters: Their role and efficacy in sunscreens and suncare products. *Inorganica Chimica Acta* 360 (**3**) pp 794.

Smith, C. J., Shaw, B. J. and Handy, R. D. (2007). Toxicity of single walled carbon nanotubes to rainbow trout, (Oncorhynchus mykiss): Respiratory toxicity, organ pathologies, and other physiological effects. *Aquatic Toxicology* 82 (**2**) pp 94.

Sondi, I., Goia, D. V. and Matijevic, E. (2003). Preparation of highly concentrated stable dispersions of uniform silver nanoparticles. *Journal of Colloid and interface Science* 260 (**1**) pp 75.

Sondi, I. and Salopek-Sondi, B. (2004). Silver nanoparticles as antimicrobial agent: a case study on E. coli as a model for Gram-negative bacteria. *Journal of Colloid and interface Science* 275 (**1**) pp 177.

Sotiriou, G. A. and Pratsinis, S. E. (2010). Antibacterial Activity of Nanosilver Ions and Particles. *Environmental Science & Technology* 44 (**14**) pp 5649-5654.

Soto, K. F., Carrasco, A., Powell, T. G., Garza, K. M. and Murr, L. E. (2005). Comparative in vitro cytotoxicity assessment of some manufactured nanoparticulate materials characterized by transmission electron microscopy. *Journal of Nanoparticle Research* 7 (**2**) pp 145-169.

Spalla, O. (2002). Nanoparticle interactions with polymers and polyelectrolytes. *Current Opinion in Colloid & Interface Science* 7 pp 179-185.

Spencer, R. G. M., Bolton, L. and Baker, A. (2007). Freeze/thaw and pH effects on freshwater dissolved organic matter fluorescence and absorbance properties from a number of UK locations. *Water research* 41 (**13**) pp 2941-2950.

Sposito, G. (1989). *The Chemistry of Soils*, Oxford University Press.

Stathis, E. C. (1948). Determination of Silver with Ascorbic Acid. *Anal. Chem.* 20 (**3**) pp 271-271.

Steiner, M. and Lazaroff, N. (1974). Direct Method For Continuous Determination Of Iron Oxidation By Autotrophic Bacteria. *Applied Microbiology* 28 (**5**) pp 872-880.

Stipp, S. L. S., Hansen, M., Kristensen, R., Hochella, M. F., Bennedsen, L., Dideriksen, K., Balic-Zunic, T., Leonard, D. and Mathieu, H. J. (2002). Behaviour of Fe-oxides relevant to contaminant uptake in the environment. *Chemical Geology* 190 (**1-4**) pp 321-337.

Stolpe, B., Hassellov, M., Andersson, K. and Turner, D. R. (2005). High resolution ICPMS as an on-line detector for flow field-flow fractionation; multi-element determination of colloidal size distributions in a natural water sample. *Analytica Chimica Acta* 535 (**1-2**) pp 109-121.

Stone, V., Johnson, G. D., Wilton, J. C., Coleman, R. and Chipman, J. K. (1994). Effect of oxidative stress and disruption of Ca2+ homeostasis on hepatocyte canalicular function in vitro. *Biochem Pharmacol* 47 pp 625 - 632.

Stumm, W. and Morgan, J. J. (1996). *Aquatic Chemistry; Chemical Equilibria and Rates in Natural Waters*, John Wiley & Sons

Suber, L., Sondi, I., Matijevic, E. and Goia, D. V. (2005). Preparation and the mechanisms of formation of silver particles of different morphologies in homogeneous solutions. *Journal of Colloid and interface Science* 288 (**2**) pp 489.

Sun, Y. and Xia, Y. (2002). Shape-Controlled Synthesis of Gold and Silver Nanoparticles. *Science* 298 (**5601**) pp 2176-2179.

Taillefert, M., Lienemann, C.-P., Gaillard, J.-F. and Perret, D. (2000). Speciation, reactivity, and cycling of Fe and Pb in a meromictic lake. *Geochimica et Cosmochimica Acta* 64 (**2**) pp 169.

Tan, M. H., Commens, C. A., Burnett, L. and Snitch, P. J. (1996). A pilot study on the percutaneous absorption of microfine titanium dioxide from sunscreens. *Australas J Dermatol* 37 pp 185 - 187.

Thang, N. M., Geckeis, H., Kim, J. I. and Beck, H. P. (2001). Application of the flow field flow fractionation (FFFF) to the characterization of aquatic humic colloids: evaluation and optimization of the method. *Colloids and Surfaces A: Physicochemical and Engineering Aspects* 181 (**1-3**) pp 289-301.

Theron, J., Walker, J. A. and Cloete, T. E. (2008). Nanotechnology and water treatment: Applications and emerging opportunities. *Critical Reviews In Microbiology* 34 (**1**) pp 43-69.

Thevenot, P., Cho, J., Wavhal, D., Timmons, R. B. and Tang, L. (2008). Surface Chemisitry influences cancer killing effect of TiO_2 nanoparticles. *Nanomedicine* 4 pp 226-236.

Thill, A., Zeyons, O., Spalla, O., Chauvat, F., Rose, J., Auffan, M. and Flank, A. M. (2006). Cytotoxicity of CeO2 Nanoparticles for Escherichia coli. Physico-Chemical Insight of the Cytotoxicity Mechanism. *Environmental Science & Technology* 40 (**19**) pp 6151-6156.

Tiede, K., Hassellöv, M., Breitbarth, E., Chaudhry, Q. and Boxall, A. B. A. (2009). Considerations for environmental fate and ecotoxicity testing to support environmental risk assessments for engineered nanoparticles. *Journal Of Chromatography A* 1216 (**3**) pp 503-509.

Tipping, E. and Higgins, D. C. (1982). The effect of adsorbed humic substances on the colloid stability of haematite particles. *Colloids and Surfaces* 5 (**2**) pp 85.

Tipping, E., Rey-Castro, C., Bryan, S. E. and Hamilton-Taylor, J. (2002). Al(III) and Fe(III) binding by humic substances in freshwaters, and implications for trace metal speciation. *Geochimica et Cosmochimica Acta* 66 (**18**) pp 3211-3224.

van der Perk, M. (2006). *Soil and Water Contamination*, Taylor and Francis.

Van Hyning, D. L., Klemperer, W. G. and Zukoski, C. F. (2001a). Characterization of colloidal stability during precipitation reactions. *Langmuir* 17 (**11**) pp 3120-3127.

Van Hyning, D. L., Klemperer, W. G. and Zukoski, C. F. (2001b). Silver Nanoparticle Formation: Predictions and Verification of the Aggregative Growth Model. *Langmuir* 17 (**11**) pp 3128-3135.

Van Hyning, D. L. and Zukoski, C. F. (1998). Formation Mechanisms and Aggregation Behavior of Borohydride Reduced Silver Particles. *Langmuir* 14 (**24**) pp 7034-7046.

Velikov, K. P., Zegers, G. E. and van Blaaderen, A. (2003). Synthesis and characterization of large colloidal silver particles. *Langmuir* 19 (**4**) pp 1384-1389.

Verwey, E. J. W. (1947). Theory of the Stability of Lyophobic Colloids. *The Journal of Physical and Colloid Chemistry* 51 (**3**) pp 631-636.

Villalobos-Hernandez, J. R. and Muller-Goymann, C. C. (2006). Sun protection enhancement of titanium dioxide crystals by the use of carnauba wax nanoparticles: The synergistic interaction between organic and inorganic sunscreens at nanoscale. *International Journal of Pharmaceutics* 322 (**1-2**) pp 161.

Wallace, P. R. (1947). The Band Theory of Graphite. *Physical Review* 71 (**9**) pp 622-634.

Warheit, D. B., Webb, T. R., Sayes, C. M., Colvin, V. L. and Reed, K. L. (2006). Pulmonary Instillation Studies with Nanoscale TiO2 Rods and Dots in Rats: Toxicity Is not Dependent upon Particle Size and Surface Area. *Toxicological Sciences* 91 (**1**) pp 227-236.

Waychunas, G. A., Kim, C. S. and Banfield, J. F. (2005). Nanoparticulate Iron Oxide Minerals in Soils and Sediments: Unique Properties and Contaminant Scavenging Mechanisms *Journal of Nanoparticle Research* 7 (**4-5**) pp 409-433.

Weng, L., Van Riemsdijk, W. H. and Hiemstra, T. (2008). Humic Nanoparticles at the Oxide−Water Interface: Interactions with Phosphate Ion Adsorption. *Environmental Science & Technology* 42 (**23**) pp 8747-8752.

White, J. M. L., Powell, A. M., Brady, K. and Russell-Jones, R. (2003). Severe generalized argyria secondary to ingestion of colloidal silver protein. *Clinical & Experimental Dermatology* 28 (**3**) pp 254-256.

Wiesner, M. R., Lowry, G. V., Alvarez, P., Dionysiou, D. and Biswas, P. (2006). Assessing the Risks of Manufactured Nanomaterials. *Environmental Science & Technology* 40 (**14**) pp 4336-4345.

Wigginton, N. S., Haus, K. L. and Hochella, M. F. (2007). Aquatic environmental nanoparticles. *Journal Of Environmental Monitoring* 9 (**12**) pp 1306-1316.

Wilkinson, K. J., Balnois, E., Leppard, G. G. and Buffle, J. (1999). Characteristic features of the major components of freshwater colloidal organic matter revealed by transmission electron and atomic force microscopy. *Colloids and Surfaces A: Physicochemical and Engineering Aspects* 155 pp 287-310.

Wilson, M. A., Tran, N. H., Milev, A. S., Kannangara, G. S. K., Volk, H. and Lu, G. Q. M. (2008). Nanomaterials in soils. *Geoderma* 146 (**1-2**) pp 291-302.

Yoon, K.-Y., Hoon Byeon, J., Park, J.-H. and Hwang, J. (2007). Susceptibility constants of Escherichia coli and Bacillus subtilis to silver and copper nanoparticles. *Science of The Total Environment* 373 (**2-3**) pp 572.

Yoon, K. Y., Byeon, J. H., Park, C. W. and Hwang, J. (2008). Antimicrobial Effect of Silver Particles on Bacterial Contamination of Activated Carbon Fibers. *Environmental Science & Technology* 42 (**4**) pp 1251-1255.

Zattoni, A., Reschiglian, P., Montalti, M., Zaccheroni, N., Prodi, L., Picca, R. A. and Malitesta, C. (2007). Characterization of titanium dioxide nanoparticles imprinted for

tyrosine by flow field-flow fractionation and spectrofluorimetric analysis. *Inorganica Chimica Acta* 360 (**3**) pp 1063-1071.

Zhang, W.-x. (2003). Nanoscale Iron Particles for Environmental Remediation: An Overview. *Journal of Nanoparticle Research* 5 (**3 - 4**) pp 323.

Zhang, X., Sun, H., Zhang, Z., Niu, Q., Chen, Y. and Crittenden, J. C. (2007). Enhanced bioaccumulation of cadmium in carp in the presence of titanium dioxide nanoparticles. *Chemosphere* 67 (**1**) pp 160.

Zhao, X. C., Striolo, A. and Cummings, P. T. (2005). C-60 binds to and deforms nucleotides. *Biophysical Journal* 89 (**6**) pp 3856-3862.

Zhou, Q., Maurice, P. A. and Cabaniss, S. E. (2001). Size fractionation upon adsorption of fulvic acid on goethite: equilibrium and kinetic studies. *Geochimica et Cosmochimica Acta* 65 (**5**) pp 803-812.

Zhu, H., Han, J., Xiao, J. Q. and Jin, Y. (2008). Uptake, translocation, and accumulation of manufactured iron oxide nanoparticles by pumpkin plants. *Journal Of Environmental Monitoring* 10 (**6**) pp 713-717.

Zhu, X., Zhu, L., Chen, Y. and Tian, S. (2009). Acute toxicities of six manufactured nanomaterial suspensions to Daphnia magna. *Journal of Nanoparticle Research* 11 pp 67-75.

Zodrow, K., Brunet, L., Mahendra, S., Li, D., Zhang, A., Li, Q. and Alvarez, P. J. J. (2009). Polysulfone ultrafiltration membranes impregnated with silver nanoparticles show improved biofouling resistance and virus removal. *Water research* 43 (**3**) pp 715-723.